Competitive Thermokinetics and Non-linear Bushfire Behaviour

Andrew Lawrence Sullivan

A thesis submitted for the degree
of Doctor of Philosophy of
the Australian National University

Department of Theoretical Physics
Research School of Physical Sciences & Engineering
ANU College of Science

October 2007

Typeset in Palatino by TEX and LATEX 2$_\varepsilon$.

Declaration

This thesis contains no material which has been accepted for the award of any other degree or diploma in any university. To the best of the author's knowledge and belief, it contains no material previously published or written by another person, except where due reference is made in the text.

Andrew Lawrence Sullivan
24 October, 2007

Acknowledgements

A project this size does not happen without the help of quite a few people and while I can't list all the people who have aided and abetted me over the past few years, I would like to put into print the names of those without whom this work would have been very much poorer:

Foremost, I would like to thank my family: my wife, Jo, and my children, Taelor and Cameron, for whom my couple of years at the ANU (my new work) has been a pleasant diversion from the tedium of home, school and daycare; and my Mum and Dad, who have always encouraged and supported my exploration of new things with a sense of wonder and enjoyment.

My CSIRO (and, later, my Ensis) next-level managers: Jim Gould, Brian Richardson, Tim Vercoe and Sadanandan Nambiar, who supported my project proposal even when, I'm sure, they didn't really have any idea of what I was talking about and allowed me $2\frac{1}{2}$ years at 80% full-time to attempt it; and the CSIRO Centre for Complex Systems Science, John Finnigan and Rachel Williams, for providing the necessary external support for my project proposal that got me here. Also many thanks to the International Association of Wildland Fire for the inaugural 2007 IAWF-Wildland Fire Scholarship for Graduate Studies that enabled me to finish this thesis in my allotted time.

My PhD supervisors: Rowena Ball, Ian Enting and Jim Gould, for providing a challenging and constructive environment in which to explore the complexity that is bushfire behaviour and for providing critical comments and suggestions along the way. In particular, I would like to thank Jim for taking on the challenge that was my project, for allowing me the time and space to seriously tackle the issue of bushfire behaviour as a complex system within the scope of my CSIRO/Ensis work, and for making my PhD such a vital professional development endeavour (and also for suggesting my temporary relocation to the ANU in order to actually get some work done!).

My librarians at the various institutions, for work above and beyond the call of duty: Laurelle Tunks, Pamela Lockwood and Ailsa George (CSIRO/Ensis); Annette Stiles (ANU); and the little robot program that handled all the interlibrary loan requests.

My colleagues at CSIRO/Ensis: Phil Cheney, Ian Knight, Peter Ellis, Sean Cheney, Juanita Myers, Miguel Cruz, Matt Plucinski, Stuart Matthews, Brendan Pippen, Elizabeth Botha and Tivi Theiveyenathan (Australia) and Grant Pearce and Stuart Anderson (New Zealand) for providing valuable feedback, commentary and discourse on the nature of bushfires, particularly Ian and Phil for providing a sounding board for many new and counter-intuitive ideas.

The staff and students of the Department of Theoretical Physics in the ANU Research School of Physical Sciences and Engineering (in particular those with whom I shared the basement of the Sir Mark Oliphant Building for a year): Murray Batchelor and Vladimir Bazhanov (Heads of Department), Trina Merrell, Bob Dewar, Brian Kenny, Sergey Sergeev, Michael Bortz, Matthew Hole, Sangeetha Gnanapragasam, Farzand Abdullatif, Josh Garretson, Peggy Kao, Madeleine Smith, David Botman, Norman Oelkers, Andre Stoffel, Phillip Brydon, Emma Kirby, Graham Dennis, Peter Evans, Santi-

ago Callabero, Jolyon Bloomfield, Aroon O'Brien, Miklos Gulasci, Taira Vora, Natasha Devine, and Mathew McGann.

The staff and students of the wider world of the Research School: Neil Manson, Anna Cirjak, Liudmila Mangos (student admin), Julie Dalco, James Irwin (IT), Margaret Kahn (APAC), Kevin Lonsdale, Lyndell Paseka, Adrian Sheppard, Holger Averdunk, Paul Veldkamp, Jo Harrison, Matt Sellars, and Elliot Fraval for many enlightening and constructive morning and afternoon tea discussions.

Finally I wish to acknowledge the work of Dave Grohl who provided such a fine soundtrack for much of this PhD study.

For Noel Phillip (Phil) Cheney and Alan Grant McArthur.
Two scientists who have taught me what it is to be a bushfire researcher:
to study, observe, report and, above all, to think.

This universe, which is the same for all, has not been made by any god or man, but it always has been, is, and will be, an ever-living fire, kindling itself by regular measures and going out by regular measures.

Heraclitus of Ephesus
535 - 475 BC

The only real voyage of discovery consists not in seeking new landscapes, but in having new eyes, in seeing the universe with the eyes of another, of hundreds of others, in seeing the hundreds of universes that each of them sees.

Marcel Proust
1871 - 1922

We are going to study a problem that no one has managed to approach objectively, one in which the initial charm of the object is so strong it still has the power to warp the minds of the clearest thinkers...

The Psychoanalysis of Fire (1938)
Gaston Bachelard
1884 - 1962

Burn baby burn! Disco inferno
Burn baby burn! Burn that mama down

Disco Inferno
from *Disco Inferno* (1976)
The Trammps

Abstract

The prediction of the behaviour and spread of bushfires has always been fraught with a large number of unknowns, not the least of which has been the seemingly capricious nature of fire itself. Operational bushfire prediction systems, developed as they are using empirical methods, aim to predict the long-term mean spread of a bushfire based on its steady-state behaviour. This is done with the knowledge that the short-term behaviour might be very different to that predicted as a result of short-term (often at scales much less than can be readily measured) changes in wind, fuel, topography, and the apparent non-linear response of the fire. Such non-linear, short-term and, to all intents and purposes, unpredictable, fire behaviour can result in firefighters being caught unawares by changes in the behaviour of a bushfire, potentially leading to fatalities.

Recent efforts to capture the non-linear behaviour of bushfires have focussed on the interaction between the release of energy from the fire and the atmosphere, primarily through the convection column established above the fire. These generally take the form of large, computationally-intensive physical models based on the chemistry and physics of combustion and heat transfer. To make these models computationally tractable, simplifications and approximations are made in both the chemistry and physics, eschewing some of the fine scale detail of the combustion and turbulence in order to concentrate on the large scale interactions. However, this thesis shows that in doing so, much of the fundamental non-linearity in the combustion of biomass fuel is lost.

The primary component of all biomass fuel is cellulose, a substance that, due to its chemical structure as a polymer of condensed glucose ($[C_6H_{10}O_5]_n$), is one of the most adaptable and valuable substances known to mankind, providing clothing, paper, housing, energy, animal feed and dietary roughage. It is highly structured, insoluble in water, very stable over a wide range of temperatures and highly resistant to non-specific enzymatic attack. Its chemical structure also provides cellulose with a rather unique set of attributes when it is heated. Competitive nucleophilic attack following thermolysis of the glycosidic link joining two glucose residues results in two possible eventual morphologies under continued heating: the formation of charcoal through dehydration, decarbonylation and cross-linking reactions with a net exothermicity, or the formation of volatiles through cyclisation and depolymerisation with a net endothermicity and higher activation energy.

In this thesis I propose that much of the non-linearity observed in the behaviour of bushfires—the asymmetrical spread of fires under the action of wind, the formation of parabolic headfire shape, the inconsistent fire spread under essentially consistent conditions—is a result of the competitive nature of the thermal degradation of cellulosic fuels and, more particularly, the interaction of the ambient wind with the thermal and chemical feedbacks within the competitive combustion processes.

A zero-dimensional thermokinetic model of the thermal degradation of cellulose, based on the conservation of mass and energy, was obtained from the literature and extended and modified to represent secondary oxidisation reactions of the primary thermal degradation products—representing flaming and glowing combustion. An extensive se-

ries of numerical experiments were undertaken using this model to explore the effect of wind on the rates of fuel substrate loss, energy and species production. Results showed that all reactions were highly temperature sensitive, and that the model replicated the onset of ignition (providing the initial substrate temperature was significant enough) through the exothermic reaction enthalpies. It was also shown that while both charcoal and volatilisation reactions occur simultaneously (and thus glowing and flaming combustion), the ratio of the two products varies as a function of the wind temperature. The formation of charcoal was favoured under the action of ambient-temperature wind; the formation of volatiles was favoured under the action of elevated (i.e. near reaction-zone) temperature wind.

A commercial computational fluid dynamics package was used to investigate the spatial implications of the effect of competitive combustion of cellulosic fuels in a 3-dimensional environment. A simplified two-path, two-step version of the cellulose combustion chemistry showed that a low speed ambient temperature wind produces an asymmetry in the perimeter spread biased in the direction of the wind suggestive of the parabolic headfire shape. An asymmetry also occurs in the location of the formation of charcoal, forming preferentially over volatiles at the rear of the fire where the ambient temperature of the wind has the greatest impact. In no wind, no asymmetry was present in either the perimeter shape or the formation of the products. These results support the proposition that the interaction of the wind with the thermal degradation reactions controls the ratio of charcoal to volatiles formed. Ambient temperature wind is present on the windward edge of the fire perimeter, resulting in the formation of more charcoal, leading to more glowing combustion; passage of the air over the burnt and burning regions heats the air such that at the leeward edge of the fire perimeter the wind temperature is much greater than ambient, resulting in the formation of more volatiles leading to more flaming combustion.

The understanding of the role of wind, in particular wind temperature, in the thermal degradation of cellulosic fuel was used to construct a framework for a model of fire spread (as a function of the cross product of the direction of the wind and the normal to the tangent of the fire perimeter) that would be more computationally feasible than a complete fundamental model of the combustion chemistry and physics in the form of differential equations or a cellular automata. This framework provides a basis for the explanation of the importance of headfire width in determining the rate of forward spread of a fire.

Implications of the nature of the combustion of cellulosic fuels are many and wide ranging. From the sequestration of carbon and formation of CO_2 during biomass burning to post-fire mop-up, the competitive formation of charcoal and volatiles in the thermal degradation of cellulose plays a critical role in the behaviour of bushfires. A robust understanding of this role will lead to safer and more effective suppression.

Contents

List of Figures

List of Tables

Chapter 1

Introduction

In which the background of the subject of bushfire behaviour is introduced, some history of bushfire research around the world is discussed, the issues of predicting bushfire behaviour and spread from models of fire behaviour are explored and an outline of this thesis presented. It is proposed that much of the non-linear behaviour of bushfires can be attributed to the interaction of the wind and the unique chemistry of the thermal degradation of cellulosic biomass fuel.

A fire started beside a shed on a farm and quickly spread to an adjacent feed paddock. The local urban brigade was called to put out the fire but the fire was more than they could handle. Someone suggested the local volunteer brigade be called in. Despite some doubt from the professional guys, the volunteers were called in.

The volunteers arrived in a dilapidated old fire tanker. They rumbled straight past the stunned professional firefighters and drove right into the middle of the rapidly spreading head of the grassfire and stopped. The firemen jumped out and frantically sprayed water in all directions. They soon had the head fire snuffed out, leaving only the mildly burning flanks and rear of the fire to suppress.

Watching all of this, the farmer was impressed. To show his gratitude to the vollies who saved his feed he wrote them a cheque there and then for $1,000. A local reporter who had appeared on the scene asked the vollie crew leader what he was going to do with the money. The crew leader looked at the reporter with surprise. "That ought to be obvious," he said. "The first thing we're gonna do is fix the brakes on our tanker."[1]

1.1 Background

1.1.1 Bushfires and their behaviour

In Australia and many other parts of the world, the term 'the bush' refers to any part of the landscape that is of a rural or undeveloped character and generally refers to any

[1] This and other jokes in this thesis have been obtained from a number of sources. Refer to the Afterword for more information.

part of the countryside outside the cities, towns or built-up areas[2]. Thus any fire that burns in this region, whether it is intentional (such as a prescribed fire) or unintentional (such as a wildfire) is generically called a bushfire, regardless of the type of fuel in which the fire burns or the nature of the fire itself. In the United States such regions are called 'wildlands' and thus such fires are known as wildland fires. Bushfires therefore include fires in all types of vegetation—and may include structural fires if the fire is not restricted to the structure.

Bushfire has been an integral part of the Australian environment for millions of years. Much of the vegetation has evolved to cope with fire (Smith 1979; Springett 1979; Kemp 1981) and indeed in many cases has evolved to require fire to propagate (Kemp 1981; Gill 1981; Pyne 1991), developing characteristics such as coarse bark and slowly decaying leaf litter to promote the spread of bushfire. Australia's climate and vegetation is such that somewhere, at some time of the year, weather patterns will occur that will bring hot dry winds from the centre of the continent. Coinciding with drought and an ignition source, this will produce the possibility of wide spread conflagration that cannot be controlled until the weather moderates.

Evidence suggests that the Aborigines developed methods to use fire for access, hunting, encouraging of green pick, and for warfare (Hallam 1975). The arrival and spread of Europeans in the late 18th century resulted in changes in Aboriginal populations and fire regimes (Pyne 1991). While fire was found to be extremely useful for land clearing and pasture rejuvenation by European settlers, implementation of European land and farm management practices, where intense agricultural activity replaced land clearing and fire (particularly naturally occurring fires such as those ignited by lightning) was excluded, reduced the frequency of bushfires but also resulted in an increase in the amount of fuel and thus the intensity of wildfires when they did occur. Development of infrastructure such as settlements and townships increased the perceived value of assets at risk and thus the potential for significant damage.

Black Thursday, 6 February 1851, was one of the first events of large-scale conflagration to be recorded following European settlement. Fires on this day covered over a quarter of what today is the State of Victoria—approximately 5 million hectares[3]. Twelve people were killed and over a million cattle and sheep destroyed. Table 1.1 lists several severe wildfire events in Australia that have had a significant impact on Australians and the way we think about bushfires. While major bushfires generally occur each year somewhere in the country, severe events appear to occur on a cycle of 11 to 15 years (Luke and McArthur 1978).

1.1.2 Fire events and galvanisation of fire research

The need for bushfire research has been driven mainly by the occurrence and impact of severe wildfire events. Indeed, much of the world's general fire research is driven by the impact of fire events that provide impetus and funding for research. However, short political and social memories mean that such effects are short-lived, resulting in a boom-

[2]The Concise Oxford English Dictionary (5th Ed.) defines the bush as 'woodland, untilled district, (especially of partly-settled countries)'.

[3]While the term 'megafire' has recently been coined to describe the recent occurrences of large coincident fire events (Williams 2004)—largely attributed to anthropic climate change—extensive intense bushfires have been around for quite some time.

Table 1.1: Severe bushfire events that have had a significant impact upon Australia.

Name	Date	Location	No. of Fires	Area (MHa)	Fatalities	Structures
Black Thursday	6/2/1851	Victoria	unknown	≃5	12	unknown
Black Friday	13/1/1939	SE Aust.	unknown	1.5-2.0	71	650
Hobart	7/2/1967	Tasmania	100+	0.3	62	1446
Western District	14/2/1977	Victoria	69	0.1	5	450+
Ash Wednesday	16/2/1983	SE Aust.	100+	0.4	76	2400
Sydney	12/1993 - 1/1994	E NSW	800+	0.8	4	300+
Alpine Region	1/2003-3/2003	SE Aust.	unknown	3.0	10	500+
Wangary	10-11/1/2005	SA	1	0.08	9	90+

Sources include: Bond *et al*. (1967); McArthur (1969); Cheney (1976); Luke and McArthur (1978); Keeves and Douglas (1983); Rawson *et al*. (1983); Sullivan (2004); Gould (2006).

bust cycle for fire research that follows the occurrence of fire events (Williams 1982). In the case of bushfires, much of this research was left to those for whom the problem of less publicly significant but much more frequent bushfire events impacted immediately upon their livelihood. These were the foresters and other land managers.

In the US, the extensive fires of 1910 provided a galvanising effect for the then recently formed US Forest Service that provided the first direction for conducting research into the behaviour of bushfires (Pyne 2001). The work of Hawley (1926) and Gisborne (1927, 1929) pioneered the notion that understanding of the bushfire phenomenon and the prediction of the danger posed by a bushfire could be gained through measurement and observation and theoretical considerations of the factors that might influence such fires. In Canada, forest protection from wildfires was long recognised as an important problem for the forestry industry and an intensive study into fire behaviour was commenced at the Petawawa Forest Experiment Station in Ontario in 1929 (Wright 1932).

In Australia, it was not until the devastating fires of Black Friday, 13 January 1939, that such a galvanising effect was to be had, at least for the eastern states (Pyne 1991). In the west it was not until the Dwellingup fire of January 1961 (Rodger 1961) that Western Australia was galvanised toward bushfire mitigation and research into the behaviour, spread and danger posed by bushfires.

While there had been considerable research conducted into bushfires (the study of fire danger and behaviour and the factors that affect them) before the Second World War, it was generally driven by the individual needs of the various state-based forestry agencies to protect their own forestry assets. It was not until the early 1950s that a concerted effort was undertaken to develop a national professional bushfire behaviour research capacity. In 1953, the Forestry and Forest Timber Bureau, part of the Commonwealth Department of National Development, employed Australia's first full-time bushfire researcher, Alan Grant McArthur, an ex-New South Wales forester, to conduct research into bushfire behaviour and to develop a national fire danger rating system.

1.2 Bushfire research activities

1.2.1 Fire danger and fire behaviour

The primary aim of early bushfire research was to define and predict the likely danger and difficulty of suppression posed by a fire burning under given fuel and meteorological conditions. Such a prediction could then allow those charged with fighting of

bushfires to plan the daily allocation of suppression resources based on daily forecast weather. Later, such predictions would be used to issue public warnings of fire danger, such as total fire bans, which were aimed at reducing the likelihood of fire ignitions on days of extreme fire weather.

These fire danger prediction systems were generally simple tools that took observations of fuel conditions (moisture content, fuel load, degree of curing, etc.) and forecast meteorological conditions (air temperature, relative humidity, wind speed) and provided an index of fire danger, commonly on a scale of 1-100. The index was then generally divided into 5 or 6 ratings of likely fire danger: nil, low, moderate, high, very high or extreme, which were then used to issue warnings, set suppression readiness levels and predict likely difficulty of suppression.

As fire suppression planning became more sophisticated, the need for predicting the behaviour of the fire, not just its likely level of danger, was recognised. The ability to predict the likely spread of a bushfire would allow firefighting agencies to better plan the attack and suppression of bushfires while the fire was active. The primary element of fire behaviour that was needed for suppression planning was the speed of the fire in the direction of the prevailing wind (i.e the rate of forward spread, or more simply, the rate of spread (ROS), of the fire). Such information could allow the prediction of the movement of the most active part of the fire perimeter, the head of the fire, and thus generally the focus of suppression activities, as well as provide estimates of the growth of the fire area and perimeter length.

In the US in the late 1930s and early 1940s, workers of the US Forest Service brought a rigorous approach to the measurement and modelling of the behaviour of bushfires (Curry and Fons 1938, 1940; Fons 1946). Similar efforts occurred in Australia and Canada, again driven mainly by the needs of state and national forestry agencies. During this period, much of the research effort in the US, Canada and Australia was state or locality-based, although generally conducted in conjunction with federal agencies.

In Australia in the mid-1950s, McArthur commenced work on the development of fire danger rating systems for the two main fuel types of concern in Australia: native eucalypt forest (McArthur 1958) and grasslands (McArthur 1960). This was done in conjunction with many state-based forestry researchers (e.g. Luke (1953); Douglas (1957); Luke (1961); McArthur and Luke (1963); Peet (1965)) by conducting extensive series of experimental fires. As a forester of some experience, McArthur also recognised the utility of the long-held practice of controlled burning in reducing fuels to reduce the impact of wildfires and developed guidelines for use of prescribed fire in native forest (McArthur 1962). The development of these guidelines provided the basis for the development of operational wildfire spread prediction systems for grasslands (McArthur 1966) and forest (McArthur 1967; Cheney 1968) that remained in use for more than 30 years. In 1997, the grassland fire spread prediction system was replaced by a more robust system based on larger experimental fires (Cheney *et al*. 1998). In 2007, the forest fire spread prediction system was also replaced by a more robust system that incorporated the influence of shrub fuels (Gould *et al*. 2007).

Concurrently with McArthur's work, the US Forest Service and Canadian Forestry Service were developing national systems of their own for the operational prediction of fire behaviour in their particular fuel types. The Canadian Forestry Service, through its regional research facilities, undertook extensive experimental fire behaviour studies

in a wide variety of forest types. These experiments led to the development of several preliminary fire behaviour prediction systems before the introduction in 1970 of the Canadian Fire Weather Index (Canadian Forest Service 1970; Van Wagner 1987) and in 1992 of Canadian Fire Behaviour Prediction (CFBP) System (Forestry Canada Fire Danger Group 1992), which together formed the basis for the Canadian Forest Fire Danger Rating System (CFFDRS) (Stocks *et al*. 1991). Work continues to extend the various systems to crown fire spread (Stocks *et al*. 2004).

The US Forest Service undertook extensive laboratory experimentation in wind tunnels using artificial fuel beds to investigate fire behaviour (Anderson 1964; Rothermel and Anderson 1966; Anderson 1969). Rothermel (1972) developed a model of fire spread based on the heat balance approach of Frandsen (1971) and the wind tunnel results (augmented with wind speed data of McArthur). The model was incorporated into the US National Fire Danger Rating System (Deeming *et al*. 1977; Burgan 1988) and a fire behaviour prediction system known as BEHAVE (Andrews 1986) and is still in use today. Work on revising Rothermel's model is under way (Catchpole *et al*. 1998).

While research into bushfires has been conducted to various extents in many other parts of the world over the years, including South Africa, Russia, and the Mediterranean, for the most part the majority of the work was carried out in the US, Canada and Australia. With the formation of the European Union in 1990, significant funding was made available for bushfire research in Europe. The result is that for the past decade and a half, European countries such as France, Spain, Portugal and Greece have had an increasing impact in the field.

1.2.2 Predicting bushfire perimeter spread

From the earliest time of planned fire suppression there has been a need to predict the movement of the entire fire perimeter across the landscape. The plotting of predicted locations of the head fire on a wall map enabled the fire suppression planner to place the future position of the fastest-moving part of the fire in the landscape and identify key locations for suppression access and action as well as major topographical and geographical features that might affect the behaviour of the fire. Predicting the spread of the entire fire perimeter provided information about likely ecological and economical impacts of the predicted burnt area and the impact of future weather on probable spread, which allowed consideration of the cost of possible suppression strategies. Plotting fire spread on a wall map, even if only the likely position of the head fire, might well be considered the first attempt at fire spread simulation.

All current operational fire spread prediction systems aim to predict the mean rate of forward spread of a fire based on estimates of the mean current or forecast meteorological conditions (i.e. wind speed, temperature and relative humidity) and some mean characteristic of the fuel in which the fire is burning. In the case of the McArthur Mk V Forest Fire Danger Meter (McArthur 1973), the characteristic of the fuel is the amount of available fuel per unit area (i.e. fuel load). In the case of BEHAVE, it is fuel moisture content, bulk density, packing ratio and load. The CFBP requires fuel moisture content and qualitative data on fuel type. Both BEHAVE and CFBP combine fuel attributes into pre-defined fuel models for easier implementation.

These operational systems were designed to be implemented using simple, straightforward technology widely available at the time of their development. The US and Cana-

dian systems initially took the form of nomograms and tables of fire behaviour. The Australian systems were implemented as circular cardboard slide rules (indeed, Australian fire authorities requested even the new grassland system be made available as a circular slide rule). With the advent of cheap computing power in the 1970s and 1980s, these systems were soon adapted to be run on computers (Cohen and Burgan 1979; Noble *et al*. 1980; Crane 1982; Van Wagner and Pickett 1985) that provided faster and potentially more comprehensive estimates of a fire's rate of forward spread.

It has long been recognised that the shape of a free-burning bushfire commencing from a point ignition resembles that of an ovoid or ellipsoid (Mitchell 1937; Curry and Fons 1940). It has also long been recognised that free-burning bushfires spreading for some time tend toward a parabolic head fire shape curved in the direction of the wind (Curry and Fons 1938; Fons 1946), allowing estimation and mapping of the spread of the perimeter. McArthur (1966) determined a relation between the speed of the wind and the ellipse parameters length and breadth for grassfires in which the ellipse becomes more narrow and elongated under stronger winds. Alexander (1985) developed a relationship between wind speed and ellipse parameters for wind-driven forest fires on level ground. As with McArthur's relationship for grass, the ellipse narrows and elongates with increased wind speed.

Van Wagner (1969) proposed a simple fire perimeter propagation model based on the expansion of an ellipse given linear rate of spread values for the head, flanks and rear of the fire. Utilising ellipse geometry and assumptions regarding constant linear spread, Van Wagner derived relations for the rate of area and perimeter increase of a fire. A similar approach was used by King (1971) to simulate the rate of spread of mass ignitions used in aerial prescribed burns using circular spread (i.e. the perimeter shape of spread in low to nil wind). It was not until the increased availability of substantial computing ability in the 1970s that the desire to predict the spread of the entire perimeter across the landscape, rather than just the spread of the most active part, became achievable (Albini 1975; Kourtz *et al*. 1977; Anderson *et al*. 1982; Anderson 1983).

Kourtz and O'Regan (1971) approached the problem of fire spread simulation from a computer science perspective, modelling of fire spread across a landscape using a cell-to-cell contagion method. This approach was modified to use the predicted rate of forward spread from a combination of the Canadian and US fire behaviour models (Kourtz *et al*. 1977). Green *et al*. (1983, 1990) produced similar simulation models for Australian fire behaviour models.

Anderson *et al*. (1982) proposed a deterministic method based on Huygens' wavelet propagation principle that could be used in conjunction with a model of forward spread. In this method, a fire perimeter is treated as a continuous line represented by a series of linked points. Each point on a fire perimeter is considered a theoretical source of a new fire, the characteristics of which are based upon the given fire spread model and the prevailing conditions at the location of the origin of the new fire. The new fires around the perimeter are assumed to ignite simultaneously, to not interact, and spread according to a template shape based on an ellipse aligned in the direction of the wind. The exterior of all the new fires forms the new fire perimeter at that time.

The development of geographical information systems (GIS) in the late 1980s and early 1990s led to the inevitable linking of spatial data with bushfire spread algorithms resulting in the development of bushfire spread simulations as part of decision support

systems (Beer 1990). These systems include Farsite (Finney 1998) in the US, SiroFire (Coleman and Sullivan 1996) in Australia and Prometheus (CWFGM Steering Committee 2004) in Canada.

There have been many concerted efforts to model the behaviour and spread of bushfires from first principals (based primarily on the fundamental laws of motion and thermodynamics (e.g. Pagni and Peterson (1973); Grishin *et al*. (1983); Linn (1997); Linn *et al*. (2002); Linn and Cunningham (2005); Porterie *et al*. (1998, 2000, 2007); Mell *et al*. (2006, 2007), see reviews by Weber (1991a) and Sullivan (2007b)). However, the difficulties of obtaining suitable formulations of the governing equations that adequately capture the complex and interconnected nature of the processes involved in biomass combustion in the open over the range of scales involved in bushfire spread, while still remaining computationally tractable, have meant that the resultant physical models are difficult to validate, have extensive data and computation requirements, are generally orders of magnitude slower than real time, and thus have yet to gain acceptance for operational use by fire management agencies. These models, however, are finding use in pre-fire planning, post-fire effects modelling, and general fire dynamics research.

1.3 Unusual bushfire behaviour

1.3.1 Quasi-steady behaviour

The initial aim of operational fire behaviour prediction systems is to provide an estimate of the long term (i.e. 1–6 hours) *mean* behaviour and rate of spread of a bushfire based on mean quantities of fuel and weather conditions with the full understanding that the actual behaviour and spread rate might be considerably different over the shorter term. This long term average represents a *quasi-steady* value for rate of spread (Cheney and Gould 1997) and allows the developers of empirical fire spread models to incorporate several factors that may act to vary the rate of spread of a fire over the shorter term. These factors include the growth phases observed in bushfires commencing from point ignitions (Luke and McArthur 1978; Van Wagner 1985; McAlpine and Wakimoto 1991; Cheney and Gould 1997), as well as the short term variation in rate of spread that results from the spatial and temporal changes in fuel, topography and wind affecting the fire (Van Wagner 1977; Albini 1982; Weise and Biging 1997).

It is because of the high degree of spatial and temporal variation of the primary independent variables that mean values have been used in the development of operational fire behaviour prediction systems. Even if the system development itself was based on exactly measured laboratory experiments, the nature of these variables in the field has meant that significant effort has been expended developing methodologies for determining the mean field values of those variables for predictive purposes (McArthur 1966; Albini and Baughman 1979; Rothermel 1983; Andrews 1986; Sullivan and Knight 2001). For meteorological variables such as wind speed, temperature, relative humidity, the meteorological measurement procedures standardised by the World Meteorological Organisation (1988) have become the default standard for operational fire meteorology observations and thus most operational fire behaviour prediction systems are based on such measures. For example, wind speed is measured operationally at a height of ten metres in an open area in which the closest obstacle is more than ten times its height away from the anemometer. Measurements are averaged over a period of 10-20 minutes in or-

der to achieve a meaningful quantity that represents the bulk movement of air across the measurement site without undue influence from the gust and lull structure of turbulence embedded in the flow (World Meteorological Organisation 1988). Thus an operational fire behaviour prediction system developed using some other more practical measure of wind speed must provide a conversion so operational meteorological observations can be used directly (e.g. Rothermel (1983)).

1.3.2 Unexpected changes in behaviour

Unexpected changes in the quantities of fuel, topography and wind from those used to carry out a fire behaviour prediction will, of course, result in variation from the predicted value. Observations of periods or areas less than that required for a meaningful average value will also result in incorrect predictions. The use of long-term averages (wind, terrain, fuel, ROS) allows the rate of spread over the landscape to be made with some degree of confidence (e.g. over the long-term, fire spread over hilly topography is said to approach that of flat ground (Cheney 1968)). Detailed measurements of short-term (i.e. 5 s) wind speed and rate of spread were found to be poorly correlated in both grassfires (Cheney *et al*. 1993) and northern jack pine/black spruce forest fires (Taylor *et al*. 2004). Indeed, Cheney *et al*. (1993) found that the instantaneous ROS varied by up to ± 0.7 m s^{-1}. The spatial separation of the wind measurement site/s and the fire also introduces possible error (Sullivan and Knight 2001).

However, even using the highest quality observations of independent variables to predict fire behaviour over the required period and within the range of conditions in which the prediction system was developed will not necessarily result in an accurate prediction of the actual fire behaviour. Detailed measurements of strictly controlled laboratory experiments (e.g. Rothermel and Anderson (1966); Dupuy (1995); Catchpole *et al*. (1998)) found considerable variation in fire ROS despite constant wind, fuel and slope conditions. This capricious nature of fire—seemingly chaotic behaviour around some mean value—is widely accepted in both the research and operational bushfire communities as part of the nature of bushfire. Indeed, both the developers and users of operational fire spread prediction systems do not expect such systems to be perfectly accurate but to provide only a practical prediction upon which planning may be based.

As an example, Figure 1.1 shows the performance of the CSIRO Grassland Fire Spread Meter (CSIRO 1997) against the normalised data[4] used to develop it (Cheney *et al*. 1998). Even with the effects of fuel moisture content, degree of curing, and fuel condition removed from the data, the variation in ROS is considerable. At one standard deviation (i.e. 68% confidence interval), the range of ROS at a mean wind speed of 20 km h^{-1} is 4 km h^{-1} around a mean speed of 7 km h^{-1} (i.e. 5–9 km h^{-1}).

As a result, while operational fire spread prediction systems are useful for determining mean rate of spread over many hours (such as required for suppression planning and public warning purposes), they do not provide any insight into the short term fire behaviour and rate of spread for firefighters on the ground. Short term behaviour that may lie within a standard deviation or two of the mean behaviour may be allowable in the prediction of spread over an hour or two but means that to all intents and purposes the behaviour is unusual and thus unpredictable by the operational fire spread predic-

[4]Data normalised for fuel moisture content, degree of curing and using 10-minute mean wind speed.

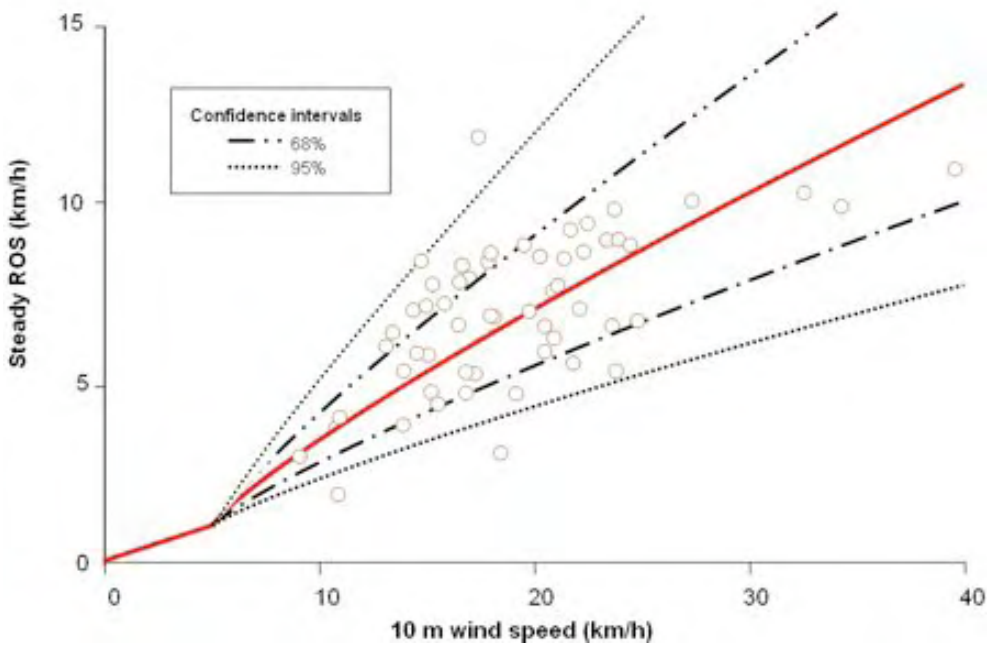

Figure 1.1: Comparison of the CSIRO grassland fire spread model (red line) for grazed pasture and the data (normalised for fuel moisture content and curing) on which it was based. (Source: Cheney *et al*. (1998))

tion system. Such short term behaviour can include rapid increases in rate of spread as well as decreases that may mislead observers and catch firefighters unaware. In the most severe situation, particularly where firefighters are undertaking indirect suppression[5], unexpected changes in fire behaviour can result in firefighters being overrun by the fire and killed or seriously injured (Cheney *et al*. 2001).

There have been many attempts to improve the ability of operational fire spread prediction systems to predict the 'unusual' or unpredictable behaviour of fires that is commonly observed in bushfires. Byram (1954) identified the situation where the behaviour of a fire (rate of spread and intensity) increased dramatically with no forewarning and no apparent change in burning conditions. This dramatic increase in fire behaviour has been termed variously 'blow-up', 'boil-up', 'eruption', or 'extreme or erratic behaviour', amongst others (e.g. Byram (1954); Tolhurst and Chatto (1998); Viegas (2005, 2006)). Attempts to address the issue of this unusual fire behaviour have focussed on the interaction between the fire and the atmosphere, as Byram (1959b, p.101) identified this interaction as being the most involved of all the interactions concerning a fire and its environment.

1.3.3 Investigation of atmospheric interactions

Byram (1954) found that 'blow-up' fires generally occurred when the atmosphere was unstable and a low level jet existed near the surface such that an inversion of the wind profile was present—that is, wind speed reduced with height. It was these fires of ex-

[5]Suppression activity where firefighters carry out fireline construction some distance from the fire edge.

treme behaviour that caused the most difficulty for suppression and posed the highest threat to the safety of firefighters. Byram conducted an analysis of the forces involved, namely the buoyant force of the fire and the dynamic force of the wind, and developed a non-dimensional ratio, the energy criterion or convective number, N_c, between what he called the power of the wind, P_w, and the power of the fire, P_f. This was elaborated recently by Nelson (1993, 2003):

$$N_c = \frac{P_f}{P_w} = \frac{\frac{gI}{c_p \theta_a}}{\frac{\rho\,(u-r)^3}{2}} = \frac{2gI}{\rho\, c_p\, \theta_a\, (u-r)^3}, \tag{1.1}$$

where I is fireline intensity (kW m^{-1}), ρ is air density (kg m^{-3}), c_p is the specific heat of dry air at constant pressure (J kg^{-1} K^{-1}), g is gravity, θ_a is the absolute ambient air temperature, u is mean wind speed (m s^{-1}) and r is rate of forward spread of the fire (m s^{-1}).

Clark *et al*. (1996a) conducted numerical experiments of a coupled atmosphere-fire model with a similar approach based on the Froude number, which they called the convective Froude number, F_c:

$$F_c = \sqrt{\frac{(u-r)^2}{g\frac{\Delta\theta}{\theta_a} D}}, \tag{1.2}$$

where $\frac{\Delta\theta}{\theta_a}$ is the convective buoyancy (the ratio of the difference between the ambient potential temperature, θ_a, and the potential temperature in the convection column θ_c), and D is the flame depth (m), the depth of the flaming zone of the fire front.

Both Byram and Clark *et al.* suggested that these non-dimensional analyses would identify critical behaviour of bushfires. When the dynamic forces dominate the buoyant forces, ($F_c > 1 > N_c$), there would be little interaction between the fire and the wind, and when the buoyant forces dominate the dynamic forces ($F_c < 1 < N_c$) then the fire would not be affected by the wind to any great extent. When the forces involved were in balance, ($F_c \simeq N_c \simeq 1$), for some height above the fire, there would be a high level of interaction between the atmosphere and the fire, and the fire would exhibit critical behaviour that would lead to 'blow-up' behaviour.

However, Byram (1959b) found that not all blow-up fires could be correlated with $N_c \simeq 1$ and, conversely, not all conditions of $N_c \simeq 1$ could be correlated with blow-up fires. Jenkins *et al*. (2001) suggested that the critical conditions would occur at values of F_c less than unity when the buoyant forces are slightly greater than the dynamic wind forces. Sullivan (2007a) found that there was no correlation between F_c and behaviour of large experimental grassland fires. Potter (1996, 2002, 2005) developed a number of upper atmosphere measures in an attempt to provide a robust quantification of the fire-atmosphere interaction. More recent work (Mills 2005a) has found that extreme fire behaviour is also associated with 'dry slots', the passage of extremely dry air from the upper atmosphere over the active fire, which Byram also identified.

1.3.4 Non-linearity of bushfire behaviour

While the focus of unusual fire behaviour has been on 'blow-up' fire behaviour (i.e. dramatic or sudden increases in fire behaviour leading to dangerous conditions), unusual fire behaviour can also include decreases in fire behaviour. A much more general term

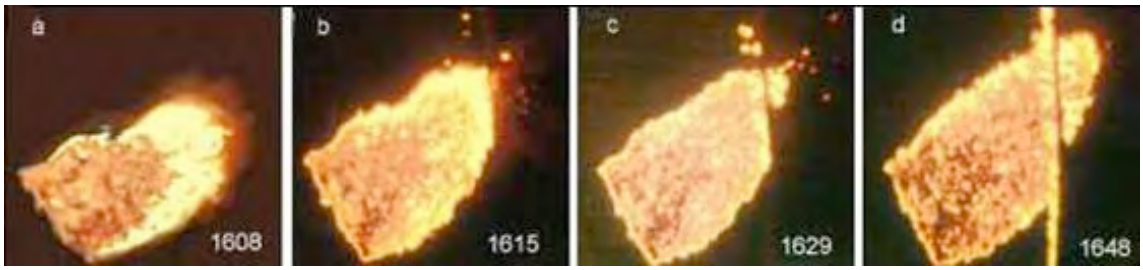

Figure 1.2: A series of infra-red line scan of experimental fire in dry eucalypt forest from Project Aquarius, Nowa Nowa Block 10, 19/2/1985. (a) The experimental fire, lit from a 200-m-long ignition line, has burnt for 48 mins and has just reached a 30-m-wide bare earth fuel break. (b) 1615 hours: The fire's forward spread has been halted and has begun to throw spot fires over the break. (c) 1629 hours: The spot fires have begun to coalesce. (d) 1648 hours: The spots have coalesced and reformed the shape of the head fire prior to hitting the break and continues to spread as though unimpeded. (Source: CSIRO Forestry and Forest Products unpublished data)

is required that does not convey the sense that all unusual fire behaviour is extreme. Erratic has been used to describe this behaviour but this also conveys inconsistency or capriciousness. The word 'non-linear' has a very strict mathematical meaning[6] but is also used to describe the behaviour of a system in which the progress from one stage to the next is not sequential or, less precisely but more generally, is not simply the sum of its parts (Scott 2005). Thus the behaviour of a bushfire which increases or decreases its intensity or speed as a result of some seemingly innocuous change in conditions can be described as non-linear, as can bushfire behaviour that doesn't change when a significant change in conditions occurs.

Two examples from field experiments are used to illustrate these aspects. Figure 1.2 is a series of infra-red line scans that show the progress at irregular times of an experimental fire conducted as part of Project Aquarius (Loane and Gould 1986; Gould *et al*. 1996) in dry eucalypt forest of southeast Victoria. This fire was lit from a 200-m ignition line and allowed to burn unimpeded for some time. Figure 1.2(a) shows the fire at time 1608, some 48 minutes after ignition. The fire has just reached a 30 m bare-earth firebreak along the right hand side of the image. Figure 1.2(b) shows that 7 minutes later the fire has ceased its forward spread due to the break and has begun to throw spotfires a short distance over the break. Figure 1.2(c) shows that at 1629 the spot fires continue to fall across the break and are beginning to coalesce. In Figure 1.2(d) at 1648, 40 minutes after the fire hit the firebreak, the spots have coalesced, reforming the shape of the fire prior to hitting the break, and the fire continues to actively spread, despite the presence of the firebreak and a backburn put in along the windward side of the break (the vertical line running through the head fire). The fire eventually burns out all of the neighbouring plot.

The second example is a set of experimental fires carried out in the grasslands of the Northern Territory at Annaburroo Station (Fig. 1.3) (Cheney *et al*. 1993). These fires were lit simultaneously with different ignition lengths: 100 m, 50 m and a point ignition. The 100-m fire spread the fastest with an average speed of 1.25 m s^{-1}. Initially, the 50-m fire

[6] A system that is not subject to the principle of superposition.

spread much faster than the point ignition fire (Fig.1.3a and b) but after about two and half minutes of spread (Fig. 1.3c), the point ignition fire was spreading at the same speed as the 50-m fire. Differences in the initial widths of the fires affected their speed, but also so did the shape of the head-fire (Cheney *et al*. 1998). This work led to the understanding of scale dependence in rate of spread that called into question operational fire spread models developed in narrow wind tunnels.

While these examples of bushfire behaviour cannot be described as blow-up or erratic, the behaviour is certainly non-linear for the prevailing conditions and is indicative of the complex nature of bushfire behaviour. Such non-linearity in behaviour is beyond any empirical system of fire behaviour prediction (indeed, such behaviour almost defines the word 'outlier' in statistical analysis and is generally removed from consideration) and can lead to deaths where such behaviour is not expected.

1.4 This thesis

The non-linear nature of bushfires has been well described in the general literature (without actually being defined as such) and has been accepted as part of the erratic nature of the phenomenon. Many attempts have been made to provide a physical explanation of the cause of such non-linear behaviour but for a field of research that has interested mankind for hundreds if not thousands of years and which in the current era can trace its roots back nearly 90 years, there is much about bushfire behaviour that has not been adequately explained.

Why do bushfires spread faster with a wind? Why is there a difference between the behaviour of head fires and the behaviour of back fires? Why do bushfires tend toward a parabolic head fire shape? What causes bushfires to suddenly change behaviour with no obvious (or only very minor) change in conditions? Why do fires exhibit stop-start spread behaviour? Why is there little to no correlation between the short-term speed of the wind and the fire? Why is there a difference between the ash left by a head fire and back fire? Why does low fuel moisture content play such a critical role in fire behaviour? Why do bushfires seem to integrate significant changes in fuel and weather under some circumstances and not others? Why does a fire that has been smouldering for considerable time suddenly burst into flame? Why is it so difficult to put out smouldering fires during mop-up?

No doubt some of these questions will remain unanswered adequately for some time to come, while others may be answered for practical purposes without need for an exact answer. It is the aim of this thesis to propose a physical mechanism by which some of the non-linear behaviour of bushfires may be explained and perhaps lead to a greater fundamental understanding of the nature of bushfire behaviour. It is proposed in this thesis that it is the unique chemical makeup of biomass fuel, the way that it thermally degrades, and the interaction of this process with the wind that leads to the non-linear behaviour of bushfires and provides an explanation for much of the observed behaviour of bushfires.

Cellulose, the primary constituent of biomass fuel, has long been recognised for its unique qualities that have found many uses in the form of construction material, paper and clothing, as well as a source of heat when burnt in the form of wood. Cellulose provides dietary fibre (roughage) in food and forms the basis for many man-made poly-

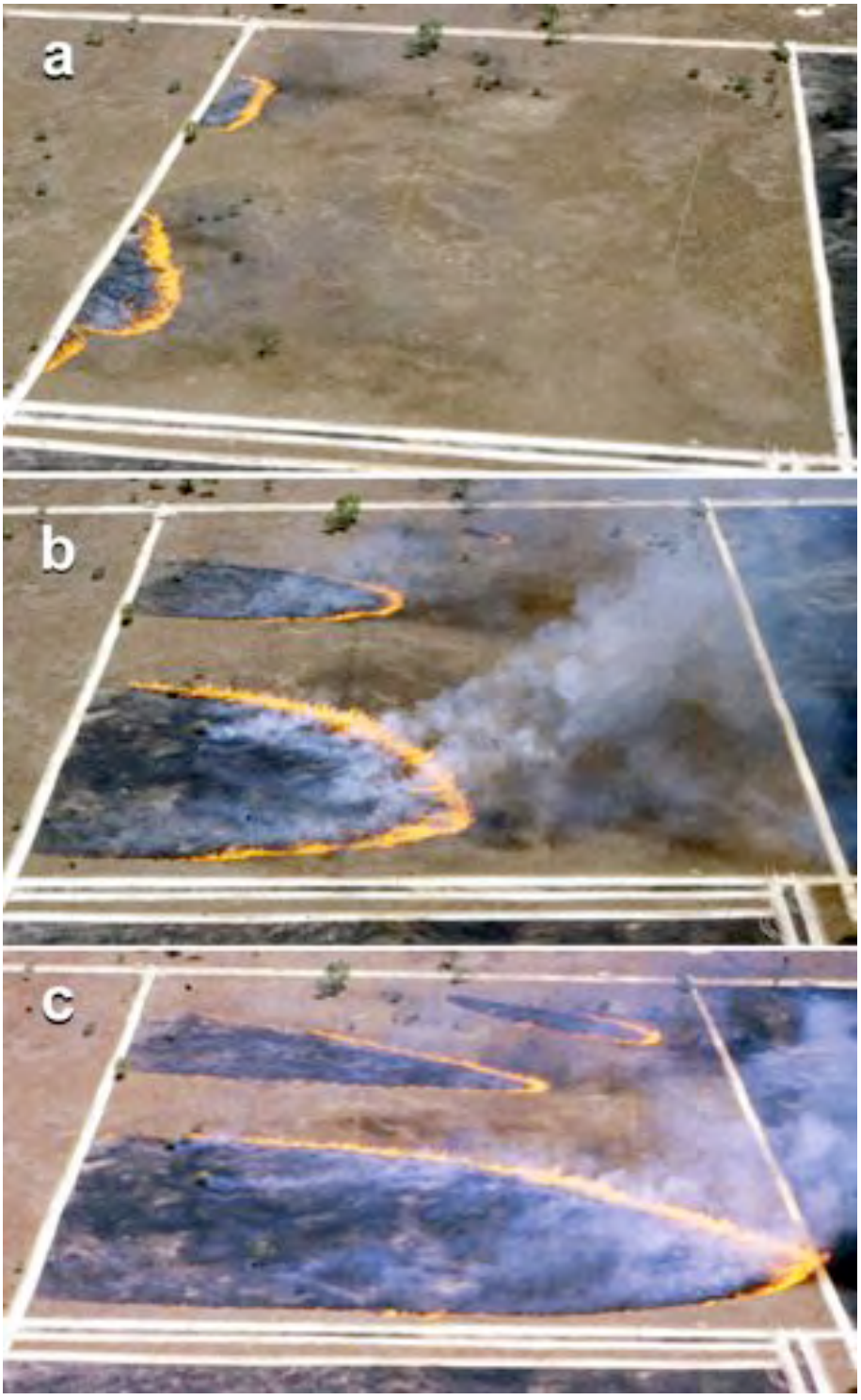

Figure 1.3: Sequence of photos showing the development of three fires lit simultaneously (from left to right: 100-m ignition, 50-m ignition, and point ignition) during experiments at Annaburroo Station in the Northern Territory. (a) 40 s since ignition: The 50 m and 100 m fires have spread a similar distance. The point ignition is barely discernible. (b) 1 min 40 s since ignition: The 100-m fire is spreading faster than the 50-m fire. The point ignition fire is now visible. (c) 2 min 40 s since ignition: The 100-m fire has reached the end of the block. The 50 m and the point ignition fires are now spreading at roughly the same speed. (Source: Cheney and Gould (1995).)

mers such as rayon. Conversion of raw wood to charcoal (from Old English, literally to 'turn to coal') was found to provide much more heat energy during combustion than the combustion of the raw wood itself and has been used since the early ages.

The process involved in charcoal formation has been understood empirically for millennia and involves the thermal degradation of cellulosic material (such as biomass) in the presence of moisture and the absence of oxygen. In the absence of moisture and the presence of oxygen, the cellulosic material can undergo a volatilisation reaction and flaming combustion, resulting in useless ash. A unique aspect of cellulosic thermal degradation is that the reactions that lead to charcoal formation and to volatile formation are *competitive*, that is a segment of cellulose can undergo charring or volatilisation but not both.

Charcoal and its production from wood is intricately linked to the development of metallurgy and the beginnings of technology 5000 years ago (Harris 1999). The much higher temperature of combustion of charcoal enabled the smelting of metals that was not possible burning ordinary wood. Purpose-built charcoal kilns or retorts that enabled the strict control of air flow and moisture into the combustion zone were used to manufacture charcoal from a very early period. The widespread demand for charcoal as fuel led to mass deforestation of central Europe and Britain during the middle of the previous millennium. Up until the innovation of coke (produced from bituminous coal) around 1700, charcoal was the primary fuel for the production of iron. (Interestingly, the metallurgy industries are again considering biomass charcoal as fuel in an attempt to address greenhouse gas and carbon accounting issues.)

The competitive processes of charcoal formation and volatilisation of cellulose fuel provides a source of non-linearity in the combustion of biomass fuel and this thesis explores the dynamic nature of these processes when combustion is open to the influence of wind, as is found in a free-burning bushfire. The interaction between the competitive chemistry of cellulosic thermal degradation and the wind results in complex nonlinear behaviour that may provide an explanation for much of the observed behaviour of bushfires, including the formation of parabolic head fire shapes, the difference between backing and heading fires and the formation of different types of ash after the fire.

The focus of this thesis is the thermokinetics of the thermal degradation process and the interactions with an ambient wind flow. These are explored through numerical techniques and simulation. An outline of this thesis follows.

Chapter 2 provides an overview of the fundamentals of chemistry and physics that are involved in cellulosic fuel combustion in regard to bushfires, detailing the physical and organic chemistry of the thermal degradation and combustion of biomass fuels and the transfer of heat released to unburnt fuel through the physics of thermodynamics, fluid dynamics and heat transfer.

Chapter 3 presents the implications for the competitive combustion detailed in Chapter 2 and proposes an hypothesis which defines this thesis. Observational evidence from a unique set of large-scale field experiments in the literature is given to support the hypothesis and an inadvertent null-hypothesis test from the literature is used to further support the hypothesis.

Chapter 4 modifies and extends a model of the reaction kinetics of the thermal degradation and combustion of cellulose obtained from the literature. This model is in the form of a zero-spatial dimension set of coupled ordinary differential equations and is

used in Chapter 5 to investigate the dynamics of the system and the role of a number of key variables. The results of the simulations shows that the temperature of the system and thus the reaction rates are tightly connected with the magnitude and temperature of the advection to which the system is exposed and thus whether the system undergoes charring or volatilisation.

Chapter 6 places the reaction kinetics developed thus far into a spatial context and uses computational fluid dynamics (CFD) to explore the effects of advection on the reaction kinetics around a fire perimeter. A CFD model is constructed in the commercial CFD package FLUENT and simulations are run that show that the shape of the head fire is a function of the chemistry of combustion in conjunction with the wind.

Chapter 7 develops a framework for a model based on the concepts of Complex Systems Science (CSS) and the competitive combustion of cellulosic fuels explored in the preceding chapters. Requirements for a model incorporating different combustion characteristics around the fire perimeter are given and a basic framework for such a model presented.

Chapter 8 presents the conclusions of this thesis and discusses a range of implications of the findings of this study. These include implications for fire behaviour prediction and firefighter safety, particularly in relation to changes in wind direction, for fire suppression and post-fire mop-up, for carbon sequestration in black carbon and carbon dioxide emission from biomass burning.

Throughout this thesis the term 'competitive combustion' is used to describe the competitive thermal degradation of a cellulosic fuel and the subsequent non-competitive oxidation of the products.

Chapter 2

Some fundamentals of fire

In which an overview of the fundamentals of combustion and fire spread in biomass fuels in the context of bushfires is given, covering the basic physical and organic chemistry of the thermal degradation of cellulose, the primary component of all biomass fuels, the oxidation of the released products, through to the physical mechanisms of heat transfer by which bushfires propagate through the fuel. A brief summary of fire spread modelling is given.

An engineer, a physicist, a mathematician, and a mystic were asked to name the greatest invention of all time. The engineer chose fire, because it gave humanity power over matter. The physicist chose the wheel, because it gave humanity the power over space. The mathematician chose the alphabet, because it gave humanity power over symbols. The mystic chose the thermos bottle.

"Why a thermos bottle?" the others asked.

"Because the thermos keeps hot liquids hot in winter and cold liquids cold in summer."

"Yes," they said. "So what?"

"Think about it," said the mystic reverently. "That little bottle—*how does it know*?"

2.1 Introduction

Bushfire spread is the complicated combination of the release of energy (in the form of heat) from chemical reactions in the process of combustion and the transport of that energy to surrounding unburnt fuel, the subsequent ignition of that fuel and the ongoing cycle of these processes. The former is the domain of chemistry (more specifically, *chemical kinetics*) and occurs on the scale of molecules, and the latter is the domain of physics (more specifically, *thermodynamics* and *heat transfer*) and occurs on scales ranging from millimetres up to kilometres (Table 2.1). It is the interaction of these processes over the wide range of temporal and spatial scales that makes the physical modelling of bushfire behaviour a most difficult problem.

This chapter presents the important aspects of the chemistry and physics of the combustion of cellulosic fuels as they relate to bushfires. As the focus of this thesis is on

Table 2.1: The major biological, physical and chemical components and processes occurring in a bushfire and the temporal and spatial (vertical and horizontal) scales over which they occur.

Type	Time scale (s)	Vertical scale (m)	Horizontal scale (m)
Combustion reactions	$10^{-20} - 10^{-2}$	$10^{-4} - 10^{-2}$	$10^{-4} - 10^{-2}$
Fuel particles	–	$10^{-3} - 10^{-2}$	$10^{-3} - 10^{-2}$
Fuel complex	–	$10^{0} - 2 \times 10^{1}$	$10^{0} - 10^{2}$
Flames	$10^{-2} - 3 \times 10^{1}$	$10^{-1} - 10^{1}$	$10^{-1} - 2 \times 10^{0}$
Radiation	$10^{-9} - 1 \times 10^{1}$	$10^{-1} - 10^{1}$	$10^{-1} - 5 \times 10^{1}$
Conduction	$10^{-2} - 10^{1}$	$10^{-2} - 10^{1}$	$10^{-2} - 10^{1}$
Convection	$10^{0} - 10^{2}$	$10^{-1} - 10^{2}$	$10^{-1} - 10^{1}$
Turbulence	$10^{-1} - 10^{3}$	$10^{0} - 10^{3}$	$10^{0} - 10^{3}$
Spotting	$10^{0} - 10^{3}$	$10^{0} - 3 \times 10^{3}$	$10^{0} - 10^{5}$
Plume	$10^{0} - 10^{5}$	$10^{0} - 10^{5}$	$10^{0} - 10^{2}$

the role of the chemistry of thermal degradation in bushfire behaviour, this is covered in more detail than the physics of heat transfer, which is covered in most texts on the subject.

2.2 Chemistry of combustion

The chemistry of combustion involved in bushfire is necessarily a complex and complicated matter. This is in part due to the complicated nature of the biology of the fuel itself but also in the range of conditions over which combustion can occur which dictate the evolution of the combustion processes.

While the basic understanding of the processes of combustion of biomass fuels in general has been around since the beginning of the industrial revolution, it took some time before it became prevalent in bushfire research. Gisborne (1947) summarised the fundamentals of bushfire behaviour for the time, in which the basic process of combustion was identified as a chemical reaction involving the oxidation of fuel that released heat energy. The conditions necessary for this reaction required the presence of fuel heated to a temperature sufficient to initiate the reaction and oxygen with which the fuel could react. Byram's (1959a) seminal work of forest fuel combustion has provided much of the basis for the operational understanding of bushfire behaviour and the development of prediction systems in use today. However, while the current texts of the field (e.g. Chandler *et al*. (1983a,b); Pyne *et al*. (1996)) have to a limited extent expanded upon the knowledge of combustion in the field, much of the material available in the realm of bushfire behaviour has not taken up the advances in the understanding of combustion that have been made in the field of biomass combustion in the intervening decades. The simplified understanding of the chemical processes involved in the combustion of bushfire fuels (e.g. Byram (1959a); Vines (1981)) obscures the true complexity of the chemical reactions involved in the thermal degradation and oxidation of cellulosic fuels and in some cases is fallacious.

This section details the understanding of the chemistry of combustion of cellulosic fuels that has been developed predominantly in the field of industrial energy conversion via biomass burning. Much of the understanding has come from strictly controlled laboratory investigation of the combustion of cellulose fuel.

2.2.1 Fuel chemistry

Bushfire fuel is composed of the live and dead plant material of the biomass consisting primarily of leaf litter, twigs, bark, wood, grasses, and shrubs (Beall and Eickner 1970). Under some conditions, particularly severe fire weather situations, the fuel can also include all components of the biomass that would not normally burn under milder conditions, such as fallen logs, tree canopies, and, possibly, the trees themselves (Gould and Sullivan 2004). The fuel represents a considerable range of physical structures, chemical components, age and level of accumulation and biological decomposition, depending on the type, age and history of the particular biomass.

The primary chemical constituent of biomass fuel is cellulose which has the chemical formula $(C_6H_{10}O_5)_n$. Cellulose is a polymer of a glucosan monomer (Shafizadeh 1982; Williams 1982) and is a non-reducing carbohydrate (Morrison and Boyd 1983, p.1112). Glucosan, or D-glucose, is a variant of glucose, the primary source of energy of all living organisms, and has the empirical chemical formula $C_6H_{12}O_6$ (Fig. 2.1). Cellulose is the most abundant organic material on the Earth (O'Sullivan 1997) and is present in bacteria, algae, fungi and some animals in addition to plants.

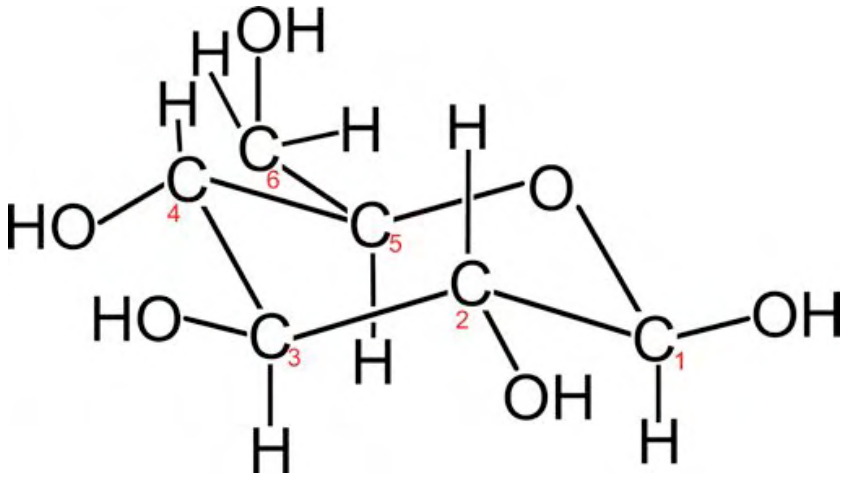

Figure 2.1: Full schematic of chemical structure of D-glucose, showing the chair-like conformation of the molecule's ring. Carbon atom numbering convention is shown in red. (After Morrison and Boyd (1983, p. 1080))

It is common in the field of organic chemistry to reduce the full diagrammatic structure of a molecule to what is called the skeletal formula. In this form, neither carbon atoms or their valence hydrogen atoms are shown in order to simplify the diagram. Only functional groups are shown on the skeleton of the molecule; the carbon and hydrogen atoms are implied at the vertices of the skeleton such that there are always four bonds associated with each vertex. Figure 2.2 shows the D-glucose molecule in Figure 2.1 in the form of its skeletal formula. Additional stereochemistry information can be shown by use of wedges to represent bonds out of the plane of the page, dashed lines to represent bonds into the plane of the page and plain lines to represent bonds in the plane of the page.

Cellulose is a linear, unbranched polysaccharide of D-glucose monomers in $\beta(1,4)$ linkage (Fig. 2.3), ranging in length from 200-10000 units (O'Sullivan 1997) with molecular weights 250,000–1,000,000 or more (Morrison and Boyd 1983, p. 1113). Here, the

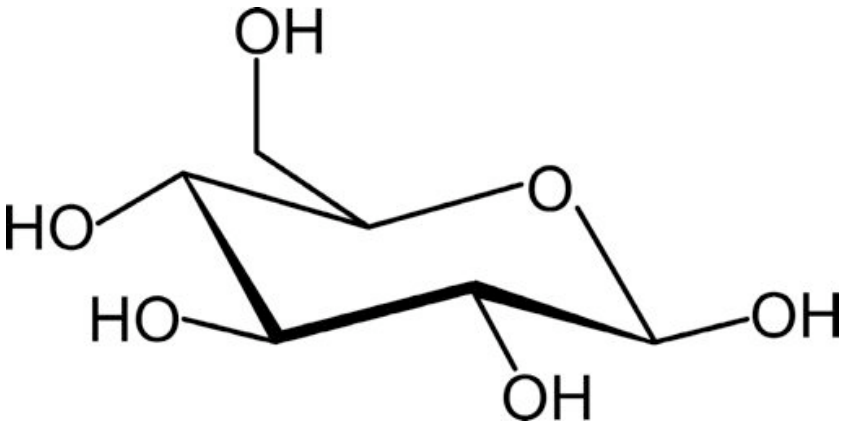

Figure 2.2: Skeletal formula of D-glucose, where only functional groups are shown on the hydrocarbon skeleton. Carbon and hydrogen atoms are implicit at each vertex such that four bonds are represented at each vertex. Wedges indicate bonds coming out of the plane of the page.

D- prefix refers to one of two configurations, around the chiral centre of carbon-5 (C-5), of which only the D- variant (also known as dextrose) is biologically active. The $\beta(1,4)$ refers to the configuration of the covalent link between adjacent glucose units, called a glycosidic bond. There are two possible geometries around C-1 of the pyranose (or 5-membered) ring: in the β anomer the hydroxyl group on C-1 sits on the opposite side of the ring to that on C-2; in the α anomer it is on the same side. The glycosidic bond in cellulose is between C-1 of one β-D-glucose residue and the hydroxyl group on C-4 of the next unit (see Figure 2.3). The bond is formed through the process of condensation or dehydration between two glucosan units (i.e. a water molecule is produced in the joining of two D-glucose residues in this manner).

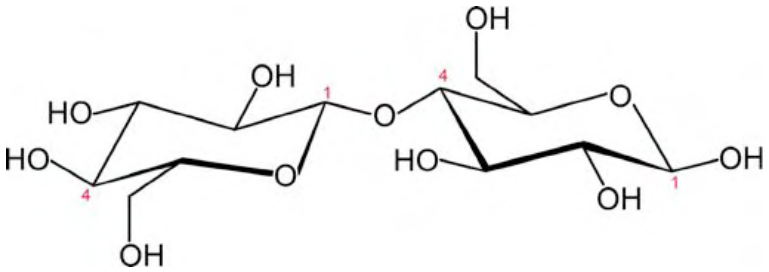

Figure 2.3: Skeletal formula of short 2-unit (i.e. disaccharide) cellulose (known as cellobiose) chain in β(1-4) bond in which two D-glucose monomers are joined through dehydration of the hydroxyl groups at C-1 and C-4 respectively, forming a glycosidic bond.

Unlike starch, a similar polysaccharide used by plants to store excess glucose (which utilises an α(1-4) bond), the natural cellulose polymer is a straight chain with no coiling and adopts an extended rod-like morphology that can take on two polymorphs (O'Sullivan 1997). Parallel chains of cellulose can form hydrogen bonds—a non-covalent linkage—in which surplus electron density on hydroxyl group oxygens is distributed to hydrogens with partial positive charge on hydroxyl groups of adjacent residues (Fig. 2.4). Multiple parallel chains thus bonded form a crystalline structure with two possible alignments, depending on the arrangement of the C-6 hydroxyl group, forming cellulose

Iα and cellulose Iβ[1] (Baker *et al*. 2000). This crystalline structure is very rigid and forms the basis of the microfibrils of plant cells, where bundles of up to 1000 cellulose chains are bonded in parallel, and contribute to its high tensile strength (Jane 1956). Segments of naturally occurring cellulose can exhibit regions of both crystalline structure with ordered alignment of both inter- and intra-molecular bonds and amorphous structure in which the bonding is disordered (Broido *et al*. 1973) but not entirely random (O'Sullivan 1997). The difference in the structures was shown by Zhbankov *et al*. (2002) to be a consequence of differing angles of rotation of functional groups around C-5 and C-6.

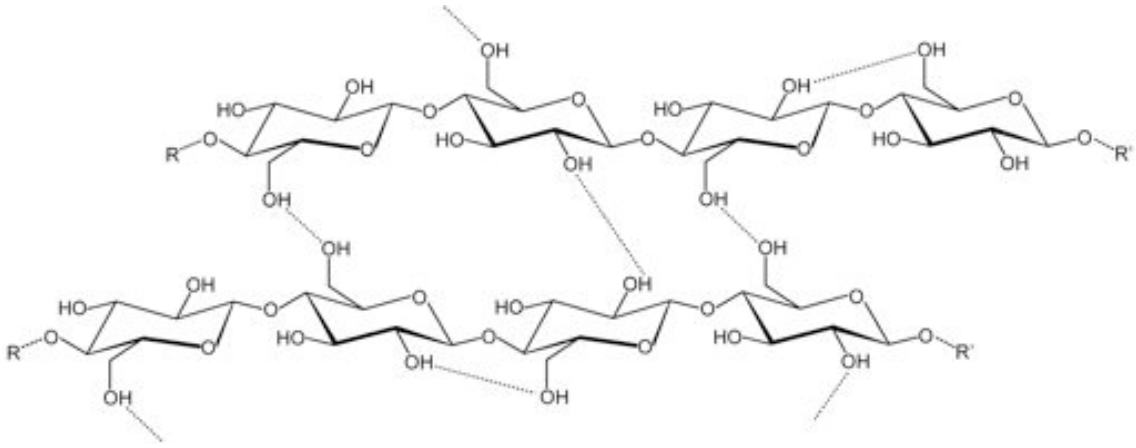

Figure 2.4: Schematic of chemical structure of a portion of neighbouring cellulose chains, indicating some of the intra- and inter-molecular hydrogen bonds (dashed lines) that may stabilise the crystalline form of cellulose. R and R′ indicate continuation of the cellulose chain.

As a result of this structure, cellulose is an extraordinarily stable polysaccharide: it is insoluble in water, relatively resistant to acid and base hydrolysis, and inaccessible to all hydrolytic enzymes except those from a few biological sources. This means that cellulosic fuels take a long time to biologically degrade (i.e. decompose) and require considerable energy to thermally degrade. In contrast to starch, which has a crystalline-to-amorphous transition (i.e. breakdown of interchain hydrogen bonds) at 60–70°C in water, it takes 320°C and 25 MPa for cellulose to become amorphous in water (Deguchi *et al*. 2006).

Other major chemical components of bushfire fuel include hemicelluloses (copolymers of glucosan and a variety of other possible, mainly sugar, monomers) and lignin (an aromatic polymer consisting of phenylpropane monomers) in varying amounts, depending upon the species, cell type and plant part (See Table 2.2). Minerals, water, salts and other extractives (such as terpenes—isoprene polymers—and resins—fats, fatty acids and fatty alcohols) and inorganics also exist in these fuels. The cellulose is the same in all types of biomass, differing only in the degree of polymerisation (i.e. the number of monomer units per polymer) (O'Sullivan 1997).

Cellulose is the most widely studied substance in the field of wood and biomass combustion. By comparison, few studies have been carried out on the combustion of hemicelluloses or lignin in isolation (Di Blasi 1998), due perhaps to the relative thermal instability of these compounds. Generally, studies are conducted on compounds (e.g.

[1]Man-made celluloses are known as cellulose II and III.

Table 2.2: Approximate analysis of some biomass species (Shafizadeh 1982; Mok *et al*. 1992).

Species	Cellulose (%)	Hemicelluloses (%)	Lignin (%)	Other[a] (%)
Shafizadeh (1982)				
softwood	41.0	24.0	27.8	7.2
hardwood	39.0	35.0	19.5	6.5
wheat straw	39.9	28.2	16.7	15.2
rice straw	30.2	24.5	11.9	33.4
bagasse	38.1	38.5	20.2	3.2
Mok et al. *(1992)*				
Eucalyptus saligna	45	15	25	15
Eucalyptus gummifera	38	16	37	9
sweet sorghum	36	18	16	30
sugar cane bagasse	36	17	17	30
Populus deltoides	39	21	26	14

[a] *Other* can consist of organic compounds such as starch or inorganic material such as salts, minerals, water and extractives.

lignocellulose (Orfao *et al*. 1999)). The degradation of biomass is generally considered as the sum of the contribution of its main components (Güllü and Demirbaş 2001), although extrapolation of the thermal behaviour of the main biomass components to describe the kinetics of complex fuels is only a rough approximation (Di Blasi 1998). The presence of inorganic matter in the biomass structure can act as a catalyst or an inhibitor for the degradation of cellulose; differences in the purity and physical properties of cellulose and hemicelluloses and lignin also play an important role in the degradation process (Di Blasi 1998).

2.2.2 Combustion reactions

Combustion processes

The term 'combustion' is generally used to describe a self-sustaining, high-temperature oxidation reaction (Babrauskas 2003, p. 14), however it is equally applicable to the description of the complete reaction process from unburnt fuel to spent ash and residue (Luke and McArthur 1978). The mechanism involved in these processes is complicated and is not yet fully understood but is thought to be a free radical chain reaction that is extremely exothermic yet requires a very high temperature for its initiation (Morrison and Boyd 1983, p. 115).

Byram (1959a, p. 64) identified three stages of combustion: 1) preignition, in which fuels are heated, dried and partially distilled; 2) ignition and combustion of distilled gases; 3) combustion of residual charcoal. As we will see, this is not nearly an accurate description of what happens in a bushfire but does serve as a suitable platform from which to begin.

The key aspect of biomass combustion in the context of bushfire is that it is not strictly a linear sequence of events as portrayed by Byram and other authors in the field of bushfire behaviour (e.g. Gisborne (1947); Vines (1981); Pyne *et al*. (1996)). While there are several stages identifiable in the process of bushfire spread, they are not necessarily sequential, as assumed in many models of combustion (e.g. Albini (1985); de Mestre *et al*. (1989)), and can occur simultaneously in many instances, a function of the individual rates of the chemical reactions. Rather than identifying combustion phases by the sequence in which they might occur, it is simpler to identify the processes involved.

The most basic process is heating of the fuel, usually by heat transfer (i.e. radiation, convection and conduction) from adjacent, already burning fuel (but at least initially from a pilot source such as a flame or spark). The fuel undergoes *drying*, in which free and bound water in and on the fuel evaporate. *Thermal degradation*, is the primary chemical reaction in combustion in which the fuel undergoes a fundamental change in its structure through a series of reactions including dehydration (the formal chemical reaction rather than the commonly misconceived notion of simply drying out) and depolymerisation, producing combustible gas (volatiles) and solid phase products (charcoal).

Secondary reactions of these gas and solid phase products, primarily oxidation in air, can then occur. *Gas phase oxidation* results in what we see as flaming combustion. *Solid phase oxidation* results in what is seen as glowing or smouldering combustion. While both forms of oxidation can and do occur simultaneously to varying degrees, the reaction rate of the former is much faster than the latter, resulting in the apparent delay of the charcoal oxidation after the fire front has passed. All reactions can occur simultaneously and some reactions occur at the expense of others. The dynamic nature of these reactions can result in very complex global behaviours.

Reaction rates

Chemical reactions occur when reactant molecules are brought together in the correct orientation with sufficient kinetic energy to break or form bonds between or within the reactants (Morrison and Boyd 1983, p. 55). The minimum energy required for a reaction to occur is called the activation energy, E_a. The rate at which a reaction occurs proportional to the concentration of the reactant and may be expressed quantitatively as (Moore 1963, p. 254):

$$-\frac{dc}{dt} = k[c], \tag{2.1}$$

where c is the reactant concentration, t is time and k is the reaction rate constant. According to Eyring theory, k is related to the total number of collisions that occur per second, the fraction of collisions that occur per second at or above E_a (i.e. effective collisions) and the fraction of effective collisions that occur in a favourable orientation. Thus the reaction rate constant comprises three factors:

$$k \propto \text{collision factor} \times \text{energy factor} \times \text{orientation factor}. \tag{2.2}$$

The theoretical expression for k has the same form as that observed empirically for many reactions and is known as the Arrhenius Law (Moore 1963, p. 273):

$$k = A \exp^{(-E_a/RT)}, \tag{2.3}$$

where A is a pre-exponential factor that subsumes the collision and orientation factors, R is the universal gas constant (8.314472 J K^{-1} mol^{-1}) and T is the absolute temperature of the reactants. The energy factor, $\exp(-E_a/RT)$ (derived from the Boltzmann velocity distribution of the molecules), reveals the critical role of temperature in the rate constant through the exponential dependence—a small increase in temperature results in a large increase in the rate constant. The pre-exponential factor, A is also dependent on temperature, but this dependence is proportional to $\sqrt{T}$ and is so much weaker than the exponential dependence of the energy factor that A is usually considered to be a constant.

Reaction enthalpy ΔH_R is the change in enthalpy when a reactant forms product following a reaction: $\Delta H_R = \Delta H_f(products) - \Delta H_f(reactants)$, where ΔH_f is the standard state heat of formation of reactant or product. When ΔH_R is positive, the process absorbs heat and is said to be endothermic. When ΔH_R is negative, the process releases heat and is said to be exothermic.

The role of negative reaction enthalpy and the temperature sensitivity of the rate constant in ignition is discussed in the next section.

Reaction rate temperature sensitivity

The study of the transport and transfer of energy in a system is called thermokinetics (Le Goff 1999) and reveals a great deal about the temperature dependence of chemical reactions. The exponential dependence of the Arrhenius reaction rate constant on temperature is critical to the onset of ignition or thermal runaway in an exothermic system of reactions. In such a system, the rate of heating is exponential with temperature. The rate of heat losses is linear (or a relatively weak power law) in the temperature. The enthalpy balance of a single reactant undergoing first order conversion can be given (e.g. Ball *et al*. (1999a) as:

$$V\bar{C}\frac{dT}{dt} = -\Delta H V c A \exp\left(-E_a/RT\right) - L(T - T_a), \tag{2.4}$$

where V is volume (m^{-3}), $\bar{C}$ is the weighted volumetric specific heat (J $m^{-3}K^{-1}$), T is the system temperature (K), ΔH is the reaction enthalpy, c is the concentration of the reactant, L is the linear heat loss coefficient (J s^{-1} K^{-1}) and T_a is the temperature of the surroundings. This equation is the simplest model for a combustion process and was first analysed by Semenoff (1928).

If the enthalpy balance is expressed in terms of dimensionless quantities, where $x = c/c_0$ (c_0 is the concentration of reactant at time $t = 0$), $\theta = RT/E_a$, $\tau = tA$, $l = LE_a/(-\Delta H R V c_0 A)$, and $C = (\bar{C}E_a/Rc_0\Delta H)$, we have:

$$C\frac{d\theta}{d\tau} = x\exp\left(-1/\theta\right) - l(\theta - \theta_a), \tag{2.5}$$

where the first term on the right represents the heat production rate while the second term represents the heat loss rate. If a heuristic assumption of an infinite supply of reactant (i.e. $x = 1$) is made, the exponential rate has no free parameters.

Figure 2.5 plots the two terms against θ for 3 values of l and $\theta_a = 0.1$ and shows graphically the effect of thermokinetics. With $l = 0.3$ (Fig. 2.5a), three intersections or steady states occur where the production of heat is equal to the linear loss of heat. At P1, there is little to no reactant conversion. As θ increases, the heat loss rate continues to increase but the heat production begins to increase rapidly. At P2, the heat production rate exceeds the heat loss rate and thermal runaway or ignition is inevitable. The third intersection point (P3) is the point at which thermal quenching of the reaction occurs when the rate of increase of the heat production begins to decrease and is exceeded by the heat loss rate (but this point can't be reached unless the system temperature has already passed the point of no return and ignited). In reality, the system would generally have consumed all the fuel before this occurs (i.e. the heat production rate would reach a maximum and then decrease as the fuel is depleted).

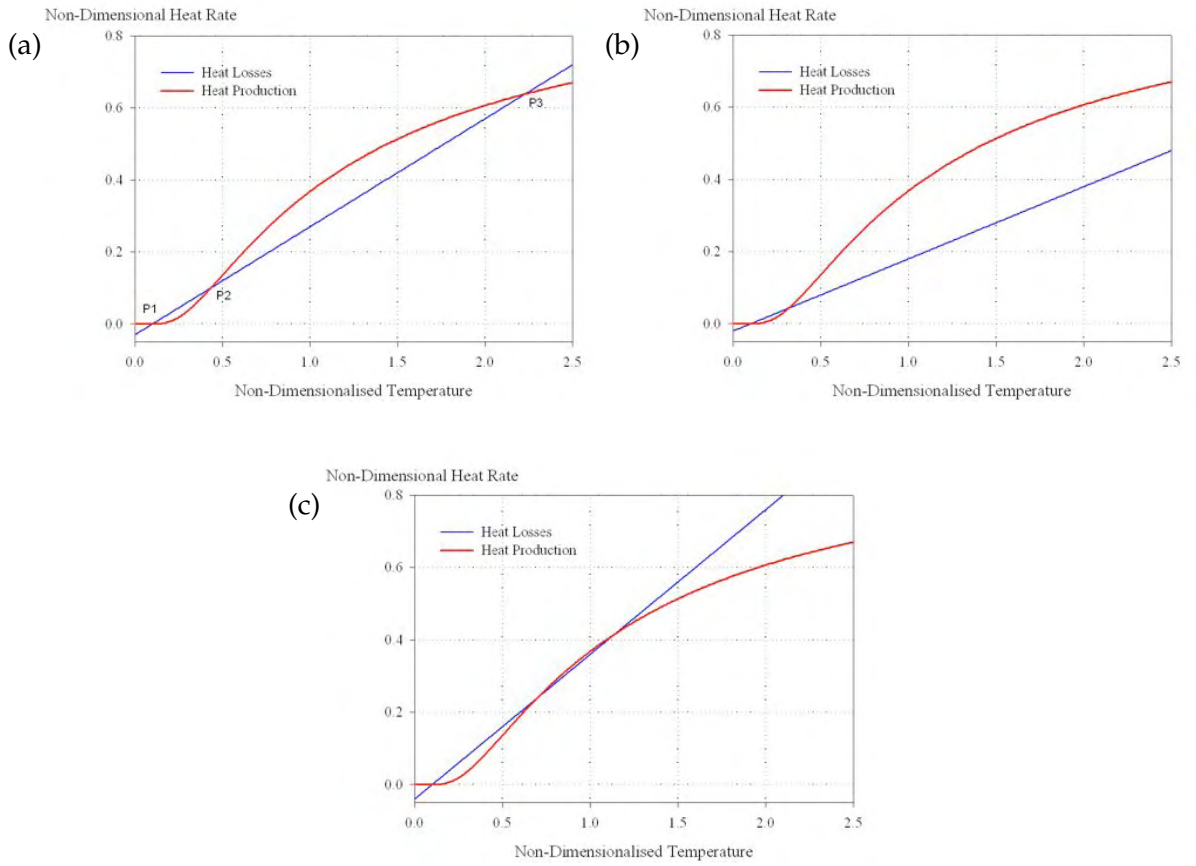

Figure 2.5: Non-dimensional heat loss rate and heat production rate plotted against non-dimensional temperature (θ) showing the exponential temperature dependence of the heat reaction release rate (red line) and typically linear heat loss rate (blue line). (a) With loss coefficient, $l = 0.3$, three intersections (marked P1, P2 and P3) occur, indicating where the heat loss rate equals the heat production rate. Between P2 and P3, the heat generation rate exceeds that of heat loss and ignition is inevitable. (b) With a lower loss coefficient of$l = 0.2$, the onset of thermal runaway occurs at a lower temperature and over the range here does not cease. (c) With a higher loss coefficient of $l = 0.4$, ignition is marginal.

At a lower heat loss coefficient, $l = 0.2$, (Fig. 2.5b), the onset of thermal runaway occurs at a lower temperature and will not be subject to thermal quenching until much higher temperatures. As the heat loss rate becomes even less efficient, a point of tangency is reached below which there is no possibility of cooling the reaction. At a higher heat loss coefficient, $l = 0.4$, (Fig. 2.5c), the onset of thermal runaway and ignition is only marginal, and under even higher loss coefficients will not occur at all.

A commonly-held misconception in bushfire literature is that of a specific fuel-related 'ignition temperature'. This assumption is not strictly true but can be explained using a dynamical systems understanding (Nelson 1997). The assumption relies on the combustion reactions having a high activation energy and therefore being so temperature sensitive that the reaction occurs dramatically over a very small temperature range after a long incubation period during which the fuel undergoes heating with relatively little change. This temperature sensitivity of high activation energy is illustrated in the numerical experiments that are described in Chapter 4.

2.2.3 Thermal degradation

Thermal degradation (also known as thermal decomposition, thermolysis or thermal scission) is the process by which a compound breaks into two or more component molecules (scission) when heated. It is an endothermic reaction as energy is required to break the chemical bonds of the original molecule. In the absence of oxygen, this degradation is called *pyrolysis* (in the literature (e.g. Babrauskas (2003, p. 18)) the term pyrolysis is often used incorrectly to describe any form of thermal degradation). Scission by the action of water is known as hydrolysis (i.e. cleavage by water).

Under the application of heat, cellulose will undergo random cleavage at a glycosidic bond joining two D-glucose units somewhere along the polymer chain (Fig. 2.6). More often than not, this will occur in a region of amorphous cellulose. The result is two cleaved ends of the cellulose chain, one positively charged and one negatively charged. The positive fragment forms a resonance-stabilised carbocation; electron density on the hemi-acetal oxygen can be distributed to stabilise the positive carbon centre on C-1 (Ball *et al*. 1999a). The negative fragment will form a non-reducing end.

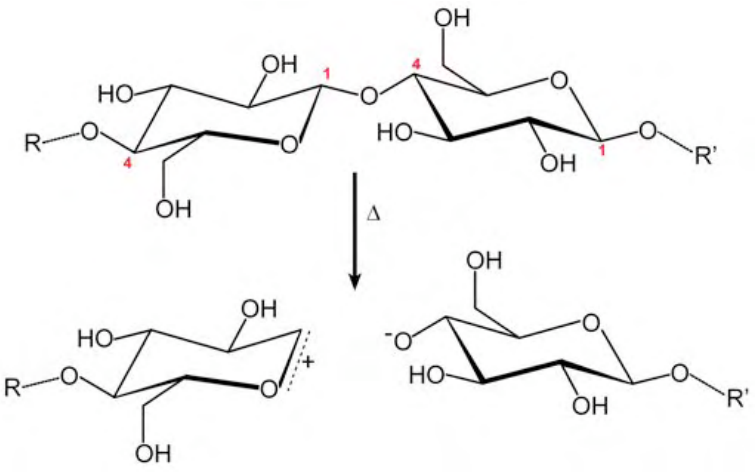

Figure 2.6: Skeletal formula showing the thermolysis of a cellulose chain at the glycosidic bond at C-4–C-1, resulting in a resonance-stabilised positive carbonium ion on the left and non-reducing negative ion on the right.

There are two possible outcomes from this step, depending on the conditions in which this reaction occurs. These are mutually exclusive and thus competitive. The first is intramolecular nucleophilic[2] attack of the resonance-stabilised positive centre on C-1 through donation of the electron density on the C-6 hydroxyl oxygen (Ball *et al*. 2004) (Fig. 2.7) in a process that leads to *volatilisation*. The second is rehydration via intermolecular nucleophilic action in the presence of moisture (Fig. 2.9, p. 29). Subsequent heating results in reactions that lead to the formation of charcoal in the process known as *charring*. The formation of the stabilised carbocation is critical to the competition by the nucleophiles. It can survive as an entity for long enough to allow capture of a water molecule.

[2]From the Greek, literally "nucleus loving"

Volatilisation

Intramolecular nucleophilic attack (formally known as 'nucleophilic addition') in which the oxygen from the hydroxyl group on C-6 forms a covalent bond with C-1 via cyclisation (i.e. formation of a ring), resulting in the formation of a levoglucosan end in the cellulose chain (Fig. 2.7). The hydrogen released from the hydroxyl group on C-6 is taken up by the other cleaved end of the cellulose chain where it binds to the oxygen on C-4, restoring the hydroxyl group there and resulting in a non-reducing (i.e. it is non-reactive) end of that half of the cellulose chain.

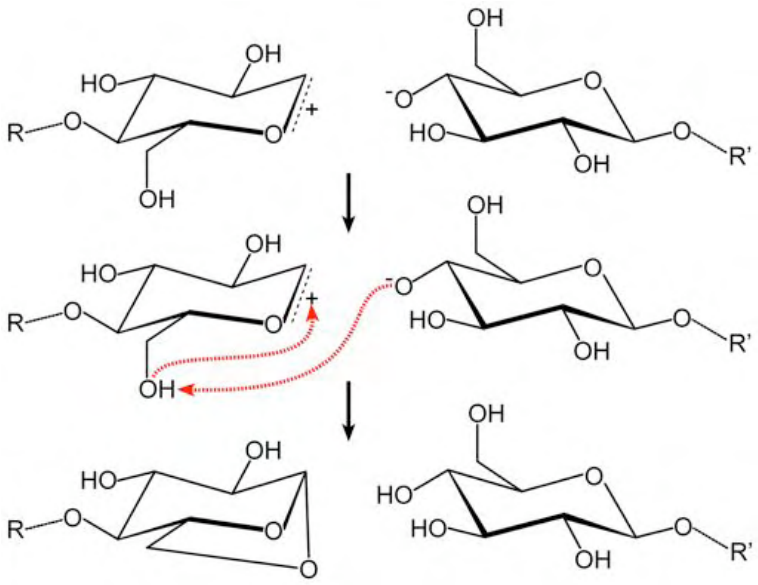

Figure 2.7: Skeletal formula showing the intra-molecular nucleophilic addition resulting in cyclisation between C-6 and C-1 through the hydroxyl group on C-6, resulting in a levoglucosan end on the cellulose chain. The other half of the cleaved chain forms a non-reducing end.

The levoglucosan end of the cellulose chain is stable to the reactions of decarbonylation and dehydration that lead to charring under additional heating. However, the levoglucosan end can undergo depolymerisation via direct intra-chain heterolytic scission of the glycosidic linkage in a process known as transglycosylation (Mamleev *et al*. 2007a,b) (Fig. 2.8), picking up the required hydrogen ion from a water molecule or from the hydroxyl group on C-6 of the next unit in the chain and forming the highly volatile species levoglucosan (1,6-anhydro-β-D-glucopyranose). Mamleev *et al*. (2007b) found that although transglycosylation can occur at any point along the levoglucosan-end chain, once the process starts at the end unit, it is more likely to proceed sequentially along the chain, leading to the common description of the polymer 'unzipping' (Williams 1982).

Levoglucosan is gaseous at the temperature of thermal degradation ($\simeq$ 400-600 K) but is a solid at ambient temperatures and is described as a 'tar' (Williams 1982). It is the source of a wide range of species following further thermal degradation that readily oxidise in secondary reactions, resulting in what is seen as flaming combustion. Wodley (1971) identified nearly 40 products from the thermal decomposition of levoglucosan—many of which were products of reactions between initial volatiles—including pentane, acetalaldehyde, furan, furfural. Wodley (1971) further noted that other workers identified 20 additional compounds including formaldehyde and formic acid.

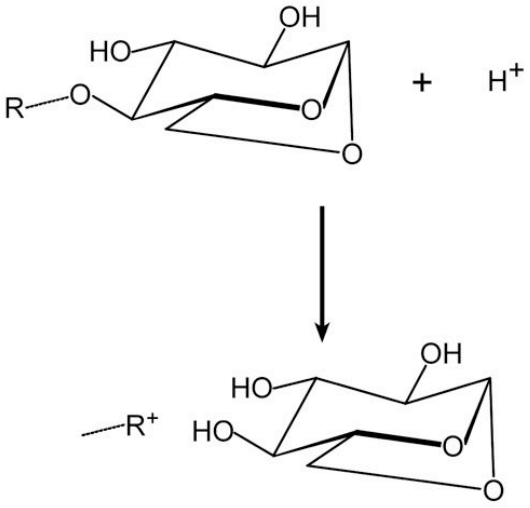

Figure 2.8: Depolymerisation of levoglucosan-end of cellulose chain through scission at the glycosidic bond results in the formation of free levoglucosan, the primary species of volatilisation.

The basic stoichiometric equation for the formation of levoglucosan is:

$$(C_6H_{10}O_5)_n \rightarrow (C_6H_{10}O_5)_{n-1} + C_6H_{10}O_5. \tag{2.6}$$

This reaction path has been found to be slightly endothermic (reaction enthalpy, ΔH, $\simeq$ 300 J g^{-1} (Antal and Várhegyi 1995; Ball *et al*. 1999a)) and to have a relatively high activation energy ($E_a \simeq$ 240 kJ mol^{-1} (Bradbury *et al*. 1979; Antal and Várhegyi 1995; Di Blasi 1998)).

Charring

In the presence of moisture, the intra-molecular nucleophilic addition from the hydroxyl group on C-6 seen in the formation of the levoglucosan end competes against a water molecule for the chance to bond with the positive centre at C-1 of the carbocation (Fig. 2.9, shown as a one-step reaction). In this case a hydroxyl group is formed at C-1, resulting in a very stable end that has 'lost' the opportunity to volatilise (i.e. cyclisation of the oxygen of the hydroxyl group on C-6 cannot occur). This product is known as hydrolysed cellulose. The released hydrogen ion from the water molecule bonds to the negative ion forming a non-reducing end that is relatively unreactive because it lacks the hemiacetal–carbonyl group of the reducing end. However, this nucleophilic addition is reversible—that is, the addition cation may eliminate, yielding the (relatively) stable thermolysis carbocation and giving a competing nucleophile another chance.

Further heating of the hydrolysed cellulose causes the elimination of water (dehydration), carbon monoxide (decarbonylation) and carbon dioxide (decarboxylation) resulting in cross-linking of the carbon skeleton of the structure and the formation of the unsaturated[3] anhydrous carbohydrate commonly known as charcoal (also activated cel-

[3] A saturated carbohydrate is one in which all covalent bonds are single bonds. A mono-unsaturated carbohydrate is one in which there exists one double or triple bond between carbon atoms. A poly-unsaturated carbohydrate is one in which there are many double or triple bonds between carbon atoms.

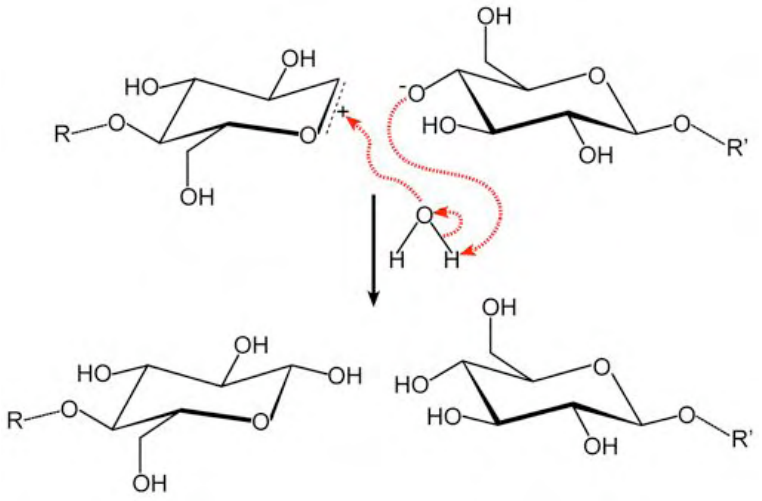

Figure 2.9: Skeletal formula showing the (reversible) inter-molecular nucleophilic addition by a water molecule on the positive carbonium ion as a one-step reaction, forming hydrolysed cellulose on the left and a non-reducing end on the right.

lulose, particularly early on in the process when there is relatively little desaturation and much of the original substrate remains).

The dehydration reaction generically occurs via Lewis acid catalysis (represented here for convenience as a hydrogen ion), resulting in the formation of a carbon-carbon double bond. The generic reaction is illustrated in Figure 2.10a. In practice, this might occur as illustrated in Figure 2.10b.

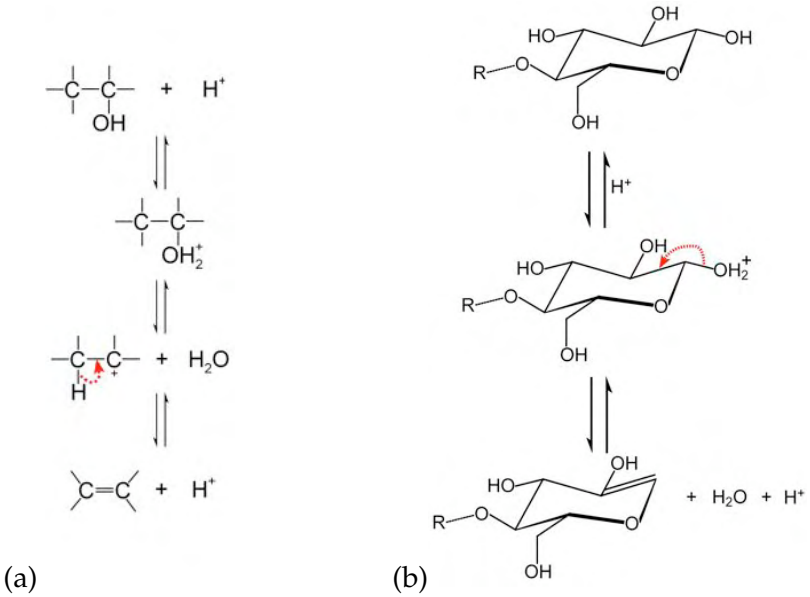

Figure 2.10: (a) Generic dehydration via Lewis acid catalysis (shown as a hydrogen ion), resulting in formation of a carbon-carbon double bond. (b) Possible dehydration of hydrolysed cellulose with Lewis acid catalysis resulting in desaturation of the carbon skeleton.

Acid catalysis can also open the hemiacetal ring of the hydrolysed cellulose end unit—a characterising step in charcoal forming reactions (Drysdale 1985)—forming an aldehyde group (Fig. 2.11a). This formation can then undergo dehydration (Fig. 2.11b).

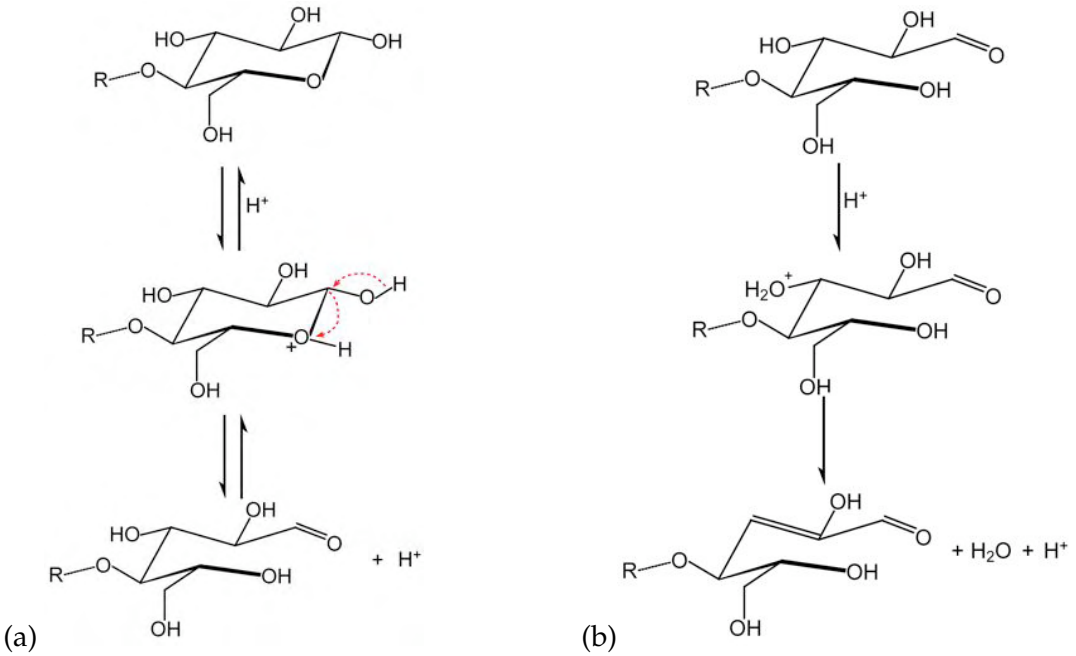

Figure 2.11: (a) Formation of aldehyde group by decyclisation of the hydrolysed cellulose end unit via Lewis acid catalysis resulting in the opening up of the hemiacetal ring. (b) Possible resultant dehydration of a hydroxyl group via Lewis acid catalysis forming a conjugate carbon-carbon double bond in the carbon skeleton.

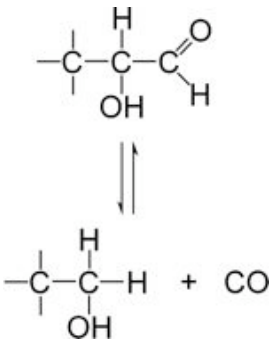

Figure 2.12: Under thermal stress, an aldehyde group will undergo decarbonylation, eliminating a carbon monoxide molecule.

An aldehyde group under thermal stress will undergo decarbonylation. A generic representation of this reaction is shown in Figure 2.12. It should be noted that aldehydes are easily oxidised to carboxylic acids (-COOH), suggesting that oxidation may play a minor role in charring.

Cross-linking of adjacent activated cellulose chains may occur through dimerisation via acid catalysis with water. Figure 2.13 shows a generic interchain dimerisation of carbon-carbon double bond groups.

The charcoal[4] formed from these charring and cross-linking reactions is not a particular species but a range of anhydrous species of indeterminate molecular weight, from mono-unsaturated species that have eliminated only one water molecule, carbon dioxide

[4]It is common in the literature to see this substance referred to as char but since the word 'char' is a verb (Concise Oxford English Dictionary (5th Ed.)), the noun 'charcoal' is preferred in this thesis to describe the product of the process of charring of biomass fuel.

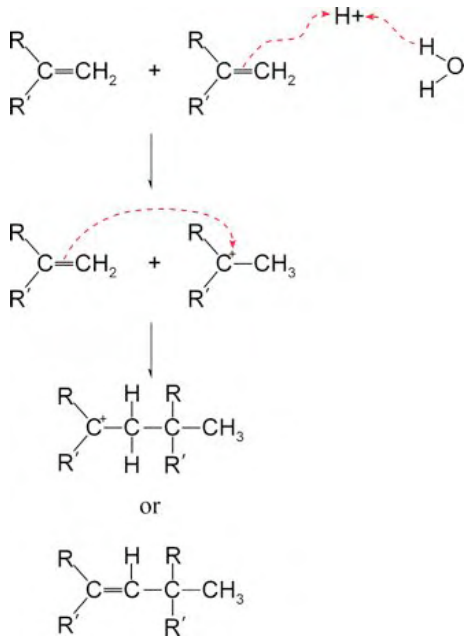

Figure 2.13: A generic representation of interchain dimerisation of adjacent carbon-carbon double bond groups. This reaction may cause cross-linking of adjacent activated cellulose chains.

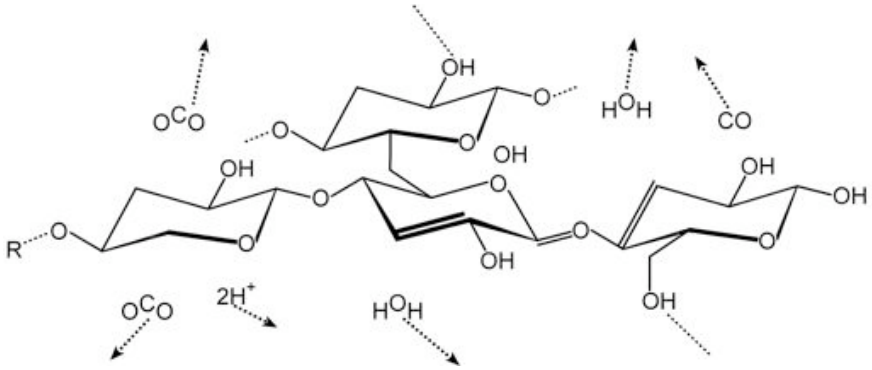

Figure 2.14: Skeletal formula showing the possible results of charring reactions that lead to cross-linking between chains, desaturation of hydrolysed cellulose and the formation of charcoal species: dehydration (loss of H_2O), decarbonylation (loss of CO) and decarboxylation (loss of CO_2). Conjugate double bonds between carbon atoms (i.e. alternating double and single bonds) occur as a result of the loss of functional groups and decrease the saturation of the compound.

or carbon monoxide, through polyunsaturated carbonaceous species where more than one functional group has been lost (Fig. 2.14), to pure carbon in which all functional units have been eliminated. Depending on the extent of saturation, the resultant can be known as activated charcoal.

For the purposes of illustration in this thesis, we consider a single charcoal species, $C_{11}H_4$, which is a suitably polyunsaturated hydrocarbon. However, due to the possible initial thermolytic cleavage of the cellulose chain at any point along a possibly very long polymer and subsequent functional group elimination through charring, the charcoal species could be quite large (i.e. molecular weight of 10000 or more).

The stoichiometric equation for the formation of our simple charcoal species is:

$$(C_6H_{10}O_5)_n \rightarrow (C_6H_{10}O_5)_{n-2} + C_{11}H_4 + CO_2 + 8H_2O. \quad (2.7)$$

While the initial glycosidic thermolysis is endothermic, the subsequent possible decarboxylation, decarbonylation and dehydration reactions result in a net exothermicity. This reaction path has a relatively low activation energy ($E_a \simeq$ 110-200 kJ mol^{-1}(Diebold 1994; Di Blasi 1993)) and a reaction enthalpy of $\Delta H \simeq$ -1–2 kJ g^{-1} (Milosavljevic *et al*. 1996; Ball *et al*. 1999a).

2.2.4 Oxidation reactions

The most apparent reaction involved in combustion is the oxidation of the thermal degradation products. It is these reactions in the gas phase (levoglucosan) and solid phase (charcoal) that exhibit much of the mass loss of the fuel and the morphology of 'fire'—that is the release of heat, light and the appearance of flame. Much of the study of combustion in bushfire research has concentrated on the transfer of heat from flames to unburnt fuel. Understanding the source of energy in the flames is critical in correctly determining the rate and magnitude of transfer of this energy.

Gas phase oxidation

Gas phase oxidation of the volatilised levoglucosan and its derivative products appears as flame and is highly complex and disordered due to both the chemistry involved and the susceptibility of the reactions to turbulence in the oxidant and fuel flows. Studies of emissions from combustion of bushfire fuel (such as Wodley (1971); Hurst *et al*. (1994); Greenberg *et al*. (2006)) show that the number of oxidation products is quite considerable and often the result of many intermediate reactions. The simplest stoichiometric reaction for levoglucosan oxidation is:

$$C_6H_{10}O_5 + 6O_2 \rightarrow 6CO_2 + 5H_2O. \quad (2.8)$$

However, this reaction assumes that intermediate reactions, consisting primarily of oxidation reactions of derivative products (produced through sequential thermal degradation), are complete (and also assumes that intermediate reactions can be expressed in terms of only initial and final products). But the number of pathways that such reactions can take is quite large, and not all paths will result in completion to carbon dioxide and water.

As an example of a gas-phase hydrocarbon oxidation reaction, Williams (1982) gives a non-exhaustive list of 14 possible pathways for the combustion of CH_4, one of the many possible intermediates of the thermal degradation of levoglucosan, to H_2O and CO_2. In this case, intermediate species included CH_3, H_2CO, HCO, CO, OH and H_2. Additionally, elemental carbon can form and be present as soot. This reaction is further complicated by reactions with nitrogen present in the atmosphere that can lead to the formation of a variety of nitrogen oxide (NO_X) species as well as toxins such as dioxins and polycyclic aromatic hydrocarbons (Reisen *et al*. 2006).

The resultant flames are turbulent diffusion flames with a relatively thin reaction zone between fuel and oxidant. As a result, the oxidation reactions are often mixing-limited (that is, the oxidation reaction does not occur because the fuel and oxidant cannot

be brought together in the correct stoichiometric ratio) and can result in large volumes of volatiles that separate from the reaction zone and subsequently burn out some height above the fire (Cheney and Sullivan 1997). At any stage in the reaction process, any pathway may stop (through loss of energy or reactants) and its products be advected away to take no further part in combustion. It is these partially combusted components that form the bulk of what appears as smoke. The more turbulent the reaction zone, the more likely that reaction components will be removed prior to complete combustion, hence the darker and thicker the smoke from a head fire, as opposed to the lighter, thinner smoke from less turbulent flames.

These oxidation reactions are highly exothermic and very fast. Oxidation of levoglucosan requires an activation energy, E_a, of approximately 190 kJ mol^{-1} at a reaction rate constant of about 2.55 $\times 10^{13}$ s^{-1} and has a reaction enthalpy, ΔH, of approximately -14 kJ g^{-1} (Parker and LeVan 1989)

Solid phase oxidation

Oxidation of the solid phase charcoal appears predominantly as glowing or smouldering combustion. It is generally a more straightforward reaction than that of the gas phase in that there is not the complicated intermediate pathways that can be interrupted by turbulence in the mixing of reactants. However, due to the range of possible species that are called charcoal, the range of possible reactions is similarly large. Activation energies for these species vary, with higher carbon concentration species having much higher activation energies for oxidation than their more saturated cousins. Pure carbon requires temperatures in the order of 1000 K to oxidise, whereas more saturated species require in the order of 700 K (Harris 1999).

The basic stoichiometric reaction for the solid phase oxidation of our charcoal species is:

$$C_{11}H_4 + 12O_2 \rightarrow 11CO_2 + 2H_2O. \tag{2.9}$$

This reaction, too, can lead to a range of intermediate species that can remain if the reaction stops for any reason, such as if reactants are cooled below the reaction's activation energy. It is also possible for oxygen in the air to be excluded from the reaction surface of the solid by the presence of reaction products such as ash as they build up and form an insulating layer, resulting in cessation of the reaction. Generally, however, solid phase reactions will continue to completion. When it does, there is a characteristic fine white ash residue composed mainly of minerals, salts and other inorganic components of the fuel that do not combust.

The solid phase oxidation reaction is highly exothermic ($\Delta H \simeq$ -32 kJ g^{-1}), over twice that of the volatile gas phase oxidation, but has a lower activation energy ($E_a \simeq$ 180 kJ mol^{-1}) and occurs at a much slower rate ($A \simeq 1.4 \times 10^{11}$ s^{-1}) (Eghlimi *et al*. 1999; Branca and di Blasi 2004). Due to the slow reaction rate, much of the charcoal oxidation occurs after the passage of the fire front, perhaps leading to the impression that glowing combustion occurs after flaming combustion. Much of the significant heat released is localised in the fuel bed, which is the reason why charcoal combustion has found such a niche in industrial and domestic use.

In addition to being a source of energy through its oxidation, the formation of charcoal may act to insulate the fuel bed, acting as a thermal barrier between the heat gen-

erated through the gas or solid phase oxidation and the unburnt fuel (Watt *et al*. 2001). Partially combusted solid-phase products and combustion residue such as mineral ash can also act to reduce the heating of unburnt fuel such that in some circumstances it may remain unburnt (Cheney and Sullivan 1997).

2.2.5 Discussion

The desaturation of the anhydrous cellulose to charcoal species is visually apparent by a shrinkage in the substrate and a change in its colour. The colour change is similar to that of the browning of cooking food, a result of the glycosidic reaction between reducing sugars and free amino groups in proteins (van Boekel 2001) and first described by Maillard in 1912. Saturated hydrocarbon compounds absorb light only in the ultraviolet (Barrow 1973, p. 330) and so appear white in the visible spectrum. As the number of carbon-carbon double bonds in the compound increases through dehydration, decarbonylation or decarboxylation, the electronic absorption spectrum broadens and shifts toward the infra-red into the visible (Coblentz 1905; Swanson 1948). This results in the absorption of more visible spectrum light and a darkening of the substrate. This can proceed until only carbon black remains.

This discoloration process is also evidenced in the yellowing and weakening of acidic paper through acid hydrolysis (Zou *et al*. 1994), which is essentially the same process as charring only much slower, and also in the difference in colour between saturated, mono- and poly-unsaturated fats (white to dark yellow respectively).

The key morphological difference between the two competing thermal degradation pathways is that fuel that has undergone the charring process retains the shape of the original substrate (Williams 1982)—i.e, one can still discern the form of the virgin fuel in the charcoal. The cross-linking reactions that occur during charring act to retain the original shape of the fuel. Fuel that has undergone volatilisation does not retain any of the original fuel's structure and becomes amorphous.

The main source of heat into the combustion process comes from the rapid exothermic oxidation of the gas phase levoglucosan and other decomposition products. These species are buoyant and are generally convected away from the solid fuel. As a result the transport of the heat generated from these reactions is extremely complex and brings us to the physics of heat transfer.

2.3 Physics of combustion and heat transfer

The physics involved in the combustion of bushfire fuel and the behaviour of bushfires is, like the chemistry, complicated and highly dependent on the conditions in which a fire is burning. The primary physical process in a bushfire is that of heat transfer. Williams (1982) gives nine possible mechanisms for the transfer of heat from a fire:

1. Diffusion of radicals
2. Heat conduction through a gas
3. Heat conduction through condensed materials
4. Convection through a gas
5. Liquid convection
6. Fuel deformation

7. Radiation from flames
8. Radiation from burning fuel surfaces
9. Firebrand transport.

Mechanisms 1, 2 and 3 could be classed as diffusion at the molecular level. Mechanisms 4 and 5 are convection (although the presence of liquid phase fuel in biomass combustion is extremely rare and short-lived (Boutin *et al*. 1998)). Mechanisms 7 and 8 are radiation. Mechanisms 6 and 9 could be classed as solid fuel transport. This roughly translates to the three generally accepted forms of heat transfer (conduction, convection and radiation) plus solid fuel transport, which, as Emmons (1966) points out, is not trivial or unimportant in bushfires. The effect of conduction is rather limited in bushfire fuel where fuel elements are discrete and heterogeneous in regard to continuity and distribution (even in the most homogeneous fuels, such as grasslands, the fuel elements are not contiguous). Convection may be generalised to advection to include any transfer of heat through the motion of gases (i.e. both forced and free convection).

Thus the primary physical processes driving the transfer of heat in a bushfire are advection and radiation. In still or low wind conditions, the dominating process is that of radiation (Weber 1989). In conditions where wind is not insignificant, it is advection that dominates (Grishin *et al*. 1984). However, it is not reasonable to assume one works to the exclusion of the other and thus both mechanisms must be considered. The following sections detail the governing equations that are employed to model these physical processes.

2.3.1 Advection

Advection is the general motion of fluid and is studied predominantly using fluid dynamics. Fluid dynamics is a large and active area of research and only the basic outlines of the principles are given here. A considerable number of texts on the general application of fluid dynamics (e.g. Batchelor (1967); Turner (1973)) and combustion theory (e.g. Williams (1985)) provide a more in-depth discussion.

A fundamental aspect of fluid dynamics and its application to the understanding of the motion of gases is the concept of continuity. The molecules of a gas are considered to be *continuous* and thus to behave as a fluid rather than a collection of independent particles. In conjunction with other key foundations of physics in general such as thermodynamics and the conservation of quantities, a set of governing equations to describe the motion of fluids can be constructed. The fluidised *equations of motion* form the basis of all fluid dynamics modelling.

General governing equations

A description of the rate of change of the density of particles in relation to the velocity of the particles and distribution of mass of particles provides a method of describing the continuity of the particles (Elliot 1993). By taking velocity moments of the density distribution (i.e. multiplying by powers of the velocity and integrating with respect to the velocity ($\int \mathbf{u}^k d\mathbf{u}$, where k is the moment index: 0, 1, 2...), the fluidised equations of motion are obtained which can be used to describe the continuity, conservation of mass, momentum and energy, etc. (Elliot 1993).

When *k*=0, the integration of density distribution results in the equation of continuity. If the particles are considered to have mass, then the continuity equation also describes the conservation of mass (Batchelor (1967, p. 74); Williams (1985, p. 625)):

$$\frac{\partial \rho}{\partial t} + \nabla.(\rho \mathbf{u}) = 0, \tag{2.10}$$

where ρ is density, t is time, and $\mathbf{u}$ is the fluid velocity (with vector components u, v, and w) and $\nabla.$ is the Laplacian or gradient operator (i.e. in three dimensions $\mathbf{i}\frac{\partial}{\partial x} + \mathbf{j}\frac{\partial}{\partial y} + \mathbf{k}\frac{\partial}{\partial z}$). This is called the *fluidised* form of the continuity equation and is presented as a partial differential equation. Concisely, it says that the rate of accumulation of mass in a volume element is the same as the rate at which mass flows out of the volume element.

However, in order to solve this equation, the evolution of $\mathbf{u}$ (i.e. $\frac{\partial u}{\partial t}$) is needed. This incompleteness is known as the closure problem and is a characteristic of all the fluid equations of motion. The next order velocity moment (k = 1) can be taken and the evolution of the velocity field determined. This results in an equation for the force balance of the fluid or the *conservation of momentum* equation (Batchelor (1967, p. 136); Williams (1985, p. 625)):

$$\frac{\partial \rho \mathbf{u}}{\partial t} + \nabla.(\rho \mathbf{u})\mathbf{u} + \nabla p = 0, \tag{2.11}$$

where p is pressure. This equation balances the rate of increase of momentum with the inertial, pressure and viscous forces, and is, at its most basic, the application of Newton's Second Law ($F = ma$) to small volumes of fluid; it is more formally known as the Navier-Stokes equation (here presented in its simplified inviscid form for illustration). However, the evolution of p is then needed to solve this equation. This can be determined by taking the second velocity moment (k=2) which provides an equation for the conservation of energy in the same manner as the First Law of Thermodynamics (Williams (1985, p. 626)):

$$\rho \frac{\partial E}{\partial t} + \nabla p - k\nabla T - \phi = \text{constant}, \tag{2.12}$$

where E is energy, k is the Boltzmann constant (coefficient of heat conduction), T is absolute temperature and ϕ is the energy dissipation function (which takes into account irreversible production of heat through dissipation of mechanical energy). This equation describes the fact that the sum of the thermal, chemical and kinetic energy in the system is equal to the sum of the energy lost from, and the work done by, the system.

This equation, too, needs a further, equally incomplete, equation to provide a solution for the evolution of energy. One can either continue determining higher order moments *ad nauseum* in order to provide a suitably approximate solution (as the series of equations can never be truly closed but will asymptote to an exact answer) or, as is more frequently done, utilise an equation of state to provide the closure mechanism. In fluid dynamics, the equation of state is generally that of the ideal gas law (i.e. $pV = nRT$).

The above equations are in the form of the Euler equations for illustrative purposes. In the case of bushfire, where chemical reactions provide additional sources and sinks of mass, momentum and energy, the right hand side of the fluidised equations of motion may be non-zero and will depend on additional models of gas phase and solid phase species formation and consumption as well as chemical and enthalpy source closure (Cox 1998). Similar non-fluidised equations for the conservation of mass and energy for the solid phase can be constructed (assuming that solid phase fuel does not move and thus

not have momentum (Porterie *et al*. 2000)). A typical conservation equation for a species places the accumulation rate of a given species in a given volume equal to the sum of convection of the species out of the volume, diffusion of the species into the volume and production of the species via chemical reaction.

Due to the complexity of the governing equations, they often cannot be solved analytically and must be solved numerically. A branch of fluid dynamics called computational fluid dynamics (CFD) has arisen that utilises computers to numerically solve the equations of motion. Many methods exist to numerically solve the set of equations of motion (Shampine 1980) and much effort is exerted in developing faster and more efficient numerical solver methods (Ferziger and Perić 1996). The method of choice depends on many factors, including the form of the equations (e.g. Lagrangian, Eulerian), the spatial dimension of the equations (i.e. 1D, 2D or 3D), the method of discretisation of the equations (finite difference, finite element/volume), the spatial and temporal resolutions used, the treatment of boundary conditions, the computational capability, and the co-ordinate system involved.

Due to the considerable computational resources required to solve them precisely at the necessary scales (for example, using the method of direct numerical simulation (DNS) (Ferziger and Perić 1996, p. 249)), trade-offs are made in order to improve the speed of computation at the cost of precision. Buoyancy and turbulence are two aspects of fluid flow that that are particularly difficult to solve exactly via DNS and are instead modelled via separate mechanisms to improve computational feasibility.

Buoyancy, convection and turbulence

The action of heat release from the chemical reactions within a combustion zone results in heated gases, both in the form of combustion products as well ambient air heated by, or entrained into, the combustion products. The reduction in density caused by the heating of the gas increases the buoyancy of the gas and results in the gas rising as a plume via convection. The interaction of the rising gas with an air flow can then lead to turbulence in the flow (Turner 1973).

Because modelling of a bushfire necessarily requires modelling of atmospheric processes, the regime of the flow is of high-order Reynolds number (in the order of 60,000-90,000) which is well outside the bounds of laminar flow (Jiménez 2006). Thus turbulence is a key component of air flow in the open. Turbulence acts over the entire range of scales in the atmosphere, from the fine scale of flame to the scale of the atmospheric boundary layer. Non-linearity produces eddy motions of smaller and smaller scales until viscous dissipation causes the cascading of energy to smaller scales to stop (Richardson 1922; Kolmogorov 1941). Interaction of the flow with elements on the earth's surface, such as terrain, vegetation or structures, through the effect of drag and mechanical disturbances, can increase the rate at which energy is cascaded down the scales (Finnigan and Brunet 1995; Finnigan 2000).

Turbulence mixes heated gases from the fire with ambient air and acts to increase the entrainment of cooler air into the convection column. Turbulence also mixes the heated gases of the fire with unburnt solid phase fuels around the fire and to immerse the fuel in flame, resulting in greater transfer of heat and increased fuel ignition rates (Finney *et al*. 2006). This aspect of turbulent buoyant flow in and around the fuel is critical to the understanding of the behaviour of bushfires, particularly in complicated

fuel structures. Turbulence also affects the transport of solid phase fuel, such as that of firebrands, resulting in spotfires downwind of the main burning front (see Section 2.3.3). It can also act to increase the rate of solid phase combustion by improving gas-solid interface exchange and removing insulating ash.

The study and modelling of turbulence is a very active research field. Suitably formulated Navier-Stokes equations can be used to incorporate the effects of buoyancy and turbulence as separately modelled components (such as turbulent kinetic energy, energy dissipated via the energy cascade or Boussinesq's eddy viscosity for the modelling of turbulence or a renormalised perturbation variable for modelling the effects of buoyancy (McComb 2006)) in such a way that the small-scale turbulent fluctuations do not have to be directly simulated.

The methods for solving the Navier-Stokes equations represent a spectrum of approaches: from DNS, which explicitly computes everything up to and including the energy dissipation scales; Reynolds-averaged Navier-Stokes (RANS) simulations (Ferziger and Perić 1996, p. 265), in which the solution variables in the instantaneous (exact) Navier-Stokes equations are decomposed into the mean (ensemble-averaged or time-averaged) and fluctuating components; and large-eddy simulations (LES) (Mason 1994) which explicitly computes large scale eddies directly but treats the dissipation and inertial cascade at smaller scales using sub-grid-scale approximations. The formulation of equations used in RANS are are not closed due to use of unknown Reynolds stress terms and must be closed through estimated eddy viscosities (such as the $\kappa - \varepsilon$ method involving the evolution of fluctuating kinetic energy (κ) and eddy dissipation (ε) (Jiménez 2006)) or Reynolds stress evolution methods (known as the Reynolds stress transport model (RSM) (Launder *et al*. 1975)), in which the RANS equations are closed by equations for the Reynolds stresses.

All these methods provide a direct estimation of the kinetic energy associated with turbulent motion into the conservation of energy equation. The application of rigorous statistical methods from quantum field theory (i.e. renormalisation group theory (RNG) (Yakot and Orszag 1986; McComb 2004)) have led to improved formulations of some of these turbulence models (McComb 2006).

Atmospheric interactions

In addition to the exchange of heat released from the fire to the flow of the air immediately around the fire, the interaction of the transport of the gas phase products from the combustion processes with the wider-scale atmosphere flow also plays a significant role in determining the behaviour of the fire (Clark *et al*. 1996a). If only a subsection of the atmosphere in which the fire is present is modelled, suitable boundary conditions and the interactions across those boundaries are needed to adequately model the larger scale effects of the fire. For example, the condition of the atmosphere, particularly the lapse rate (the negative rate of change of air temperature with increasing height which dictates the ease with which heated parcels of air rise within the atmosphere), controls the impact the buoyancy of the heated air from the combustion zone will have on the atmosphere and the fire (Byram 1959b).

Changes in the ambient meteorological conditions, such as changes in wind speed and direction, moisture, temperature, lapse rate, etc, both at the surface and higher in the atmosphere, can have a significant impact on the state of the fuel (moisture content),

the behaviour of a fire, its growth, and, in turn, the impact the fire can have on the atmosphere itself. Structures in the atmospheric flow such as fire whirls or, on a larger scale, pyro-cumulus cloud (Mills 2005b), can be generated. These structures might themselves in turn affect the spread and behaviour of the fire.

Topographic interactions

The topography in which a fire is burning also plays a part in the way in which energy is transferred to unburnt fuel and the ambient atmosphere. The ground acts as an impervious boundary that defines the bottom of the atmosphere (the atmospheric boundary layer) and acts as a source of friction to the flow over it (Gibson and Launder 1978). Vegetation on that boundary increases the amount of friction through the roughness length and provides the layer (and the fuel) through which the fire moves (Finnigan 2000).

It has long been recognised that fires burn faster upslope than they do down (McArthur 1967; Van Wagner 1977). This is thought to be due to increased transfer of radiant heat due to the change in the geometry between the fuel on the slope and the flame, however recent work by Wu *et al*. (2000) suggests that there is also increased advection in these cases.

The complicated interaction of the topography with the atmosphere results in changes to the flow over the land surface. The surface, particularly complex geometry surfaces as found in hilly or mountainous terrain, induces turbulence in the air flow over it by causing flow separation and the formation of eddies (Belcher and Hunt 1998) and can lead to wind directions at odds with the bulk (synoptic) motion of the air (e.g. gully or valley winds). Differential solar heating of the surface can lead to the generation of local vortices (commonly called whirlwinds or willy-willies) and also differential in fuel moisture contents. Diurnal heating and cooling of the ground can result in generation of upslope (anabatic) or downslope (katabatic) winds.

2.3.2 Radiant heat transfer

Radiant heat is a form of electromagnetic radiation emitted from a hot source and is in the infra-red wavelength band ($\simeq 0.7\mu\text{m} - 1000\mu\text{m}$). In flame, the primary source of the radiation is thermal emission from hot carbon particles (generally in the form of soot) (Gaydon and Wolfhard 1960), although band emission from electronic transitions in molecules also contributes to the overall radiation from a fire.

The general method of modelling radiant heat transfer is through the use of a radiant transfer equation (RTE) such as that of the Stefan-Boltzmann equation:

$$q = \sigma T^4, \tag{2.13}$$

where q is the blackbody emissive power per unit area (W m^{-2}) of the source surface, σ is the Stefan-Boltzmann constant (5.67×10^{-8} J K^{-4} m^{-2} s^{-1}) and T is the radiating temperature of the surface (K).

While it is possible to approximate the radiant heat flux from a fire as a surface emission from the flame face, this does not fully capture the nature of the radiation as a volumetric emission from the full thickness of flame (Sullivan *et al*. 2003a) and can lead to inaccuracies in flux estimations if precise flame geometry (e.g. view factor—the ge-

ometric relation between the emitting surface and receiving surface), temperature and surface emissivity equivalents, are not known.

More complex solutions of the RTE, such as treating the flame as a volume of radiation emitting, scattering and absorbing media, can improve the prediction of radiant heat but are necessarily more computationally intensive (Knight and Sullivan 2004); varying levels of approximation (both physical and numerical) are frequently employed to improve the computational efficiency. The Discrete Transfer Radiation Model (DTRM) (Lockwood and Shah 1981) solves the radiative transfer equation throughout a domain by a method of ray tracing from surface elements on its boundaries and thus does not require information about the radiating volume itself. Discrete Ordinate Method (DOM) (Raithby and Chui 1990) divides the volume into discrete volumes for which the full RTE is solved at each instance and the sum of radiation along all paths from an observer calculated. The differential approximation (or P1 method) (Cheng 1964) solves the RTE as a diffusion equation which includes the effect of scattering but assumes the medium is optically thick. Knowledge about the medium's absorption, scattering, refractive index, path length and local temperature are required for many of these solutions, decreasing their ease of implementation and leading to increase use of approximations and simplifications in complex scenarios, such as bushfires.

Descriptions of methods for solving these forms of the RTE are given in texts on radiant heat transfer (e.g. Drysdale (1985)). Sacadura (2005) and Goldstein *et al*. (2006) review the use of radiative heat transfer models in a wide range of applications.

Transmission of thermal radiation can be affected by smoke or band absorption by certain components of the atmosphere (e.g CO_2, H_2O) (King 1972). In the case of bushfires, transmission to surface fuel can also be affected by interception by the trees and other obstructions.

2.3.3 Solid fuel transport (firebrands)

Spotting (the ignition of small spotfires downwind of a main bushfire front by firebrands lofted by the main fire's convection) is a major contributing factor to the difficulty of suppression of a bushfire (Cheney 1968). While long-distance ($>$ 1 km) spotting is predominantly a high-intensity forest fire phenomenon, spotting over shorter distances (0-50 m) occurs under all intensities in nearly all fuel types. In forests, firebrands may consist of bark, leaves, branches or flower/seed capsules (McArthur 1967). In grass fuels, firebrands may consist of seed heads, clumps of grass, or animal dung (Cheney and Sullivan 1997).

The transport of firebrands is highly probabilistic (Ellis 2000) and not readily amenable to a purely deterministic description. This is due in part to the wide variation in firebrand sources and ignitions (type, period of ignition, height, etc.), combustion characteristics and the particular flight paths any firebrand might take.

The maximum distance that a firebrand may be carried is determined by the height to which the brand is lofted (this, in turn, is determined by the intensity of the fire, the velocity of updraught of the convection and the terminal velocity of the firebrand), the height at which the firebrand was released, and the wind profile aloft and the change in terminal velocity as the firebrand burns (Albini 1979; Ellis 2000). Whether the firebrand lands alight and starts a spotfire is dependent upon the nature of the firebrand, how it was ignited, its in-flight combustion properties (including flaming lifetime) (Ellis 2000),

and the ignition properties of the fuel in which it lands (e.g. moisture content, bulk density, etc.) (Plucinski 2003).

Spotting is the main mechanism by which bushfires cross breaks in fuel and topography (see Figure 1.2, p. 11). In general, the majority of firebrands initiated in a bushfire will be consumed in the convection column and thus not fall out of the column alight (Ellis 2000). However, if the energy in the convection column is reduced (for instance, when the fire encounters a fuel break and runs out of fuel to burn), the updraught velocity in the column is reduced, causing the firebrands to fall out of the column before they are consumed and thus land alight, increasing the chance of a spotfire starting.

2.3.4 Fuel drying and wetting

The moisture content of the fuel (known as fuel moisture content (FMC)) is an important factor in determining the ignitability and combustibility of a fuel (Byram 1959a; Pompe and Vines 1966). Bushfire fuel consisting primarily of dead leaf (litter) material has lost all moisture associated with the live plant (that is live FMC is zero). Any moisture present in the dead fuel comes from either free water that has soaked in from the surface (i.e. rain, dew, etc.) or water vapour adsorbed from the atmosphere and given time can achieve an equilibrium FMC associated with the moisture in the atmosphere (King and Linton 1963).

However, FMC will follow a diurnal adsorption/desorption trend as solar radiation, air temperature and air moisture vary through the day. As direct measurement of FMC is labour intensive and time-consuming, methods such as the use of a fuel simulacrum (e.g. commonly wooden sticks of known dry mass) or models of FMC are employed. The physical processes that determine fuel moisture in litter fuel are a complex interaction of transfers of radiation, heat and water (Matthews 2006). These transfers include long and short wave radiation into and out of the fuel bed, the vertical transport of heat and water (both gas and liquid phase) between fuel and the atmosphere and the fuel and the soil layer beneath, and adsorption and desorption of water into the fuel itself. Empirical models based on the correlation of FMC with readily measurable variables such as air temperature and relative humidity (e.g. McArthur (1967) are often employed operationally. However these are generally limited to a small operational range (e.g. part-shade, afternoon, adsorption phase) and often cannot cope with free water such as rain or dew (Viney 1991).

2.3.5 Discussion

Fluid dynamics has been applied to the modelling of the motion of the atmosphere over the Earth's surface and has resulted in the development of not only general circulation models of the planetary atmosphere motion at the largest scale, but also general weather forecasting models at the intermediate or mesoscale (Pielke *et al*. 1992) and local weather models at the synoptic scale (e.g. Leslie and Skinner (1994)). The application of the same principles to smaller scales has produced models of local wind flow over complex terrain (Belcher and Hunt 1998; Butler *et al*. 2006) or ocean surfaces (used to predict winds for yacht racing) (Batt and Leslie 1998), as well as the flow over and around complex geometries such as aircraft, buildings and even cities.

While the development of understanding of the processes involved in atmospheric motion has been underway since the late 19th Century with the development of the Navier-Stokes equations, the understanding of turbulence still presents a considerable challenge for researchers (Jiménez 2006). The two opposing factors in the full simulation of turbulent atmospheric flows are the need for high precision solutions to the complete set of equations describing the flow and the speed at which those equations can be solved using modern computers. Due to the extreme number of degrees of freedom in the turbulent atmosphere system (the Reynolds number of the flow—approximately 60,000–90,000 in the atmosphere—equates to the number of degrees of freedom of the system), the cost of direct computations of the solutions makes the approach impractical (Jiménez 2006). As a result, a number of computational methods have been developed to approximate aspects of the turbulent flow to reduce the computational cost.

It is only in the last few decades that these intricate models of atmospheric motion have been extended to include terms for a source of heat and movement of that heat source within the system in a self-consistent manner. Equations of motion specifically formulated to deal with buoyant reactive flows that include energy release from combustion (Anderson and Jackson 1967; Rehm and Baum 1978; Grishin *et al*. 1983) form the basis of a number of physical models of fire spread. As with the simulation of turbulence, the simulation of the transfer of heat (e.g. from flames), the movement of solid fuel firebrands, and the spread of the bushfire and its interaction with the atmosphere and terrain, are necessarily filled with approximations and simplifications in order to make the problem tractable. However the effects of interactions of turbulence with reactions kinetics, soot formation and radiant heat transfer associated with the turbulent combustion characteristics of fire are still beyond the capabilities of even the largest computers (Cox 1998). It is very much a developing research area and advances in the field are ongoing.

2.4 Modelling of bushfire spread

Like most efforts to build models of natural phenomena, the range of approaches used to model bushfire behaviour is best described as a continuum (Karplus 1977). In the context of bushfire, these can range from the purely physical (those that are based on fundamental understanding of the physics and chemistry involved in the combustion of biomass fuel and behaviour of a bushfire) through to the purely empirical (those that have been based on phenomenological description or statistical regression of observed fire behaviour).

It is useful, however, to divide the methods that have been applied to bushfire modelling into a number of categories. Weber (1991a) proposed a system by which models were described as physical, empirical or statistical, depending on whether they account for different modes of heat transfer, make no distinction between different heat transfer modes, or involve no physics at all. Pastor *et al*. (2003) proposed descriptions of theoretical, empirical and semi-empirical, again depending on whether the model was based on purely physical understanding, of a statistical nature with no physical understanding, or a combination of both. Grishin (1997) divided models into two classes, deterministic or stochastic-statistical. These schemes, however, are rather limited given the combination of possible approaches and, given that describing a model as semi-empirical or

semi-physical is a 'glass half-full or glass half-empty' subjective issue, a more robust convention is required.

Thus it is proposed that models of fire behaviour be divided into four broad categories: physical, quasi-physical, empirical and quasi-empirical. In this context, a physical model is one that attempts to represent both the physics and chemistry of fire spread; a quasi-physical model attempts to represent only the physics, relying on prescribed values for heat release; an empirical model is one that contains no physical basis at all (and is generally only statistical in nature); a quasi-empirical model is one that uses some form of physical framework upon which to base the chosen statistical modelling. Empirical and quasi-empirical models can be further subdivided into field-based and laboratory-based, depending on the source of observational data. The four proposed categories may be expanded to five with the inclusion of mathematically analogous models. Mathematical analogous models are those that utilise a mathematical concept rather than a physical one for the modelling of the spread of a bushfire and thus may not necessarily include any fire-related attributes.

Sullivan (2007b,c,d) conducted a comprehensive survey of all fire spread and simulation models published since 1990 based on these categories. Those models that endeavour to account for the chemistry of combustion as well as the physics of heat transfer (i.e. physical models), which include Grishin (1997); Larini *et al*. (1998); Linn *et al*. (2002); Mell *et al*. (2007) and Porterie *et al*. (2007), all employ simplified chemistry models in a common need to develop a tractable model of fire behaviour and achieve computational feasibility. Generally, single-step reaction chemistry is employed with prescribed stoichiometry assuming gas-gas oxidation (i.e. flaming combustion). As a result, much of the interesting (i.e. nonlinear) aspects of the combustion of cellulosic biomass fuel detailed in the first part of this chapter is missing from these models, leading the authors of these works to attempt to seek the source of non-linearity in bushfire behaviour in the complicated interactions of the fire with the atmosphere of which, of course, there is plenty. The models of Linn and Mell *et al.* are discussed in greater detail in the next chapter.

Other methods of bushfire modelling, such as empirical and quasi-empirical models and their associated simulation forms, are unable to include any form of non-linear behaviour due to the structure of these models which are invariably linear in form. Only the model of Clark *et al*. (1996a,b), in which a quasi-empirical fire spread model was coupled to a mesoscale meteorological model solving the equations of motion for the atmosphere, demonstrated non-linear behaviour in the interaction of the fire with the atmosphere. However, the reliance on the quasi-empirical fire spread model limits its potential to explore other avenues of non-linearity. Mathematically analogous models may be able to emulate non-linear behaviour but generally this behaviour is present in the form of the equations implemented and will not necessarily reflect observed fire behaviour.

2.5 Conclusion

This chapter has précised the fundamentals of the chemistry and physics of combustion involved in the spread and behaviour of a free-burning bushfire. Due to the cellulosic polymer nature of biomass fuels the thermal degradation and resultant oxidation of ther-

mal degradation products is complex. The competitive nucleophilic addition following thermal scission of the cellulose chain provides two possible pathways for the thermal degradation of cellulose: intramolecular nucleophilic addition resulting in cyclisation, depolymerisation and the formation of the gas phase levoglucosan which quickly breaks down to form a host of other volatile gas phase species, or intermolecular nucleophilic addition via a water molecule resulting in a stable end that forms hydrolysed cellulose and under further heating dehydrates and cross-links to form a species of charcoal. The differences in activation energy, reaction rate, enthalpy and thermochemical feedbacks mean that the two pathways are intricately linked in a highly dynamic way.

Oxidation of these thermal degradation products results in the release of considerable energy in the form of heat and light. In the case of gas phase volatiles this is in the form of flames. In the case of charcoal this is in the form of glowing solid/gas combustion. The transfer of this heat to adjacent unburnt fuels is through advection of the heat gases associated with the flame, radiation of heat from the flames and burning charcoal or conduction of heat through contiguous solid phase fuel. Advection is predominantly modelled through the use of fluid dynamics in the form of the Navier-Stokes equations. This enables the consideration of buoyancy, convection and turbulence as well as atmospheric and topographic influences. Radiant heat transfer is modelled through forms of the radiant transfer equation that relates the emissive power to the temperature of the radiating body. Other considerations are the transport of burning solid fuel in a process known as spotting, and the adsorption and desorption of moisture from the surrounds by the fuel.

A continuum of models has been developed to incorporate a selection of the chemical and physical processes involved in the combustion and spread of bushfire. Practical considerations mean that often model authors must prioritise which processes can be incorporated completely, which can be approximated and which must be ignored. Often the chemistry is approximated or ignored completely with the focus of the model being the larger scale physics of the heat transfer mechanisms. The following chapters will explore the importance of the chemistry of thermal degradation of fuels in the behaviour of bushfires.

Chapter 3

Competitive combustion in bushfires

In which the implications of the competitive thermal degradation of cellulose in regard to bushfires are discussed, leading to this work's hypothesis. It is proposed that it is the interaction of the molecular scale competitive nature of the thermal degradation of cellulosic fuels and the forced convection effect of the wind that is a major source of the macroscale non-linear behaviour observed in bushfires. Experimental evidence for the occurrence of this cause is given and the results of physical modelling published in the literature used as a null-hypothesis test.

A physical scientist has been carrying out a series of experiments and has developed an empirical relation that seems to explain his data. Being a bit uncertain about his mathematical skills, he asks a mathematics professor at the local university to check his work and make sure he hasn't got something wrong in the formulation.

A week later, the mathematics professor emails him, telling him the equation is invalid. By then, however, the scientist has used his equation to predict the results of further experiments and is getting excellent results, so he asks the mathematics professor to check again.

Another week goes by, and the scientist drops by the maths professor's office to see how he is doing. The maths professor finally agrees the equation does work. "But," he says, "only in the trivial case where the numbers are real and positive."

3.1 Introduction

The knowledge that biomass fuels can undergo different thermal degradation pathways depending on the combustion conditions has existed since well before the industrial revolution and the conversion of much of the forest of Europe and Britain to charcoal (Harris 1999). In this context of industrial use, the promotion of one thermal degradation path over the other through the controlled use of moisture (in the case of charcoal manufacture) or the exclusion of water (in the case of gasifiers), has clearly illustrated the role of water in the thermal degradation of cellulosic fuel, primarily through nucleophilic addition on the carbocations resulting from thermolysis of the cellulose chain.

Extensive experimental investigation of these reactions via such methods as thermogravimetric analysis (TGA) under a large range of controlled conditions has led to the development of many models of the thermal degradation of cellulose (Antal and Várhegyi 1995; Antal *et al*. 1998; Di Blasi 1998). Di Blasi (1993) identified three main types of reaction kinetic models, encompassing: a single global one-step reaction for the entire system, multiple one-step reactions to describe the formation of several species, and two-step semi-global reactions that incorporate primary and secondary reactions.

The simplest model assumes a global one-step first order reaction (Antal and Várhegyi 1995) in which a single-step reaction is used to describe degradation of solid fuel by experimentally measured rates of weight loss. Generally yields of products are held proportional. However, in the case of thermal degradation processes occurring at the surface of condensed (i.e. solid) phase fuels where both the physical and chemical compositions of interacting species are changing with respect to time, the kinetics of these processes involve a complex interplay of competing reactions that may not be adequately depicted by simple kinetic models (Flynn 1980).

Broido and Nelson (1975) and Bradbury *et al*. (1979) put forward models in which cellulose takes an intermediate form (active cellulose or anhydrous cellulose) as a result of reactions that do not result in mass loss, and then undergoes competitive reactions (as a result of the nucleophilic competition described in Chapter 2) to form either volatile tars or charcoal. In the case of Broido's model, charcoal is formed via a series of reactions[1], with differing activation energies for each path. Koufopanos *et al*. (1991) proposed an extension to the Broido-Shafizadeh model in which a secondary reaction between the volatiles and charcoal produced further charcoal, gases and volatiles but of different composition. Shafizadeh and Chin (1977) proposed a three-path reaction mechanism in which charcoal, tar and gases all form in competition.

The Broido-Shafizadeh model (described in some literature as 'classic' (Mamleev *et al*. 2007a)) forms the basis of many models of cellulosic biomass thermal degradation. Often it is modified such that the substrate does not undergo an intermediate step before competitive formation of volatiles and charcoal (Di Blasi 1998). This model is characterised by a high activation energy volatilisation pathway that is slightly endothermic and a low activation energy charring pathway that is exothermic. Várhegyi *et al*. (1993, 1997) showed experimentally that the presence of water acted as a catalyst for the formation of charcoal to the detriment of volatilisation. Figure 3.1 shows a modified Broido-Shafizadeh model with water catalysis (Ball *et al*. 1999a).

In this model of cellulosic thermal degradation there are thermal and chemical feedbacks (Fig. 3.2) between the two paths such that if heating rates are low and/or moisture is present, the charring pathway is promoted at the expense of the volatilisation pathway. If sufficient energy is released in this process (or additional heat is added) or moisture evaporated, then the volatilisation pathway becomes statistically favoured over the charring pathway. However, if the heat released is advected away from the reactants or moisture is trapped, then the charring path becomes statistically favoured. These two competing pathways will oscillate until conditions become totally self-supporting or thermal degradation stops.

[1] Any model that consists of two competing reactions preceded by an intermediate initiation step all with relatively high activation energies is referred to as the Broido-Shafizadeh model (Antal and Várhegyi 1995) in reference to these two models (e.g. the model by Koufopanos *et al*. (1989) for biomass fuels)

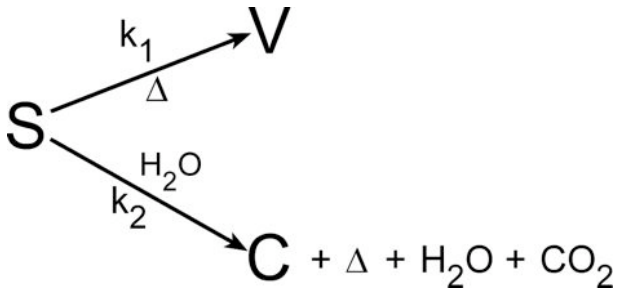

Figure 3.1: Schematic of the competing paths possible in a simple two-path model of the thermal degradation of cellulose substrate (S). Volatilisation into levoglucosan (V) is endothermic. Charcoal formation (C) occurs at a lower activation energy in the presence of moisture. This path is exothermic and forms water. Δ is heat, k_n is the reaction rate constant. (After Várhegyi *et al*. (1993) and Ball *et al*. (1999a)).

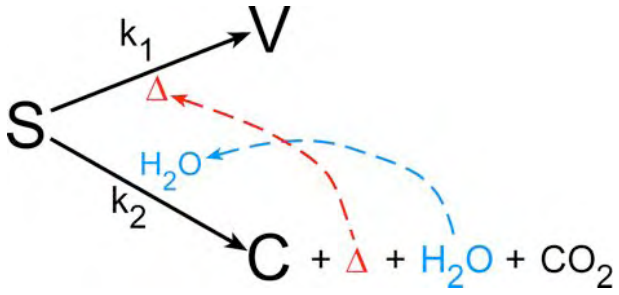

Figure 3.2: Chemical and thermal feedback paths (dashed lines) can encourage either volatilisation or charring. (After Di Blasi (1998) and Ball *et al*. (1999a)).

However, it is recognised that the thermal degradation of biomass fuels is the combination of both chemical (reaction kinetics) and physical (mainly heat transfer) processes (Koufopanos *et al*. 1991) and thus the transfer of heat from exothermic reactions plays a significant role in the thermal degradation process. If not suppressed, secondary reactions with the products of the primary thermal degradation reactions will occur, i.e. if conditions are suitable, oxidisation of the levoglucosan (as flame) and charcoal and associated products (as smouldering or glowing combustion) will provide large amounts of energy to the system (Fig. 3.3).

When these subsequent reactions release enough energy then the entire process becomes self-supporting through the additional thermal feedbacks (Fig 3.4). These additional sources of energy are orders of magnitude greater than those released through the thermal degradation processes and thus provide the bulk of the energy released by biomass combustion.

In the case of bushfire, where the fire is moving through the fuel, the thermal degradation processes occur continuously as the leading edge of the combustion zone moves into unburnt fuel. And, of course, the processes occur all around the perimeter of the bushfire where the local conditions can vary quite markedly.

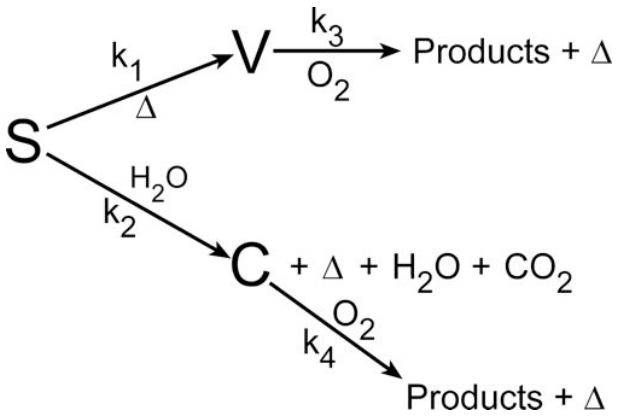

Figure 3.3: Simplified pathways of secondary reactions to complete combustion of levoglucosan and charcoal products of thermal degradation via oxidation.

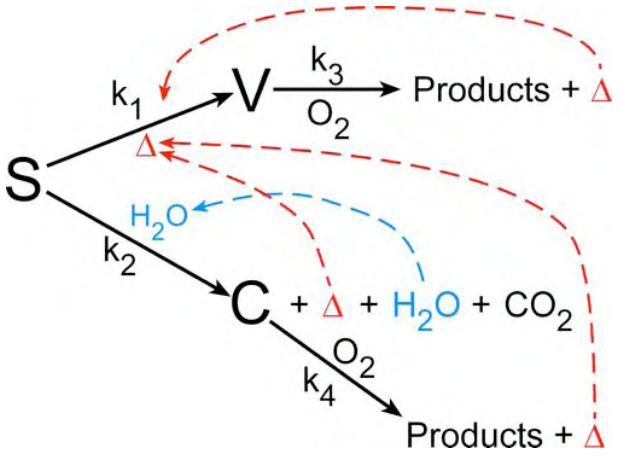

Figure 3.4: Chemical and thermal feedback paths (dashed lines) from both thermal degradation and subsequent oxidation of released products (levoglucosan and charcoal) can lead to self-supporting reactions.

3.2 Competitive combustion in bushfires—a hypothesis

While the above general model has been accepted in one form or another in the industrial biomass combustion field, the role of competitive combustion in biomass fuels has not been investigated in the context of bushfires. The fact that the conditions in which bushfires occur are, unlike in an industrial setting, uncontrolled and open to the vagaries of weather and changes in terrain and fuel, means that the combustion process, which is already highly complicated, becomes even more so. But it does not change the nature of the combustion process itself.

The key difference between the combustion of biomass fuel in an industrial burner and that of a bushfire is that the wind plays a critical role in determining the behaviour of the fire (where and how fast it moves, the angle of the flames, etc). That is, the wind plays a critical role in the combustion process. In Figure 3.4, the thermal feedback from the secondary reaction of volatiles (e.g. oxidation of the levoglucosan and flaming combustion) and charcoal (e.g. smouldering combustion) is open to the action of the wind. In particular, the flaming combustion occurs some height above the level of the thermally

degrading fuel bed and thus can be advected away from the fuel, reducing the impact of the considerable heat being released by this mechanism. As a result, it is possible that the endothermic reaction of volatilisation and subsequent loss of heat from combusting products can drive the thermal degradation reaction toward charring. Additionally, the cooling effect of the ambient wind can have the same result.

It is hypothesised that, all else being equal (such as fuel structure and continuity), it is this critical interaction between the wind and the combustion chemistry that drives not only the behaviour and speed of the fire but also the shape of the perimeter, the distinctive difference in behaviour between heading fires and backing fires, and the difference in the residue left behind by these types of fires.

We will first consider the evidence that supports such a hypothesis, ranging from observational evidence from experimental fires, to an essentially unintentional null-hypothesis test in the literature from well-established physical models of bushfire spread. In the following three chapters we will explore the nature of the interaction through reaction thermokinetics modelling and computational fluid dynamics.

3.3 Observational evidence

This section relies upon the results obtained from field experiments conducted in grassland fuels by the National Bushfire Research Unit of the CSIRO Division of Forestry[2], Canberra, Australia, during the 1970s and '80s in the Northern Territory (Cheney *et al*. 1993; Cheney and Gould 1995, 1997; Cheney *et al*. 1998). These experiments investigated the role of fuel and weather attributes in determining the rate of forward spread of large unrestricted grass fires. A large number of experimental fires were conducted in flat grassland and open woodland in a range of grass species, fuel (both natural and modified) and weather conditions. Plots ranged in size from 100×100 m to 1+ km. Fires were generally lit from lines 35–175 m long with some point ignitions. During each experiment fire perimeters were defined by markers thrown at regular intervals or, later, by a series oblique aerial photographs. This information was then used to produce a map of fire spread intervals and analysed to produce such measurements as rate of spread, head fire width, and flame depth and augmented with ocular estimates of flame front geometry.

An example of a series of aerial photographs of one such experiment is shown in Figure 3.5. This fire, Annaburoo experimental fire CO64, was lit from a 50-m-long ignition line perpendicular to the prevailing wind on the up-wind edge of a 100×100 m plot consisting of untreated *Themeda australis* grass. Mean rate of spread across the plot was 1.19 m s^{-1}, mean wind speed at a height of 2 m was 4.67 m s^{-1}.

While the results of these well-documented experiments have been incorporated into operational grassland fire spread prediction system (CSIRO 1997; Cheney *et al*. 1998), the data collected represent a unique insight into the behaviour of large, free-burning fires in relatively simple fuels and are a valuable source for continued analysis of bushfire behaviour (e.g. Linn and Cunningham (2005); Morvan *et al*. (2006); Mell *et al*. (2007); Sullivan (2007a); Cunningham and Linn (2007)).

[2]Now Ensis, a joint venture between CSIRO Forestry and Forest Products and SCION (formerly New Zealand Forest Research).

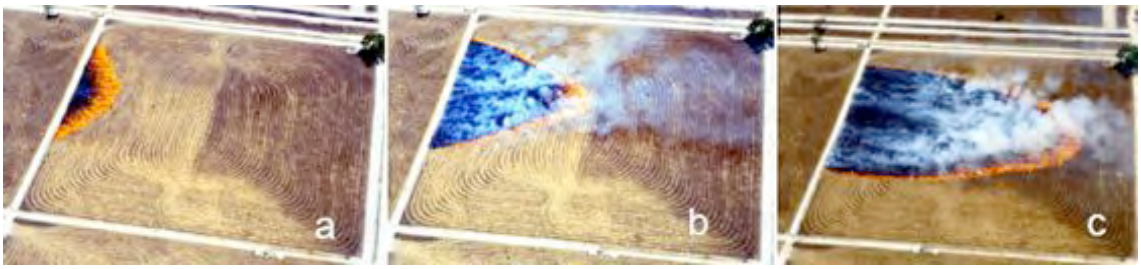

Figure 3.5: Sequence of oblique aerial photographs of Annaburoo experimental fire C064 burning in untreated *Themeda australis* grass at three times following ignition: a) 24 s, b) 50 s, and c) 82 s. This fire was lit from a 50-m-long ignition line perpendicular to the prevailing wind on the up-wind edge of a 100 $\times$ 100 m plot. (Source: Sullivan and Knight (2004).)

3.3.1 Flame characteristics

The defining attribute of a head fire is the relatively tall height of the flames when compared to those at the back or flanks of the fire. This is generally associated with the direction of the wind such that the flames of the head fire lean over unburnt fuel. The head fire is also associated with thick dark smoke, high flame intensity, dynamic behaviour and fast spread in the direction of the wind. Flames at the back of the fire, by contrast, are associated with thin pale smoke, low flame intensity, mild, steady behaviour and slow spread into the wind.

Figure 3.6 shows the final spread interval of Annaburoo experimental fire B101 (CSIRO Forestry and Forest Products, unpublished data). The fire was ignited in *Themeda australis* grass that was cut and retained from a 50-m-long line and in this image has been burning for 118 seconds in an average wind of 5.5 m s^{-1}. The head fire is clearly delineated by very deep and tall flames leaning in the direction of spread with the wind and a narrowing of the head fire into a parabolic shape. The depth and height of the flames reduces along both flanks heading towards the back of the fire where the flames are very low, in some places indiscernible, and produce very little smoke. There is very little outward spread of the flanks or into the wind at the rear of the fire in comparison with the length of the ignition line.

At any point in time, the conditions (fuel, moisture, temperature and relative humidity) around the perimeter are, to all intents and purposes, constant. The only differences are the direction of the wind with respect to the spread of the fire and the mode in which the fuel is consumed. In backing flames, the fuel is consumed from the base of the fuel bed up; in heading flames, fuel is consumed from top of the fuel bed down (Cheney and Sullivan 1997). Clearly there is something more than the way the fuel is consumed that contributes to the amount of flame produced at the head compared to the back—orders of magnitude more flame by volume in some instances—that cannot be explained by physical conditions alone.

While the difference in the rate of combustion and net heat flux around the perimeter obviously plays a part, this is driven by the difference in the rate of volatilisation, i.e. where there is more heat being transferred to unburnt fuel, there is a resultant greater rate of volatilisation and thus subsequently more flame and more heat to transfer. The direction of transfer of the heat is dictated by the direction of the air flow in and around

Figure 3.6: Aerial photograph of Annaburoo experimental fire B101, 118 seconds after ignition. The fire was lit in *Themeda australis* grass that has been cut and retained from a 47-m-long ignition line. Average wind speed was 5.5 m s^{-1}, average rate of spread was 1.95 m s^{-1}. The difference in structure between the flames at the head of the fire and those at the back is clearly shown. The wind is blowing from the bottom left corner of the photograph to the top right, as suggested by the direction of the passage of smoke. (Source: CSIRO Forestry and Forest Products unpublished data.)

the flaming zone which is driven by the mean wind direction. As a result the net heat flux is greater at the head than at the rear or flank. The low net heat flux at the rear of the fire

3.3.2 Ash residue

In post-fire investigations it is often only the ash residue left behind that gives any indication of the direction of spread of a fire. Figure 3.7 is a sequence of images showing the development of the ash patterns of Annaburoo experimental fire E26 (Cheney and Sullivan 1997). This fire was lit from a point and underwent several phases of spread, resulting in the laying down of a fine white ash when the flames were low, and the laying down a black ash when the fire behaviour lifted and began to spread forward consistently.

The laying down of the white ash during the period of low flame concurs with the proposition that predomination of non-flaming combustion is associated with the formation and subsequent combustion of charcoal. When flames are tall and fire behaviour active, the thermal degradation is dominated by the volatilisation pathway, resulting in amorphous residue after oxidisation that is not further combusted and which appears as black ash.

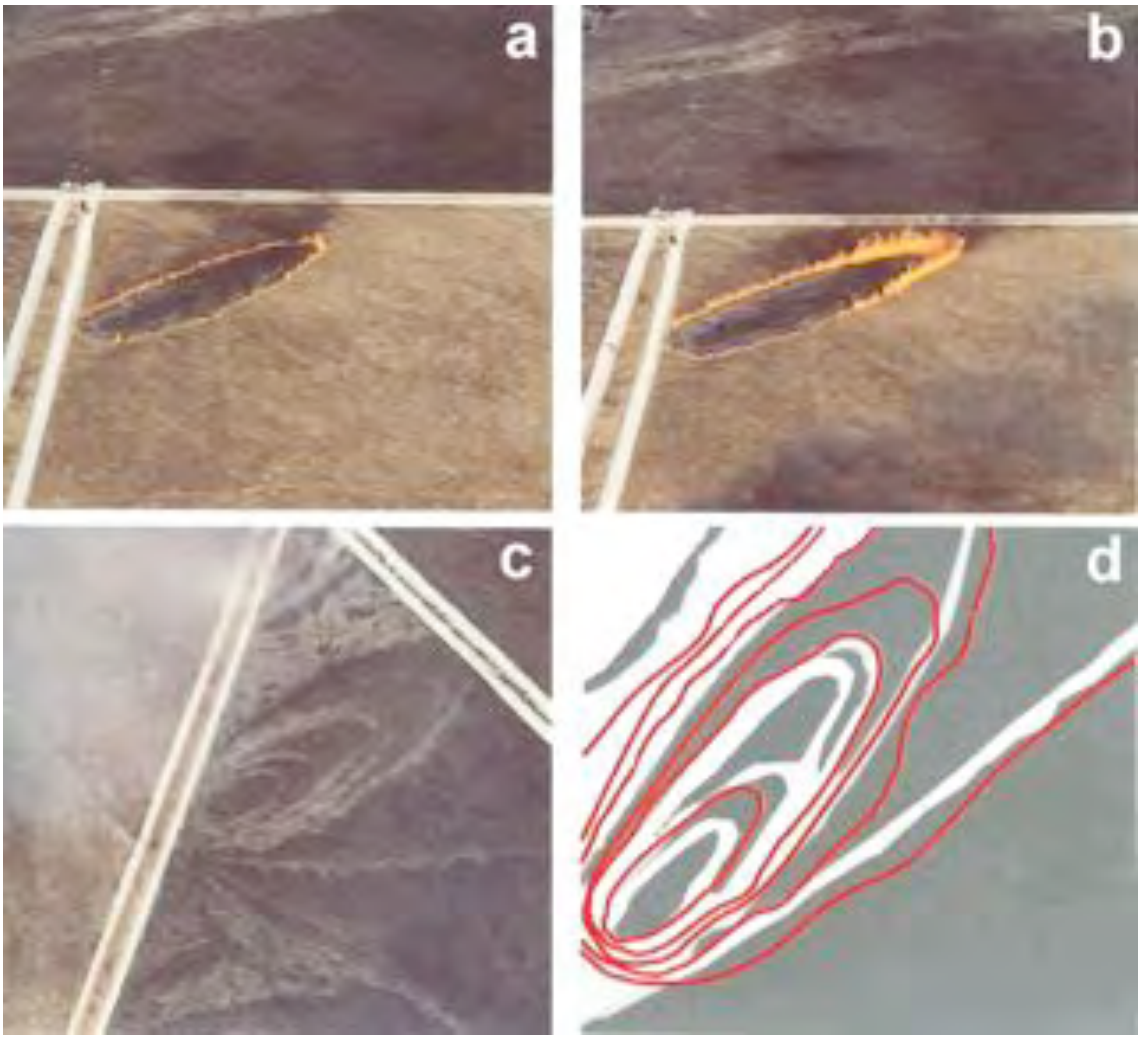

Figure 3.7: Sequence of oblique aerial photographs of Annaburoo experimental fire E26 showing the development of alternating white and dark ash patterns. This fire was lit from a point and went through some of the following phases: (a) 3.1 minutes after ignition, a lull dominates the spread and flames are low and flame depth thin. (b) 3.6 minutes after ignition, the fire is spreading as a heading fire with tall flames and lengthened flame depth. (c) Final ash patterns left after the fire has burned out. (d) The measured spread pattern of E26 (in red) superimposed on a map of the ash pattern left behind. (Source: Cheney and Sullivan (1997).)

3.3.3 Flame residence time

Flame residence time, t_r, is defined as the period of time for which flames remain burning at one particular location. Generally, it is calculated using measurements of rate of forward spread, r, and flame depth, d_f:

$$t_r = \frac{d_f}{r}, \tag{3.1}$$

where r is in m s^{-1}and d_f in m. This quantity is assumed to be constant for a particular fuel type—Anderson (1969) found residence time to be a function of the ratio of surface area to volume of a fuel particle (Mell *et al*. 2007). However, analysis of the Annaburoo

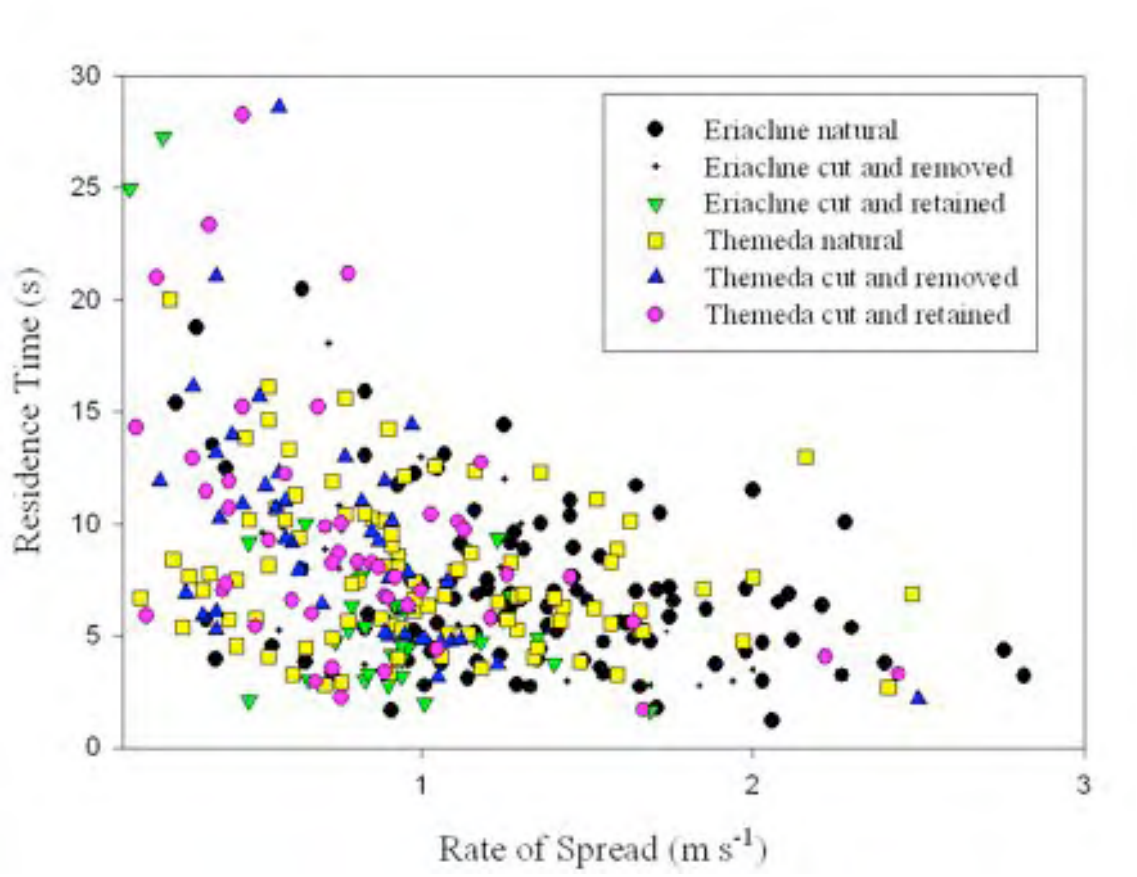

Figure 3.8: Residence time of all Annaburoo grassland experimental fires separated by fuel treatment. A distinct exponential decay curve trend can be seen in the data with slower spreading fires burning for longer and faster spreading fires burning for less, asymptoting to a value consistent with the accepted residence time for grass fuels. (Data from: Cheney *et al*. (1993).)

data shows that the residence time is not constant (Fig. 3.8), resulting in generally longer residence times for slower moving fires. As the rate of spread increases, the residence time asymptotes to a relatively stable value that is consistent with the commonly accepted value for residence time for grassy fuels, $t_r = 5$ s (Cheney and Sullivan 1997).

While the increase in residence time for lower speed fires is not consistent, with many fires still exhibiting low residence times, there is enough of a trend in the data (exponential function: $t_r = 5.4 + 12.68e^{-1.98r}$, correlation coefficient = 0.211) to suggest that slower spreading fires are burning differently from the faster spreading variety. This difference is possibly a result of the statistical favouring of the slower charcoal production and glowing combustion path over the faster volatilisation and flaming path impeding the spread of the fire, resulting in a longer period over which both modes of combustion occur. As the fire spreads faster, the volatilisation path is favoured to the near exclusion of the charring path, rate of spread increases and the residence time decreases as a result of the faster reaction rates of gas phase oxidation.

It is possible that the difference in measured residence time is an artifact of the method used to measure the flame depth (Cheney[3] pers. comm., 2006) in that slower moving fires presented more depth of flame to allow a more accurate measurement com-

[3]N.P. Cheney, Honorary Research Fellow, CSIRO.

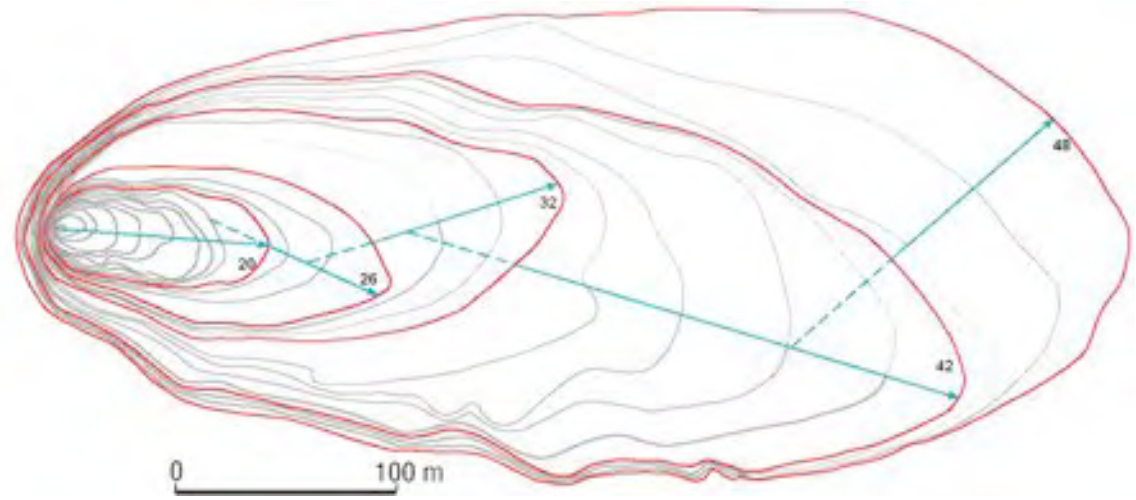

Figure 3.9: Interpreted map of sequential fire perimeters (isochrones) of Gunn Pt experimental fire 50 in open forest starting from a point ignition and showing the incremental increases in head fire width with changes in wind direction. Isochrones are at 2-minute intervals. Changes in wind direction allow the flanks to become heading or backing fires by turns. ROS increases with these changes, despite wind speed remaining relatively constant. (Source: Cheney and Gould (1995).)

pared to faster moving fires presenting less flame depth. But the separation of the data into fuel treatments (Fig. 3.8) shows that treated fuels (whether mown and removed or mown and retained) neatly delineate much of the higher residence times, suggesting that there is no bias in the residence time data due to measurement technique.

3.3.4 Perimeter shape

It has been long observed that free-burning fires spreading under generally consistent wind form an elongated shape closely resembling an ellipse or egg shape (Mitchell 1937; Curry and Fons 1940) and this has been used to great advantage in a number of fire spread simulation algorithms (Anderson *et al*. 1982; Knight and Coleman 1993; Richards 1995; Richards and Bryce 1996). The aspect ratio of the ellipse has been related to the wind speed (McArthur 1966; Alexander 1985), with stronger winds producing thinner, longer ellipses. Cheney and Gould (1995) found that slight changes in wind direction act to broaden the fire perpendicular to the mean wind direction (Fig. 3.9), resulting in an increase in the rate of spread of the fire. More significant changes in wind direction causes the flanks of the fire to become, in turns, heading or backing fires, depending on the direction of the wind (Cheney and Gould 1995; Cheney and Sullivan 1997) which cause those parts of the perimeter to increase or decrease rate of spread accordingly.

The only difference between the head of a fire and the back of the fire is the relation of the direction of the wind to the perimeter. The only physical difference in the wind is the temperature of the wind. The wind affecting the back of the fire (that part burning into the wind) is unaffected by the fire and thus of ambient temperature; the wind affecting the head of the fire has passed over the hot burnt and burning ground and is thus much hotter than ambient. The current understanding of bushfire dynamics does not suggest a reason that this should affect the behaviour of the combustion zone. However, the sensitive dependence of the combustion chemistry on temperature (through the exponential

Arrhenius reaction rate) is critical to determining which combustion path will dominate. The exothermic but lower activation energy pathway of charcoal formation may dominate when ambient temperature (i.e. $<$ 310–315 K) wind is applied and acts to cool the thermally degrading fuel in the combustion zone (generally $>$ 600 K). If such convective cooling is not effected, either because the wind has been heated to much greater than ambient temperature or the wind is not applied because it is deflected then the higher activation but endothermic pathway of volatilisation may dominate, leading to a greater portion of flaming combustion.

Formation of the parabolic head fire shape has been simulated using models that allow wind flow to interact with a buoyant heat source representing the fire (e.g. Linn *et al*. (2002); Sullivan and Knight (2004); Clark *et al*. (2004); Mell *et al*. (2007)). However, these models assume that the combustion chemistry is constant around the perimeter and thus, while they may predict the head fire shape well, do not predict well the spread of other parts of the perimeter where the combustion chemistry is different to that of the head fire.

3.4 Null-hypothesis evidence

The current state of the art in the physical modelling and simulation of bushfire spread is represented by a handful of models from around the world (Sullivan 2007b), including FIRETEC (Linn *et al*. 2002) and WFDS (Mell *et al*. 2007). One aspect that is common to these physical models is the necessary simplification of the combustion chemistry in order to produce a computationally tractable model of bushfire spread. Both FIRETEC and WFDS reduce the thermal degradation and combustion chemistry to a single-path, single-step reaction in which flaming combustion represents all combustion in the fire. As a result, their output represents an inadvertent null-hypothesis test for this current work.

3.4.1 FIRETEC

FIRETEC (Linn 1997; Linn *et al*. 2002; Linn and Cunningham 2005) is a coupled multiphase transport/wildland fire model based on the principles of conservation of mass, momentum and energy. It is fully 3-dimensional and employs a fully compressible gas transport formulation to represent the coupled interactions of the combustion, heat transfer and fluid mechanics involved in wildland fire (Linn *et al*. 2002). It attempts to represent the average behaviour of the gases and solid fuels in the presence of a wildland fire. Many small-scale processes such as convective heat transfer between solids and gases are represented without each process actually being resolved in detail (Linn 1997; Linn and Harlow 1998).

While formulations for representing reactions for pyrolysis, char burning, hydrocarbon combustion and soot combustion are given, a simplified chemistry model is employed that reduces combustion to a single solid-gas phase reaction (Linn *et al*. 2002):

$$N_{wood}(wood) + N_{O_2}(oxygen) \rightarrow (products) + heat, \tag{3.2}$$

where N_{wood} and N_{O_2} are stoichiometric coefficients that describe the net amount of wood and oxygen consumed through pyrolysis and all of the intermediate reactions

when a unit mass of 'inert' products is formed. These are estimated from Drysdale (1985). It is assumed that the rates of exothermic reaction in areas of active burning are limited by the rate at which reactants can be brought together in their stoichiometric proportions (i.e. mixing limited). This rate is calculated using a simplified reaction model based on turbulent diffusion:

$$F_{wood} = \rho_{wood}\rho_{O_2}\sigma\Pi, \tag{3.3}$$

where F is a reaction rate, ρ_x is species density and σ is the turbulent diffusion coefficient which is calculated on length scales corresponding to vegetation geometry and the turbulent kinetic energy and Π is a probability density function for the temperature within the resolved volume and is a function of the stoichiometric coefficients and the relative densities of the reactants.

3.4.2 WFDS

The Wildland Fire Dynamic Simulator (WFDS) (Mell *et al*. 2007), is a fully 3D model based upon the unique formulation of the equations of motion for buoyant flow of Rehm and Baum (1978). WFDS assumes a two-stage endothermic thermal decomposition (water evaporation and then solid fuel 'pyrolysis'). It uses the temperature dependent mass loss rate expression of Morvan and Dupuy (2004) to model the solid fuel degradation and assumes that pyrolysis occurs at 400 K. Solid fuel is represented as a series of layers which are consumed from the top down (which the authors admit is not suitable for fuels in which there is significant vertical flame spread and air flow through the fuel such as in forests) until the solid mass reaches a predetermined char fraction at which point the fuel is considered consumed. Char oxidisation is not accounted for.

WFDS assumes combustion occurs solely as the result of fuel gas and oxygen mixing in stoichiometric proportion (and thus is independent of temperature):

$$\mathrm{C_{3.4}H_{6.2}O_{2.5}} + 3.7(\mathrm{O_2} + 3.76\mathrm{N_2}) \rightarrow 3.4\mathrm{CO_2} + 3.1\mathrm{H_2O} + 13.91\mathrm{N_2}. \tag{3.4}$$

Due to the relatively coarse scale of the resolved computation grids within WFDS (1.5 m $\times$ 1.5 m $\times$ 1.4 m), detailed chemical kinetics are not modelled. Instead, a mixture fraction within a resolved volume is used to represent the mass ratio of gas-phase fuel to oxygen using a fast chemistry or flame sheet model which then provides the mass loss flux for each species. The model assumes that the time scale of the chemical reactions is much shorter than that of mixing. Thermal radiation transport assumes a gray gas absorber-emitter for which the absorption coefficient is a function of the mixture fraction and temperature for a given mixture of species and solved using a finite volume radiation solver. A soot production model is not used; instead it is an assumed fraction of the mass of fuel gas consumed. Mechanical turbulence, through the dynamic viscosity of the flow through the fuel, is modelled as a subgrid parameter via a variant of the Large Eddy Simulation (LES) method.

3.4.3 Results

Figure 3.10 shows the published plan view output from FIRETEC (Fig. 3.10a) and WFDS (Fig. 3.10b), simulating the spread of a grassfire, and the rectified spread map of Annaburoo experimental fire CO64 (Fig. 3.10c). The FIRETEC output is a simulation

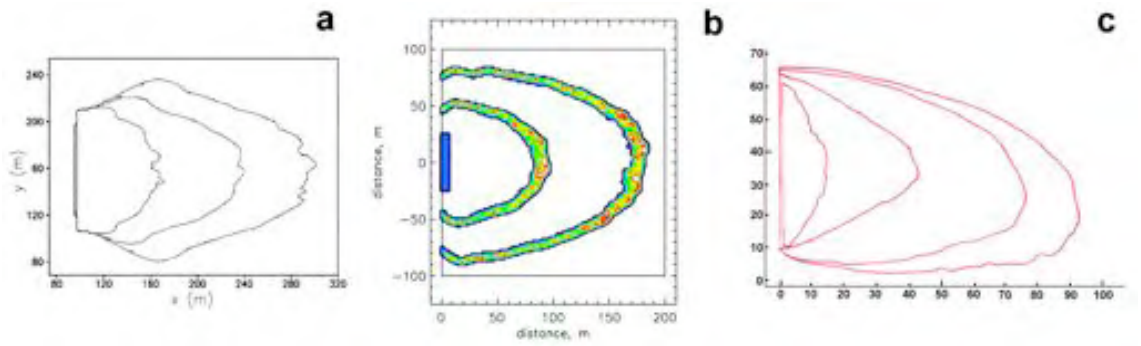

Figure 3.10: Output from (a) FIRETEC and (b) WFDS of simulation of grassfire spread in constant wind and (c) an isopleth map from Annaburro experimental fire CO64. (a) Plan view of FIRETEC perimeter at 50 s, 100 s and 150 s since ignition in constant 6.0 m s^{-1} wind, ignition line 100 m long. (Source: Linn and Cunningham (2005).) (b) Plan view of WFDS perimeter at 27, 53 s and 100 s since ignition in constant 4.6 m s^{-1} wind, ignition line (in blue) 50 m long. (Source: Mell *et al*. (2007).) (c) Isopleth map of the spread of CO64 with perimeters at 27 s, 53 s and 85 s in mean wind speed of 4.67 m s^{-1}, ignition line 50 m long. (Source: Cheney *et al*. (1993).) It can be seen that the physical models overestimate the rate of lateral spread of the flanks compared to the experimental fire. A slight change in the direction of the wind during the experiment has resulted in off-axis spread.

of a 100-m ignition line fire in grass fuel 0.7 m high and a constant ambient wind of 6 m s^{-1} from the left 'inflow' boundary. The WFDS output is a simulation of CO64, a 50-m ignition line in grass fuel 0.21 m high, 100% curing and a constant ambient wind of 4.6 m s^{-1} from the left 'inflow' boundary. Both models hold the inflow wind direction and speed constant throughout the simulation.

In the case of the results from WFDS, the rate of forward spread of the simulation is in general agreement with that observed from CO64. Both simulations, however, exhibit considerable lateral or flank spread, particularly that of WFDS, which acts to increase the width of the fire. This degree of widening is not evident in the experimental fire. WFDS increases its width from the initial width 100% after 53 s of spread and 170% after 100 s, compared to 6% after 53 s and 20% after 85 s observed in CO64. FIRETEC also exhibits significant bowing of the flank perimeter which is not evident in the real fire.

It is argued here that combustion around the perimeter is a statistical combination of volatilisation and charcoal formation (in which both pathways are always present) with the relative extent of each mechanism depending on the orientation of the section of perimeter with the wind direction. At the rear of the fire perimeter, where the combustion zone is open to the convective cooling of the ambient wind, the combustion will be dominated by charring. At the head of the fire, where the wind has passed over hot burnt ground and burning fuel and is much hotter than ambient, combustion will be dominated by volatilisation. At the flanks, changes in the wind direction due to inconsistent wind may result in the pathways alternating in response to changes in the temperature of the wind.

Assuming only volatilisation around the entire perimeter (as both FIRETEC and WFDS do) may contribute to the over-estimation of the rate and magnitude of heat output from the combustion and, subsequently, the transfer of that heat and the rate of spread of that section of the perimeter.

The key point here is not the concern that these models overestimate flank spread and thus the increase in width of the fire, but the fact that these models increase the width of the simulated fires *in the absence of variation in direction of the inflow wind*. The simulations shown in Figure 3.10 are a result of conditions in which the inflow wind speed and wind direction are held constant. That is there is no variation in wind direction that will result in the increase in the width of a bushfire in the open as illustrated in Figure 3.9 (p. 54). In contrast, the off-axis spread of the experimental fire and the slight change in the direction of spread of the fire reveal that there was a slight change in the direction of the wind during the experiment. Even with that slight change in wind direction, there is not the increase in lateral spread as simulated by the two models. Additionally, FIRETEC does not exhibit any spread of the rear of the fire into the wind, again perhaps as a result of assuming volatilisation and flaming combustion as the mechanism of spread (WFDS does model backing spread but it is not applicable in the simulation results presented due to the presence of a firebreak on the upwind edge). This overestimation in lateral spread of the flanks will result in incorrect and unnatural perimeter expansion.

Linn and Cunningham (2005) argued that the high degree of lateral spread (the 'bulges' apparent in Figure 3.10a) are a result of the effect of unresolved sub-grid scale turbulence on the net heat transfer, however the grid-scale wind vectors do not indicate such turbulence would result in the magnitude of spread normal to the direction of the local wind. The lack of backing spread is similarly consigned to a lack of resolved velocity within the grass. Both models have significantly large computational grid sizes (in the order of 1–2 m in the horizontal plane) in comparison with the scale of the combustion processes being simulated. This might be sufficient to provide necessary resolution for the head fire but may not be suitable for other parts of the perimeter such as the flank and back. This lack of spatial resolution may also play a role in the inability of these models to adequately simulate the spread of the perimeter of a bushfire.

A non-local chemistry model in which the formation of char and tar are competing processes was proposed by Colman and Linn (2003) for FIRETEC, illustrating that the role of such competitive combustion was considered important, but does not appear to have been implemented at the time of this writing. Colman and Linn (2005, 2007) implemented a restricted non-local model in which volatilisation and oxidisation of the gas phase volatile is separated (i.e. a 2-step reaction) in an effort to improve the modelling of flame and radiation but this had the effect of slightly increasing the width of the fire perimeter.

3.5 Conclusions

While the role of nucleophilic competition in the thermal degradation of cellulosic biomass fuel has long been studied in the realm of industrial applications (mainly in energy conversion and the production of charcoal), it has not been applied to the behaviour of bushfires. The complex and highly variable conditions in which bushfires occur (in regard to weather, fuel and topography) have meant that attempts to model the behaviour of bushfires has focussed on other, more readily measurable, aspects. The growing field of numerical simulation has started to deal with the fundamental processes involved in the behaviour and spread of bushfires across the landscape; however,

presently these have necessarily resorted to simplifications and approximations in order to achieve tractable and computationally feasible models.

It is apparent from large field-based experimental fires that much of the phenomenological aspects of bushfires may be explained by the fundamental processes involved in the initial competitive thermal degradation and the action of combustion of cellulosic fuels. The roles of moisture and temperature have been shown to greatly influence the selection of pathway, either volatilisation or charring and, indeed, are used in industrial burners to control product yield.

The role of advection, however, has not been considered in the literature on industrial biomass burning, apart from in the guise of purge gas flow (e.g. inert gas, such as N_2, used to flush reactors to halt secondary oxidation reactions). In the controlled conditions of most industrial burners, air flow is very strictly managed and thus the variation of the air is not seen to play an important role in combustion dynamics. In bushfires, wind is the single most important variable determining the behaviour and rate of spread of the fire. How the wind affects the chemistry of combustion has not been adequately addressed.

The thermal degradation reactions have been found to be highly temperature sensitive. Changes in the temperature of the system of reactants will greatly vary the types and rates of reactions. Ambient wind, being in the order of 200–300 K cooler than the initial thermal degradation temperatures should play a significant role in the combustion kinetics of biomass fuel. The observational evidence presented above shows that much of the behaviour of bushfires may be explained by this critical role of the cooling action of the wind.

The next three chapters of this thesis will explore the effect of ambient temperature wind on the reaction kinetics and the spatial implications for the shape of the fire perimeter.

Chapter 4

A thermokinetic model of competitive cellulosic combustion

In which a zero-spatial dimension dynamical model from the literature is introduced and discussed. The model, designed to describe the thermokinetics of the thermal degradation of cellulose in a thermogravimetric experiment, is then modified and extended to include the secondary reactions of oxidation of the charcoal and volatilised levoglucosan, formed in competition, in the presence of a constant ambient air flow. A series of sample numerical experiments is then undertaken to illustrate the utility of the model. More detailed numerical experiments are presented in the next chapter. The model is shown to simulate the steady increase in system heat and the onset of ignition of thermal degradation products.

An engineer, a physicist, and a mathematician were shown a pasture with a herd of sheep and told to put them inside the smallest possible amount of fence. The engineer went first. He herded the sheep into a circle and then put the fence around them, declaring, "A circle will use the least fence for a given area, so this is the best solution."

The physicist went next. She created a circular fence of nearly infinite radius around the sheep and then steadily reduced the radius, drawing the fence tight around the herd. She declared, "This will give the smallest circular fence around the herd."

The mathematician went last. After giving the problem a little thought, he put a small fence around himself and then declared, "I define myself to be on the outside."

4.1 Introduction

Ball *et al*. (1999a) developed a dynamical model of the thermokinetics of the thermal degradation of cellulose to simulate the results of thermogravimetric (TGA) experiments. This model is a zero-spatial plus time dimensional model[1] that considers only the evolu-

[1]That is it has only time as a dimension and does not consider the spatial aspects of what is being modelled.

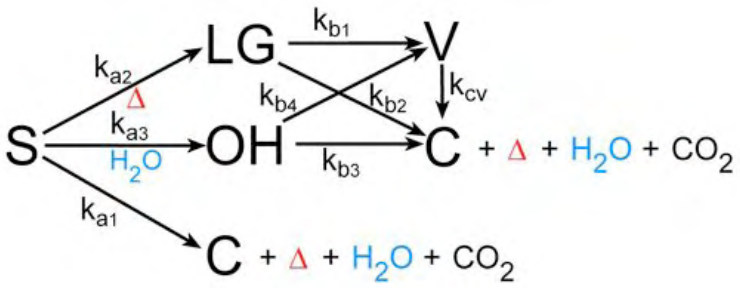

Figure 4.1: Schematic of the complete thermal degradation model of Ball *et al*. (1999a). A three-path, two-step model in which crystalline cellulose can form hydrolysed cellulose (*OH*), levoglucosan-end cellulose (*LG*) or charcoal (*C*) directly. *OH* and *LG* can then degrade further through depolymerisation or cross-linking reactions to form *C* or volatile levoglucosan (*V*). k_{xn} indicates the rate for each reaction.

tion of the mass of system variables and the heat generated as a result of the thermokinetics. It is based on the competitive asymmetric chemistry between two nucleophiles which compete for the positively charged carbon centre on C-1 of the carbonium ion formed through thermolysis of a glycosidic bond in the cellulose chain. The nucleophiles are either a molecule of water or an -OH group on C-6 on the glucosyl end of the cleaved chain. If the water molecule is successful, a reducing chain fragment with the tendency to undergo the bond-forming reactions (i.e. dehydration, decarbonylation and decarboxylation) that produce charcoal will result. If the -OH group is successful, a levoglucosan-end that is resilient to the bond-forming reactions and that depolymerises to levoglucosan and thence to other volatile products will result.

4.1.1 Ball *et al.*'s (1999a) thermal degradation model

To capture the minimal vital aspects of the thermal degradation of cellulose in their dynamical model, Ball *et al*. (1999a) chose a modified Broido-Shafizadeh (Broido and Nelson 1975; Bradbury *et al*. 1979) mechanism composed of a three-path, two-step configuration (Fig. 4.1). Broido (1976) determined from experimental weight loss data that under moderate heating cellulose undergoes an "incubation" period before branching into either depolymerisation or char formation reactions. He concluded that although there was no weight loss during this period, the fuel did undergo important changes that dictated which subsequent path would dominate under further heating. The product of the incubation period has been called "activated" cellulose. The incubation period correlates to the formation of hydrolysed cellulose and levoglucosan-end cellulose in Figure 4.1.

In this model, the thermal degradation of cellulose can undergo charcoal formation by two semi-independent processes:

1. dehydration and decarbonylation at reducing ends created by thermolysis in the amorphous regions of the substrate;
2. direct inter- and intra-chain cross-linking in the crystalline regions.

The initiation, rate and final products of the amorphous cellulose degradation depends upon the supply of water from dehydration and external sources (Várhegyi *et al*. 1993), whereas the degradation of crystalline cellulose is less dependent on the supply of water. Thus the thermal degradation of the amorphous component of the cellulose

undergoes nucleophilic competition and the crystalline undergoes conversion directly to charcoal.

The model in Figure 4.1 is described by the following chemical reaction equations :

$$S \xrightarrow{k_{a1}} nC + mW + pG, \tag{4.1}$$

$$S \xrightarrow{k_{a2}} LG, \tag{4.2}$$

$$S + W \xrightarrow{k_{a3}} OH, \tag{4.3}$$

$$LG \xrightarrow{k_{b1}} V, \tag{4.4}$$

$$LG \xrightarrow{k_{b2}} nC + mW + pG, \tag{4.5}$$

$$OH \xrightarrow{k_{b3}} nC + mW + pG, \tag{4.6}$$

$$OH \xrightarrow{k_{b4}} V, \tag{4.7}$$

$$V \xrightarrow{k_{cv}} nC + mW + pG, \tag{4.8}$$

where *S* is the cellulosic fuel substrate, *C* is charcoal, *OH* is hydrolysed cellulose, *LG* is levoglucosan-end cellulose, *V* is volatile (i.e. levoglucosan), *W* is water, *G* is non-volatile gas product (primarily CO_2), *n, m* and *p* are yield parameters, and k_{xn} are reaction rates for each reaction.

Reaction 4.1 represents the low energy direct charcoal formation from crystalline cellulose. Reactions 4.2 and 4.3 represent a simplification of the semi-global competition of the nucleophiles to form either a cellulose fragment with a levoglucosan end (*LG*) or a hydrolysed cellulose fragment (*OH*). Reactions 4.4 – 4.7 illustrate the second-step formation of final thermal degradation products (*V* or *C*). Reaction 4.4 represents the depolymerisation of levoglucosan-end cellulose to *V*; reaction 4.5 represents the possible polymerisation and cross-linking reactions of levoglucosan-end cellulose to *C*; reaction 4.6 represents the cross-linking reactions of hydrolysed cellulose to *C*; reaction 4.7 represents possible depolymerisation and volatilisation of hydrolysed cellulose to *V*. There is also a possibility of subsequent charring of levoglucosan (reaction 4.8).

4.1.2 Ball *et al.*'s (1999a) dynamical thermokinetic model

Dynamical systems, in the form of differential equations, have long been used to model chemical reactions (e.g. Gavalas (1968)). More recently such mathematical models have been shown to simulate the thermokinetics of competitive chemical reactions in which reaction rates are proportional to the total mass of common reactant rather than different fractions or states of the reactant mass (i.e. independent-parallel reactions) (Ball *et al*. 1999b).

A dynamical thermokinetic model was constructed from the reactions 4.1 – 4.8 using the principles of conservation of mass and energy (Ball *et al*. 1999a). Mathematical uniqueness of solutions and compliance with the second law of thermodynamics (i.e. entropy of the system increases) were assumed (Ball *et al*. 1999b).

Conservation of energy determines that the enthalpy of the system shall be a constant:

$$Vol[c_S h_S(T) + c_X h_X(T) + c_Y h_Y(T)] = \text{constant}, \tag{4.9}$$

where Vol is the volume of the system, c is the density, and h is the enthalpy of formation of each species where $_S$ is the substrate and $_X$ and $_Y$ are the products formed in competition, and T is the temperature of the system.

Conservation of mass gives:

$$c_S + c_X + c_Y = c_{S(0)}, \tag{4.10}$$

where $c_{S(0)}$ is the initial mass of the substrate at time $t = 0$. Combining these equations and differentiating with respect to time and using the constant-volume approximation ($dV/dt \approx 0$) and the definition of heat capacity:

$$C_p = \left(\frac{\partial h}{\partial T}\right)_p, \tag{4.11}$$

in which C_p is the specific heat at constant pressure, p, provides the basis for the model.

The resultant dynamical thermokinetic model of Ball *et al*. (1999a) is:
Evolution of cellulose substrate:

$$\frac{dS}{dt} = -k_{a1}S - k_{a2}S - k_{a3}SW, \tag{4.12}$$

Evolution of levoglucosan-end fragments:

$$\frac{dLG}{dt} = k_{a2}S - k_{b1}LG - k_{b2}LG, \tag{4.13}$$

Evolution of hydrolysed cellulose:

$$\frac{dOH}{dt} = k_{a3}SW - k_{b3}OH - k_{b4}OH, \tag{4.14}$$

Evolution of water:

$$\frac{dW}{dt} = mk_{a1}S - k_{a3}AW + mk_{b2}LG + mk_{b3}OH + mk_{vc}V + f(W_f - W), \tag{4.15}$$

Evolution of volatiles:

$$\frac{dV}{dt} = k_{b1}LG + k_{b4}OH - k_{vc}V - fV, \tag{4.16}$$

Evolution of charcoal:

$$\frac{dC}{dt} = nk_{a1}S + nk_{b2}LG + nk_{b3}OH + nk_{vc}V, \tag{4.17}$$

Evolution of gases:

$$\frac{dG}{dt} = pk_{a1}S + pk_{b2}LG + pk_{b3}OH + pk_{vc}V - fG, \tag{4.18}$$

Evolution of source temperature:

$$\frac{dT_s}{dt} = \beta, \tag{4.19}$$

Evolution of the temperature of the system:

$$\frac{dT}{dt} = [(-\Delta H_v)(k_{b1}LG + k_{b4}OH) + (-\Delta H_c)(k_{a1}S + k_{b2}LG + k_{b3}OH + k_{vc}V)fC_g(T_f - T) + l(T_s - T)]/\bar{C}, \quad (4.20)$$

where f is a volumetric flow-through of a simulated purge or carrier gas stream, W_f is the moisture content of the stream and T_f is the temperature of the stream (taken to be 550 K). ΔH_v is the enthalpy of formation (J g^{-1}) of the volatiles, ΔH_c is the enthalpy of formation of the charcoal, $\bar{C}$ is the weighted overall heat capacity of the system (J g^{-1} K^{-1}), T is the system (substrate) temperature, T_s is the source temperature, and β is the (constant) rate of source temperature increase. The reaction rate constants, k_{xn}, are temperature dependent and given by the formula:

$$k = A\exp(-E_a/RT), \quad (4.21)$$

where A is the pre-exponential factor (s^{-1}), E_a is the activation energy for the reaction (J mol^{-1}), R is the universal gas constant (8.314472 J K^{-1} mol^{-1}) and T is the temperature of the reactants (K). Values for these and other thermal parameters were obtained by Ball *et al*. (1999a) from experimental TGA results presented in the literature and are given in Table 4.1.

Table 4.1: Kinetic parameters used in Ball *et al*. (1999a)

Parameter	**A** (s^{-1})	**E_a** (kJ mol^{-1})	**Enthalpy** (J g^{-1})
k_{a1}	6.7×10^{5}	110	
k_{a2}	2.8×10^{19}	240	
k_{a3}	6.9×10^{22}	220	
k_{b1}	3.2×10^{14}	198	
k_{b2}	1.3×10^{10}	153	
k_{b3}	1.3×10^{10}	145	
k_{b4}	3.2×10^{12}	198	
k_{cv}	1.3×10^{10}	153	
ΔH_c			-1000
ΔH_v			300

4.1.3 Discussion

It can be seen from Table 4.1 that the two reactions with the fastest pre-exponential factors, k_{a2} (Eq. 4.2) and k_{a3} (Eq. 4.3), also have the highest activation energy and are the two key reactions in competition. Once thermolysis and nucleophilic addition have occurred, the subsequent reactions to form either levoglucosan or charcoal are relatively slow and have much lower activation energies. The evolution of temperature in the system (Eq. 4.20) couples the energy exchange between the stream flow and the system, and the source temperature and the system. The enthalpy of formation of charcoal provides energy to the system, whereas the enthalpy of formation of volatiles removes energy from the system. A weighted overall specific heat of the system of gases, charcoal and volatiles is used to convert system energy to system temperature.

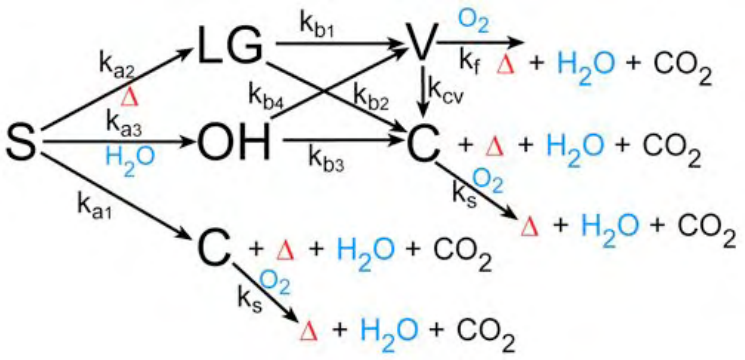

Figure 4.2: Schematic of the thermal degradation model of Ball *et al*. (1999a) extended to include the oxidation of the volatile and charcoal species. It is a three-path, three-step model in which the volatile and charcoal formed in competition oxidise in the process of flaming and glowing combustion respectively.

Ball *et al*. (1999a) found that under conditions in which charcoal formation is promoted, anomalous heating effects would result. Subsequent analysis of the thermal feedbacks in the competitive thermal degradation of cellulose using bifurcation analyses (Ball *et al*. 2004) identified that, in situations where heat and mass transfer in cellulosic fuel are restricted (such as in furnishings, insulation and stock piles), the use of flame retarding treatments which suppress the endothermic volatilisation pathway in favour of the exothermic charcoal formation may in fact increase the risk of flaming combustion. The build-up of heat from the positive feedback in the charcoal formation may overcome the flame retarding capability of the treated fuel and result in the fuel bursting into flame because of the greater reservoir of heat in the fuel.

4.2 An extended, modified zero-spatial dimension thermokinetic model

The Ball *et al*. model was designed specifically to simulate experimental TGA of the thermal degradation only of cellulose fuels under controlled laboratory-like conditions and thus does not include any subsequent oxidation of the thermal degradation products. The aim of this current work was to extend and modify the model to simulate the combustion of the volatiles and charcoal, their contribution to the heat of the system, and the effect of an ambient stream flow (i.e. wind) on the dynamics of the system. The extended model, as with the Ball *et al*. model, is of zero spatial dimension in that the spatial characteristics of the reactions are not taken into account, but does consider the temporal evolution of the reactions.

The primary extension to the Ball *et al*. model undertaken here is that of the secondary reactions describing the oxidation of the volatile and charcoal species produced from the thermal degradation reactions (Fig. 4.2) using rate constants, reaction enthalpies and activation energies obtained from TGA analysis presented in the literature. These processes are more open to the action of the wind than the thermal degradation reactions and thus present a potential for great variation with changes in the flow variables of speed and temperature.

The primary modification to the Ball *et al*. model is removal of the controlled source temperature and its increase rate, β. It is this mechanism that allowed the original model to simulate TGA experiments in which the rate of mass loss of the substrate is correlated to the temperature and rate of increase of the temperature of the substrate. The modification removes the external source and makes the temperature of the substrate a function only of the heat released from reactions within the system. This self-consistent temperature mechanism provides a realistic feedback between the energy released through combustion of thermal degradation products and the formation of those products.

4.2.1 Additional reactions

The additional reactions for the oxidation of the volatile and charcoal species, resulting in the release of considerable heat, are:

$$V + O \xrightarrow{k_f} qW + rG, \tag{4.22}$$

$$C + O \xrightarrow{k_s} sW + tG. \tag{4.23}$$

The impact of these two reactions on the model is to introduce additional sinks to the evolution equations for *V* and *C*, and additional sources for *W* and *G*; *O* represents O_2 as reactant; *G* represents CO_2 as product. The model assumes that O_2 is infinite, or at least not limited, and thus O_2 mass is not tracked. Although this is not realistic, it is not an unreasonable first approximation considering that stoichiometrically oxygen is always available (Beer 1991). The critical aspect of these reactions is the location of the associated heat release. In Equation 4.23 the heat is contained in the fuel strata. In Equation 4.22 the heat is released at some height above the fuel and open to turbulent mixing.

Because there are now two phases of water to be considered—the gas phase water released through combustion in the secondary oxidation reactions and the condensed or bound phase released through dehydration in the charcoal formation reaction—the evolution of water must be split into two, W_g and W_b, and the evaporation of bound phase water to gas phase water must also be included:

$$W_b \xrightarrow{k_{ev}} W_g. \tag{4.24}$$

The term 'bound phase' is used instead of liquid phase as this water may or may not be of sufficient amount to actually form liquid. Generally, it is thought that the bound phase water will exist as individual molecules that remain inside the substrate, rather than free molecules in the atmosphere as is the case with the gas phase water.

4.2.2 Modified evolution equations

The modified equations for the evolution of these quantities are given as:
Modified evolution of cellulose substrate:

$$\frac{dS}{dt} = -k_{a1}S - k_{a2}S - k_{a3}SW_b, \tag{4.25}$$

Evolution of hydrolysed cellulose:

$$\frac{dOH}{dt} = k_{a3}SW_b - k_{b3}OH - k_{b4}OH, \tag{4.26}$$

Modified evolution of volatiles:

$$\frac{dV}{dt} = k_{b1}LG + k_{b4}OH - k_{vc}V - fV - k_fV(1-f), \tag{4.27}$$

Modified evolution of charcoal:

$$\frac{dC}{dt} = nk_{a1}S + nk_{b2}LG + nk_{b3}OH + nk_{vc}V - k_sC, \tag{4.28}$$

Evolution of bound water:

$$\frac{dW_b}{dt} = mk_{a1}S - k_{a3}SW_b + mk_{b2}LG + mk_{b3}OH + mk_{vc}V + f(W_f - W) - k_{ev}W_b, \tag{4.29}$$

Evolution of gaseous water:

$$\frac{dW_g}{dt} = f(W_f - W_g) + qk_fV(1-f) + sk_sC + k_{ev}W_b, \tag{4.30}$$

Modified evolution of gases:

$$\frac{dG}{dt} = pk_{a1}S + pk_{b2}LG + pk_{b3}OH + pk_{vc}V - fG + rk_fV(1-f) + tk_sC, \tag{4.31}$$

where all variables are as previously defined and *q*, *r*, *s* and *t* are product parameters.

Initially it was thought that a single temperature evolution equation could be used but it became apparent through testing of the model that this approach was unsuitable due to the separation of the fuel phases. A dual, coupled temperature system, consisting of a substrate temperature for solid phase reactions (T_s) and gas or vapour phase temperature for gas phase reactions (T_v) (Weber 1991b; Búcsi and Rychlý 1992; Nelson 1998) was constructed:

$$\frac{dT_s}{dt} = (q1 + q2 + q4 + q5 + \epsilon_s f(T_a - T_s) + \zeta(T_v - T_s))/\bar{C}_s, \tag{4.32}$$

$$\frac{dT_v}{dt} = (q3 + \epsilon_g f(T_a - T_v) - \zeta(T_v - T_s))/\bar{C}_g, \tag{4.33}$$

where $q1$, $q2$, $q3$, $q4$ and $q5$ are the reaction enthalpies given below, T_a is the temperature of the ambient stream flow (i.e. the wind temperature), ϵ_s is a coupling factor between the ambient stream flow and the solid phases, ϵ_g is a coupling factor between the ambient stream flow and the gas phases, ζ is a coupling factor between the gas phase temperature and solid phase temperature, $\bar{C}_s$ is the weighted overall specific heat of the solid phases, and $\bar{C}_g$ is the weighted overall specific heat of the gas phases:

$$\bar{C}_s = 1.38(S + LG + OH) + 4.183W_b + 0.67C, \tag{4.34}$$

and

$$\bar{C}_s = 1.01(1 - (V + G + W_g)) + 1.1(V + G) + 2.02W_g, \tag{4.35}$$

where it is assumed that air is the dominant species.

Reaction enthalpies are:

Heat of formation (volatiles):

$$q1 = -\Delta H_v(k_{b1}LG + k_{b4}OH), \tag{4.36}$$

Heat of formation (Charcoal):

$$q2 = -\Delta H_c(k_{b2}LG + k_{b3}OH + k_v cV), \tag{4.37}$$

Heat of combustion (volatiles)–flames:

$$q3 = -\gamma\Delta H_f k_f V, \tag{4.38}$$

Heat of combustion (charcoal)–glowing:

$$q4 = -\Delta H_s k_s C, \tag{4.39}$$

Heat of vaporisation of bound water:

$$q5 = -\Delta H_w k_{ev} W_b, \tag{4.40}$$

where H_x are the enthalpies of formation and combustion for the various reactions. Values for these and the other reaction constants are given in Table 4.2. γ is a heat transfer coefficient from the flames to the solid phase and represents the net heat flux transferred to adjacent uncombusted fuel. The ζ, ϵ and γ coefficients are parameters which can be varied to explore various effects and range: ζ: $0 \rightarrow \infty$, ϵ: $0 \rightarrow 1$, γ: $0 \rightarrow 1$. Of the original set of ODEs, Equation 4.13 alone remains unmodified.

Table 4.2: Additional kinetic and thermal parameters used in the extended thermokinetics model developed here.

Parameter	A (s^{-1})	E_a (kJ mol^{-1})	Enthalpy (J g^{-1})	Reference
k_f	2.55 $\times 10^{13}$	188		Parker and LeVan (1989)
k_s	1.4 $\times 10^{11}$	183		Eghlimi *et al*. (1999); Branca and di Blasi (2004)
k_{ev}	3.41 $\times 10^{4}$	42		Sexton *et al*. (2001)
ΔH_f			-14000	Parker and LeVan (1989)
ΔH_s			-32000	Eghlimi *et al*. (1999); Branca and di Blasi (2004)
ΔH_w			2272	Sexton *et al*. (2001)

4.2.3 Discussion

When γ = 1, all the energy liberated through flaming combustion contributes to the immediate heating of the fuel substrate. This treatment of the fuel, in which the heat received is assumed to have an immediate effect on the fuel (i.e. there is no time allowed for heat to conduct into the fuel element) is termed the thermally-thin approximation. In

the case of grass fuels, such as those discussed in Chapter 3, where the diameter of a fuel element is in the order of 0.2–0.5 mm, this approximation is valid.

However, in reality turbulent diffusion flames will transfer only a small quanta of the total heat of combustion from flames to the fuel. The action of buoyancy through convection and radiation will act to distribute the heat released from this source away from nearby fuel. While there exist a number of methods of determining the radiant heat flux from flames (e.g. Lockwood and Shah (1981); Raithby and Chui (1990); Baum and Mell (1998); Consalvi *et al*. (2002); Knight and Sullivan (2004)), this task is outside the scope of this current work. In the same manner, heat from adjacent burning fuel should be included in the heat flux of the fuel substrate (Eq. 4.32) but for the sake of simplicity this is not considered here; that is, the zero dimensional model considers the combusting fuel element receives heat from adjacent burning fuel elements sufficient to raise it to combustion temperature.

For completeness it may be argued that Equations 4.29 and 4.30 should include a term representing the condensation of gaseous water back into liquid form. The role of condensation of water has long been known to be important in the onset of spontaneous combustion in cellulosic stocks such as hay bales, bagasse and coal (Stott 1960; Gray *et al*. 1984, 2002) but as this is only important when piloted ignition is not present, it is not considered here.

The extended and modified dynamical model described in this section provides the basis for numerical experiments in which initial values of primary variables and parameter values can be changed to simulate a range of numerical experimental conditions. The model can also be used to investigate the effect of various combinations of simulation conditions. It consists of 10 primary variables, 14 secondary variables and 4 key parameters, the quantities of which are normalised such that they range $0 \rightarrow 1$. This allows simplified mass comparisons to be made, although it removes any simple physical interpretation from parameters such as wind flow, heat transfer or coupling coefficients.

It is incumbent upon anyone employing a model to establish that the conditions and parameter space are valid for the purpose of the simulation and its applicability to real world conditions. In the case of this model, however, due to its construction, being zero spatial dimensional, it is difficult place this model into a real-world context that will allow it to be validated against real-world experiments.

While it is hard to visualise a zero-spatial dimension model that involves mass, a suitable approximate representation is that of a very small element of negligible size but which is large enough to interact with its environment. In this way, the fuel element can thermally degrade, release volatiles into the region above it, and be affected by the passage of ambient air over it. The reliance upon rate constants obtained from TGA experiments published in the literature provides a solid basis for the simulation results that replicate a controlled laboratory experiment of the burning of a cellulose sample.

The remainder of this chapter and the following chapter detail a number of numerical solutions to the model that represent a number of numerical experiments to investigate the effect of thermal and chemical feedbacks in the thermal degradation and combustion of cellulose. While not directly applicable to the situation of a freely burning bushfire spreading through heterogeneous fuel, it will provide an insight into the chemical and physical processes involved in the thermal degradation of those fuels.

4.3 Numerical solutions

4.3.1 Numerical solver

The set of equations were solved using XPPAuto v5.91 (Ermentrout 2002)[2]. The equations were compiled into an XPP ODE file (see Appendix 2.1) and solved using the stiff differential equation solver method (tolerance 0.001, minimum step 1×10^{-12}) for a variety of initial conditions. The variation of these conditions, primarily model parameters, constitute numerical experiments with the model and are used to explore the role of f in determination of the primary reactions.

4.3.2 Initial conditions

The set of basic initial conditions for the solutions of the set of ODEs are given in Table 4.3. Values for the stoichiometry constants are based on the complete conversion of, in the case of volatiles, $C_6H_{10}O_5$ to CO_2 and H_2O, and in the case of charcoal, $2\,C_{11}H_4$ to CO_2 and H_2O.

4.4 Sample numerical experiment: zero wind, zero moisture

4.4.1 Initial substrate temperature and substrate mass loss

The simplest scenario to illustrate the function of the model is to consider no wind ($f = 0$), no moisture ($w_b = 0$) and matched initial substrate (solid phase) and gas phase temperatures ($T_s(0) = T_v(0)$). Figure 4.3 (p. 73) shows the evolution of S and T_s for a range of initial temperatures (480 K – 580 K). Below about 520 K the reactions occur so slowly that essentially the system is non-reactive, i.e. although there is mass loss as the reactions consume substrate, there is little change in the substrate temperature. Below 480 K there is very little change in substrate mass or temperature over the period considered here (1500 s). Between 540 – 550 K the system undergoes a gradual increase in the reaction rates, resulting in the steady loss of substrate mass through conversion to volatiles and charcoal. Above 550 K, the reaction rates increase, resulting in the rapid loss of substrate mass in the formation of volatiles and charcoal which then ignite causing an extremely rapid increase in system temperature[3], in the order of $\simeq 1900\,\mathrm{K\,s^{-1}}$. The time of the occurrence of this rapid increase in system temperature is used in subsequent discussions to define the time of ignition of the system.

As the initial temperature of the system is increased the rates of these reactions increases markedly, illustrating the sensitivity of the reactions to changes in temperature. The time taken for the substrate to be consumed (or at least to become arbitrarily extremely small since it can never reach a value of zero) in this numerical experiment is

[2]XPPAuto is a Unix freeware program, developed by Bard Ermentrout, designed to solve differential and other equations (http://www.math.pitt.edu/∼bard/xpp/xpp.html). The name is short for X (Unix) Phase Plane and incorporates a number of solver routines for differential equations and can carry out bifurcation analysis (Auto).

[3]This extreme rapid increase in system temperature and rapid loss of substrate mass also caused problems for the numerical solver (evidenced by sudden ceasing of the simulation in some cases) but, as the onset of ignition was generally all that was required for the numerical simulations, this was not a significant problem (although it proved to be symptomatic in the computational fluid dynamics modelling in a later chapter).

Table 4.3: The basic set of initial conditions for solution of the extended thermokinetic model.

Variable	Symbol	Initial Value
Substrate	S	1
Levoglucosan-end	LG	0
Hydrolysed cellulose	OH	0
Volatile	V	0
Charcoal	C	0
Gases	G	0
Bound water	W_b	0
Water vapour	W_g	0
Solid phase temperature	T_s	580 K
Gas phase temperature	T_v	550 K
Ambient temperature	T_a	300 K
Stream flow (wind speed)	f	0
Time step	dt	0.1 s
Stoichiometry constants	m	0.44
	n	0.42
	p	0.14
	q	0.75
	r	0.25
	s	0.93
	t	0.07
Coupling constants	ϵ_g	0.01
	ϵ_s	0.01
	ζ	1
Heat transfer coefficient	γ	1

highly non-linear in initial substrate temperature, ranging from $\simeq$ 220 s at 580 K, $\simeq$ 890 s at 560 K, to about 1821 s at 550 K. As initial temperature is further increased, the time taken to consume the fuel is further shortened. This suggests that there is an interaction between the reactions, particularly the high-energy-release oxidation reactions, as the initial substrate temperature increases.

Figure 4.4 (p. 74) shows a graph of substrate mass versus substrate temperature. For initial substrate temperatures $\geq$ 520 K, the fuel eventually reaches ignition, however the time take for this to occur varies greatly. At an initial temperature of 540 K, it takes $\simeq$ 5000 s to achieve ignition; at 520 K, it takes $\simeq$ 30,000 s. Below 520 K, a simulation period of 400,000 s showed that the substrate temperature eventually decreased with relatively little loss in mass as the reaction rates reduced accordingly.

4.4.2 Effect of temperature coupling coefficient

When the initial temperatures of the substrate and gas phases are not matched (i.e. $T_s(0) \neq T_v(0)$), the coupling between the two quantities becomes important. Figure 4.5 (p. 74) shows the same experimental conditions as Figure 4.3a except the initial temperature of the gas phase has been held at 550 K; the temperature coupling constant, ζ is set to 1 to provide coupling between the solid and gas phase temperatures. Simulations where initial $T_s < T_v$ have increased reaction rates. Simulations where initial $T_s > T_v$

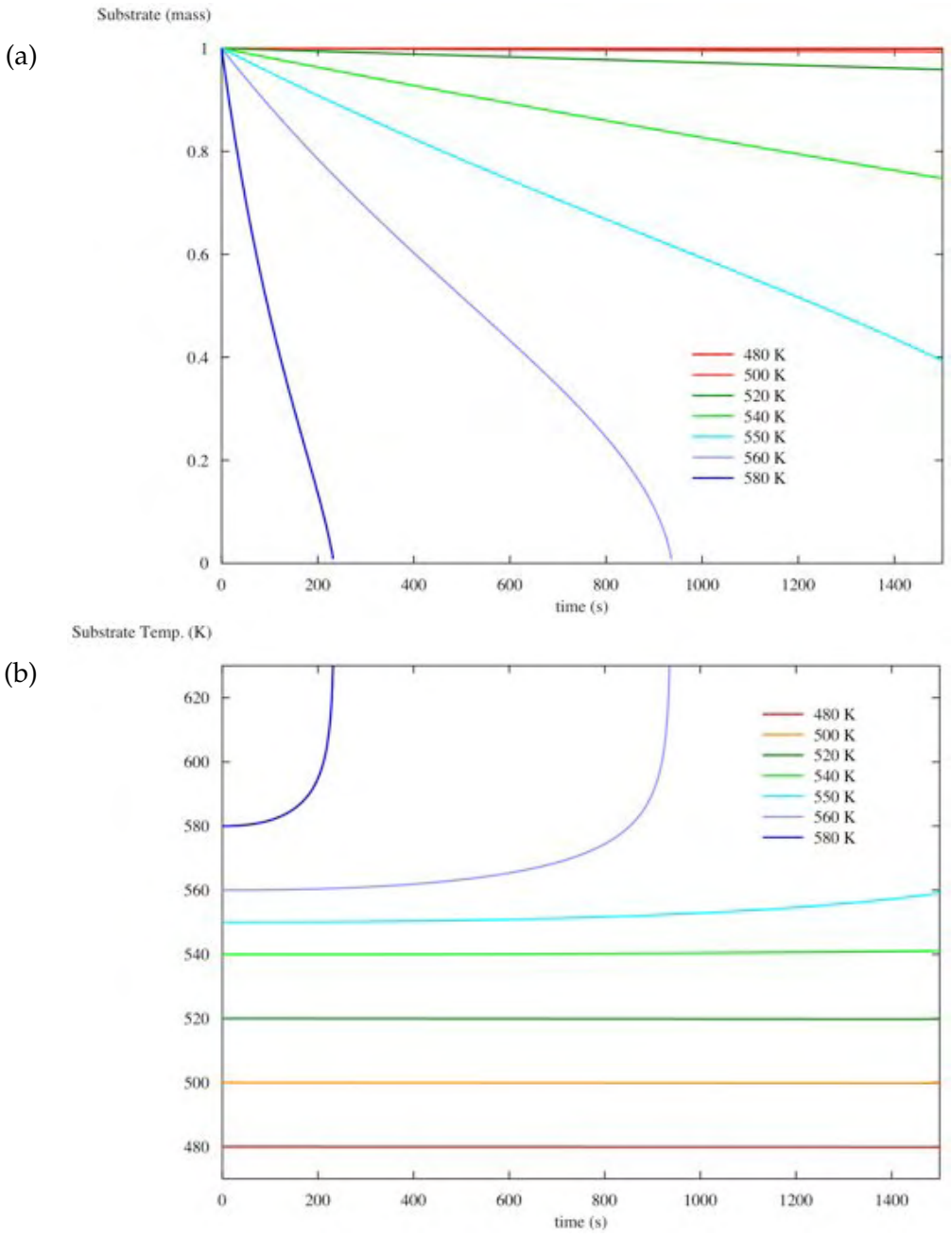

Figure 4.3: The evolution of (a) fuel substrate mass (S) and (b) solid phase temperature (T_s) for a range of matched initial solid and gas phase temperatures. Above about 540 K, the rate of loss of mass and increase of solid phase temperature increases markedly indicating that ignition of the fuel has occurred.

have decreased reaction rates (i.e. time for complete consumption at 580 K now $\simeq$ 520 s (*c.f.* 230 s), 560 K now $\simeq$ 1200 s (*c.f.* 890 s)). For all subsequent numerical experiments, T_v will be set to 550 K.

The effect of the temperature coupling coefficient, ζ, was examined using $T_s = 580$ K and ranging ζ: $0 \rightarrow 10000$ (Fig. 4.6, p. 75). Any degree of coupling between T_s and T_v is relatively robust, resulting in very little variation over the range. It is only when the two quantities are decoupled ($\zeta = 0$), that the result of the model is significantly

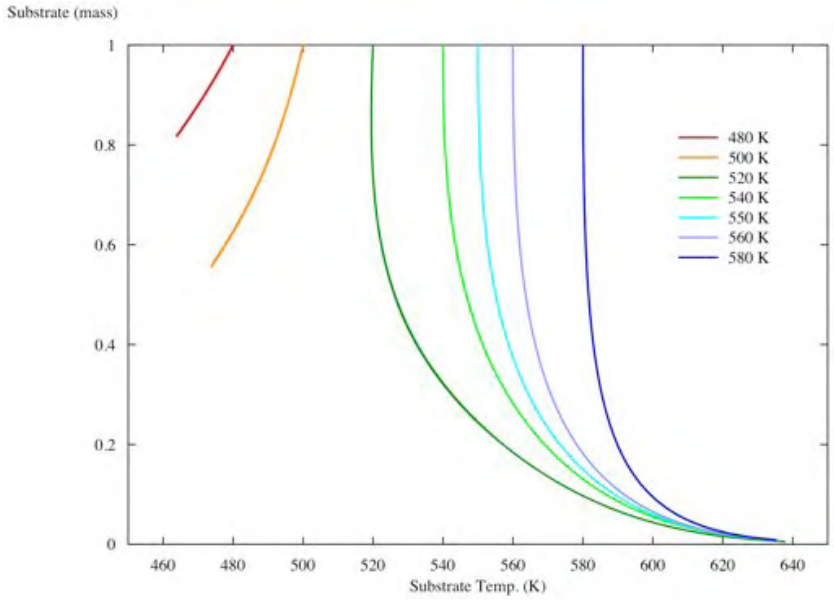

Figure 4.4: Fuel substrate mass (S) versus substrate temperature (T_s) for a range of initial substrate temperatures. For initial substrate temperatures $\geq$ 520 K, the system eventually reaches ignition, however the time taken for this to occur varies greatly.

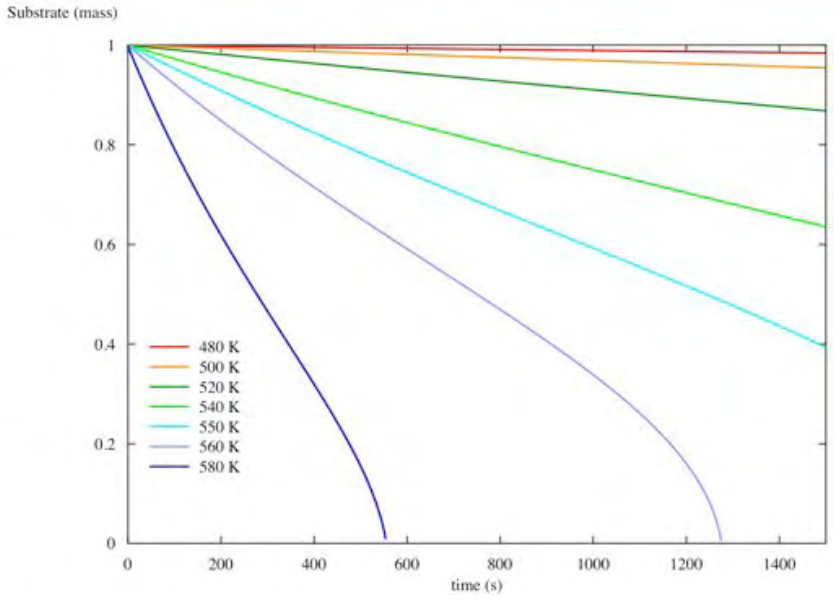

Figure 4.5: The evolution of fuel substrate mass (S) for an initial gas phase temperature of 550 K and different initial solid temperatures. In comparison with Figure 4.3a, reaction rates below 550 K have increased and reaction rates above 550 K have decreased.

changed. The relative insensitivity to changes in positive values of ζ is due to the close initial values of T_s and T_v. At more extreme differences between the two quantities, ζ would have a greater effect; however, the increased difference between the temperatures (for example, with T_v close to ambient values) would mean that the reaction rates would be very much reduced and the thermal degradation and combustion processes would cease. This suggests that the rate of the process $\zeta(T_v - T_s)$ is already comparable to the other rates in the thermal balance at $\zeta \simeq 0.1$. For the remaining experiments $\zeta = 1$.

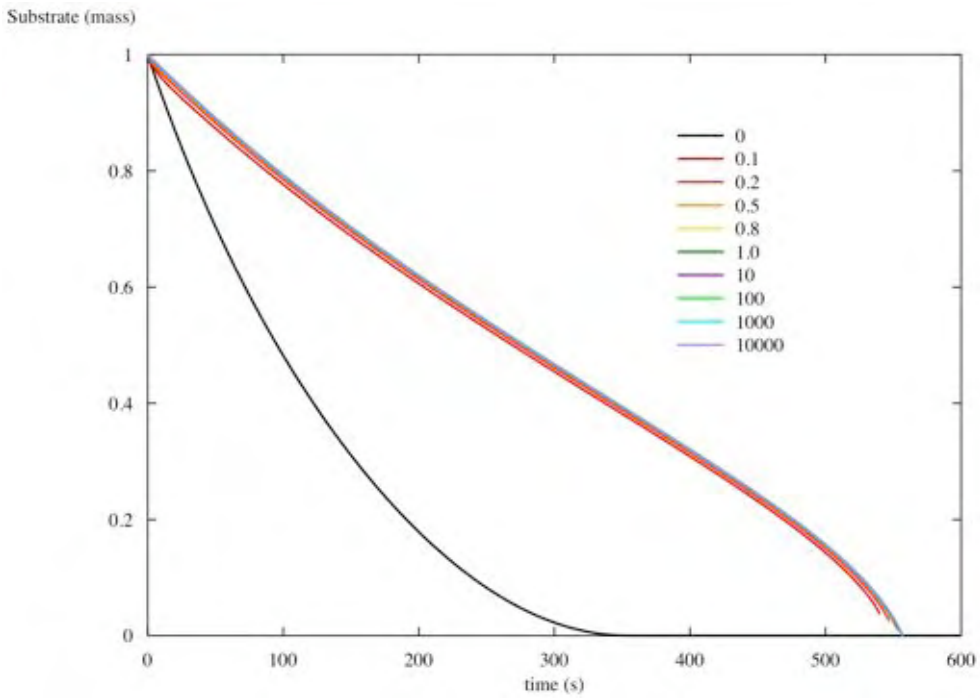

Figure 4.6: Evolution of substrate mass (S) for an initial gas phase temperature of 550 K and initial substrate temperature of 580 K for a range $0 \rightarrow 10000$ of the temperature coupling coefficient ζ.

4.4.3 Effect of initial temperature on *LG* and *OH*

Increased initial temperature results in an increase in the reaction rates of the system and an increase in the mass loss rate of the substrate. This lost mass is converted, as per the reaction equations above, to hydrolysed cellulose *(OH)* or levoglucosan-end fragments *(LG)*. These can then undergo further reactions to form charcoal *(C)* or volatile *(V)*. Figure 4.7 (p. 76) shows the effect of the range of initial temperatures on the production of *LG* and *OH* by mass. It can be see that due to the dry conditions ($W_b = 0$) the rate of production of *LG* is far in excess of the production of *OH*, by a factor of 30 in the case of the 580 K run. (The hooks at the end of the higher initial temperature runs are a result of the production of *LG* ceasing when the substrate has been consumed and *LG* itself is being consumed through conversion to *V*). The increase in production of *LG* and *OH* is highly non-linear with temperature.

4.4.4 Effect of initial temperature on *V* and *C*

The conversion of *LG* and *OH* to *V* and *C* is the next step in the reaction pathway (Fig. 4.8, p. 77). While the production rates appear similar, both increasing non-linearly with increasing initial temperature, *V* is produced in excess of *C* by a factor of more than 4.5 in most cases due to the greater amount of *LG* present. The difference in ratio of *V*:*C* and *LG*:*OH* is because there is no competition for the formation of *V* over *C* as there is in *LG* over *OH* and thus is a function only of the differences in the reaction rates.

(a)

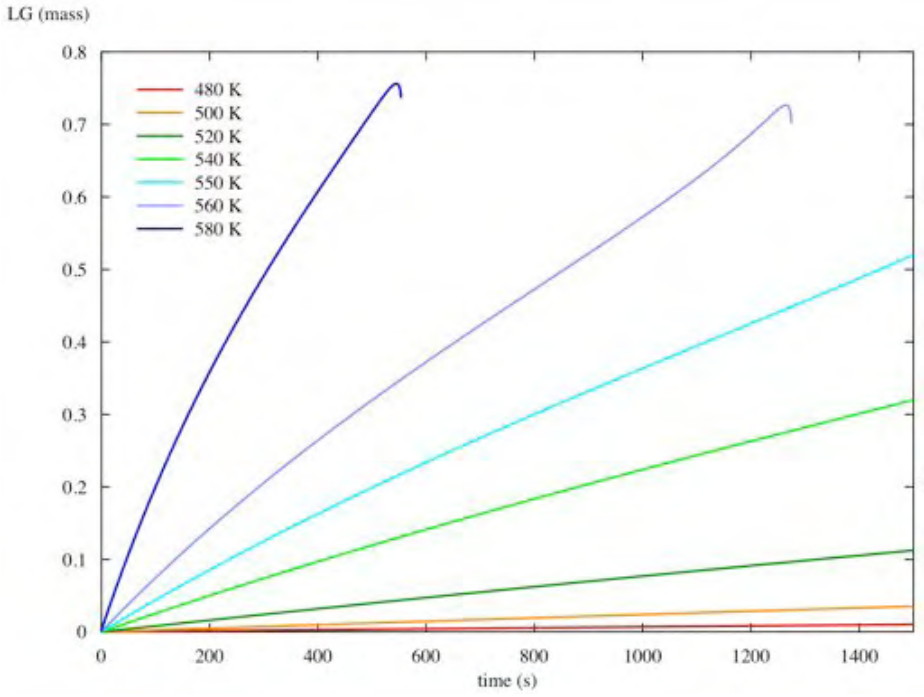

(b)

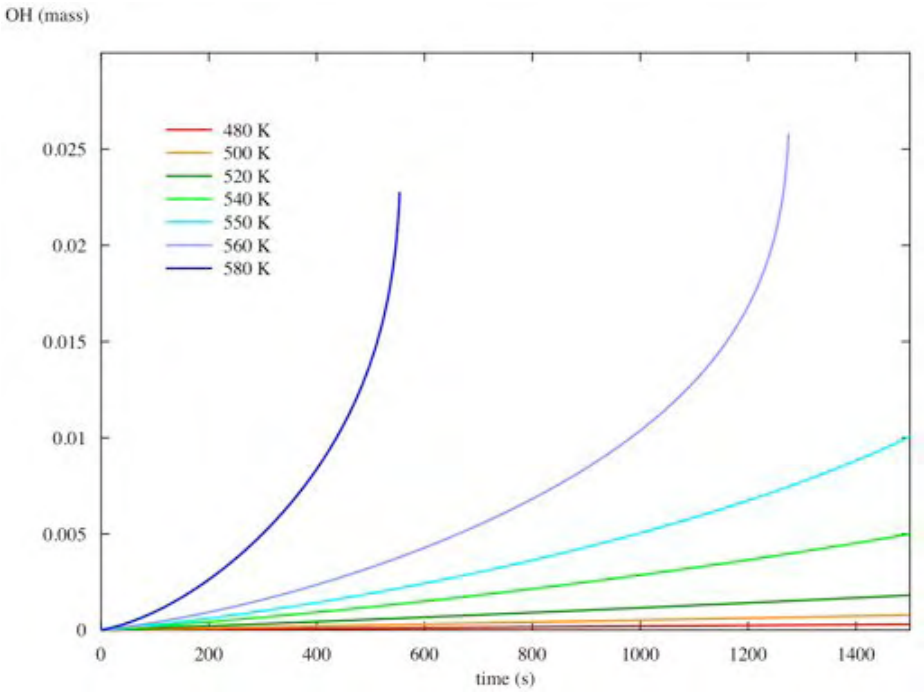

Figure 4.7: The evolution of (a) *LG* and (b) *OH* with change in initial substrate temperature. As initial temperature increases the reaction rates for both species increases. However, *LG* is produced in excess of *OH* due to the dry initial conditions, which promotes the intra-molecular nucleophilic addition over inter-molecular nucleophilic addition via water.

4.4.5 Effect of initial temperature on system energy

The production of the various species drives the consumption and production of heat in the system which in turn drives the temperature of the system and the rates at which the species are produced. Figure 4.9 (p. 78) shows the total heat produced in the system (i.e. system energy) for the range of initial temperatures. For all initial temperatures below

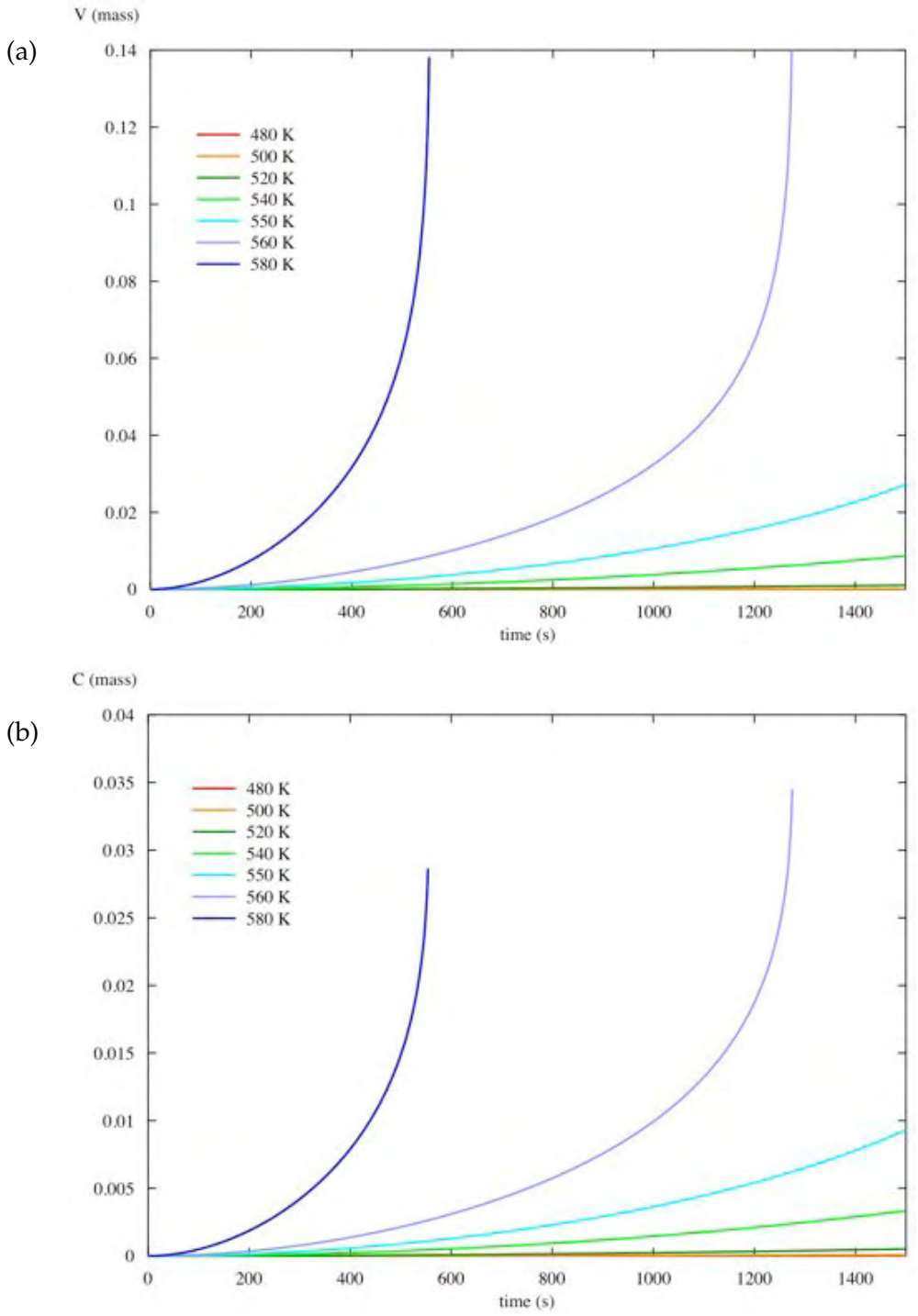

Figure 4.8: The variation of (a) *V* and (b) *C* by mass with changes in initial substrate temperature. Both species follow similar curves but *V* is produced in excess of *C* to due the greater source of *LG*. As initial temperature increases, the reaction rates for production of both species increases.

550 K, the net heat in the system remains at about zero and, while the substrate is being consumed, the system appears to be pretty much in 'quasi' equilibrium. However, if we consider the individual reaction enthalpies for the formation and combustion of *V* and *C* (Fig. 4.10, p. 79), we can see that the appearance of quasi-equilibrium is a result of the matching of the endothermic and exothermic reactions. When the system reaches a point that becomes overtly exothermic (i.e. when the system ignites), the heat in the system increases dramatically.

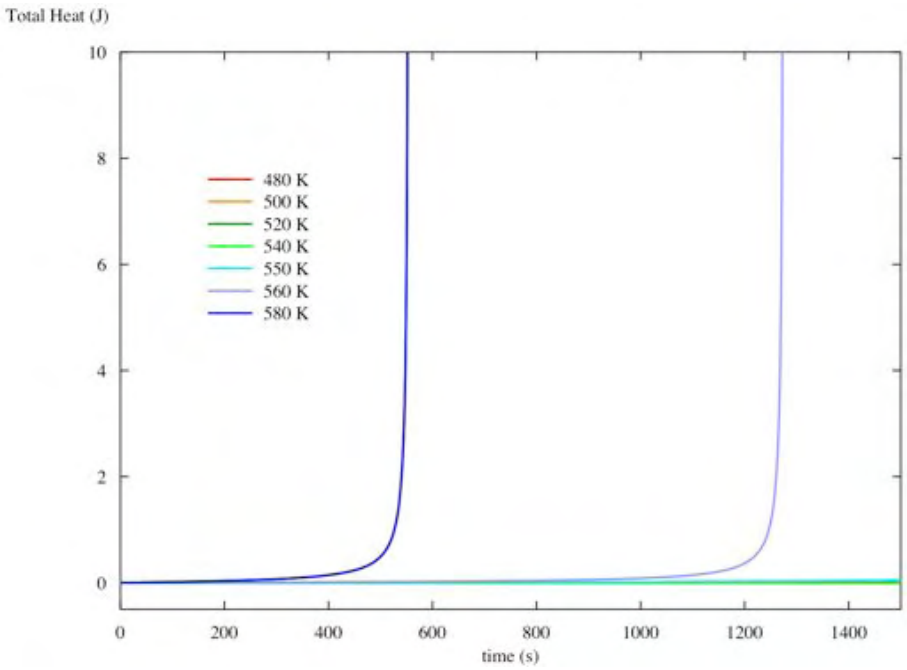

Figure 4.9: The evolution of total heat of the system for an initial gas phase temperature of 550 K and different initial solid temperatures. Total heat is the net sum of all heats of production and combustion of V and C. For all initial temperatures below 550 K, the total heat of the system remains at zero and the system remains unignited. Ignition only occurs here for initial temperatures of 560 K and 580 K.

4.5 Conclusions

A dynamical thermokinetic model of the competitive thermal degradation of cellulose based on the principles of the conservation of mass and energy was obtained from the literature. This model (Ball *et al*. 1999a) was designed to replicate the thermogravimetric mass-loss experiments commonly used to determine reaction rate constants. Parameters for heating rate, purge gas flow rate, purge gas moisture content, and reaction yields were included.

The model is based on a modified Broido-Shafizadeh mechanism for the competitive thermal degradation in which the substrate undergoes a non-mass-losing reaction following thermolysis and nucleophilic addition, either by a water molecule forming hydrolysed cellulose or an intramolecular -OH radical forming levoglucosan-end cellulose. These then undergo further cross-linking or depolymerisation reactions to form charcoal or volatile (levoglucosan). Activation energies and rate constants for the reactions were obtained from experimental results given in the literature. The model was used to explore the presence of limit cycles in the competing reactions and bifurcations in the mass-loss/system temperature phase space.

In this chapter, the model of Ball *et al*. was extended to include secondary reactions comprising oxidation of the primary products, charcoal and volatiles. The oxidation reactions result in glowing combustion in the case of charcoal and flaming combustion in the case of volatiles. Unlike the thermal degradation reactions and the glowing combustion of charcoal which are either solid phase or gas-solid interface reactions, the flaming

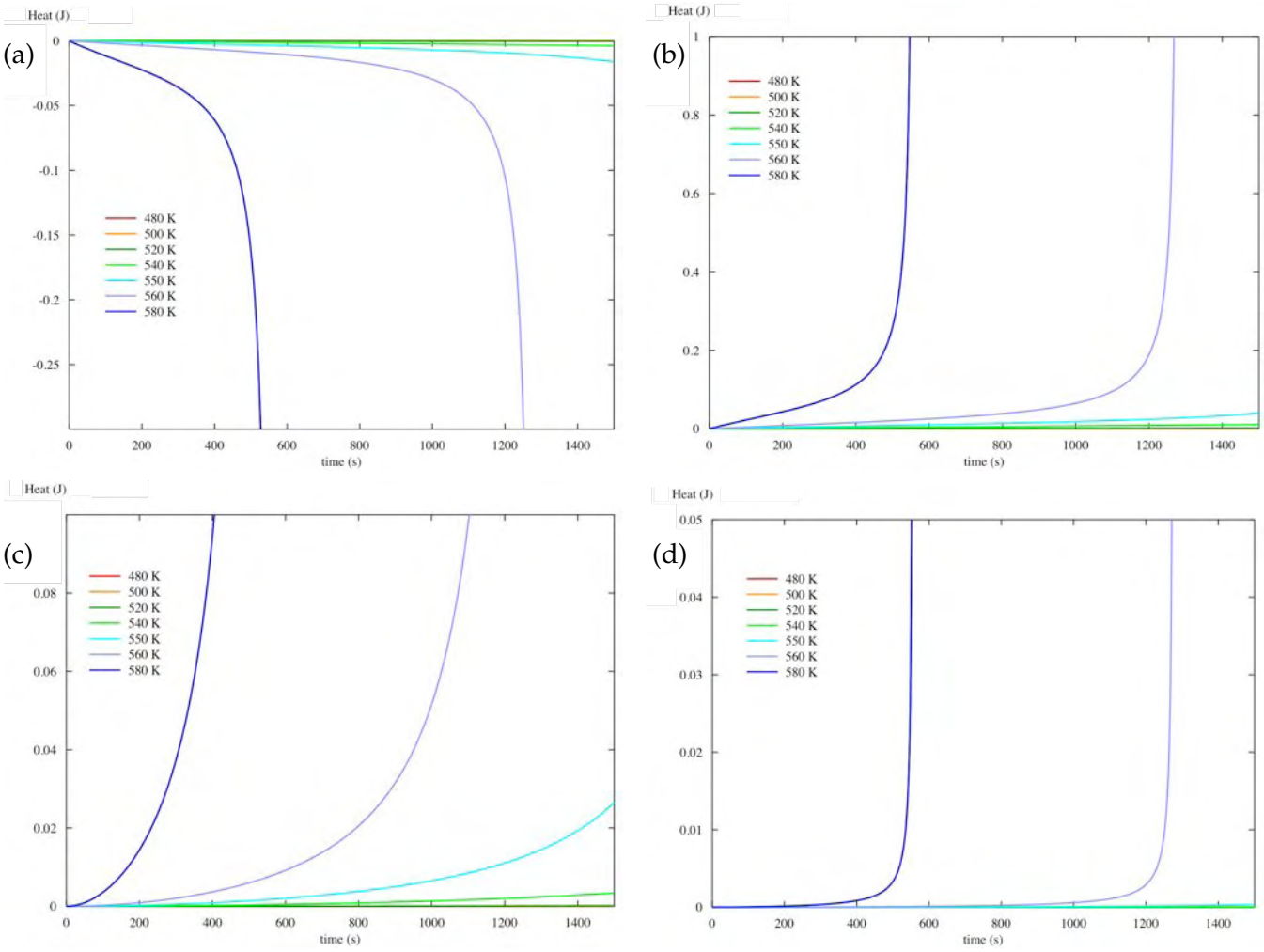

Figure 4.10: The evolution of heat from (a) formation of V, (b) formation of C, (c) combustion of V and (d) combustion of C for an initial gas phase temperature of 550 K and different initial solid temperatures. Reaction rates increase above 540 K, where ignition occurs. The heat deficit from volatile formation is compensated by the heat liberated from the formation of C and combustion of V and C.

combustion of the volatiles is solely a gas-phase reaction. As a result, the single system temperature of the original model had to be modified to two coupled temperatures, one for the solid phase substrate and one for the gas phase, in order to allow the wind flow (parameter f) affect the two phases differently. A result of this is that gas-phase reactions can occur at rates different to that of the solid-phase. Coupling parameters are then used to link the temperatures of the substrate and gas phase.

The model has zero spatial dimension and thus cannot fully simulate the spatial aspects of the full complement of reactions, in particular those involving the transfer of heat. The thermally-thin approximation is made in regard to the rate at which heat is taken up by unburnt fuel, resulting in no lag in the time it takes heat to penetrate a fuel, an approximation that is valid for fine fuel such as grass. While the model cannot hope to replicate the combustion of fuel in reality, it can be used to explore aspects of the thermal degradation of cellulosic fuel.

A sample experiment in which no wind or initial moisture content are present is used to illustrate the utility of the model. The effect of the coupling parameters is investigated and a standard set of operating values selected.

The rate of mass loss of the substrate is seen to increase with initial substrate temperature. A critical substrate temperature is identified for a given set of initial conditions below which the thermal degradation reactions peter out and the reaction stops. When the initial substrate temperature is well above the critical value, the rate of thermal degradation reactions increase to the point where the secondary reactions become significant and the products ignite. When the initial substrate temperature is just above the critical temperature, the rate of the reaction of the system increases slowly until either the substrate is consumed or the system ignites.

In the following chapter, the effects of ambient wind flow, initial moisture content and temperature of ambient wind flow are explored.

Chapter 5

Dynamical thermokinetic numerical experiments

The dynamical thermokinetic model introduced in Chapter 4 is used in a number of numerical experiments to explore the role of initial moisture, wind speed and wind temperature in the competitive thermal degradation process. The model is further modified to explore the effect of an unsteady sinusoidally-varying air flow. The results show that the temperature of the wind plays a critical role in determining the dominance of either the volatile or charcoal formation processes in the thermal degradation of cellulosic fuel.

A fire breaks out at the local university and quickly spreads across the campus. In the School of Engineering, the gathered engineers quickly realise they have to put water on the fire or the whole building will be destroyed. They make some rather hasty back-of-the-envelope calculations on the amount of water they need and, as luck would have it, manage to save everyone but end up using way too much water and destroy the whole building in the process.

In the nearby Applied Mathematics Department, the applied mathematicians, using a brand-new UFWT (Ultra fast wavelet transform) technique, calculate with a high degree of accuracy the amount of water required to extinguish the fire. They save everyone in the building as well as the building itself. When the fire brigade finally arrive, they are very impressed.

However, the Pure Mathematics building, which was right next door, burnt to the ground with the loss of all lives inside. A detailed investigation found that in the first few minutes of the fire the pure mathematicians discovered a very simple proof for the existence of an exact solution to the amount of water needed but then wasted three hours trying to prove unicity while the building burnt down around them.

5.1 Introduction

Ball *et al.*'s (1999a) thermogravimetric model of the thermal degradation of cellulose was extended and modified to include the secondary oxidation of thermal degradation products (charcoal and volatiles) in Chapter 4. The model, comprising 10 primary variables, 14 secondary variables and 4 key parameters, allows numerical experiments to be car-

ried out in which initial conditions of primary variables and parameter values can be changed to simulate a range of experimental conditions.

The primary variables that are investigated here are initial moisture content and wind (primarily strength but also temperature). In the first instance in this chapter the effects of changes to the initial values of these two variables are investigated separately before being investigated in combination.

It is recognised, however, that wind is rarely, if ever, constant. The final numerical experiment investigates the effect of a modification to the thermokinetic model in which wind is made to vary sinusoidally around a mean value. Although sinusoidally-varying wind is just as rare in reality as constant wind, the effect of a simple inconstant wind speed on the reaction kinetics as a first approximation to the time-dependent, chaotic, quasi-periodic (i.e. turbulent) flow provides an insight into the way the combustion chemistry is affected by non-steady conditions.

For the most part, the effects that are investigated are:

- substrate mass loss;
- mass changes (formation and consumption) of levoglucosan-end cellulose (*LG*), hydrolysed cellulose (*OH*), volatiles (*V*) and charcoal (*C*); and
- change in heat of the system (total, reaction enthalpies (formation, oxidation, vaporisation)).

The basic conditions for the numerical experiments are those derived from the initial experiments in Chapter 4: initial gas phase temperature of 550 K, solid phase substrate temperature of 580 K, gas-solid temperature coupling coefficient of 1, and Δt = 0.1 s.

Refer to Table A1.1 (p. 187) for a list of symbols and associated equation numbers frequently used in this Chapter. Those symbols not listed are used infrequently and defined in the text.

5.2 Initial moisture, zero wind

The primary role of bound moisture in the system reactions is to extract heat through evaporation from the energy of the system. Bound water also plays a role in the promotion of the formation of hydrolysed cellulose and charcoal at the expense of the formation of levoglucosan-end cellulose and volatiles. The following section explores the effect of moisture on a variety of system variables with no wind (i.e. f = 0).

5.2.1 Effect on water

The two roles of bound water in the model are controlled by the activation energies of the key reactions. Figure 5.1a shows the evolution of an initial amount of bound water equivalent to 0.1 substrate mass (i.e. 10%) with changing system (i.e. substrate and gas phase temperature, T_s and T_v) over the range 300–550 K. The rate of loss of water increases with increasing system temperature, as is to be expected. At 350 K, the system is approaching the boiling point of water. At and above 400 K the majority of water boils off rapidly.

Figure 5.1b shows the corresponding evolution of gas phase water vapour, W_g. The rate of increase of W_b increases with system temperature to a maximum of 0.1, the value of the initial bound water mass. However, as the system temperature approaches the

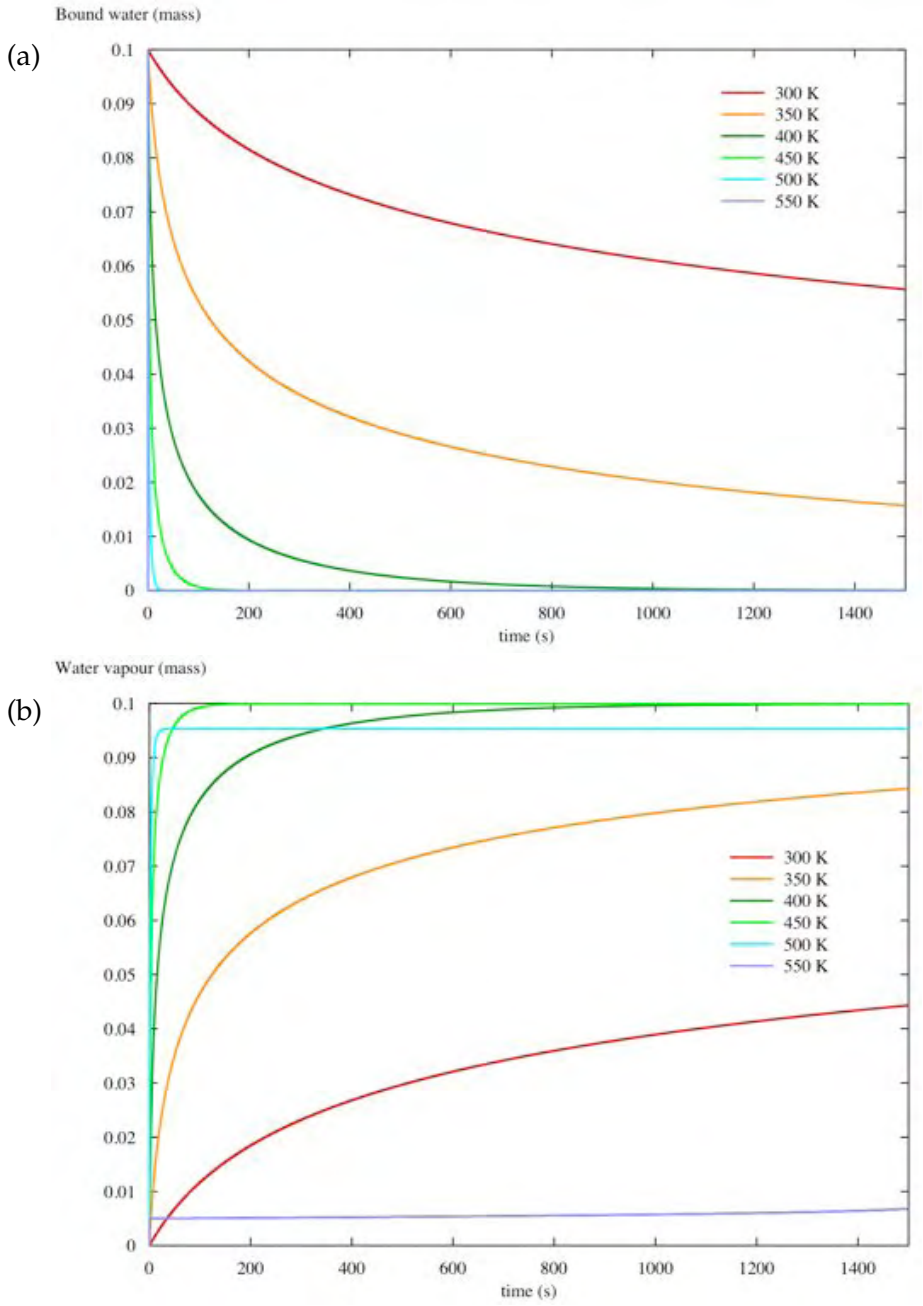

Figure 5.1: The effect of initial system temperature on (a) the evolution of initial bound moisture, $W_b = 0.1$ and (b) the associated evolution of gas phase moisture, W_g. System temperature ranges 300–550 K. Below 400 K, the rate of evaporation of water is slow. Above 500 K water is removed from the system almost instantaneously but less than 10% is converted to W_g.

temperature of ignition of the system, less of the bound water is evaporated to gas phase water. At $T = 500$ K, less than 10% of the initial bound water is converted to water vapour. The question of where the missing water went is answered by considering those reactions for which the activation energies are achieved at these elevated temperatures.

5.2.2 Effect on substrate mass

Figure 5.2 shows the evolution of the substrate mass under these conditions. As would be expected from the results of Chapter 4, under conditions in which the system has not

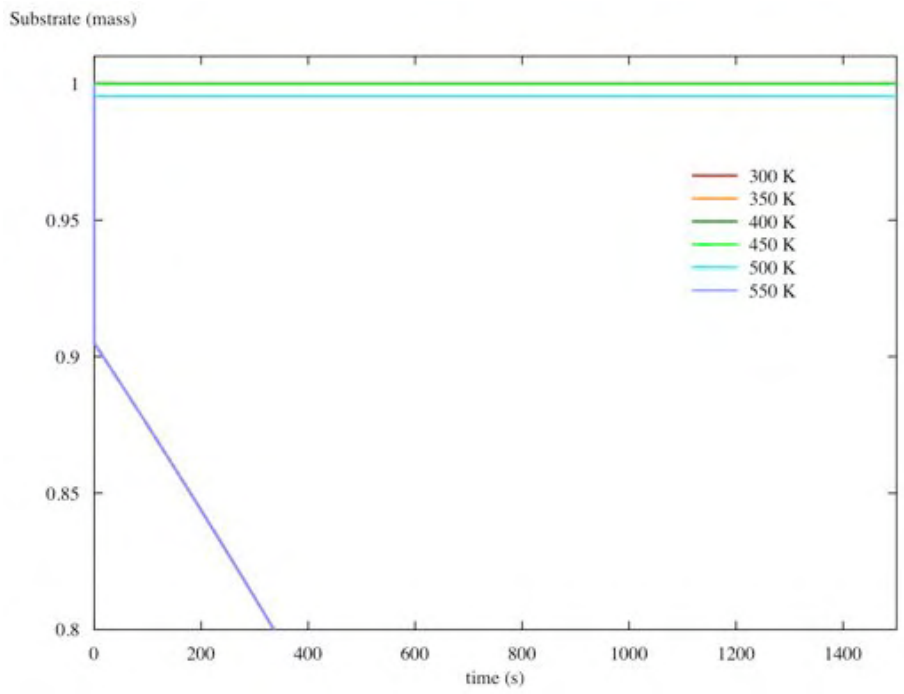

Figure 5.2: The effect of initial system temperature on the evolution of substrate mass with an initial bound water amount of $W_b = 0.1$ Below 500 K, little effect is evident on substrate mass. As the combustion reactions initiate at system temperatures above 500 K, the rate of substrate consumption increases. The effect of initial bound water is to, somewhat counter-intuitively, decrease the time taken for the substrate to be consumed.

ignited (i.e. T_s ¡ 540 K) there is little to no consumption of substrate mass due to the extremely low rates of reaction for the key thermal degradation reactions. At a temperature of 550 K, where the thermal degradation reactions begin to have effect, there is a rapid, almost instantaneous, reduction in the mass of substrate by an amount just less than 0.1 before the rate of consumption moderates, resulting in an overall decrease in the time to complete consumption of substrate when compared to the $W_b = 0$ case.

This is somewhat counter-intuitive; an increase in the amount of bound water in the system *decreases* the time for the substrate to be consumed. The accepted understanding of the influence of moisture on combustion is that increased moisture will slow or even halt combustion. While it appears in this figure that the initial substrate mass is reduced by the amount of bound water in the system, the reduction in substrate mass is a consequence of the initial and rapid conversion of the substrate to hydrolysed cellulose mass with the catalytic presence of moisture.

5.2.3 Effect on *OH*

As seen above, the effect of initial bound moisture at sub-ignition temperatures has little impact on the thermal degradation reactions. However, as the temperature increases above 500 K, the moisture becomes involved in the thermal degradation reactions, primarily in the catalytic conversion of *S* to *OH* (Fig. 5.3). Once the thermal degradation reactions commence at temperatures in excess of 540 K, the presence of moisture is very short lived ($t \simeq 0.1$ s), almost totally consumed in the formation of *OH*, driven by the very high rate constant for the hydrolysed cellulose formation reaction (i.e. $6.7{\times}10^{22}$ s^{-1}).

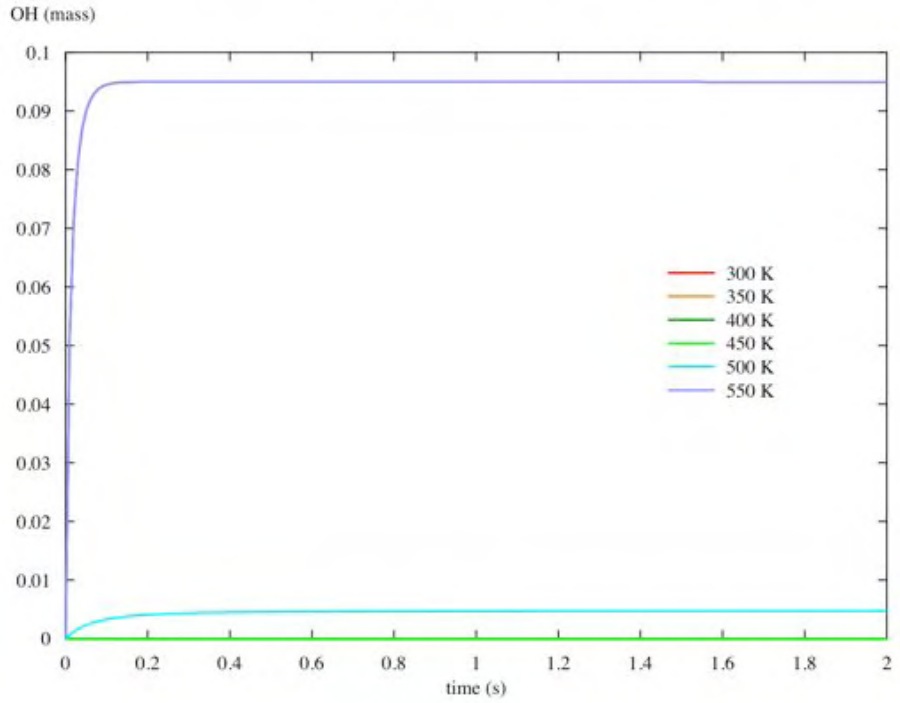

Figure 5.3: The effect of initial system temperature on the evolution of *OH* with an initial bound water amount of $W_b = 0.1$ At sub-ignition temperatures, moisture plays no part in the formation of *OH*. As ignition progresses, moisture acts as catalyst in *OH* formation, consuming almost all bound water present.

5.2.4 Effect on system heat

Figure 5.4a shows the effect of changes in initial system temperature on the energy associated with the evaporation of the initial moisture of $W_b = 0.1$. With increasing system temperature above the boiling point of water, the rate of increase in evaporation energy increases until all the water is evaporated and the net energy reaches zero. Below the boiling point, the system remains in deficit. When the system temperature is increased to the point where the activation energy of the thermal degradation is reached (i.e. $>$ 540 K), the rate of increase in energy associated with evaporation bound water present appears to be almost instantaneous. This is a result of the change in the nature of the reactions, from the relatively slow evaporation to the fast *OH* formation.

Figure 5.4b shows the evolution of the total heat of the system. It can be seen that for all but the highest temperature case, the system fails to produce excess heat, resulting in the cessation of reactions. At the highest initial system temperature, the system becomes overtly exothermic and ignites, driven by the initial formation of *OH* in the presence of the bound water.

5.2.5 Discussion

The effect of fuel moisture on the behaviour of bushfires has long been investigated (e.g. Hawley (1926); Gisborne (1933)) and is qualitatively well understood: impeding the rate of combustion and slowing rate of spread of the fire as the amount of moisture increases. This is primarily through removal of heat from the fuel via evaporation of the moisture but also by interception of heat by water vapour (King and Linton 1963; King 1972; Vines

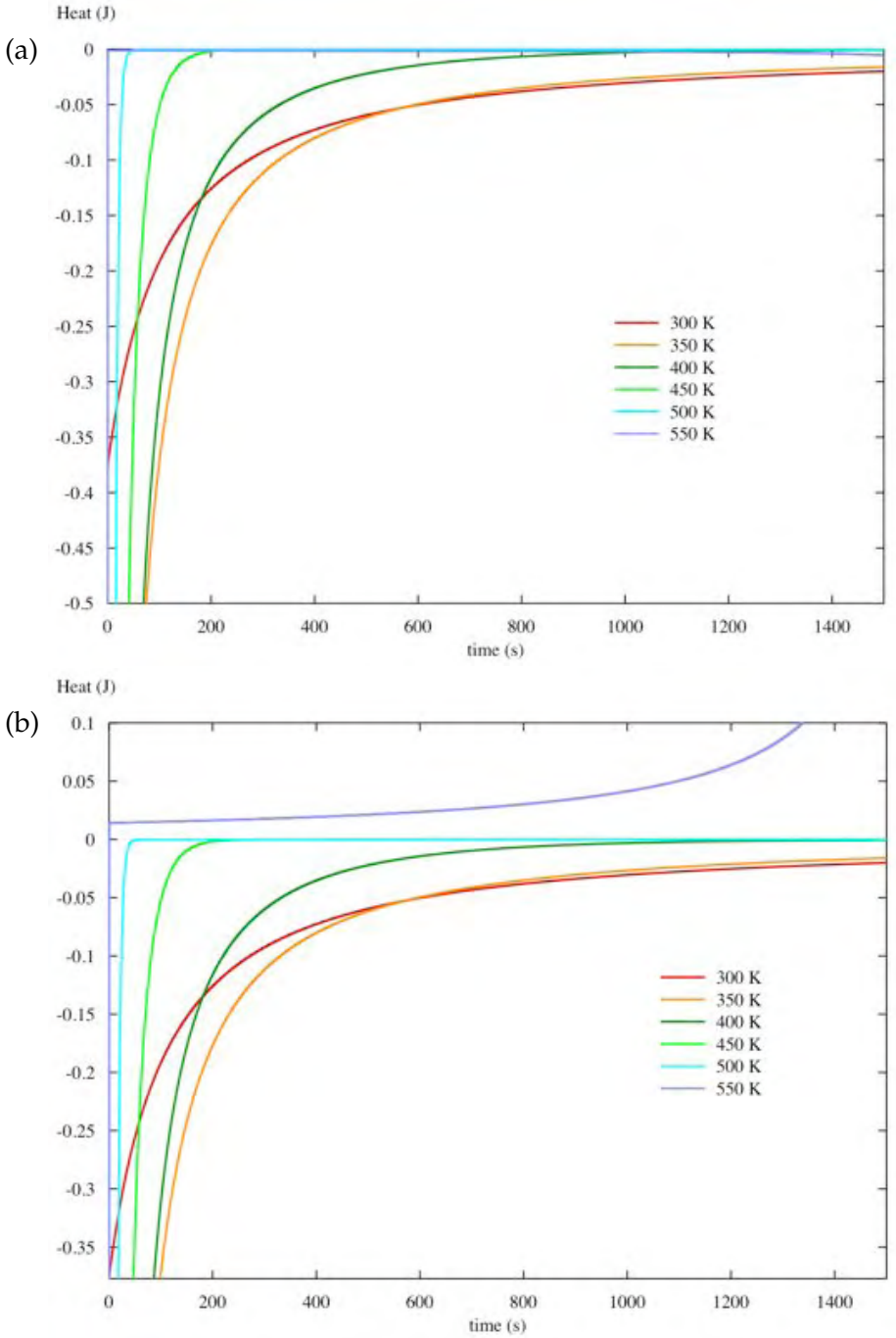

Figure 5.4: The effect of initial system temperature on (a) the heat of evaporation of the system and (b) total system energy with an initial bound water amount of $W_b = 0.1$. The time to complete evaporation decreases with increasing system temperature. At $T = 550K$ the bound water is rapidly converted to *OH* and the system eventually progresses to ignition.

1981). The performance of the model in this numerical experiment is validated by this general understanding of the impact of water in the fuel on the combustion of the fuel.

At low system temperatures the water remains in the fuel and the system energy remains in deficit meaning that ignition cannot occur. As the system temperature is increased toward and beyond that of the boiling point of water, the model shows the evaporation of the bound water out of the fuel and into the gas phase. The speed of this evaporation increases with increasing initial temperature. However, when the system

temperature is in the range where the rates of the thermal degradation reactions become dominant (i.e. $>$ 540 K), the effect of the presence of moisture in the system changes and, rather than acting as a inhibitor in the system of reactions through the loss of energy needed to evaporate the water, it becomes a catalyst in the formation of hydrolysed cellulose and acts to convert substrate fuel to *OH* at a very high reaction rate. This has the effect of almost immediately reducing the amount of substrate remaining to be consumed. Results of numerical experiments not presented here showed that the amount of substrate thus converted is almost exactly the same as the amount of initial bound water present, leading to the counter-intuitive outcome of increasing moisture content resulting in reduced time to complete consumption.

This quandry can be explained, or at least avoided, by understanding that the model can only simulate the onset of ignition from suitable combustion conditions and not the approach to ignition from ambient initial conditions (i.e. the model does not have an external heat source for pilot ignition). As such, the initial system temperature (i.e. substrate and gas phase temperatures) is imposed on the system and not the result of external heating as would be the case in the lighting of a fuel using a match, a pilot flame or adjacent burning fuel as would be found in a bushfire. Thus, when the system temperature is approaching that of ignition, any moisture that would have been present in the fuel under ambient conditions would have evaporated at a much earlier stage and not be present when the thermal degradation reactions commence.

Therefore, the results shown in Figures 5.2 and 5.3 for a system temperature of 550 K are not representative of normal combustion conditions. That is, the presence of bound water in the fuel at these initial temperatures is impossible and the consumption of initial bound water by the hydrolysed cellulose reaction would not occur. However, bound water formed by the formation of charcoal in the thermal degradation reaction *could* be present and would act as catalyst in the *OH* reactions and is therefore of interest to us.

As the remainder of this chapter is concerned with the onset of ignition at the range of elevated temperatures around the commencement of thermal degradation, no initial moisture will be considered.

5.3 Zero moisture, constant wind

In this section, the effect of a constant, non-zero wind is explored (i.e. $f > 0$). Initial moisture is zero, initial gas phase temperature 550 K, initial solid phase substrate temperature 580 K. Initially, the temperature of the wind is set to ambient, 300 K; the effect of wind temperature is investigated subsequently. The wind may also contain moisture, through the parameter W_f but this is not investigated here.

The effect of ambient temperature wind is to cool both the solid phase and gas phase species through two coupling coefficients: ϵ_s, which controls the interaction of the air flow with the solid phases, and ϵ_g, which controls the interaction of the air flow with the gas phases. For reasons of brevity, ϵ_s and ϵ_f are made equal, although in reality they would be different. These parameters would be related to the mixing potential of the two types of fuel. In the case of the solid phase fuel this might be composed of the roughness scale of the fuel and the coupling coefficient value would be much less than that of the gas phase coupling coefficient.

Refer to Table A1.1 (p. 187) for a list of symbols and associated equation numbers frequently used in this Chapter.

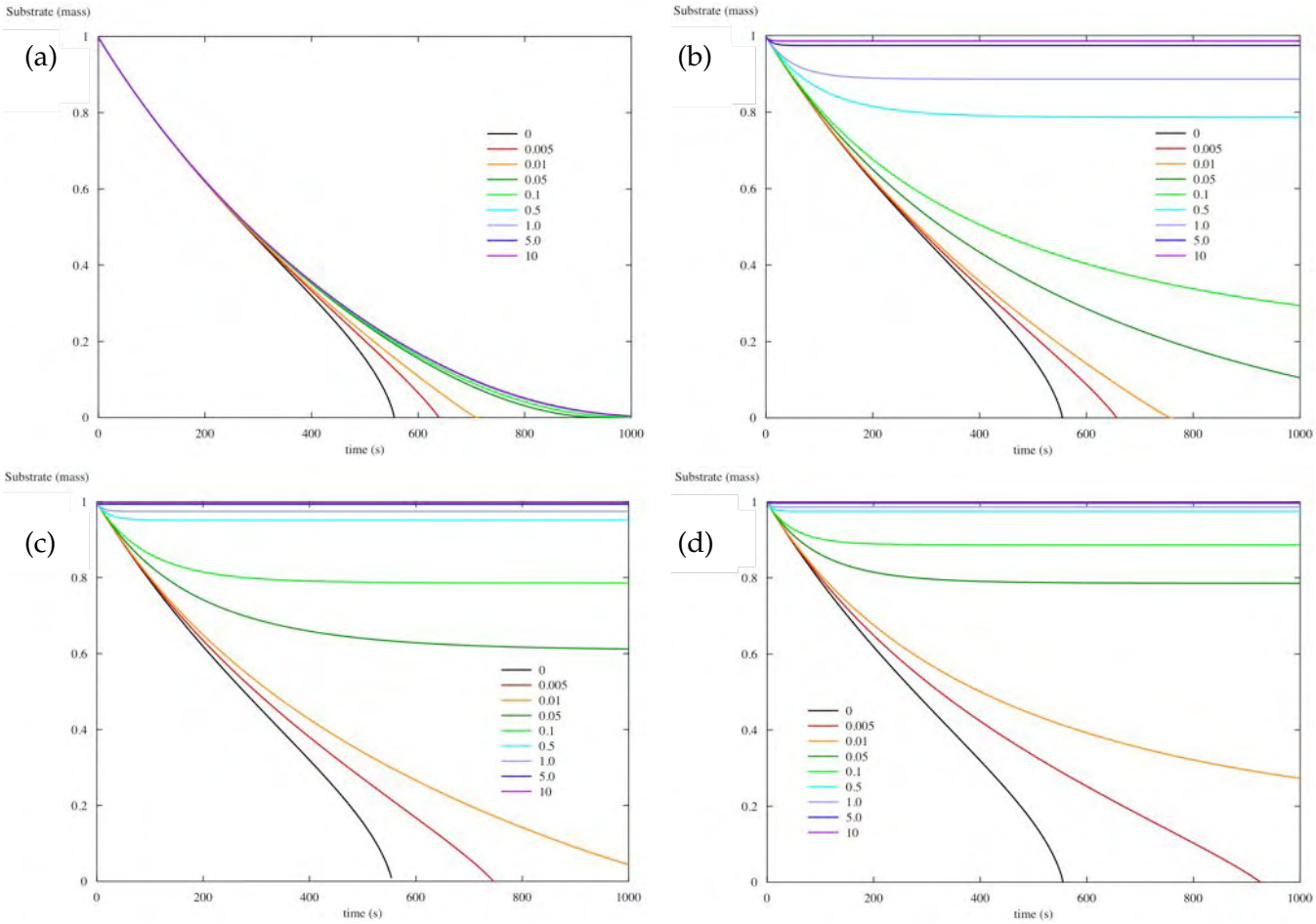

Figure 5.5: The effect of wind speed ($f : 0 \rightarrow 10$) on substrate mass for a range of coupling coefficients, (a) $\epsilon = 0$, (b) $\epsilon = 0.001$, (c) $\epsilon = 0.005$, and (d) $\epsilon = 0.01$. Increasing wind speed decreases substrate consumption rate. Increasing coupling coefficient value increases the impact of the wind on the system.

5.3.1 Effect on substrate mass

Figure 5.5 shows the effect of a range of wind speed values ($f = 0 \rightarrow 10$) on the evolution of the substrate mass for a series of coupling coefficient values ($\epsilon_s = \epsilon_f$ in [0, 0.001, 0.005, 0.01]). Setting the coupling coefficients to 0 allows us to explore the raw effect of f on the model (Fig. 5.5a). This decouples the temperature of the substrate and gas phase from the wind and limits the effect of the wind to the advection of volatiles out of the system only, reducing the impact of the combustion of the volatiles on the rest of the system. Increasing the value of ϵ acts to increase the cooling effect of the wind on the substrate and gas phase components.

Increasing wind strength acts to slow the rate at which the substrate is consumed. Increasing the coupling coefficient acts to increase the impact of the wind on the system (Fig. 5.5b-d), to the point where the system ceases reacting and the thermal degradation stops. At ϵ = 0.001, the wind strength at which reactions cease, f_c, is 0.5, at ϵ = 0.005, f_c = 0.05, and at ϵ = 0.01, f_c = 0.05.

For all subsequent simulations, $\epsilon_s = \epsilon_f = 0.01$; a value that allows a degree of coupling between the reacting system and the air flow over it.

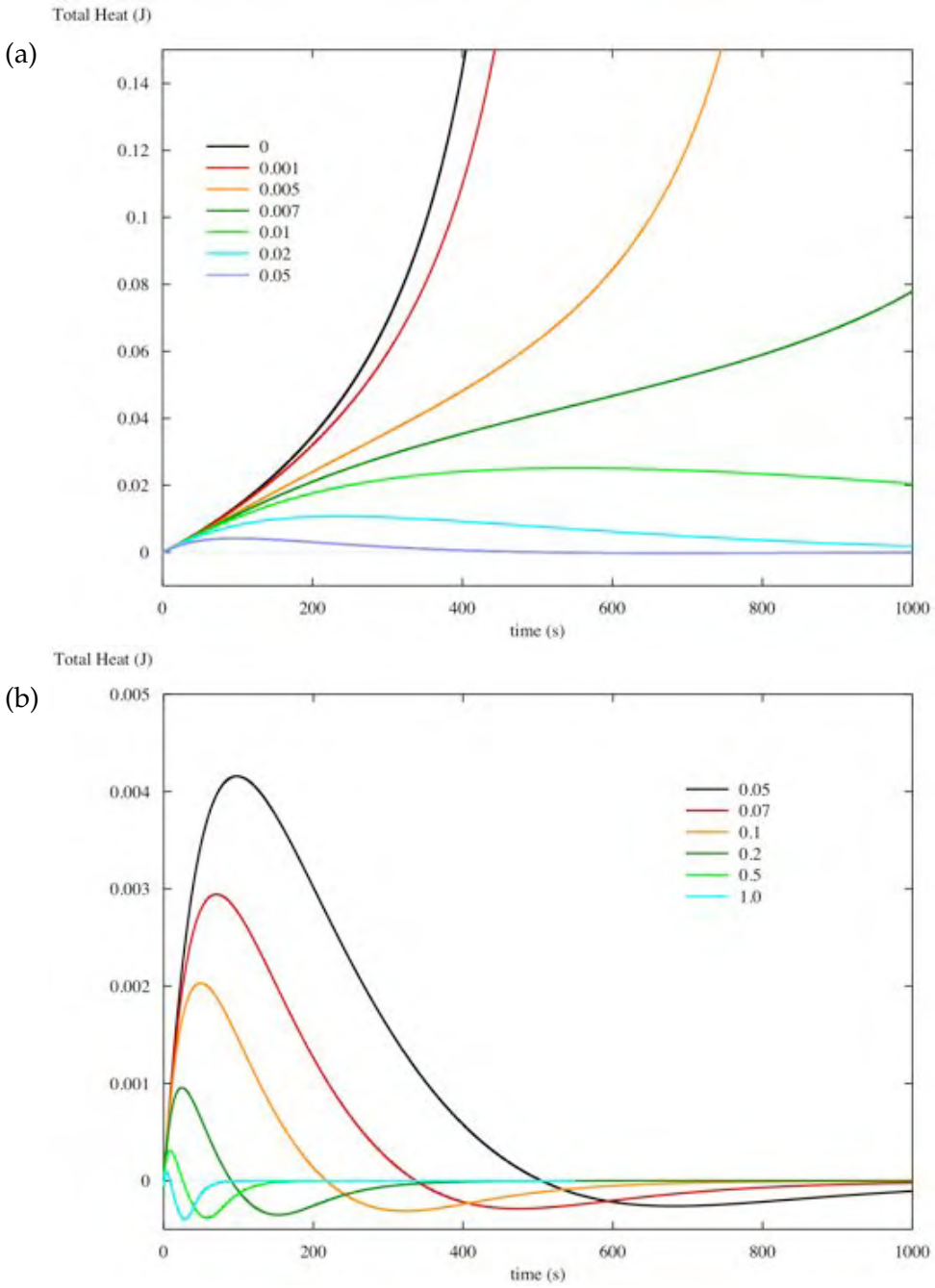

Figure 5.6: Evolution of the total heat of the system with varying wind strength, (a) $f = 0 \rightarrow 0.05$, and (b) $f = 0.05 \rightarrow 1.0$. Increasing wind speed decreases reaction rates and decreases the total heat of the system.

5.3.2 Effect on system heat and temperatures

Figure 5.6 shows the effect of increasing f on the total heat of the system over time for a range of wind strengths. Increasing f acts to decrease the rate of increase of the total energy of the system. Up to wind strengths of 0.01, the system increases in total heat, albeit at increasing lower rates, leading eventually to ignition. Wind strengths of $f \geq 0.01$ ultimately result in a decreasing of the total heat in the system and the cessation of the reactions. This is clearly evident in Figure 5.6b where, at these higher wind strengths, the total system energy becomes negative and remains at or below zero.

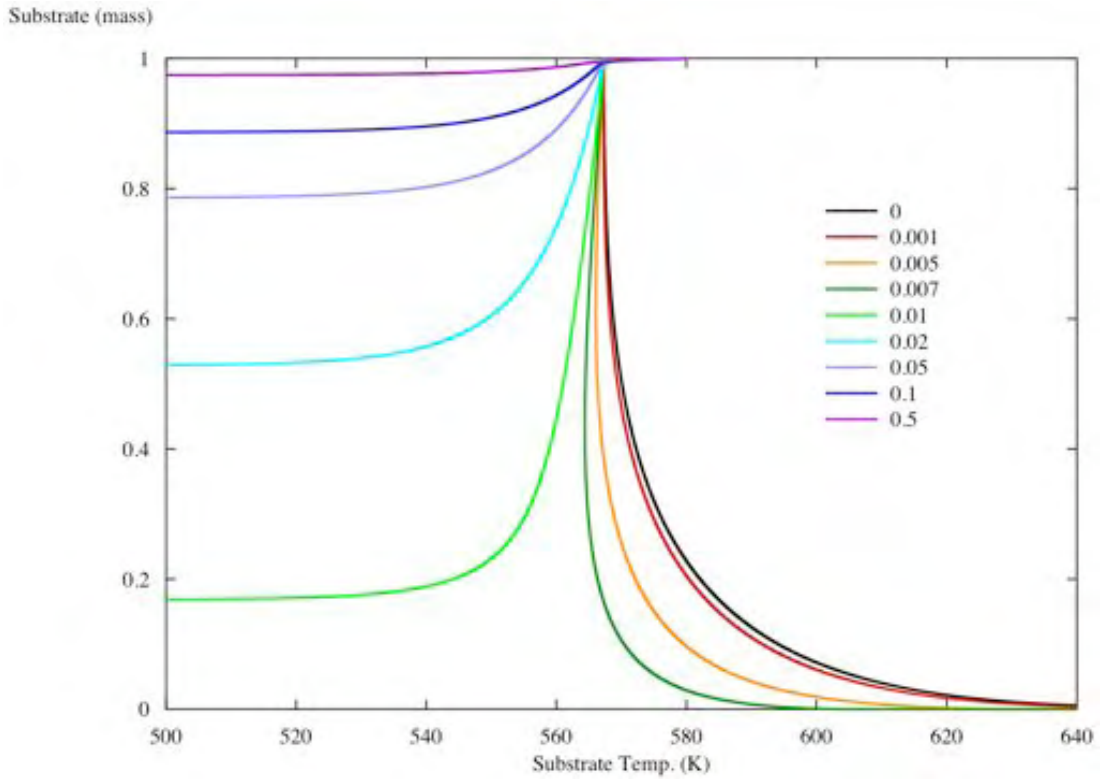

Figure 5.7: Graph of substrate mass with substrate temperature. Wind speeds less than 0.007 result in ignition eventually. At greater wind speeds, the substrate asymptotes to a value as the reactions cease.

Figure 5.7 shows substrate mass plotted against substrate temperature for a range of wind speed values ($f = 0 \rightarrow 0.5$) over extended time (i.e. the total simulation time was long enough for a complete curve to be generated, up to 30,000 s). There is an initial loss of substrate temperature for all wind speeds as the slightly cooler gas phase temperature is coupled with it. For wind strengths ≥ 0.01, the substrate temperature then decreases with increasingly less loss of substrate mass, indicating the reactions eventually cease, asymptoting to a value that may be determined from Eqs 4.32 and 4.33. At wind strengths ≤ 0.007, the reactions eventually lead to ignition and a rapid increase in substrate temperature and loss of substrate. Figure 5.8 shows the evolution of gas phase and substrate temperatures for the same wind speeds. These graphs show that the coupling of 580 K T_s and 550 K T_v result in a coupled temperature of $\simeq$ 567 K before the enthalpies of the reactions take effect. The subsequent temperatures of the two phases are very similar due to the coupling.

There exists a very robust relation between the gas phase temperature and the substrate temperature after the temperatures have engaged through the coupling coefficient (Fig. 5.9a, p. 92). Following the simulation initiation, the substrate and gas phase temperatures quickly become coupled and then maintain a path that is independent of wind speed value, coupling coefficient and, to all intents and purposes, initial substrate and gas phase temperatures. At wind speeds below 0.01, a rather complex interaction of gas phase and substrate temperatures occurs (Fig. 5.9b and c) that eventually results in the steady increase in both towards ignition. At and above 0.01, the coupling is simpler and results in the steady decrease in both temperatures until they reach ambient.

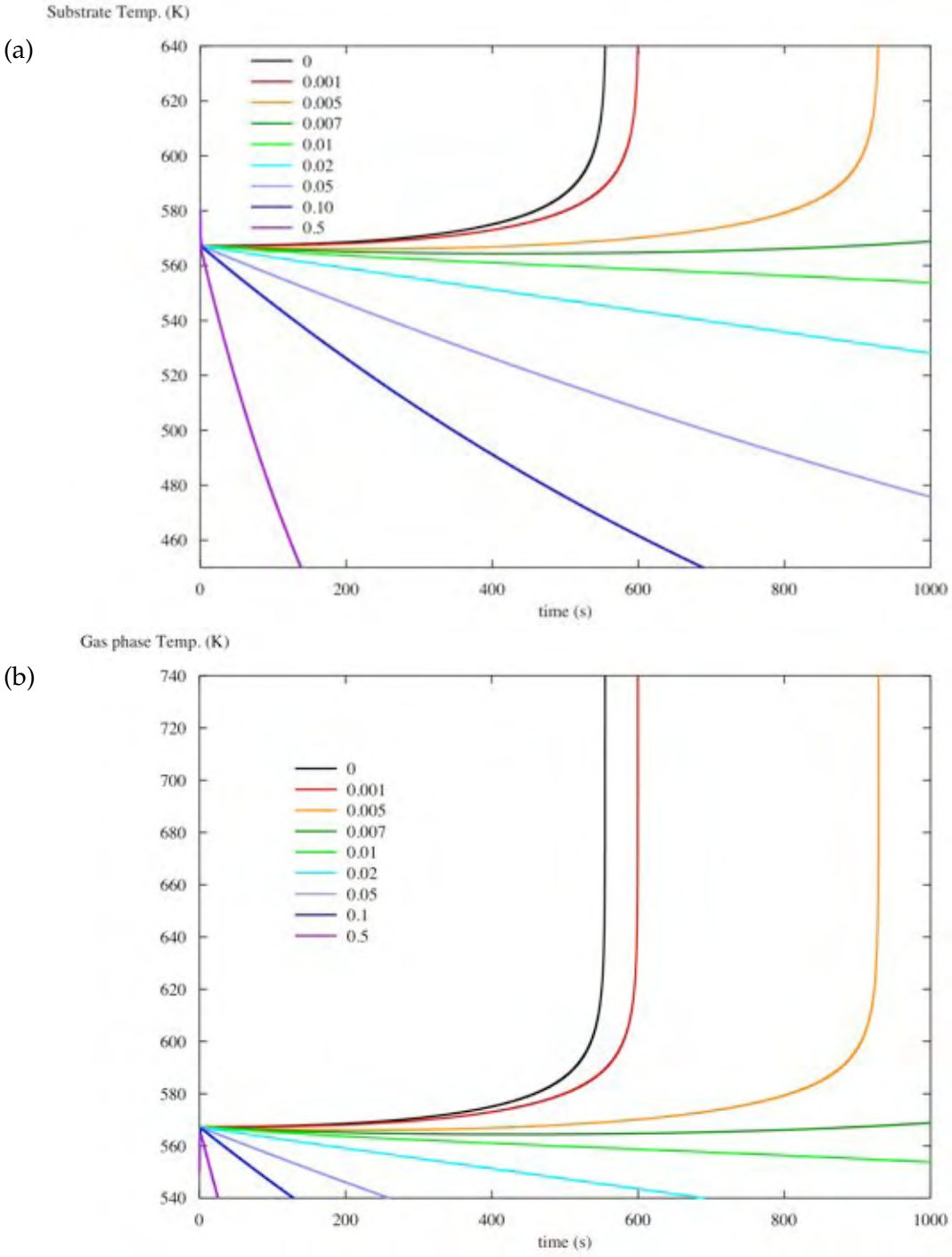

Figure 5.8: Evolution of (a) substrate temperature (T_s) and (b) gas phase temperature (T_v) for a range of wind speeds. After coupling the evolution of T_s and T_v are the same.

Figure 5.9c shows the coevolution of T_s and T_v at two wind strengths, 0.007 and 0.0077 around the point at which the gas phase and substrate temperatures become coupled. The behaviour of these temperatures reveals some rather complex dynamics. The initial trend for both wind speeds after the temperatures couple is to decrease in magnitude. After a period of time, the temperatures under both winds increase. The temperatures under the 0.007 wind continue to increase and lead to ignition. The temperatures under the 0.0077 wind decrease again and lead to reaction cessation.

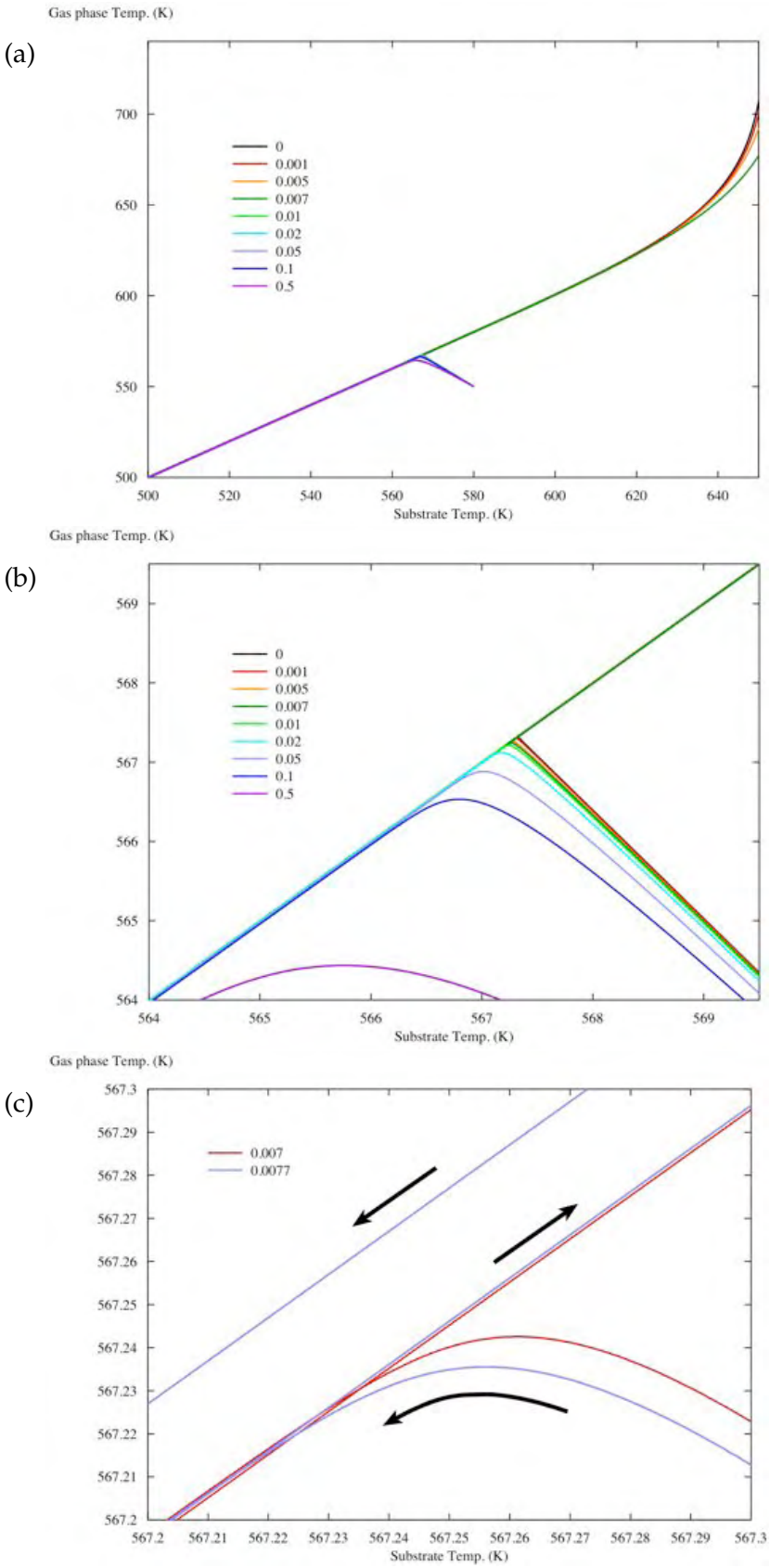

Figure 5.9: Co-evolution of the gas phase and substrate temperatures with various wind strengths (a) over a large range of temperature values, (b) over a small range of temperatures vallues around the coupling point, and (c) extreme close-up of the coupling point for $f = 0.007$ (red line) and $f = 0.0077$ (blue line). At $f \geq 0.0077$, the coupled temperatures decrease, increase and then decrease again, leading to reaction cessation. At $f < 0.0077$, the temperatures decrease and then increase, leading to ignition.

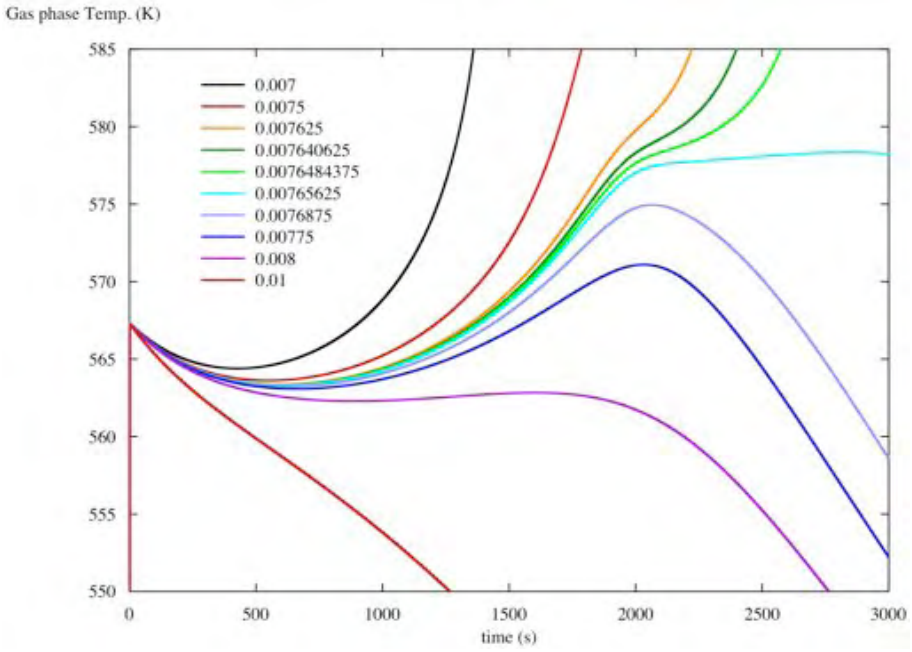

Figure 5.10: Evolution of the gas phase temperature for a range of wind speeds around a critical value that determines whether the system ignites. A binary search was used to identify a near critical wind speed, f_c, to 5 decimal places.

Obviously there is a critical wind speed value, f_c, between 0.007 and 0.01 at which the reactions either lead to an increase in system temperatures and ignition or result in a steady decrease in system temperatures. Figure 5.10 shows the evolution of the gas phase temperature for a range of wind speeds selected via a binary search of the space between 0.007 and 0.008 (i.e. sensitivity analysis). Between $f = 0.0076484375$ and $f = 0.00765625$ (a difference of 0.0000078125 and the point at which I gave up[1]) the system heads toward ignition at the lower value and peters out at the higher value, although the behaviour at $f = 0.00765625$ runs close before it too peters out. In the process it can be seen that the gas phase temperature undergoes an initial increase as it is coupled to the substrate temperature and then a slow decrease over the next 400–700 s. The system then increases in temperature until about 2100 s after ignition. If the system will go on to ignition, the temperature continues to slowly increase toward the point of ignition. If it will not, the temperature slowly decreases and the reactions peter out.

It is very likely that the value of f_c is irrational. The levels of accuracy explored here are physically meaningless as wind speed cannot be measured to anywhere near 10 decimal places but illustrates the irrationality of f_c.

5.3.3 Effect on reaction products

The production of *LG* and *OH* shows little impact due to wind at strengths less than 0.01 (Fig. 5.11). While greater wind strengths result in a greater proportion of *OH* to *LG* than at lower wind strengths, these winds speeds ultimately extinguish the reactions regardless.

If we consider the mass of *V* and *C* (Fig. 5.12, p. 95), the effect of wind is to decrease the ratio of volatiles to charcoal. In all but the highest wind speed cases (Fig. 5.12a), the

[1] It is not unreasonable to suspect that no single critical value would be found to the precision of the 64-bit computer on which these simulations were run.

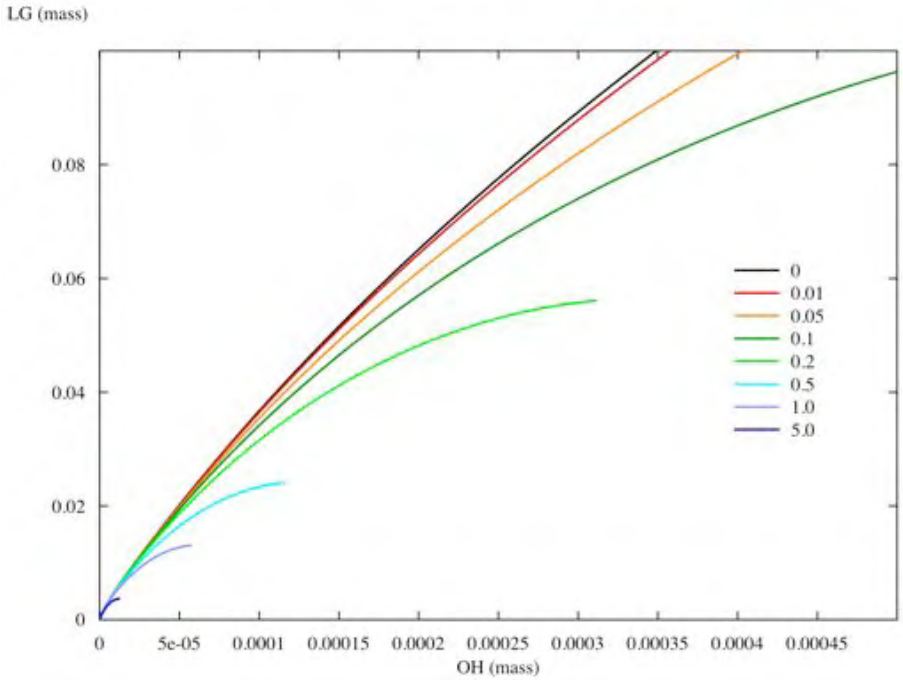

Figure 5.11: Effect of varying wind speed, f, on the production of *LG* and *OH*. At strengths less than 0.01, wind does not appear to influence the formation of these products.

amount of *V* in the system in the initial stages of reaction is much greater (by an order of magnitude) than that of *C*. As the wind speed increases so does the rate of increase of *C* in the system. However, as the reactions unfold, the later stages of degradation become dominated by production of *V*. At the higher wind strengths (Fig. 5.12b), *C* dominates. Between wind strengths of 0.007 and 0.01 there appears to be a transition from where *V* dominates to where *C* dominates. This coincides with the critical region identified in Figure 5.10.

Figure 5.12c shows the coevolution of *V* and *C* for the same wind strengths investigated in Figure 5.10. In this regime of wind, *C* dominates all but the very initial stage for all cases and the very final stages for those cases that eventually lead to ignition. In the case of $f = 0.0076484375$, *V* actually declines before it recovers and increases, leading to ignition. At wind strengths greater than this value, *C* dominates as *V* continues to decrease, leading to eventually to cessation of the reactions. However, because the mass of both *V* and *C* are a result of both production and consumption reactions, there may be other aspects not apparent in just the mass of these quantities.

The effect of wind on the heat evolved in the formation of charcoal and volatiles is not straightforward. At the broad scale (Fig. 5.13a, p. 96), increasing wind results in a relative increase in the amount of energy involved due to the formation of volatiles, implying that volatile production increases (which is opposite to that suggested by the raw comparisons of masses). At the finer scale (Fig. 5.13b), the impact of wind is even more complex. In the early stage, increasing wind, regardless of wind strength, increases the relative energy associated with charcoal formation. At strengths greater than the near-critical value identified previously (but less than 0.008), there is then a relative increase in the heat involved in the formation of volatiles (forming a slight 's'-shaped bend in the curve) but then the energies associated with both volatilisation and charcoal formation decrease, resulting in a hook-turn as the reactions peter out. In the cases of $f = 0.076875$, this results in a path that is, at the point the simulation was stopped at

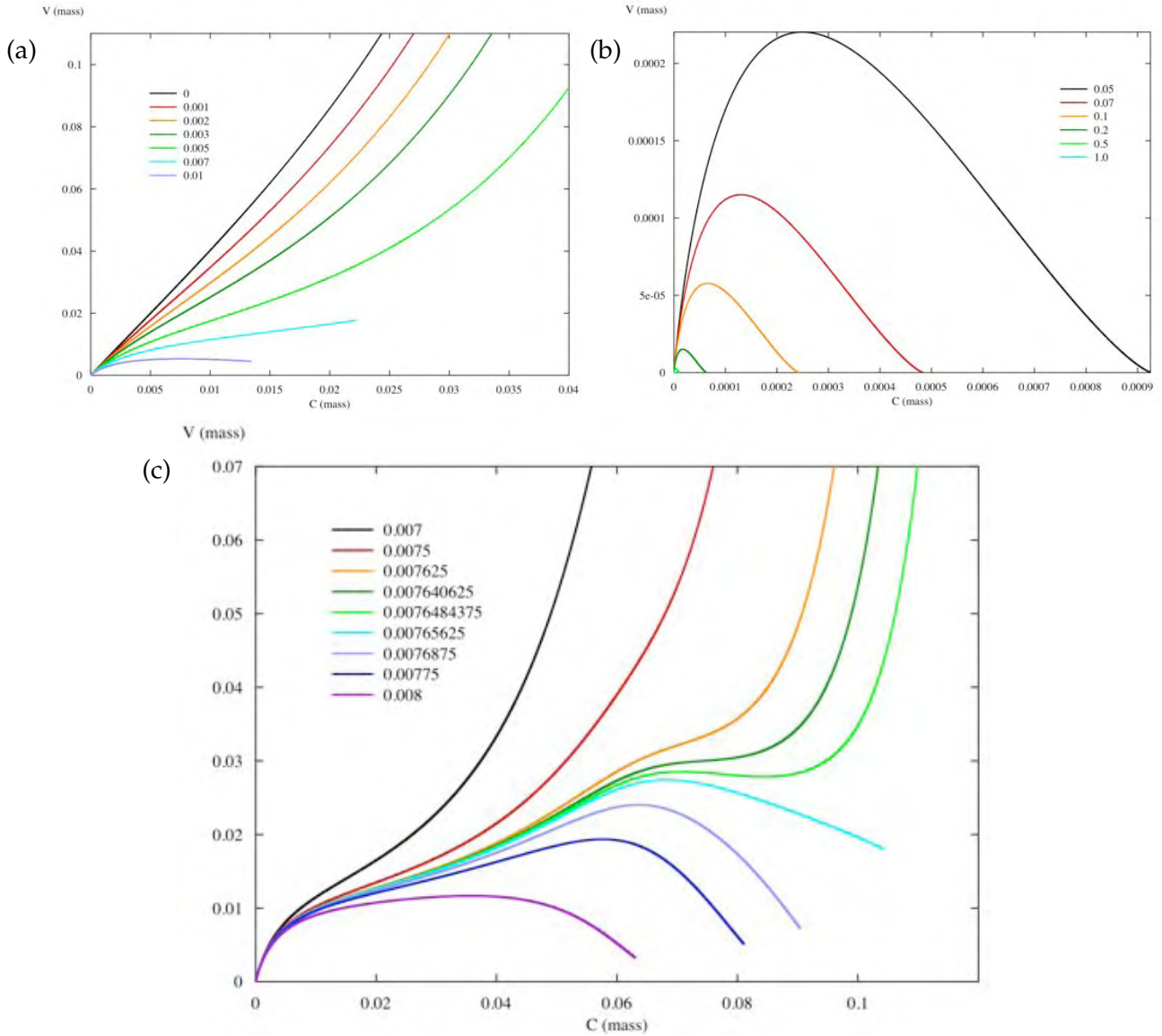

Figure 5.12: Effect of varying wind speed, f, on volatiles V and charcoal C. (a) $f = 0 \rightarrow 0.01$. (b) $f = 0.01 \rightarrow 1.0$. (c) $f = 0.007 \rightarrow 0.008$. Increasing wind speed acts to decrease the ratio of V:C.

3000 s, much greater in volatilisation than in the initial stages of the reaction. For greater wind strengths, the magnitude of the energy associated with volatilisation is less than the initial stage.

At wind strengths at or below the near-critical value—but greater than $f = 0.0075$—a dog-leg kink appears in the coevolution of the enthalpies of volatilisation and charcoal formation. In the most extreme case ($f = 0.0076484375$), there is a decrease in both the formation of charcoal and volatiles before both recover and continue on to ignition. In the lesser cases ($f = 0.007640625$ and $f = 0.007625$) there is essentially only a decrease or a pause in the energy involved in the formation of charcoal. Subsequent evolution shows the greater volatilisation energy at higher wind speeds seen in Figure 5.13a.

Figure 5.14 (p. 97) shows the effect of wind speed on the consumption of V and C through the heat released by the associated combustion reactions. At all wind speeds considered here at and around the critical wind speed value, the energy released due to volatile oxidation (i.e. flaming combustion) dominates that of the charcoal oxidation

(a)

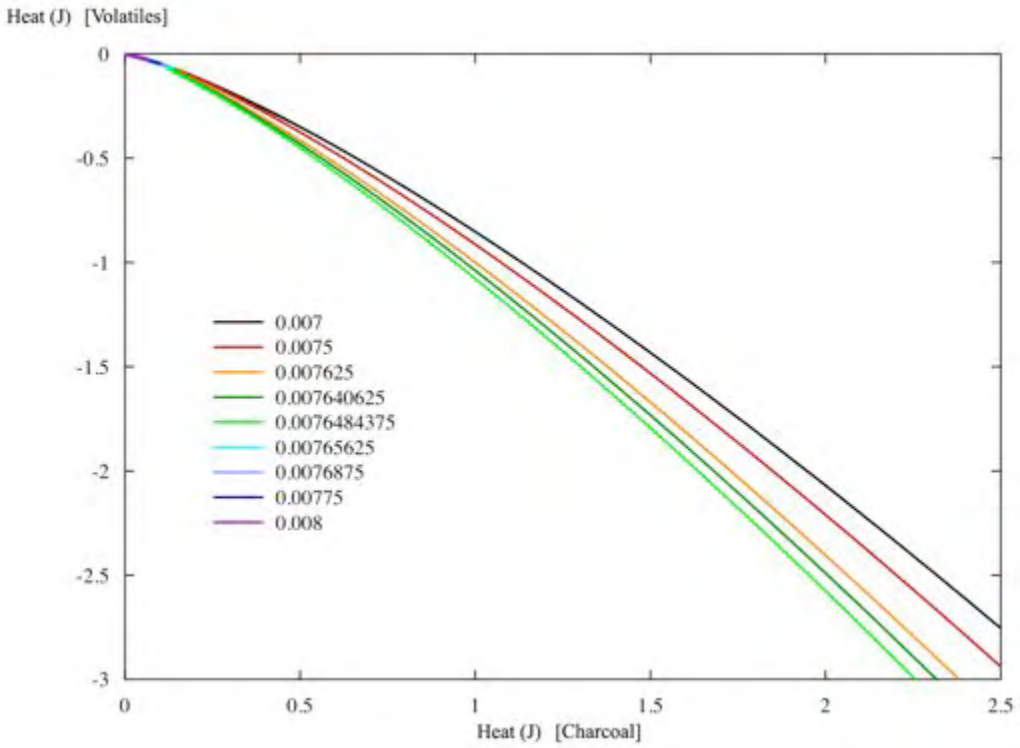

(b)

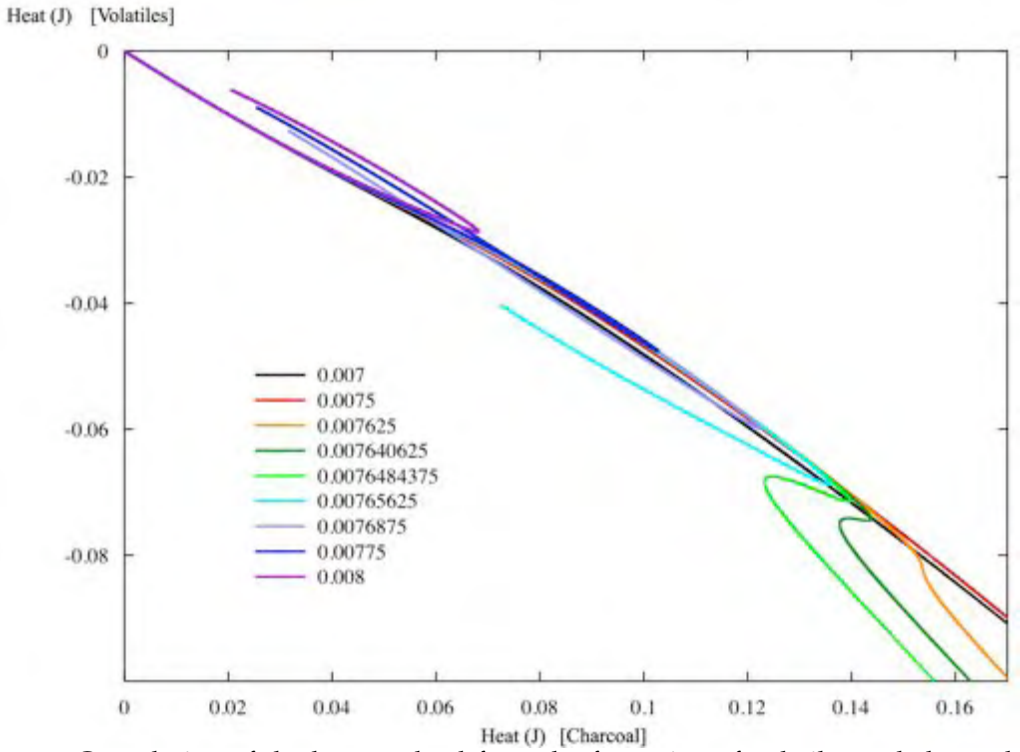

Figure 5.13: Coevolution of the heat evolved from the formation of volatiles and charcoal (a) across a broad scale of energy, and (b) at the low energy end of scale. A greater magnitude of energy is released from the formation of charcoal. Increasing wind speed generally acts to increase the magnitude of energy from the formation of volatiles, up to the near-critical wind strength.

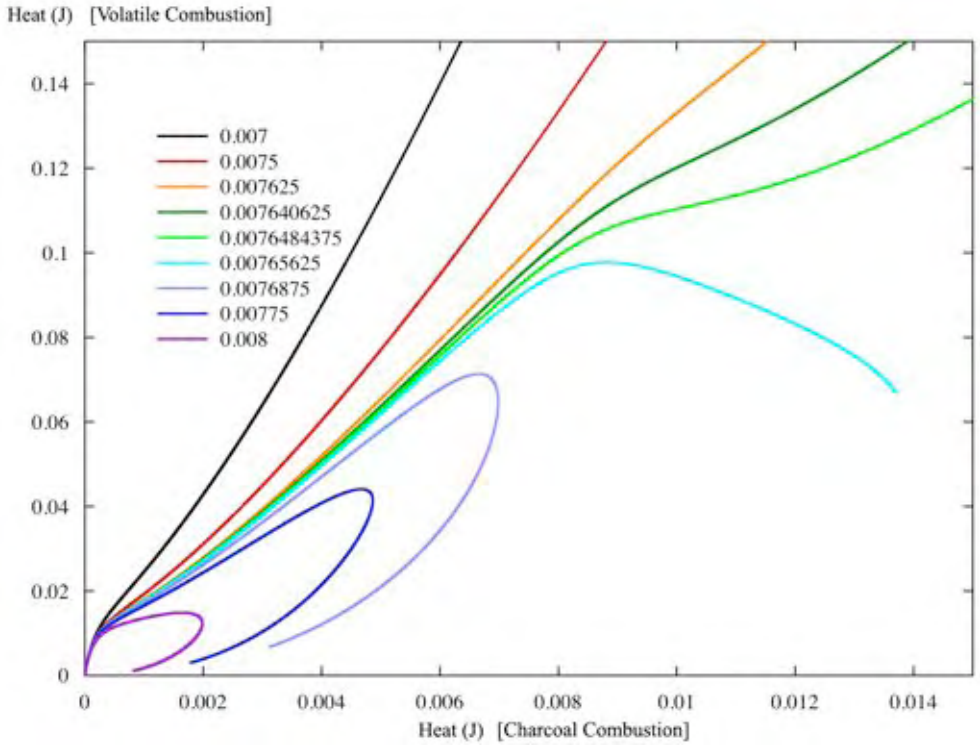

Figure 5.14: Effect of varying wind speed, f, on the heat released through combustion of volatiles and charcoal. Increasing wind speed acts to decrease the ratio of heat released due to combustion of volatiles to the heat released due to combustion of charcoal.

(i.e. smouldering combustion) by an order of magnitude. This is due primarily to the rapid reaction rate of the volatile oxidation when compared to the charcoal oxidation rate, as the amounts of volatile and charcoal consumed are comparable. As wind speed increases, the amount of energy released through charcoal combustion increases, to the point at which the energy released through volatile combustion actually decreases ($f = 0.00765625$) while charcoal combustion continues. At wind speeds in excess of this, the volatile combustion steadily decreases before the energy from charcoal combustion also decreases, leading eventually to cessation of the reactions as they peter out.

5.3.4 Effect on bound moisture

Figure 5.15 shows the effect of various wind strengths, around the near-critical wind speed identified previously, on the evolution of bound moisture in the substrate. The rapid increase in moisture at low wind speeds is associated with the onset of ignition. As the critical wind speed is approached, there is a less rapid increase in moisture content that actually achieves a local maxima and minima before the onset of ignition is achieved and the rapid increase in water occurs. At wind speeds greater than $f = 0.0076484375$ the amount of bound water in the system decreases after the maxima as the reactions begin to peter out.

It appears that these local maxima in the evolution of bound water around the critical wind speed are associated with the non-linear behaviour observed in previous figures. Figure 5.16 (p. 99) shows the relationship between bound water and two measures of charcoal in the system with various wind strengths around the near-critical wind speed: mass of C (Fig. 5.16a), and the combined heat from the formation and combustion of charcoal (Fig. 5.16b). The former shows an increase in C with bound water as wind

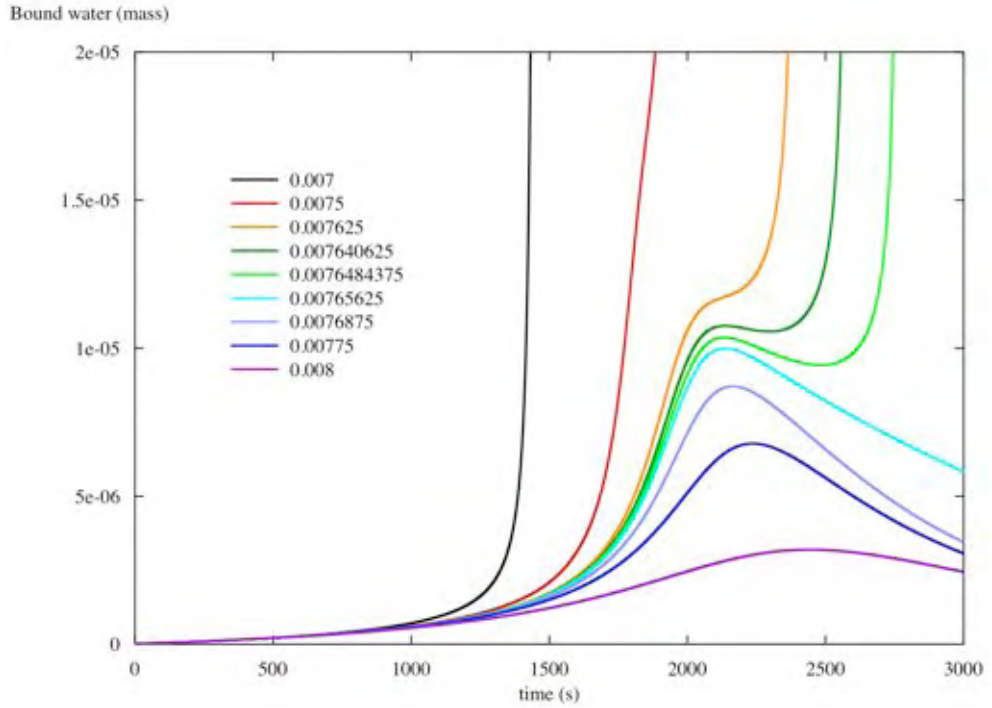

Figure 5.15: Evolution of bound moisture in the system with varying wind speed, f. The rapid increase in moisture at low wind speeds is a result of the onset of ignition and the rapid formation of water through increased reaction rates.

strength increases. Around the near-critical wind strength, the rate of increase of water decreases (in some cases becomes negative) while C increases linearly before the onset of ignition and another rapid increase in moisture. At speeds greater than the critical, C continues to increase as moisture decreases.

Figure 5.16b shows a much more complex relation between the total combined heat release associated with the formation and combustion of charcoal and bound moisture. Around the critical wind speed value there is a decrease in both charcoal-related heat and bound moisture (preceded by a decrease in charcoal-related heat) which recovers and leads to the onset of ignition. At speeds greater than the near-critical value, both moisture and charcoal-associated heat decrease as the reactions begin to peter out.

Figure 5.17 (p. 100) shows the relation between the heat involved in the evaporation of bound water in the system and the total heat of the system for different wind strengths around the near-critical wind speed. At the small scale (Fig. 5.17b), increasing wind speed decreases the rate of increase of the total heat of the system as more water is evaporated. As the near-critical wind strength is approached, however, the total heat of the system decreases as the heat expended through evaporation continues to increase. Between $f = 0.0076484375$ and $f = 0.00765625$ the fundamental dichotomy of the effect of wind is revealed. At $f \leq 0.0076484375$, the system ultimately increases in total energy of the system and eventually achieves ignition. Above this value, the total energy of the system continues to decrease (along with the production and evaporation of water) and the reactions eventually peter out and the fire goes out.

5.3.5 Effect of air flow temperature

It was noted in Chapter 2 (p. 23) that the rate constants have an Arrhenius form and thus are highly temperature sensitive. The preceding numerical experiments were all

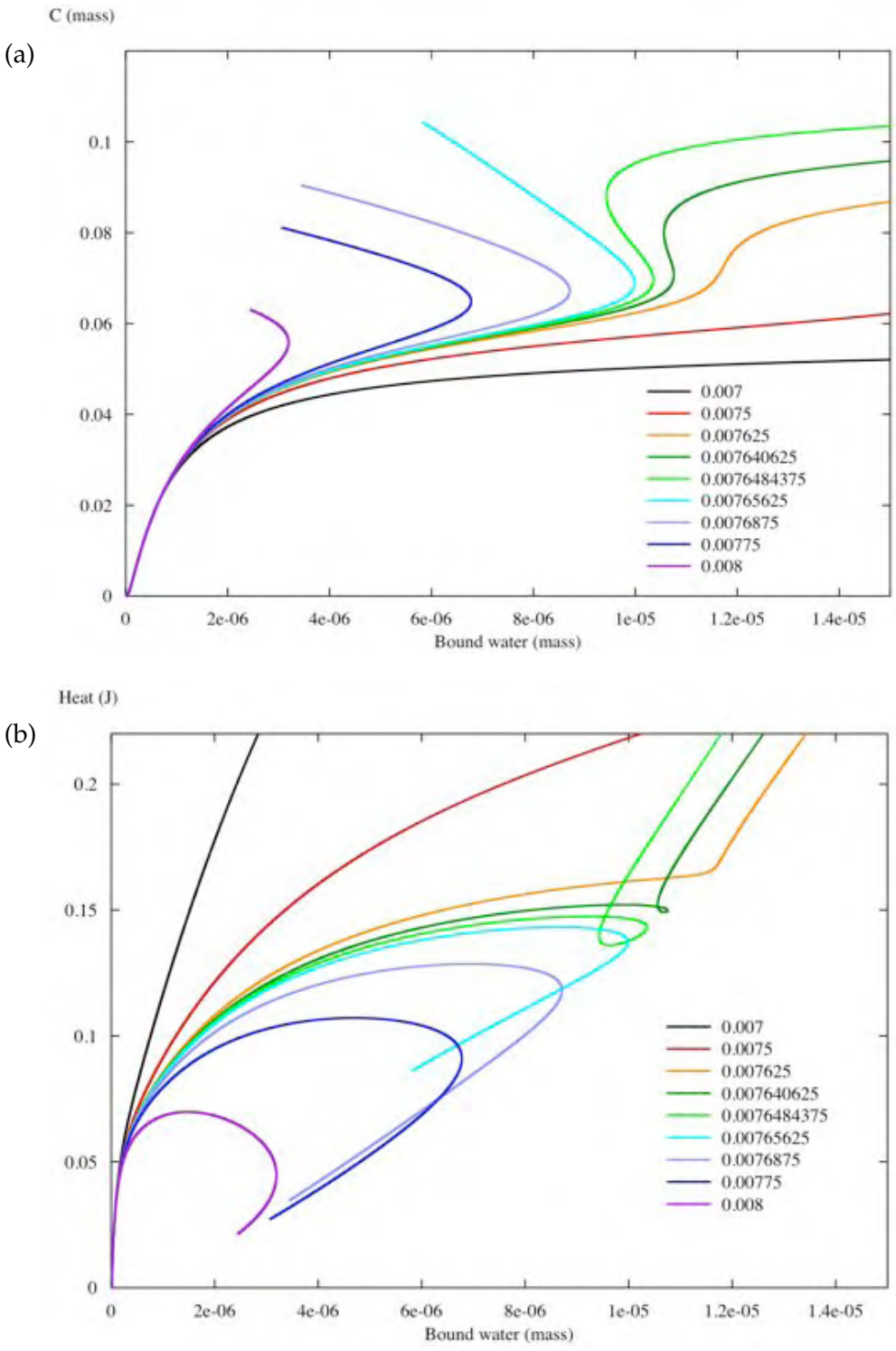

Figure 5.16: Coevolution of the amount of bound water in the substrate and (a) the mass of *C*, and (b) the combined heat of formation and combustion of charcoal. Increasing wind speed increases the amount of *C* in the system but decreases the total heat associated with the charcoal (i.e. formation and combustion) while increasing the amount of bound water.

(a)

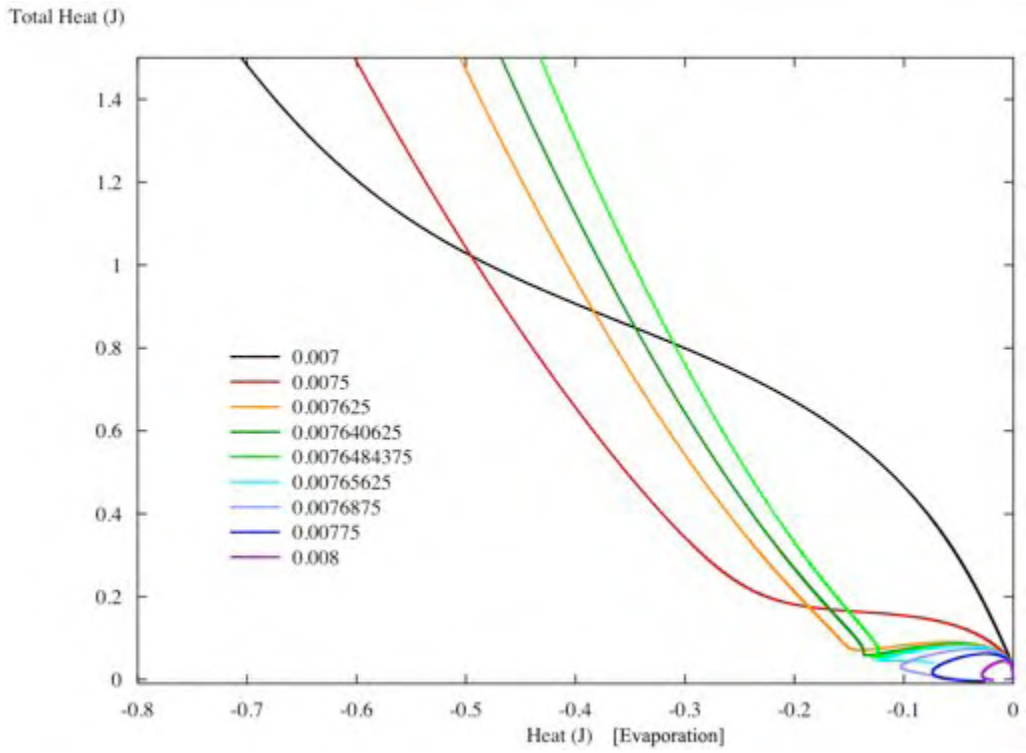

(b)

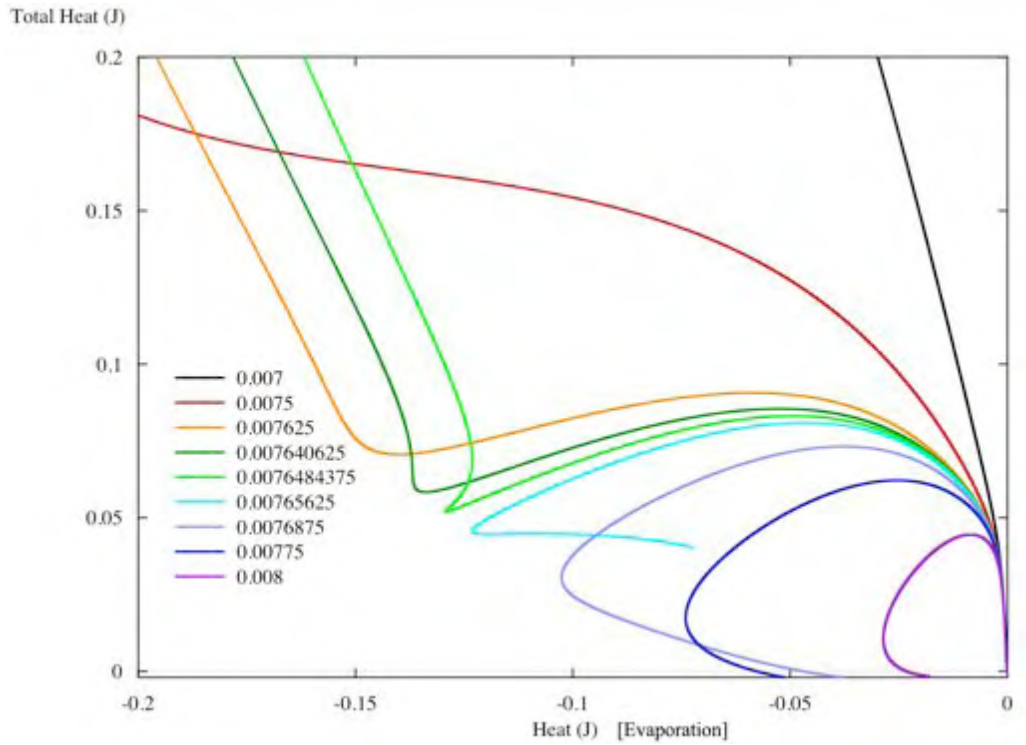

Figure 5.17: Coevolution of the heat expended due to evaporation and the total heat in the system at (a) the large scale, and (b) the small scale. A complex interrelation between wind speeds, evaporation of moisture and the total heat in the system is apparent around the near-critical value of wind strength.

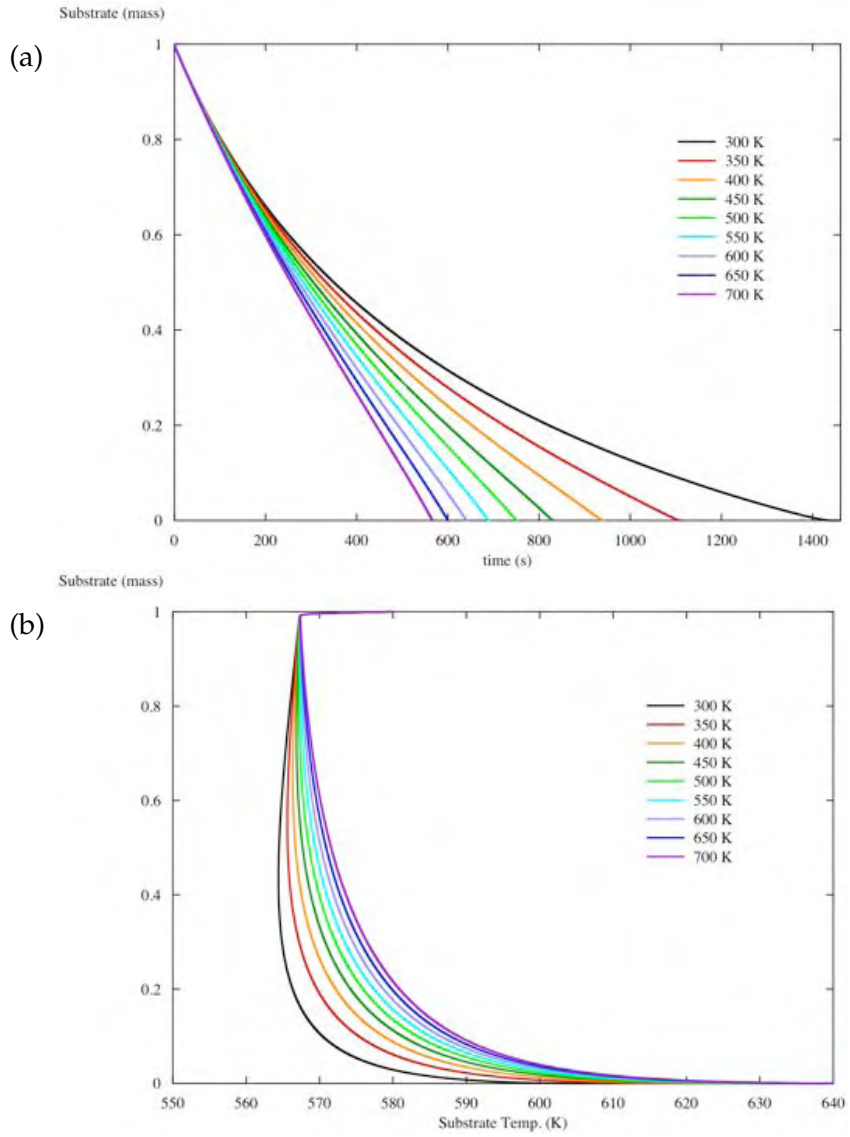

Figure 5.18: (a) Evolution of substrate mass with varying ambient wind temperature (T_a = 300 K $\rightarrow$ 700 K of constant wind strength, $f = 0.007$. (b) Coevolution of substrate mass and substrate temperature. Increasing air flow temperature increases reaction rates and decreases time for complete consumption of the fuel substrate.

conducted with a fixed air flow temperature of 300 K, simulating the flow of ambient air over the combustion zone. This replicates the conditions that would be found on the upwind or windward side of a fire (i.e. that part of the fire that is exposed to the ambient air). This section explores, albeit in much less detail, the effect of the temperature of the air flow over the range from ambient to 700 K, well in excess of the 580 K initial substrate temperature.

Due to the many possible combinations and permutations of experimental conditions, the conditions explored here are limited to a wind strength of $f = 0.007$. As a result, the potential for a critical wind speed is not determined.

Figure 5.18a shows the effect of the temperature of the ambient wind on substrate mass for the range of temperatures: T_a = 300 K $\rightarrow$ 700 K. As the temperature of the air flow increases, the rate at which the substrate is consumed increases as expected. The rate of increase of the substrate loss rate decreases exponentially with air flow tem-

perature. In each case, the initial substrate temperature (580 K) couples with the initial gas phase temperature (550 K), reaching approximately 567 K before the air temperature begins to exert its effect (Fig. 5.18b). At air temperatures less than about 500 K, the substrate temperature continues to decrease before the exothermic reactions kick-in and lead toward ignition.

Figure 5.19 shows the effect of air flow temperature on reaction products. Increasing air temperature has the effect of increasing the ratio of *LG* to *OH* (Fig. 5.19a), *V* to *C* (Fig. 5.19c), heat released by combustion of volatiles to heat released by combustion of charcoal (Fig. 5.19d), and combined heat associated with (i.e. formation and combustion) volatiles to charcoal (Fig. 5.19e). As a result of the endothermic nature of the formation of levoglucosan, the effect of the increased mass of volatile causes a decrease in the ratio of the magnitude of the heat associated with volatile formation to that associated with charcoal formation. This decrease, however, is very minor and, like the evaporation of bound water formed through the oxidation reactions, makes little difference to the total heat of the system (Fig. 5.19f).

5.3.6 Discussion

The effect of wind can be seen to advance or retard the thermal degradation reactions and thus the rate of loss of substrate mass, depending on its temperature (Fig. 5.18). Typically, ambient air temperature ($\simeq$ 290–310 K), which is in the order of 280 K below the initial substrate temperature of 580 K for these simulations, acts to cool the reaction zone through the solid and gas phase coupling coefficients and slow the reaction rates. Elevated air temperature, in the order of the temperatures associated with the onset of ignition or greater (i.e. $\simeq$ 580–700 K), act to promote the reaction rates, through the same coupling coefficients.

The strength of the wind also affects the reaction rates, acting to magnify the effect of the air temperature (Fig. 5.5, p. 88); that is, a faster cool wind results in a slower reaction rate than that found with a lower strength wind of the same temperature, and vice versa with a hot wind. At a wind temperature of 300 K, a near-critical behaviour was identified with a wind strength between 0.007 and 0.008. Between these values, the system of reactions either progressed towards ignition of the volatiles and the rapid consumption of fuel or petered out and stopped.

A binary search of the wind strength space revealed an increasingly complicated system response as the near-critical wind strength was approached (investigated to 5 decimal places without any conclusive critical value reached) (Fig. 5.10, p. 93). The response consisted of an initial decrease in system temperatures (gas phase and solid substrate) followed by a steady increase, which either continued on until ignition or decreased again to reaction cessation. Analysis of the reaction products revealed little variation in the production of *LG* or *OH*, but a shift in the dominance in the production of *V* and *C* to *C*. The exothermic charcoal formation reaction appears to support the endothermic volatilisation reaction around the near-critical wind strength values.

The critical behaviour is most evident in the sum of the enthalpies in the system (i.e. total heat), showing nearly opposite behaviour in a complicated manner in conjunction with the evaporation of bound water around the near-critical wind strength; reaction conditions that lead to ignition show a rapid increase in both the total heat and

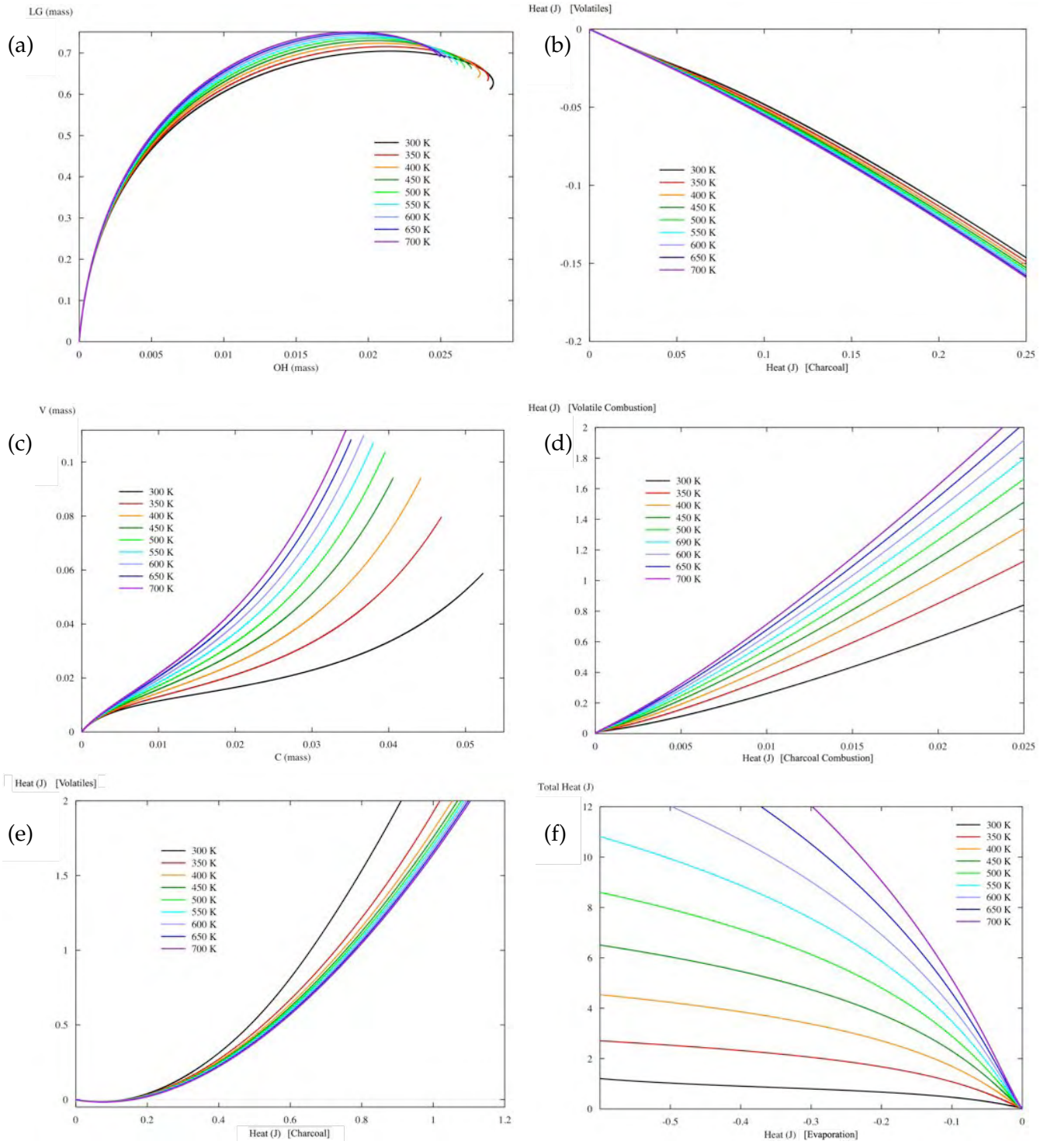

Figure 5.19: Effect of air flow temperature on reaction products and heat: (a) *LG* and *OH*, (b) heat associated with the formation of volatiles and charcoal, (c) *V* and *C*, (d) heat associated with the combustion of volatiles and charcoal, (e) heat associated with the formation and combustion of volatiles and charcoal, and (f) total heat and energy associated with evaporation.

energy associated with evaporation (led by the production of water from the oxidation reactions), whereas the reaction conditions that lead to cessation show a corresponding decrease in the heat due to evaporation and total heat in the system (Fig. 5.17).

5.4 Unsteady (sinusoidal) wind conditions

The preceding sections concerned results of a system in which the conditions were held constant. In the main, this focussed on the magnitude of the wind, f. But in the field, wind is never constant (and is more properly described as turbulent with a chaotic wave number spectrum). This section therefore deals with numerical experiments in which the wind is considered to vary sinusoidally around a mean value as a first approximation to turbulence. Effects of mean value (f_{mean}), the period of the variation (f_{period}) and the amplitude of the variation (f_{amp}) are all explored. To cover a necessarily open-ended range of possible configurations, a selected set of experimental conditions are used: $f_{amp} = 0.005, 0.01, 0.02$; $f_{mean} = 0.005, 0.01, 0.05$; and $f_{period} = 10, 30, 60, 120, 250$ s. See Appendix A2.2 (p. 193) for the ODE listing.

Refer to Table A1.1 (p. 187) for a list of symbols and associated equation numbers frequently used in this Chapter.

5.4.1 Sinusoidal wind variation

A sinusoidally-varying wind speed was chosen for its simplicity, in terms of its construction and presumed impact on the system of ODEs. Figure 5.20a shows an example of such a sinusoidal wind variation. In this case, the mean wind speed is 0.01, the amplitude is 0.02 and the period of oscillation is 60 s. All three attributes can be varied. Figure 5.20b shows two examples of mean wind speed (0.01 and 0.025) and three examples of amplitude on a wind of period 60 s. Wind speed as a scalar must remain positive, so as the mean value is reduced, so must the amplitude.

5.4.2 Effect of wind speed mean, amplitude and period

Figure 5.21a (p. 106) shows the effect on substrate mass of a sinusoidally varying mean wind speed with a period of 60 s and nominal amplitude of 0.02 (for mean wind speed values less than 0.01, the amplitude is adjusted such that the minimum wind speed is zero). When compared to simulations using constant wind of the mean strength (also see Figure 5.5c, p. 88), there is very little observable difference, suggesting, as one might expect, that a sinusoid variation around a mean wind speed behaves the same as a non-varying wind speed of the mean value. Figure 5.21b shows the relationship between substrate mass and substrate temperature for the range of wind strengths being studied. Here the effect of the sinusoidally-varying wind can be seen more clearly on the substrate temperature. It appears that the temperature of the substrate under the non-varying wind acts as the upper boundary of the substrate temperature under varying wind.

The variation in substrate mass as a result of changes in sinusoidal wind amplitude is shown in Figure 5.22a (p. 107) for two mean wind speeds ($f_{mean} = 0.005$ and $f_{mean} = 0.01$) and constant period of oscillation of 60 s. The effect of increasing amplitude in the

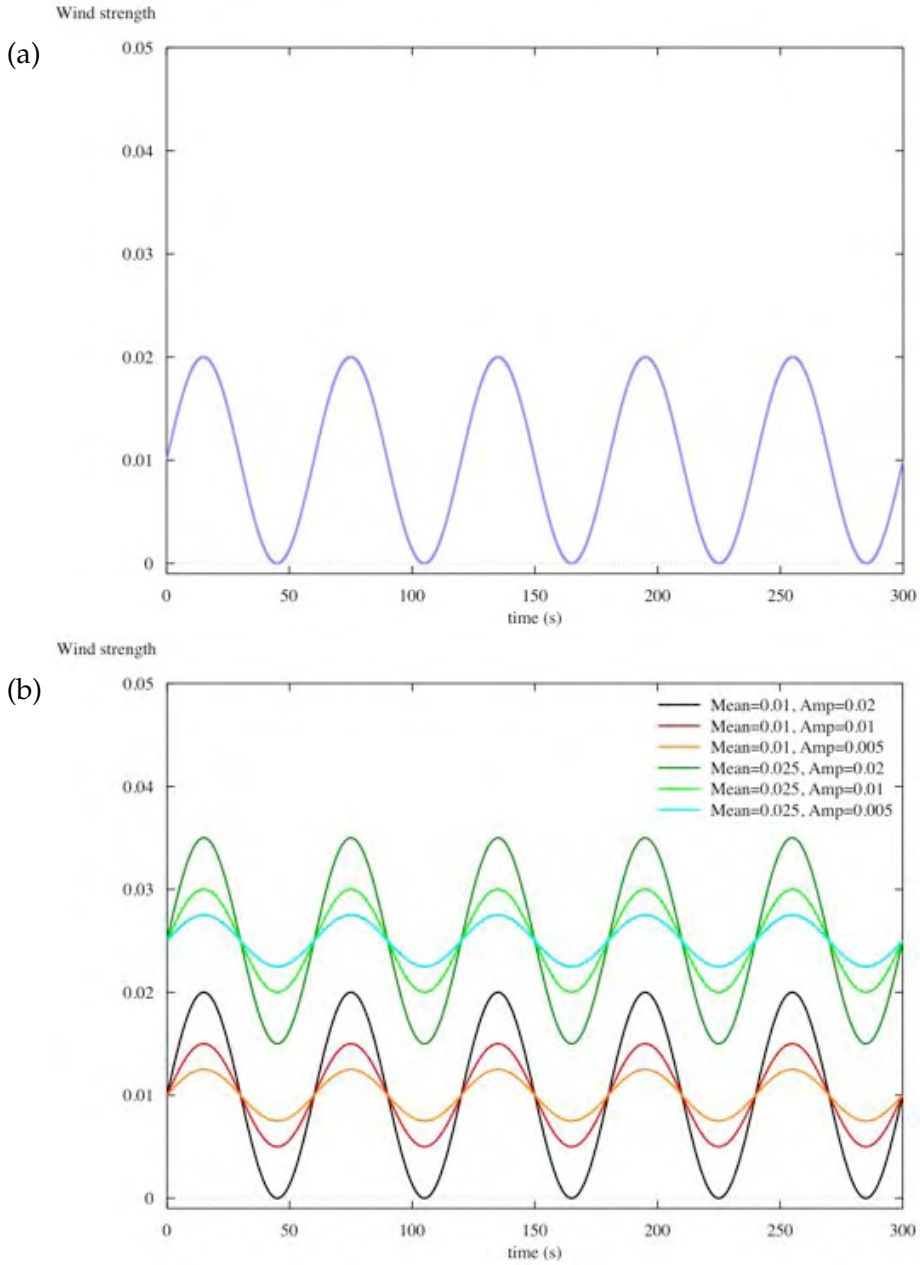

Figure 5.20: Examples of the sinusoidal wind applied as an unsteady input to the thermokinetic model: (a) A simple sinusoid, $f_{mean} = 0.01$, $f_{amp} = 0.02$, and $f_{period} = 60$ s. (b) Variations of wind with f_{mean} = 0.01 and 0.025, f_{amp} = 0.005, 0.01 and 0.02, all with f_{period} = 60 s.

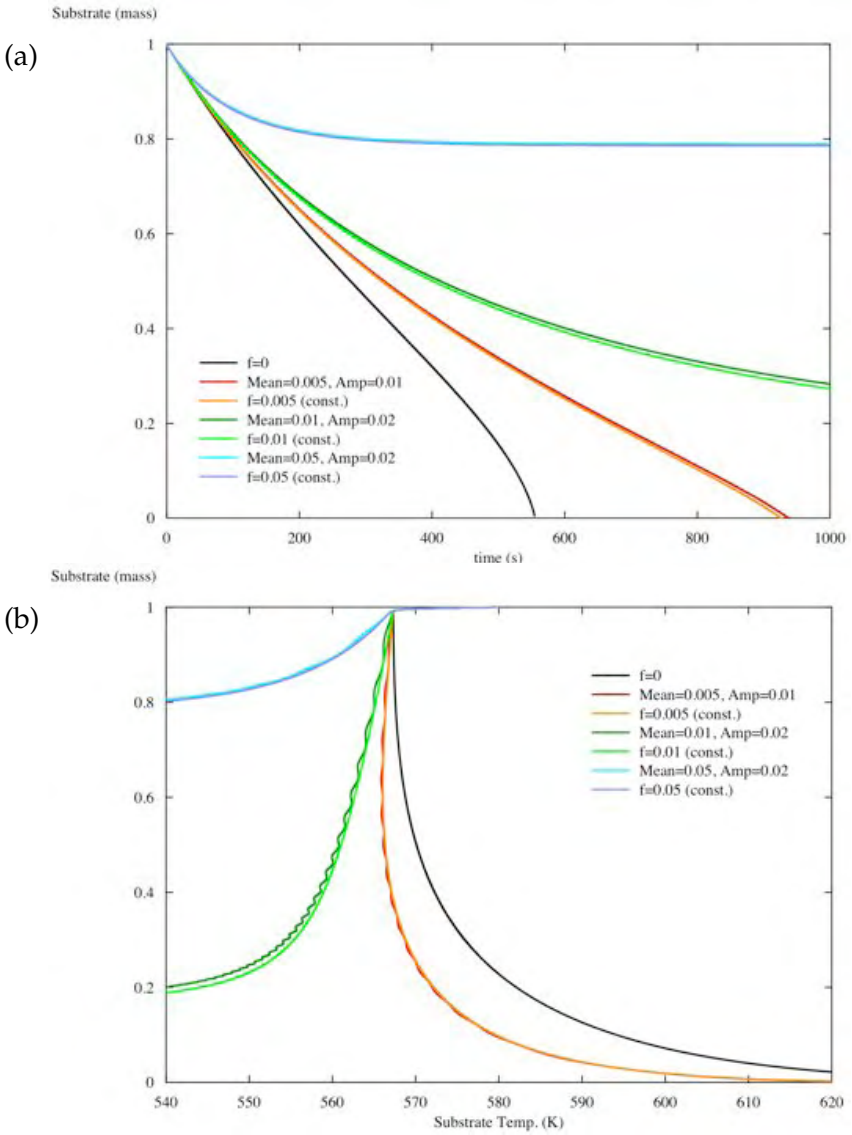

Figure 5.21: The effect of variation of a sinusoidal mean wind speed value with constant amplitude 0.02 (may be less in order to keep wind speed non-negative) and period 60 s on (a) the substrate mass and (b) substrate mass and temperature. The effect of sinusoidal wind is observed to be similar to the effect of non-varying wind at the same wind speed.

wind variation is to decrease, albeit in a very minor manner, the rate of consumption of the substrate. Decreasing amplitude results in the rate of consumption asymptoting to that of the non-varying mean wind speed, suggesting that the increased amplitude drives the reaction rates away from effect of the mean wind value.

The variation of wind oscillation period for a mean wind speed of $f_{mean} = 0.005$, $f_{amp} = 0.01$ and a range of periods ($f_{period} = 10 \rightarrow 250$ s) is shown in Figure 5.22b. The effect of increasing periodicity is to decrease the rate of consumption of the substrate. Again, this suggests that sinusoidal variation in the wind drives the reaction rates away from the effect of the mean wind value.

For all subsequent numerical experiments, a sinusoidal wind of $f_{mean} = 0.005$, $f_{amp} = 0.01$ and $f_{period} = 60$ s is used. It will in the main be compared against a non-varying wind speed of $f = 0.005$.

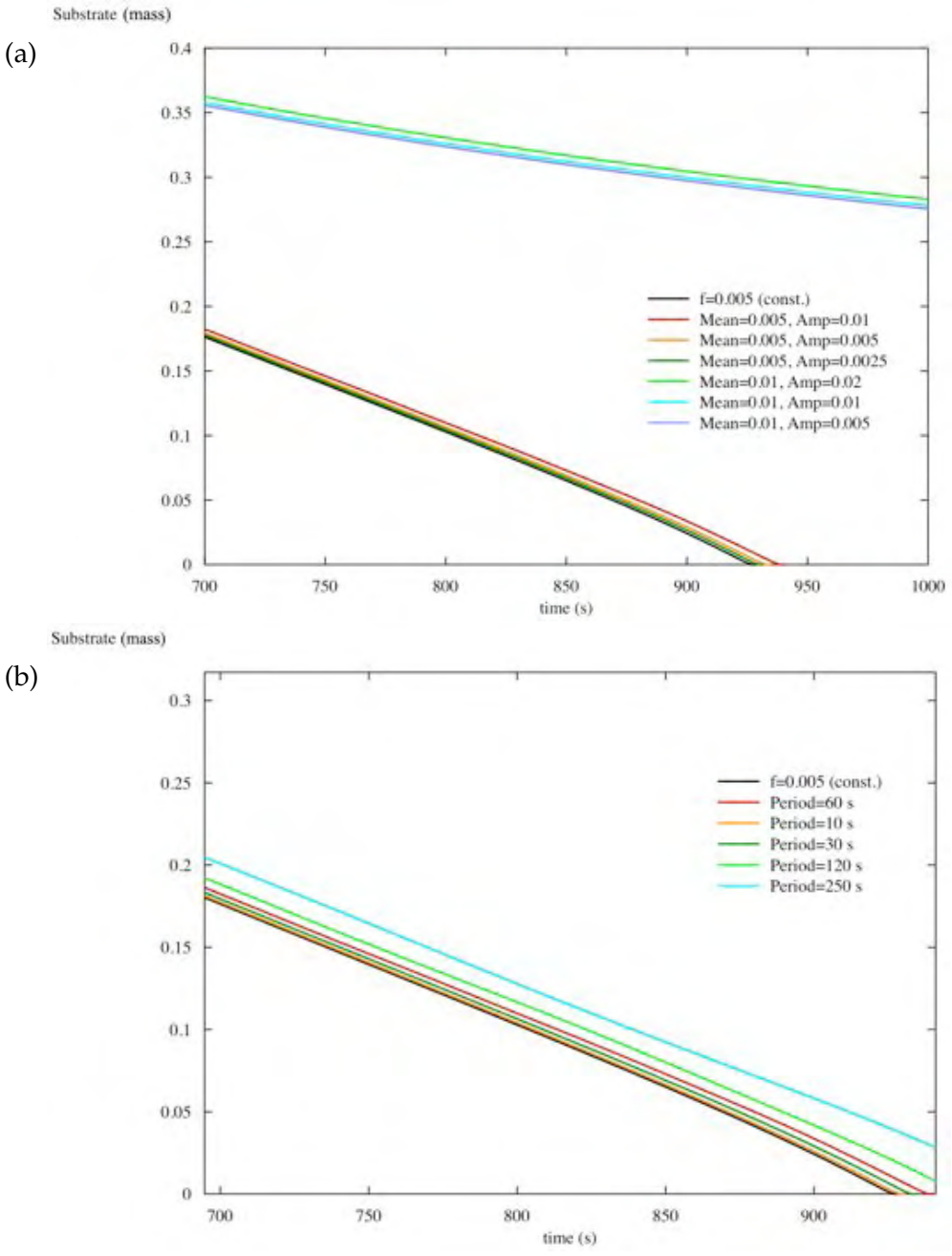

Figure 5.22: The effect on substrate mass of (a) variation of the sinusoidal amplitude of two mean wind speeds, $f_{mean} = 0.005$ and $f_{mean} = 0.01$ and $f_{period} = 60$ s; and (b) variation of sinusoidal period, $f_{period} = 10 \rightarrow 250$ s. The effect of increasing amplitude or increasing period is to decrease the rate of consumption of the substrate.

5.4.3 Effect on system heat and products

Figure 5.23a shows the evolution of the total heat in the system evolved from the formation and combustion of volatile and charcoal and evaporation of water) for a sinusoidally-varying wind ($f_{mean} = 0.005$, $f_{amp} = 0.01$, $f_{period} = 60$ s) and a constant wind, $f = 0.005$. A periodicity in the evolution of heat is discernible in the later stages of the simulation. The effect is to delay the onset of ignition of the system by 12 seconds from that of the constant wind experiment.

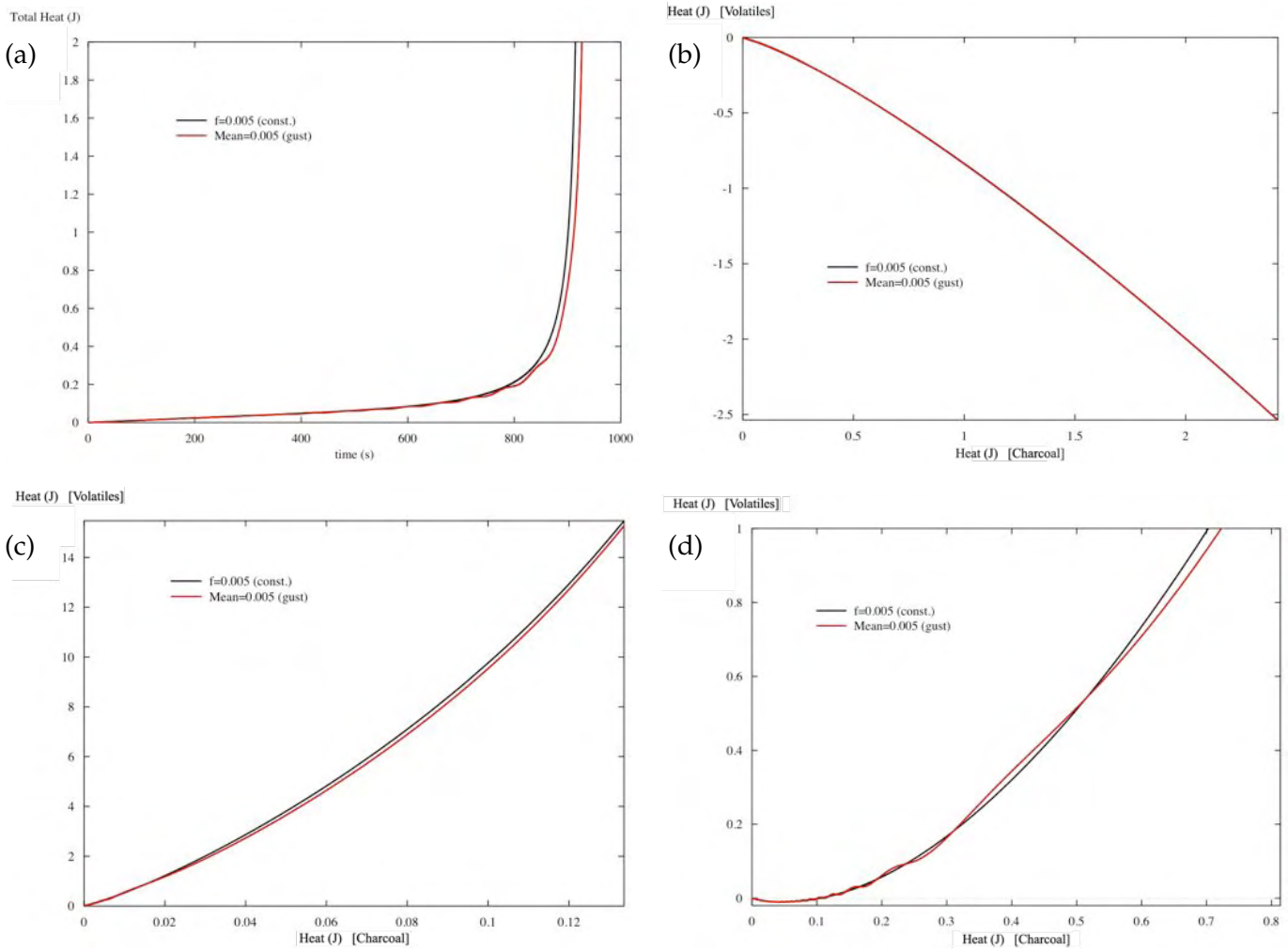

Figure 5.23: The effect of a sinusoidally-varying wind, $f_{mean} = 0.005$, $f_{amp} = 0.01$, $f_{period} = 60$ s, on (a) the evolution of total heat of the system, (b) heat from the formation of volatiles and charcoal, (c) heat from the combustion of volatiles and charcoal, and (d) the combined heat evolved from the formation and combustion of volatiles and charcoal. A slight sinusoidal variation in the total heat is apparent in the latter stages, a result primarily from the combustion reactions.

Figure 5.23b shows the coevolution of the enthalpies of formation of the volatiles and combustion. No periodicity is apparent and only a very slight difference exists between the sinusoidal and constant cases. Only in the heat released from combustion (Fig. 5.23c), and thence in the combined heat released from the formation and combustion of volatiles and charcoal (Fig. 5.23d), is a periodicity apparent. These graphs also show a more significant difference between the sinusoidal case and the constant case. More heat from the combustion of volatiles occurs under the constant case, although in the combined heats, the sinusoidal case does result in several periods where the heat from the formation and combustion of volatile exceeds that of the constant case.

The thermal degradation products *LG* and *OH* also show a lack of periodicity (Fig. 5.24a). A periodicity does appear in the mass of volatile (Fig. 5.24b), but not in *C*. This, along with the enthalpies of combustion (Fig. 5.23c) suggests that it is only the evolution of the volatiles, and then only the combustion of the volatiles, that is affected by the unsteady wind.

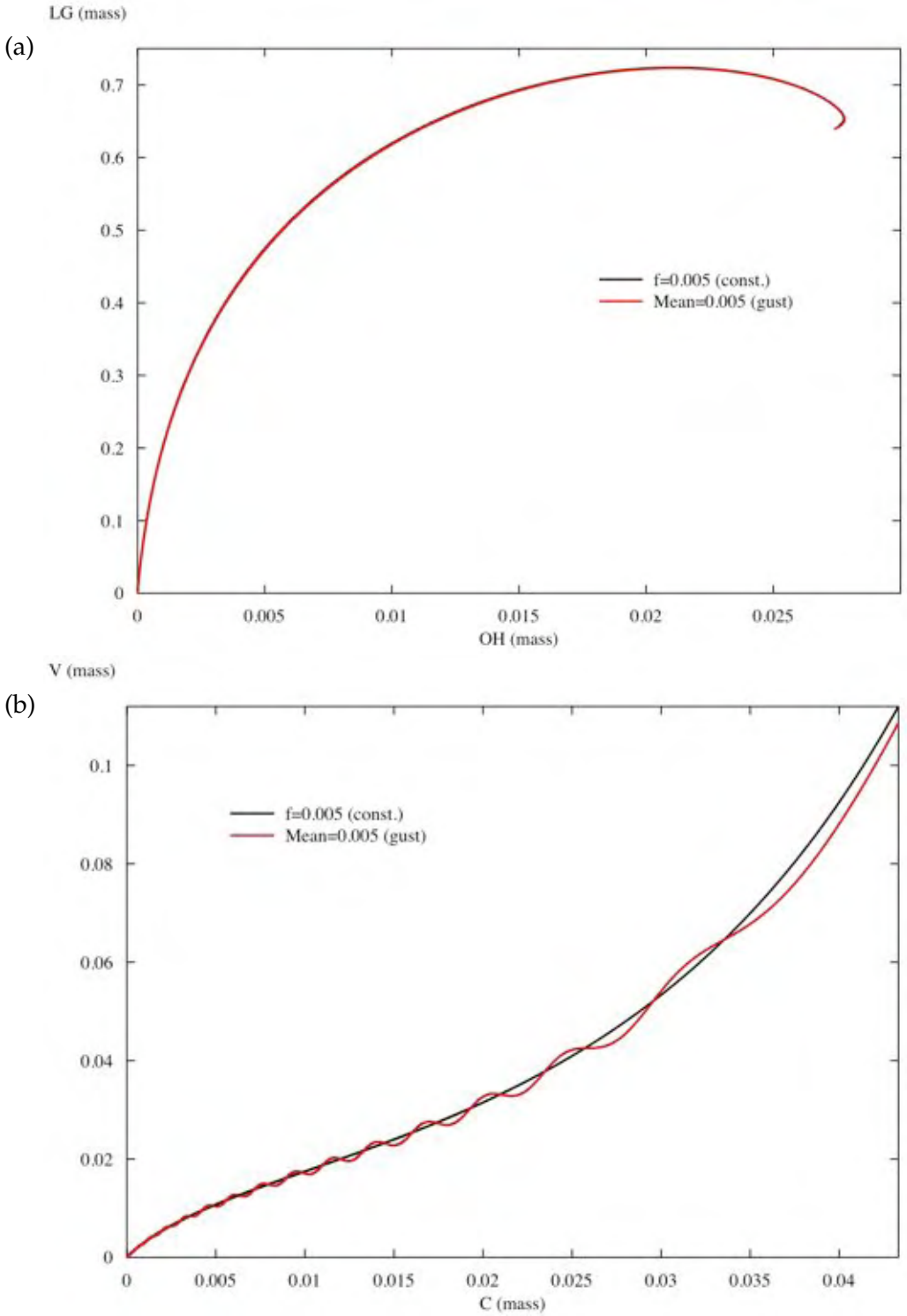

Figure 5.24: The effect of a sinusoidally-varying wind, $f_{mean} = 0.005$, $f_{amp} = 0.01$, $f_{period} = 60$ s (gust) and constant wind $f = 0.05$ (const) on (a) the coevolution of the mass of *LG* and *OH*, and (b) the co-evolution of the mass of *C* and *V*. A sinusoidal variation is present in the evolution of *V* but not in *C*.

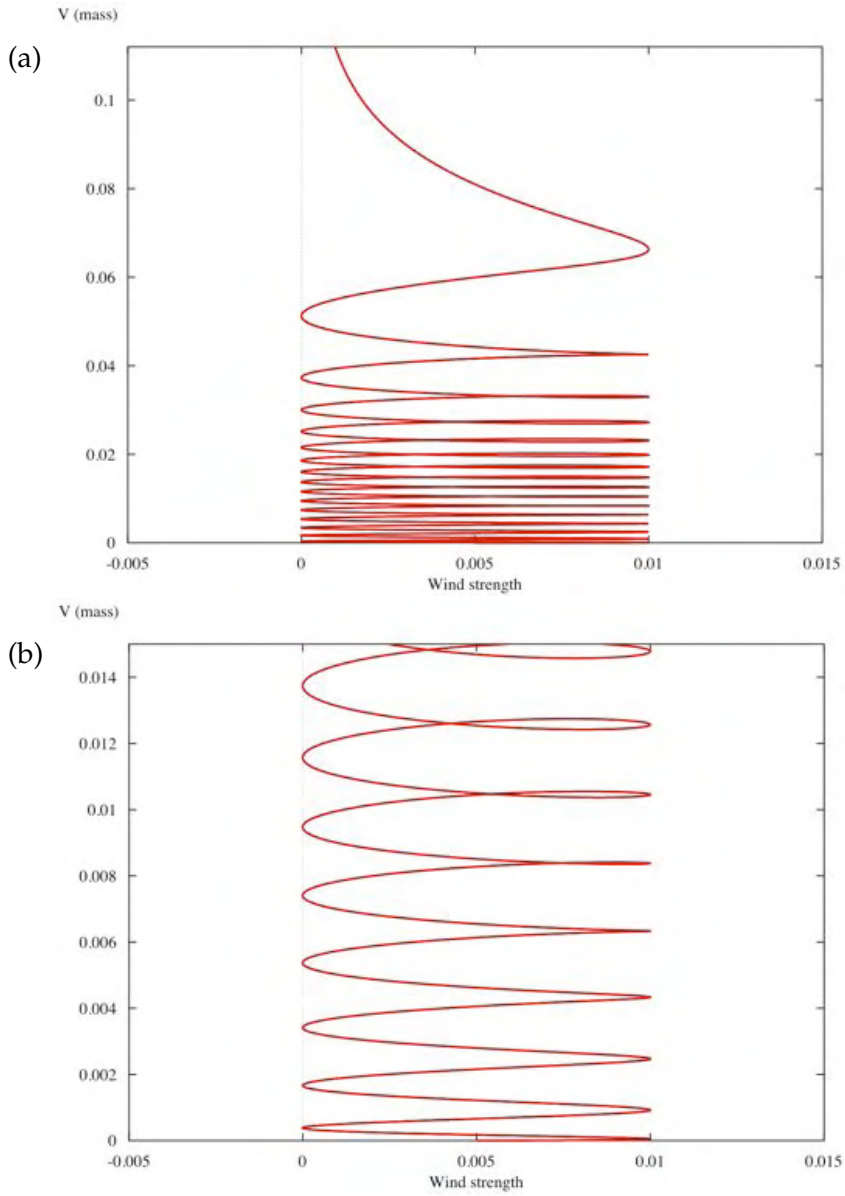

Figure 5.25: The coevolution of volatile mass with sinusoidally-varying wind, $f_{mean} = 0.01$, $f_{amp} = 0.02$, $f_{period} = 60$ s over (a) full period of reaction, (b) first half of reaction period.

Figure 5.25a shows the variation of V with the wind for the entire reaction period. A close-up of the early part of the experiment (Fig. 5.25b) shows that progression of V formation and consumption is initially independent of wind speed variation, increasing consistently. As the reactions proceed, V takes on the observed sinusoidal effect. However, this sinusoidal affect is out of phase with that of the wind, with V decreasing as the wind speed increases in the latter half of its positive period (i.e. greater than the mean value). V does not increase again until the wind has decreased to slightly more than the mean value.

5.4.4 Discussion

The effect of a sinusoidally-varying wind strength of fixed mean, amplitude and period produces results very similar to that of a constant wind strength of the same magnitude as the mean (Fig. 5.21, p. 106). Increasing sinusoid amplitude and period pro-

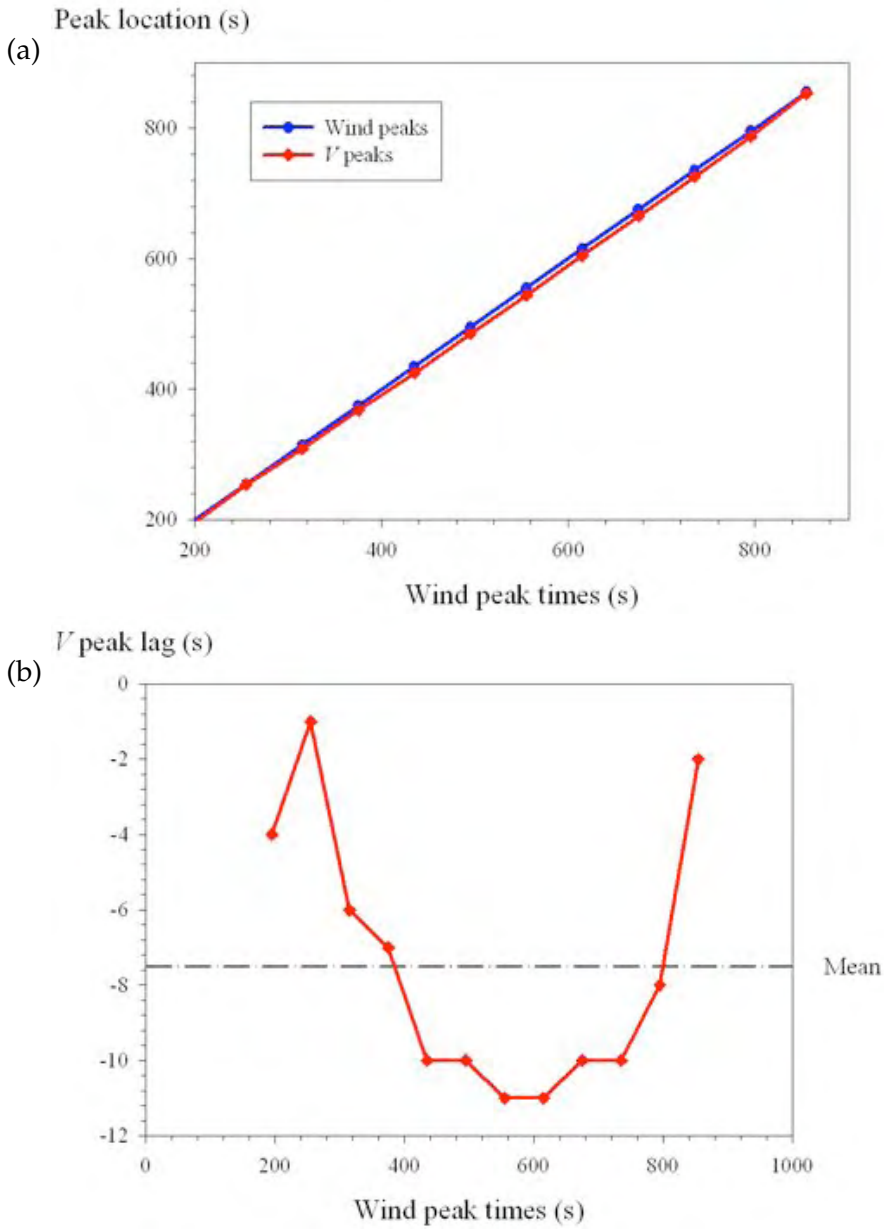

Figure 5.26: (a) A plot of the times of the maximum wind strength (blue line) and local maximum of V mass (red line). (b) The phase difference between the local peak of V and that of wind. The peak of V leads that of wind by some seconds during the middle phase of the reaction.

duces a greater difference, driving the system of reactions away from that of the constant mean wind and resulting in decreasing reaction rates and slower substrate consumption. No difference in the production of LG or OH or in the energy involved in formation of volatiles and charcoal was observed. Only a very minor effect in the heat released from the combustion of volatiles and charcoal could be seen, reflected in V and C (Fig. 5.24b, p. 109), with a significant difference occurring in the combustion of the volatiles.

Figure 5.26a plots the times of the maximum wind strength and the local maximum V for each cycle from the first phase difference up to ignition. The regular period of the wind oscillation (60 seconds) is apparent in the straight blue line. The times of the local maximum V shows a distinct non-linear difference in the middle period of the reaction

before ignition occurs. The local maximum in V consistently leads the peak in wind (Fig. 5.26b) but the magnitude of the lead varies from 1 s to 11 s, with a mean lead time of around 7.5 s.

The phase difference between the peaks of V and wind suggests that the negative impact of increasing wind on V is only felt in the final few seconds of the cycle before the wind peaks. Prior to this, an increasing wind strength has a positive effect on the net mass of V. Indeed, an increase in V also occurs under a decreasing wind, leading to the maximum rate of V at the minimum wind. However, because V is a result of both formation reactions and consumption reactions, the impact of wind on V is not straightforward. Further complicating the issue is the advection of V out of the system before oxidation.

5.5 Conclusions

A thermokinetic model of the competitive thermal degradation of cellulose from the literature (Ball *et al*. 1999a) was extended and modified in Chapter 4 to include oxidation (flaming and glowing combustion) reactions and to allow the change in temperature of the system to be self-consistent with the heat evolved from the reactions. With a basic set of initial conditions, the model was shown to simulate the progression of reactions toward ignition and an extremely rapid increase in system temperatures and substrate consumption. The model was used as the basis for a series of numerical experiments, the objective of which was, amongst other explorations, to investigate the role of advection in the competitive thermal degradation and combustion of the cellulosic fuel.

Two aspects of the system were explored: the effect of initial bound moisture, W_b, and advection or wind, through the parameter f. An additional case of sinusoidally-varying wind strength was also investigated.

The model was shown to qualitatively treat initial bound water correctly with the rate of evaporation to gas phase water increasing with increasing initial system temperature. Conditions in which initial bound water was present at temperatures when the rates of the thermal degradation reactions dominate were shown to be illogical and the counter-intuitive result of decreased substrate consumption time to be incorrect. The purpose of the model was refined to simulate the onset of ignition from suitably elevated combustion conditions and not the piloted ignition from ambient conditions. As a result the subsequent numerical experiments were limited to zero initial bound water situations, replicating the condition in which all initial bound water had been evaporated out of the fuel.

Wind is involved in two key relations in the thermokinetic model. The first is through the removal of volatile gas at a rate proportional to its strength. The second is through its temperature interacting with the temperature of the solid substrate and the gas phase above the substrate, controlled by two coupling coefficients, one for each phase. When the wind is decoupled from the temperatures of the system, the temperature of the wind has no effect on the system, although it can still remove volatile gas from the system. The effect of the coupling coefficients is to increase the effect the temperature of the wind has on the exchange of heat with the substrate and gas phase. In these experiments the coupling coefficients for both phases were kept equal, although in reality the nature of the coupling will depend on the turbulent mixing (especially for the solid phase) and

thus the roughness scale of the flows involved. For the purpose of illustrating the model and investigating the effect of wind, the coupling coefficients were set to 0.01.

Increasing wind strength of ambient air temperature (i.e. 300 K) was found to decrease the rate of substrate consumption and retard the onset of ignition. Above a certain wind strength ($f \simeq 0.0077$), the cooling effect of the wind resulted in the petering out of the reactions and eventual cessation of combustion. Around this critical wind strength, a complex system response occurred, characterised by an increase in the production of charcoal and a corresponding increase in system temperature. A binary search of wind strength space was used to try to identify an exact critical wind strength value at which the temperature of the system remained constant (that is, the endothermic reactions and exothermic reactions are in equilibrium) but none was found to 5 decimal places. The system ultimately either ignited or went out, depending on which side of the binary search space the wind speed was located. Stability analysis of the steady-state dynamics would require an infinite substrate (Ball *et al*. 2004).

Elevated wind temperatures acted to increase the rate of reactions and advance the onset of ignition, resulting in an increase in the rate of substrate consumption. The primary mechanism for this is the predominant conversion of substrate to levoglucosan and subsequently volatile gas. At ambient temperatures ($\simeq$ 300 K), the mass of volatile is of the same order of magnitude as that of charcoal; at temperatures around the onset of ignition ($\simeq$ 600 K), the amount of volatile formed is 3 times greater than charcoal. The resulting oxidation of the volatiles releases two orders of magnitude more energy than the oxidation of charcoal.

A sinusoidally-varying wind had much the same effect on the system as a constant wind of the sinusoid mean wind strength, with only a slight retardation of the reaction rates. Increasing sinusoid period and amplitude resulted in a much greater retardation in reaction rates with a corresponding decrease in the rate of substrate consumption and increase in the time to ignition. The primary effect is found in the volatile mass and combustion reactions, where volatile mass follows a sinusoidal variation in response to that of the wind. However, the peak in volatile mass leads the peak in wind strength, illustrating the complex interaction between the formation, consumption and advection of volatiles in the system.

The aim of these numerical experiments was to explore the effect of wind on the competitive thermal degradation and subsequent combustion of cellulosic fuel. The results have shown that under ambient temperature conditions, the competitive reactions are fairly evenly matched with the amount of charcoal produced in the same order as the amount of volatile produced. When the reactions lead to ignition, the initial formation of volatile, being endothermic, is supported by the exothermic charcoal formation reaction in the very early stages of the reactions. However, once the volatile oxidation reaction is initiated, the reactions become self-sustaining and system ignition occurs. When the reactions do not lead to ignition, there is a net loss of heat from the system as a result of the volatile formation. The reactions do not become self-sustaining and the reactions peter out and eventually cease.

As the wind temperature is increased toward combustion zone temperatures, all reaction rates are increased considerably. The competitive reactions are shifted toward the formation of levoglucosan-end cellulose and the resultant amount of volatile formed is three times greater than charcoal. The subsequent combustion of the volatile results in a

very rapid increase in system temperatures and substrate consumption.

The ambient wind temperature scenario would replicate the conditions found on the windward sections of a bushfire perimeter. These sections would usually be the rear and flanks of the fire. Thus the production and combustion of charcoal and volatiles would generally be equal along these sections. The elevated wind temperature scenario replicates the conditions that would be found on the leeward section of a bushfire perimeter. This section is primarily the head of the fire, in which the wind affecting the flaming zone has been heated by traversing over previously burnt and still burning ground (and thus is much hotter than ambient temperature). The significantly greater amount of volatile produced under these conditions corresponds with the greater degree of flaming combustion observed at the head of a bushfire.

The effect of ambient air temperature on the mode of combustion may also play a part in the role of convectively-induced flows ahead of a fire. In the situation where the convection of the fire causes an indraught flow to develop ahead of the fire, this flow will bring ambient temperature air into the combustion zone and thus affect the mode of combustion. However, this affect will probably be effectively countered by the relatively high rates of heat transfer in the zone immediately ahead of the flame front of a fire burning spreading freely with the wind. Fires that are limited in their capacity to spread, such as slash burns or burn-out operations, may see a greater impact from the effect of ambient temperature on the combustion mode around the perimeter due to the increased convective action and reduced radiant heating outside of the flaming zone due to flames being drawn into the centre of the fire rather than over unburnt fuel and the indraught flow.

The results of this chapter has found that wind and, in particular, the temperature of the wind, plays a significant role in the production of charcoal and/or volatile. The question remains as to how the temperature of the wind and thus the production of charcoal and volatiles varies around the fire perimeter. This is investigated in the following chapter using a computational fluid dynamics model which places the competitive reactions studied here in a spatial context.

Chapter 6

CFD modelling of competitive combustion

In which the competitive combustion model explored in a zero-spatial dimensional form in Chapter 4 is placed into a spatial context through the use of 3-dimensional computational fluid dynamics modelling in a software package called FLUENT. The design paradigm of a wind tunnel in which flow is suitably controlled is used to explore the spatial effect of wind flow (and lack of wind flow) on the competitive reaction kinetics of a fire burning along the cellulosic floor of the tunnel. It is found that a simplified two-path, two-step model of the competitive formation of volatile (levoglucosan) and charcoal and the subsequent oxidation of these products exhibits asymmetry around a fire perimeter, with a bias in the formation of charcoal on the windward side.

There is this racehorse trainer who is having problems with one of his horses. It will run but only ever follows the other horses around the track. If it doesn't win a race soon, the owner will be very upset with him, considering the amount of money she has been spent so far. Even with all his years of experience, the trainer has no idea what is wrong with the animal. After trying all conventional avenues, from veterinarians and physiologists to animal psychologists, with no luck, and with growing desperation, the trainer calls in a favour from a physicist friend to see if he can figure out what is wrong.

The physicist turns up and stands there looking at the horse. He looks at it for a long time but doesn't touch it or even approach it. The trainer begins to get nervous but then all of the sudden the physicist starts scribbling ferociously in a notebook. Finally, after filling page after page with horrendous calculations, he exclaims, "I've got it!"

"Great!" says the trainer. "What is it?"

"It's the solution to your problem. But it only works for a spherical horse in a vacuum."

6.1 Introduction

6.1.1 Computational Fluid Dynamics

Computational Fluid Dynamics (CFD) is a relatively mature sub-branch of the field of physics known as fluid mechanics in which the equations of motion for fluids (i.e. the Navier-Stokes equations as described in Section 2.3.1) are solved numerically on a computer using a variety of possible computational methods. The main use of CFD is to

analyse problems involving fluid flows which are too difficult or expensive to investigate experimentally. A growing use of CFD is the design and engineering in fields such as aerospace and automotive engineering, electronics, power generation, architecture, materials processing, and environmental applications.

Computers allow the calculation of the large array of equations required for modelling the fluid flow around complex surfaces. However, due to the complex nature of these equations and the calculations required to solve them, simplifications are required to make many problems computationally tractable, even on high-speed supercomputers (Jiménez 2006). Validation of such simulations is often a difficult task in itself and is very often performed utilising numerical techniques, only resorting to the use of experimentation such as the likes of a wind tunnel in limited circumstances.

The addition of multi-phase simulation, finite rate chemistry, and heat transfer capabilities allows CFD to model the interaction of fluids with surface and volume reactions such as that found in combustion (Cox 1998). Indeed, CFD has found a niche in the modelling, design and construction of internal combustion engines (Drake and Haworth 2007) and coal-fired power stations (Backreedy *et al*. 2005), as well as modelling reactive fluid flows such as gas dispersion in cities and transitions of stellar cores to supernovae (Oran and Gamezo 2007).

6.1.2 CFD modelling of competitive combustion

The results of the previous chapter have shown that there is a distinct change in the combustion dynamics when the temperature of the system is modified (see section 5.3.5, p. 98). Ambient temperature wind acts to steer the competitive combustion processes toward charcoal formation and glowing combustion at the expense of volatilisation and flaming combustion, whereas reaction-zone (i.e. elevated) temperature wind acts to promote volatilisation and flaming combustion at the expense of charcoal formation.

In a free-burning bushfire the thermal degradation reactions are occurring around the fire perimeter continuously as the fire progresses into unburnt fuel. The two key questions here are: 1) how does wind affect the competitive combustion in the open; and 2) what effect does this have on the mode of combustion around the perimeter?

To investigate these question it is necessary to implement the competitive combustion chemistry as detailed in Chapter 4 in a form that can be computed in three dimensions, with the interactions of the fire with the flow of air around it. This enables us to see the spatial impact of the competing combustion modes around a fire perimeter. Because we are interested in the wind (its flow and interaction with a surface fuel) as the driving mechanism in the competitive reactions, the method of CFD—and in particular the reaction kinetics modelling—is the logical choice. To that end, the CFD package called FLUENT[1] was employed.

6.1.3 FLUENT v6.2.16

FLUENT is a state-of-the-art general purpose commercial CFD software package for modelling compressible and incompressible fluid flow and heat transfer in complex

[1] produced by Fluent Inc., a wholly owned subsidiary of ANSYS, Inc.

geometries in both laminar and turbulent conditions. It is based on the finite volume method on a co-located grid. FLUENT incorporates dynamic meshing, in which FLUENT can automatically change an initial grid mesh to model flow conditions in and around moving objects based on the outcome of flow solutions. It incorporates solvers for viscous or inviscid flows, compressible or incompressible flows and multiphase (solid, liquid, gas) as well as discrete phase (i.e. particulate and droplet) flows.

It contains a large suite of codes to model heat transfer through convection, conduction, and radiation, including codes for a range of possible media. FLUENT also contains a number of models for turbulence, including a number of versions of the Reynolds-averaged Navier-Stokes (RANS) model (e.g. k-ϵ, k-ω, renormalization group, realisable), the Reynolds stress transport model (RSM), and a large eddy simulation (LES) model. It can also model periodic and buoyancy-driven flows.

FLUENT can model the mixing and transport of chemical species by solving the conservation equations describing convection, diffusion, and reaction sources for each component species. Multiple simultaneous chemical reactions can be modeled, with volumetric, wall or particle surface reactions. Combustion can be modelled directly using a comprehensive range of methods, including composition probability distribution function transport, stiff finite rate chemistry models, equilibrium mixture fraction, flamelet, premixed, non-premixed and partially-premixed combustion models, with gas/surface reactions and NO_X formation. A number of workers have employed FLUENT successfully in fully turbulent combusting flows (e.g. Xue *et al*. (2001); Bari and Naser (2005); Lignini *et al*. (2005)) and FLUENT Inc. themselves have undertaken considerable validation of solutions for a large range of numerical problems; these are available from their website[2].

While FLUENT is available as a Windows application, it was the multi-processor version run on the Australian Partnership for Advanced Computing (APAC) National Facility Supercomputer at the Australian National University, known as the SGI Altix 3700 Bx2 cluster (AC)[3], through APAC project x39, that was used for this study.

6.2 FLUENT CC-CFD model definition

While the aim of this chapter is to place the thermokinetics of the thermal degradation of cellulosic fuels explored in some detail in Chapter 5 into a 3-dimensional context, it is not feasible to literally translate the experimental conditions of that work into FLUENT, not least because the dynamical systems model was non-dimensional and FLUENT uses fully dimensional variables. That being said, it was intended that the conditions of the 3D simulations be as similar as possible to those of the dynamical system simulations.

The main design paradigm used for the FLUENT CFD model (called here the competitive combustion or CC-CFD model) was that of a fire burning through a thin fuel layer on the floor of a small rectangular-section wind tunnel. While FLUENT can easily handle much more complex geometries than that of a rectangular box, the idea was that a confined domain such as a wind tunnel would reduce the design requirements

[2]http://www.fluentusers.com (requires login and password).

[3]AC consists of 1,928 1.6 GHz Intel Itanium2 processors grouped into 59 partitions of 32 processors each. Total memory is 5.6 Terabytes. This computer ranked #71 in the list of top 500 supercomputers in 2006 (http://www.top500.org/list/2006/11/100).

and simplify the interactions of the wind with the combustion reactions. The structure of the wind field applied to the upwind (entry) end of the wind tunnel would be kept simple and any complications in the flow would result from the combustion chemistry, heat transfer and buoyancy effects of the fire itself (although, of course, there would be boundary effects from the walls).

The fuel is assumed to be composed of cellulose and to contain no moisture. The air in the system is also assumed to contain no moisture. The initial temperature of the tunnel and the air would be at ambient temperatures. The speed of the air entering from the inlet side of the tunnel would then be varied to explore the effect of the flow on the spatial dynamics of the reactions involved in the thermal degradation and oxidation reactions.

6.2.1 CFD Mesh

Two meshes (numerical grid domains) were used in this study. The first was a simple 2D mesh that was used for 'proof-of-concept' and then to develop and refine the CC-CFD model definitions. The second was a 3D mesh that allowed detailed numerical simulation of the combustion chemistry and resulting flows around the fire perimeter. The meshes were created using GAMBIT[4] 2.0.4, the mesh design application shipped with FLUENT and imported into FLUENT.

The 3D mesh (Fig. 6.1) is a 3D representation of a 3-m long, 1.6-m wide and 1-m high wind tunnel modelled using a 3-m long, 0.8-m wide and 1-m high domain that uses a symmetry face along the central axis to effectively double the width of the tunnel and thus save on computation. The mesh consists of 24000 hexahedral cells composed of 60 columns of cells in the x-direction of uniform width ($\Delta x = 0.05$ m), 20 columns in y-direction of uniform width ($\Delta y = 0.04$ m), and 20 non-uniform cells in the z-direction, increasing in height exponentially according to (Fluent Inc 2001d):

$$\frac{l_{i+1}}{l_i} = \exp\left(\frac{L}{n}\right)(x - 0.5), \tag{6.1}$$

where l_i is the length of the ith interval, l_{i+1} is the length of the next interval, L is the length of domain, n is the number of intervals in the length, and x is a user-defined ratio figure ($\simeq$2.87). This results in the smallest cell volume of size of 3.3 $\times$ 10^{-5} m^3 at the bottom of the wind tunnel where combustion will occur and the largest cell volume size of 2.2 $\times 10^{-4}$ m^3 at the top of the wind tunnel where no combustion is expected. This was done to improve computational efficiency of the simulation.

The 400 faces on the left boundary are designated inlet-velocity faces (coloured blue in Figure 6.1), the 400 faces on the right boundary are designated outflow faces (coloured red), boundary on the far side, composed of 1200 faces (coloured yellow) is designated as a symmetry boundary and allows only half the domain to be calculated and the other half to be mirrored around this symmetry boundary. The 1200 faces on the floor, 1200 faces on the near-side boundary and the 1200 faces on the roof are designated wall faces.

[4]produced by Fluent Inc., a wholly owned subsidiary of ANSYS, Inc.

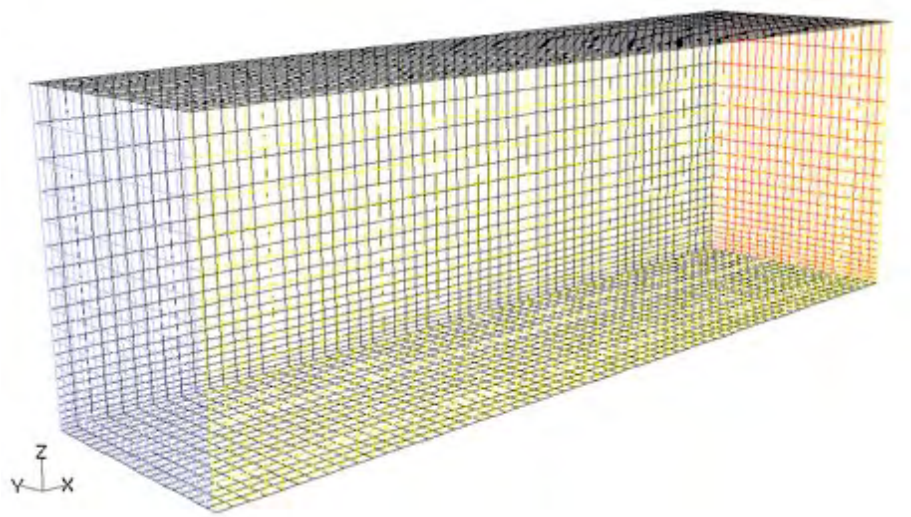

Figure 6.1: 3D mesh used for CFD modelling to investigate the role of wind flow in the combustion chemistry of cellulosic fuel. Blue indicates inlet face, red outflow face and yellow the symmetry boundary.

6.2.2 Models

This section discusses each of the components in FLUENT required for the modelling of the chemistry and physics of combustion and heat transfer. For each component, a range of models is available and these are discussed in general terms before a particular model is selected for inclusion in the CC-CFD model.

Solver

FLUENT will solve the governing equations for the conservation of mass and momentum (Eqs. 6.2 and 6.3), and (when appropriate) for energy (Eq. 6.4) and species transport using two possible methods. The first is a segregated solver in which the governing equations for mass, momentum, energy and species are solved sequentially (i.e. they are segregated or uncoupled). The second is a coupled solver in which all equations are solved simultaneously. This can be done in one of two ways: implicitly, in which for each variable the unknown in each cell is computed based on both existing and unknown values from neighbouring cells; and explicitly, in which for each variable the unknown value in each cell is computed using only known values.

Additional scalar quantities (such as turbulence or radiation including species transport) are solved sequentially after the governing equations of mass, momentum and energy. Each solver provides accurate results for a broad range of flows but in some cases one formulation may perform better (i.e. achieve a solution faster) than another (Fluent Inc 2001a, p. 1-18). Some models, such as the pre-mixed and partially pre-mixed combustion models, soot NO_X or stiff chemistry, are only available under certain solvers.

The Euler equations for conservation of mass and momentum for inviscid flow are given as:

Mass conservation (Fluent Inc 2001b, p. 8-36):

$$\frac{\partial \rho}{\partial t} + \nabla.(\rho \vec{v}) = S_m, \tag{6.2}$$

where ρ is density of the continuous phase, t is time, x is distance, $\vec{v}$ is the velocity vector, and S_m is the source mass added to the continuous phase from a dispersed second phase.

Momentum conservation (Fluent Inc 2001b, p. 8-36):

$$\frac{\partial \rho \vec{v}}{\partial t} + \nabla.(\rho \vec{v} \vec{v}) = -\nabla p + \rho \vec{g} + \vec{F}, \tag{6.3}$$

where $\rho \vec{g}$ and $\vec{F}$ are the gravitational body force and external body forces (i.e. forces that arise from interaction with the dispersed phase).

Energy conservation (Fluent Inc 2001b, p. 11-2):

$$\frac{\partial}{\partial t}(\rho E) + \nabla.(\vec{v}(\rho E + p)) = -\nabla. \left(k_f \Delta T - \sum_j h_j \vec{J}_j + (\bar{\bar{\tau}}.\vec{v}) \right) + S_h, \tag{6.4}$$

where E is the energy of the continuous phase, k_f is the effective conductivity (comprising the turbulent thermal conductivity and material thermal conductivity), h_j and $\vec{J}_j$ are the enthalpy and diffusion flux for each species concerned. The first three terms on the right hand side represent energy transfer due to conduction, species diffusion and viscous dissipation, respectively. S_h includes the heat of chemical reaction and other volumetric heat sources.

The coupled-implicit solver was selected for use in the CC-CFD model.

Energy

The solution of the energy equation is necessary for accurate solution of heat transfer equations (e.g. viscous heating in turbulence model or radiant heat transfer in the radiation model). As we are dealing with both in our CC-CFD model, the energy equation is selected to be solved.

Viscous Model

There is no single turbulence model that is universally accepted as being superior for all classes of problems (Fluent Inc 2001b, p. 10-3). As a result, FLUENT includes a selection of five primary turbulence models in addition to an inviscid model (i.e. effects of viscosity are ignored, generally where inertial forces dominate viscous forces) and a laminar flow model (i.e. no turbulence at all). The five models are:

1. the Spalart-Allmaras model, a simple one-equation model that solves for the kinematic eddy viscosity;

2. k-ϵ models, of which there are three varieties:

(a) the standard k-ϵ model, a semi-empirical two-equation model based on transport equations for the turbulence kinetic energy (k) and its dissipation rate (ϵ) which are determined independently;

(b) Renormalisation-Group (RNG) k-ϵ model, which is derived from instantaneous Navier-Stokes equations using Renormalisation Group methods;

(c) Realisable k-ϵ model, in which mathematical constraints on the normal stresses consistent with the physics of turbulent flows are applied and more exact formulations used for dissipation rate;

3. k-ω models, of which there are two varieties:

   (a) the standard k-ω model, which is an empirical model that incorporates modifications for low-Reynolds-number effects, compressibility, and shear flow spreading;

   (b) shear-stress transport k-ω model, in which the accurate standard k-ω model in the near-wall region has been combined with the free-stream independence of the k-ϵ model in the far-field;

4. the Reynolds Stress model (RSM), in which seven additional transport equations (in 3D, four in 2D) are used to solve for the individual Reynolds stresses and dissipation rate in order to close the Reynolds-averaged Navier-Stokes equations;

5. the large eddy simulation (LES) model, in which the time dependent Navier-Stokes equations are filtered such that large eddies in a flow are resolved directly and smaller eddies are modelled via sub-grid parameterisation. Can only be used in 3D.

Each turbulence model has its advantages and disadvantages, depending on the type of flow being modelled. Generally, the main issue in choosing a turbulence model is one of computational cost (CPU time and memory requirements) versus numerical gains (in terms of accuracy). While the RSM is the most elaborate turbulence model provided by FLUENT, it requires 50-60% more CPU time and 15-20% more memory than the k-ϵ and k-ω models (Fluent Inc 2001b, p. 10-12).

For the CC-CFD model, the realisable k-ϵ model was chosen in order to provide a sufficiently detailed result in the Reynolds number (i.e. turbulent) flows envisaged to result from combustion.

Radiation Model

The heating or cooling of surfaces due to radiation and heat sources and sinks due to radiation within the fluid phase are incorporated into the CFD modelling of FLUENT through the radiative transfer equation (RTE). The RTE for an absorbing, emitting and scattering medium at position $\vec{a}$ in the direction $\vec{s}$ is (Fluent Inc 2001b, p. 11-17):

$$\frac{dI(\vec{r},\vec{s})}{ds} + (a+\sigma_s)I(\vec{r},\vec{s}) = an^2\frac{\sigma T^4}{\pi} + \frac{\sigma_s}{4\pi}\int_0^{4\pi} I(\vec{r},\vec{s})\Phi(\vec{s},\vec{s}')d\Omega', \tag{6.5}$$

where $\vec{r}$ is the position vector, $\vec{s}$ is the direction vector, $\vec{s}'$ is the scattering direction vector, s is the path length, a is the absorption coefficient, n is the refractive index, σ_s is the

scattering coefficient, σ is the Stefan-Boltzmann constant (5.67×10^{-8} W m^{-2} K^{-4}), I is the radiation intensity, T is the local temperature, Φ is the phase function, and Ω' is the solid angle.

FLUENT provides a choice of five radiation models to solve the RTE and model the effect of radiant heat transfer with or without participating media (Fluent Inc 2001b, p. 11-17):

1. Discrete transfer radiation model (DTRM), a relatively simple model that approximates the radiation leaving a surface element by a single ray. It assumes all surfaces are diffuse, does not model scattering, and is CPU-intensive for a large number of rays;

2. P-1 radiation model, a simplified version of a more general model that is based on the expansion of I into an orthogonal series of spherical harmonics. It is not CPU-intensive, includes the effects of scattering but assumes all surfaces are diffuse, assumes gray radiation and is less accurate when the optical thickness of the medium is small;

3. Rosseland radiation model, derived from the P-1 model with some approximations, it is faster and requires less memory. However, it is only valid when the optical thickness of the medium is thick and can only be used with the segregated solver;

4. Surface-to-surface (S2S) radiation model, which accounts for the radiation exchange between gray-diffuse surfaces in an enclosure by utilising a view factor for the geometric relation (size, separation, orientation) between the surfaces. It does not incorporate effects of a participating media (such as scattering) and is CPU- and memory-intensive when the number of surfaces is large;

5. Discrete ordinates (DO) radiation model, which solves the RTE as a transport equation for a finite number of discrete solid angles (unlike DTRM which utilises a ray-tracing method). It can be used over the entire range of optical thicknesses, in participating media, and for surface exchange. It assumes gray or gray band radiation.

The DO model with default settings was chosen to model the radiant heat transfer in the CC-CFD model.

Species Model

FLUENT provides several models for species transport with and without chemical reactions (Fluent Inc 2001c, p. 12-1). Chemical reactions that can be modelled include gas phase reactions, surface (i.e. solid-gas interface) reactions, and particle surface (i.e. discrete phase) reactions. There are five approaches to modelling reactive flows:

1. Generalised finite-rate, based on the solution of transport equations for species mass fractions with source terms in the form of reaction rates computed from Arrhenius rate expressions. Models of these type are suitable for a wide range of applications, including combustion;

2. Non-premixed combustion, a method developed specifically for simulation of diffusion flames in which transport equations for only one or two scalars (the mixture fractions) are solved. The reacting system is treated using a 'mixed-is-burned' approach, i.e. no reaction rate used;

3. Premixed combustion, a method specifically developed for systems that are of purely the premixed (i.e. oxidiser and fuel are mixed prior to ignition) type;

4. Partially premixed combustion, a combination of non-premixed and perfectly premixed combustion methods;

5. Composition PDF transport, in which a predefined probability distribution function (PDF) is used to define the reaction results based on, for example, system temperature.

The species model chosen for the CC-CFD model was that of species transport based on the generalised finite-rate approach using reaction kinetics data provided in the simulation materials database (see Section 6.2.3, p. 124). The local mass fraction of each species is determined by the solution of a convection-diffusion equation for each species of the general form:

$$\frac{\partial}{\partial t}(\rho Y_i) + \nabla.(\rho \vec{v} Y_i) = -\nabla.\vec{J_i} + R_i + S_i, \tag{6.6}$$

where Y_i is the ith species, R_i is the net rate of production by chemical raction, S_i is the rate of creation by addition from other external sources. In turbulent flows, J_i, the mass diffusion flux of each species, is given by:

$$\vec{J_i} = -(\rho D_{i,m} + \frac{\mu_t}{Sc_t})\Delta Y_i, \tag{6.7}$$

where $D_{i,m}$ is the diffusion coefficient for species i, Sc_t is the Schmidt number (the ratio of the momentum diffusivity to mass diffusivity, set by default to 0.7), and μ_t is the turbulent dynamic viscosity.

In the CC-CFD model, both volumetric (i.e. reactions occurring in the fluid volume) and wall surface (i.e. reactions occurring only on the surface of walls) reaction types were selected as the combustion reactions we are modelling occur both on the floor surface of the wind tunnel and in the air of the wind tunnel. In volumetric reactions, turbulent flow can play a significant role in the way chemical reactions unfold. That is, the rate of mixing of the reactants due to the turbulence can control the rate at which the chemical reactions occur. Four models are available to compute chemical reaction rates:

1. the laminar finite-rate model, in which the effects of turbulent fluctuations are ignored and reaction rates are determined solely by Arrhenius expressions;

2. the eddy dissipation model, in which reaction rates are assumed to be controlled purely by turbulence (i.e. the rate of mixing) and the Arrhenius expressions are ignored;

3. the finite-rate/eddy dissipation model, in which both the finite-rate and eddy dissipation rates are calculated and the lesser of the two used;

4. the eddy dissipation concept (EDC) model, in which the eddy dissipation model has been extended to include detailed chemical mechanisms in turbulent flows. It assumes that reactions occur in small turbulent structures.

The EDC model is used in the CC-CFD model.

6.2.3 Materials

To properly model the response of all components in a CFD simulation, all components are given physical attributes, either from a comprehensive library of pre-programmed materials or from material data manually entered into the software. The attributes depend upon the phase of the material (solid, liquid or gas) and the models of turbulence, radiation and species transport chosen for the simulation solution (selected models have particular requirements in terms of physical attributes of materials needed to solve them).

Solid phase materials

There are two types of solid material used in this simulation: the walls (floor, roof, walls) of the wind tunnel, and the fuel involved in the combustion on the floor of the wind tunnel. The walls of the wind tunnel are assigned the material 'wood' from the FLUENT materials database. This material has the density of 700 kg m^{-3}, specific heat of 2310 J $kg^{-1}K^{-1}$ and thermal conductivity of 0.173 W $m^{-1}K^{-1}$.

The solid fuel involved in the combustion takes two forms, based on the combustion chemistry discussed in Chapters 2 and 3 and explored in Chapter 4. These are raw cellulose and charcoal. Both fuels are manually entered, derived primarily from wood in the case of cellulose and solid carbon in the case of charcoal.

A third condensed phase material is liquid water that is evolved from the charcoal formation reaction.

The attributes of these materials are given in Table 6.1.

Gas phase materials

The primary gas phase material is air (77% N_2, 23% O_2). Air flows into the wind tunnel from the left boundary at prescribed speeds and exits from the right boundary at rates dependent upon what happens in the wind tunnel. The other gas phase materials are those that are evolved from the combustion and thermal degradation. These, in order of decreasing amount, are: CO_2, H_2O, and levoglucosan ($C_6H_{10}O_5$).

The attributes of these materials are given in Table 6.1.

Mixture material

FLUENT treats the materials involved in chemical reactions as part of a mixture. The mixture defines the reactants, the reactions, the enthalpy, the activation energy, rate constants and products. The mixture used in the CC-CFD model was derived from 'wood-volatiles-air' from the FLUENT materials database.

The reactions that comprise the mixture material are simplified versions of those given in Chapter 4. The main simplifications involve the removal of the intermediate formation of levoglucosan-end and hydrolysed cellulose, the secondary formation

Table 6.1: Attributes[a] of reactant and product materials used in the CC-CFD model.

Material	Formula	Density (kg m^{-3})	Specific Heat (J kg^{-1} K^{-1})	Mol. Weight (kg $kgmol^{-1}$)	Std. Enthalpy (J $kgmol^{-1}$)	Viscosity (kg $m^{-1}s^{-1}$)
air	-	1.225	1006.43	28.966	-	1.7894×10^{-5}
oxygen	O_2	1.299	919.31	31.999	205026.9	1.919×10^{-5}
nitrogen	N_2	1.138	1040.67	28.013	191494.8	1.663×10^{-5}
water vapour	H_2O	0.5542	2014	18.015	-2.418×10^{8}	1.34×10^{-5}
liquid water	H_2O_l	998.2	4182	18.015	0	0.001
carbon dioxide	CO_2	1.7878	840.37	44.010	-3.935×10^{8}	1.37×10^{-05}
levoglucosan	$C_6H_{10}O_5$	1.0	1500	162	4.86×10^{7}	1.72×10^{-5}
charcoal	$C_{11}H_4$	2000	1220	136	2.57×10^{8}	-
cellulose	$(C_6H_{10}O_5)_s$	700	2310	162	-	-

[a]Based on figures from the FLUENT materials database.

of volatiles from hydrolysed cellulose, and the secondary formation of charcoal from levoglucosan-end cellulose. The reactions are thus reduced to three primary one-step reactions forming charcoal and levoglucosan and two secondary reactions involving the oxidation of these products. That is, cellulose forms only levoglucosan or charcoal. This simplification is not expected to alter the competitive behaviour of the reactions through the use of the limiting reaction rate constants and allows more simple reporting of reaction products. A more refined version may include these intermediate steps. The CC-CFD reactions are:

Charcoal 1

The primary formation of our charcoal species ($C_{11}H_4$) in the absence of water is given by:

$$2(C_6H_{10}O_5)_s \rightarrow C_{11}H_{4_s} + CO_{2_g} + 8H_2O_l, \tag{6.8}$$

where H_2O_l is liquid phase water.

Charcoal 2

It is assumed that the formation of charcoal from hydrolysed cellulose will proceed to charcoal at a rate controlled by the final charring reactions (and not the formation of hydrolysed cellulose):

$$2(C_6H_{10}O_5)_s + H_2O_l \rightarrow C_{11}H_{4_s} + CO_{2_g} + 9H_2O_l. \tag{6.9}$$

Levoglucosan

It is assumed that levoglucosan-end cellulose formed through the primary thermal degradation process will proceed to levoglucosan at a rate controlled by the final depolymerisation step (and not the formation of levoglucosan-end cellulose which is much faster). That is, cellulose proceeds directly to levoglucosan by :

$$(C_6H_{10}O_5)_s \rightarrow C_6H_{10}O_{5_g}. \tag{6.10}$$

Glowing combustion Oxidation of the charcoal is assumed to proceed to H_2O and CO_2 with no intermediates formed:

$$C_{11}H_{4_s} + 12O_{2_g} \rightarrow 11CO_{2_g} + 2H_2O_g. \tag{6.11}$$

Flaming combustion

Oxidation of levoglucosan is assumed to proceed to H_2O and CO_2 with no intermediates formed:

$$C_6H_{10}O_{5_g} + 6O_{2_g} \rightarrow 6CO_{2_g} + 5H_2O_g. \tag{6.12}$$

Pre-exponential factor and activation energy values for each reaction, as well as reaction type, are given in Table 6.2:

Table 6.2: Activation energy, pre-exponential factor and reaction type for reactions used in the CC-CFD model.

Reaction	Pre-exponential Factor (s^{-1})	Activation Energy (kJ mol^{-1})	Reaction Type
Charcoal 1	6.7×10^5	110	Wall surface
Charcoal 2	1.3×10^{10}	145	Wall surface
Levoglucosan	3.2×10^{14}	198	Wall surface
Glowing	1.4×10^{11}	183	Wall surface
Flaming	2.55×10^{13}	188	Volumetric

Unlike the thermokinetics modelling undertaken in Chapter 5 where only the reaction enthalpies of the formation of the charcoal and levoglucosan species were required to described the heat released or consumed during the formation reactions, FLUENT requires the standard state enthalpy of formation, ΔH_f, of these species (which for our charcoal species is unknown and for gas phase levoglucosan could not be found in the literature). That is, rather than dealing only in the total heat released or consumed during a reaction, FLUENT calculates the heat of reaction as the difference of the total standard state enthalpy of each reactant and product species:

$$\text{Heat of Reaction} = \sum \Delta H_f \text{Products} - \sum \Delta H_f \text{Reactants}. \tag{6.13}$$

However, knowing the heat of reaction and the textbook standard state enthalpies of reaction products, it is possible to calculate standard state enthalpies for our charcoal species and levoglucosan based on the molar stoichiometry. Thus, for charcoal, using Equations 6.13 and 6.8 and the figure of -1000 J g^{-1} (136 kJ mol^{-1} of charcoal) we get:

$$-136 = \big((1 \times \Delta H_{f_{(char)}}) + (1 \times -393) + (8 \times 0)\big) - (2 \times 0), \tag{6.14}$$

where $\Delta H_{f_{(char)}}$ is the unknown standard state enthalpy of formation for our charcoal species, the standard state enthalpy for cellobiose is taken as zero (as all species in their standard state are), and all quantities are in kJ mol^{-1}. Rearranging for $\Delta H_{f_{(char)}}$ we get:

$$\Delta H_{f_{(char)}} = -136 + 393 = 257 \text{ kJ mol}^{-1}. \tag{6.15}$$

Similar calculations for levoglucosan (Equations 6.13 and 6.10 and 300 J g^{-1} (48.6 kJ mol^{-1})) yields $\Delta H_{f_{(levo)}} = 48.6$ kJ mol^{-1}.

These values can be checked by calculating the heat of reaction (HoR) for the oxidation (combustion) reactions for each of these species and comparing with values obtained from the literature:

Charcoal combustion (Eq. 6.11):

$$\begin{aligned} HoR &= ((11 \times -393) + (2 \times -241)) - ((1 \times 257) + (12 \times 0)), \\ &= -4547 \text{ kJ mol}^{-1}, \\ &= -33.4 \text{ kJ g}^{-1} \text{ of charcoal consumed.} \end{aligned} \tag{6.16}$$

which corresponds well with the value of 32 kJ g^{-1} obtained from the literature (Eghlimi *et al*. 1999) for the heat released from the combustion of charcoal.

Levoglucosan combustion (Eq. 6.12):

$$\begin{aligned} HoR &= ((6 \times -393) + (5 \times -241)) - ((1 \times 48.6) + (6 \times 0)), \\ &= -3611.6 \text{ kJ mol}^{-1}, \\ &= -22.3 \text{ kJ g}^{-1} \text{ of levoglucosan consumed.} \end{aligned} \tag{6.17}$$

which, although considerably greater than the value of -14 kJ g^{-1} obtained from the literature (Parker and LeVan 1989) for the heat released from the combustion of volatiles, is a reasonable approximation considering the assumption of direction conversion to only CO_2 and H_2O and not the broad range of possible intermediate species that invariably occur in reality (Wodley 1971).

The comparable results between the calculated heat of reaction and the observed values in the literature suggest that the calculated standard state enthalpies for the charcoal and levoglucosan species are at least within the range of actual values.

6.2.4 Operating Conditions

The operating conditions for the CC-CFD model used an operating pressure of 101325 Pa (i.e. sea-level). Gravity was turned on. Gravitational acceleration of -9.8 m s^{-2} was applied in the z-direction (i.e. vertical). Default values for Boussinesq parameters were used. No variable-density parameters were set.

6.2.5 Boundary Conditions

Boundary conditions are the values of the attributes of each of the domain boundaries in the CC-CFD model. In the case of the walls of the wind tunnel (i.e. the roof, floor and walls), these were set to: internal emissivity 1, wall thickness 0.2 m, heat generation rate 0, material of cellulose. The walls were set to stationary, no-slip shear condition and opaque. The tunnel zone itself was set to provide chemical reaction through the volumetric reactions given in Table 6.2. Motion type was set to stationary with respect to the mesh.

Ambient conditions were selected to replicate fairly warm bushfire-like conditions. Therefore all boundary condition temperatures (i.e. wall, fluid, inlet, backflow) were set to 310 K.

The inlet to the wind tunnel was also set with a wind velocity magnitude that was used to define a set of numerical experiments. The turbulence specification method was used with turbulence intensity 10%, hydraulic diameter 1 m, (i.e. the default values). The

Reynolds-stress specification was set to turbulence intensity. The species mass fraction was set such that 23% O_2 entered the inlet.

The exit of the wind tunnel was set to type 'pressure-outlet' which allows backflow into the wind tunnel if required. As such, the backflow was set to ambient boundary conditions: temperature 300 K, backflow turbulence intensity 10%, backflow hydraulic diameter 1 m, species mass fraction of O_2 23%.

The floor of the wind tunnel differed from the roof and walls in that the floor was set to be a source of species via the wall reaction mechanism outlined in Section 6.2.3 (p. 124).

6.2.6 Ignition

An ignition source was required to initiate the reactions defined for the CC-CFD model. This was achieved by 'patching' a number of rows of cells on the floor of the wind tunnel (Fig. 6.2) to a suitably elevated temperature at which the reactions would become self-sustaining. A patch temperature in the range of 600–650 K was found in the final form of the CC-CFD to be sufficient. This value corresponds with the temperature of 580 K that was used in the zero-dimensional thermokinetic analysis of Chapter 4.

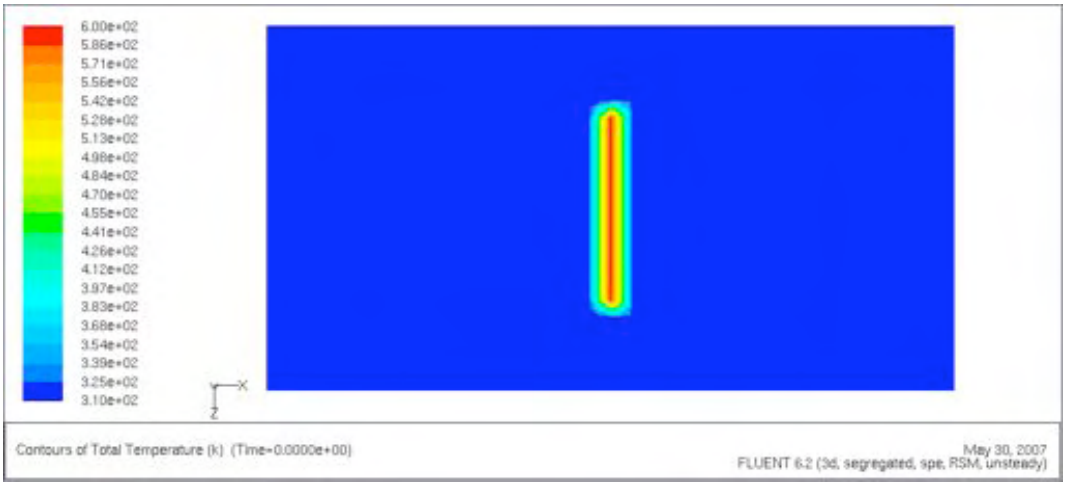

Figure 6.2: Plan view of the wind tunnel floor showing the ignition patch required to initiate combustion. The CC-CFD model is ignited by patching a number of rows of cells in the centre of the wind tunnel to a sufficiently high temperature to start the reactions. In this case, the patch temperature is set to 600 K.

6.2.7 Numerical solutions

Default values were used for the solver parameters. These included under-relaxation factors for turbulent kinetic energy, turbulence dissipation rate, turbulent viscosity, reactions, solid and discrete ordinates. Discretisation settings were left at default values; flow: second order upwind; turbulent kinetic energy: first order upwind; turbulence dissipation rate: first order upwind; discrete ordinates: first order upwind.

Simulations were initialised from all zones to set initial values for temperatures, turbulent kinetic energy, turbulent dissipation rate and air velocity, based on the boundary conditions. The ignition zone was then patched to the ignition temperature to initiate the chemical reactions. The solver was then started and iterations commenced.

Generally, FLUENT is used to determine steady-state conditions such that iterations of the solutions of the equations are undertaken and the residual (i.e. an indicator of the convergence of the equations) tracked until residuals for all conserved quantities (e.g. energy, turbulent kinetic energy, chemical species, etc.) reduce to a predetermined criteria (i.e. a suitably small value). That is, the solver is run until the solutions to the equations 'converges', which is then the solution to the problem. In our case, however, the problem (that of a fire spreading across the floor of a wind tunnel) does not lend itself to a steady-state solution as the fire will progress across the domain resulting in different solutions at each iteration and will not asymptote to a single solution.

The unsteady formulation for the solver was selected because it was recognised that the problem would not provide a steady-state solution and thus the passage of time in the solution is an explicit variable—that is, a time-dependent form of the equations are used. The iteration controls for the CC-CFD were set such that a maximum of 20 iterations (unless convergence is achieved sooner) for each time step. Initially, the length of the time step was set to 1 s, but this is changed depending on the situation in order to capture some of the faster occurring phenomena.

6.2.8 Solution representation

Visualising a 3D domain of data in a 2D media such as the printed page is difficult under the best of circumstances. FLUENT allows slices of data along predefined planes within the 3D domain to be displayed, minimising confusion while transmitting as much information as possible. While this does not give a comprehensive picture of what is happening in the 3D space, it at least provides an indication. Figure 6.3a shows the wind vector field in two orthogonal planes along the length of the wind tunnel after 10 s of simulation. The vertical plane is on the asymmetry boundary forming the centre of the wind tunnel while the horizontal plane is placed 10 cm above the floor of the wind tunnel.

The wind vectors are coloured by wind speed and show that as expected the wind field is relatively uniform throughout the entire volume with minor decreases in wind speed due to friction at the domain boundaries (roof and floor). A wind vector has been drawn for each cell inside the domain. Figure 6.3b shows the same wind field planes but now with the domain grid displayed. Each vector represents the wind speed and direction of the centre of each cell in the mesh.

Figure 6.4 (p. 131) shows the residuals for the 3D solutions displayed above. The initial solutions to the governing equations result in relatively large residuals for most quantities but these reduce with subsequent iterations and asymptote to a relatively consistent value of much less than unity, showing that the solutions are achieving a psuedo-steady state result.

(a)

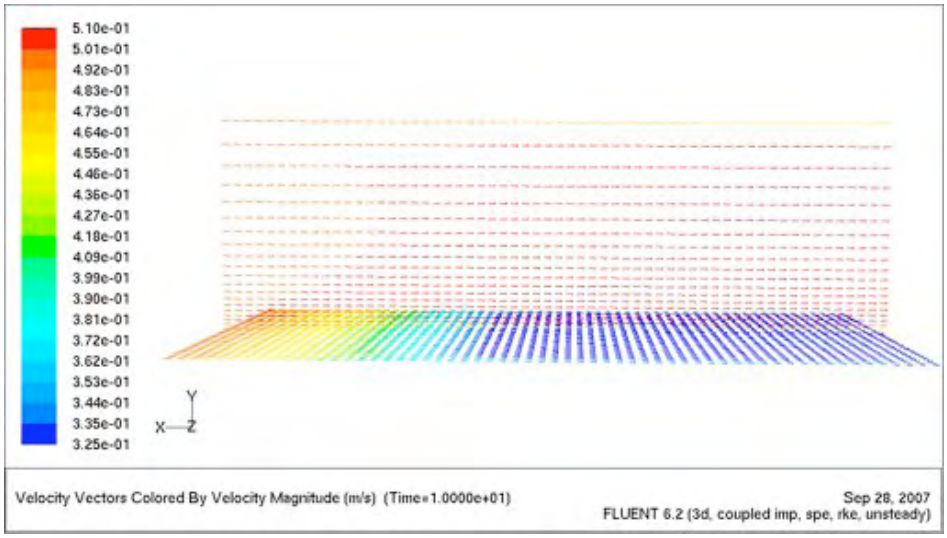

(b)

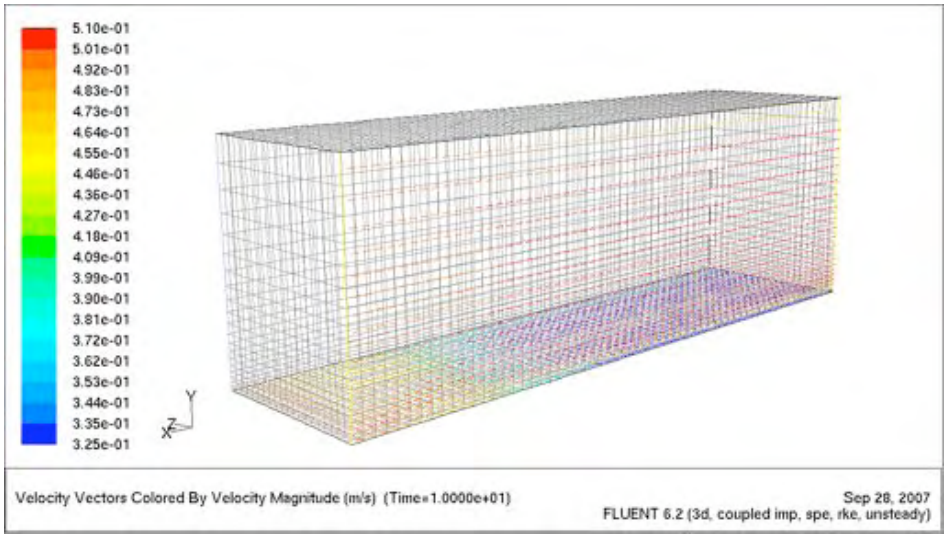

Figure 6.3: Wind vector field for the sample 3D experiment in which the reaction mechanism is turned off and no fire results. (a) Wind vectors are displayed on two orthogonal planes along the centre of the wind tunnel and are coloured by wind velocity. They show relatively uniform speed and direction throughout the domain. (b) The computational mesh has been overlaid the wind vectors of (a). A wind vector is drawn for each cell in the mesh, representing the wind speed and direction for the centre of the cell.

6.3 3D simulation experiments and solutions

6.3.1 Numerical solution issues and simplifications

The initial solution to the 'ideal' CC-CFD model, as described in section 6.2 (p. 117), suffered from numerical instability and divergence, in both the 2D and 3D formulations. Extensive experimentation showed (see Appendices A3.1, p. 197, and A3.2, p. 197) that the onset of ignition of the oxidation reactions (i.e. the reaction rates increased as the temperature increased) resulted in the generation of a fatal error ('NAN': Not a number) in the solver, due to a numerically unstable and divergent solution. Efforts to improve

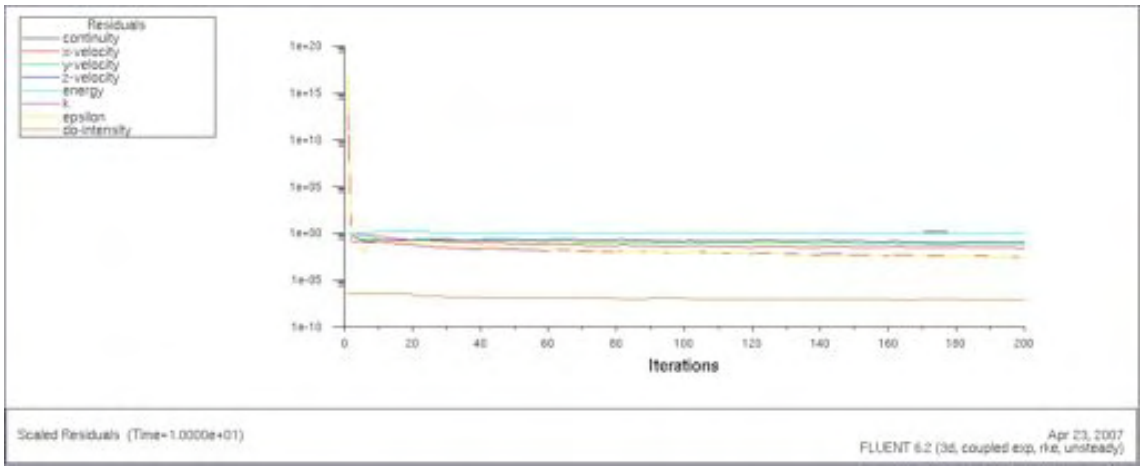

Figure 6.4: Solution residuals for the sample 3D experiment in which the reaction mechanism is turned off and no fire results. Initial residuals are relatively large but reduce as iterations progress, showing that the solutions to the governing equations asymptote to relatively steady value in this case.

numerical stability within FLUENT (see Appendix A3.2) were unsuccessful. This forced the implentation of modifications to the original 'ideal' CC-CFD model formulations in order to provide at least interim results in the time available for this study (see Appendix A3.3, p. 200).

The CC-CFD simplifications were of two types—simplification of the chemistry, primarily of the reaction products (the direction formation of charcoal from cellulose is ignored and H_2O(l) is considered a fluid rather than a condensed phased material) and the reaction rates (the fastest reaction rates are used), and the solver model (the segregated unsteady was used instead of the coupled solver). This simplified model, which was initially developed for 'proof-of-concept' in 2D, still suffered from issues with numerical instability. However, while the results presented in this section are derived from a highly simplified model of the combustion chemistry and are not conclusive due to eventual instabilities, they do provide an insight into the behaviour of the real system. See Appendix A3.3 (p. 203) for a detailed summary of the final CC-CFD model as produced by FLUENT.

As a result of the continued issues with numerical stability only two numerical experiments were conducted to explore the spatial implications of the competitive thermal degradation reactions. The first experiment simulated the spread of a line fire lit midway down the wind tunnel, transverse to a uniform wind flow of 0.5 m s^{-1}. This is a very light wind and not representative of typical winds during a bushfire but larger magnitude wind speeds caused immediate numerical instability and produced no results at all. The second experiment simulated a small square ignition in the centre of the wind tunnel with no wind. The aim of these experiments was to identify differences in the formation of charcoal and volatiles as a result of the location around the fire perimeter.

6.3.2 Numerical experiment #1: 0.5 m s^{-1}

This numerical experiment used an ignition line of length 0.9 m (in the calculation domain the ignition line is only 0.45 m long and the domain mirrored about the symmetry

boundary on the left hand edge of the domain to achieve the full length) and width 0.1 m is placed at the mid-point of the wind tunnel between the inlet and outlet. The initial domain wind speed is set at 0.5 m s^{-1}, flowing from left to right. Ambient temperature is 310 K (Table 6.3).

Table 6.3: Solver parameters used for 3D Experiment #1.

Solver Parameter	Value	Comment
Total time (s)	4	
Time step (s)	1	
Reaction	on	
Ignition	line	600 K
	(0.9 $\times$ 0.1 m)	ignition patch
Horiz. wind vel. (m s^{-1})	0.5	constant, left to right

Temperature

Figure 6.5 shows a sequence of contours of total temperature on the floor of the domain under plan view (i.e. looking down) for the first 4 seconds prior to the occurrence of divergence in the solution and cessation of the simulation due to an error. Red indicates maximum temperature of the iteration (in the order of 5000 K), blue indicates ambient temperature (310 K), with other colours interpolated between. The initial expansion of the high temperature zone as ignition occurs is clearly evident in the first time step. However, the high temperature zone does not continue to spread under the action of the wind, although there does appear to be some minor diffusion of the temperature into the surrounds. This suggests that the simulation has halted and is due to numerical instability in the solution at this time.

However, prior to the numerical instability, the expansion of the high temperature zone is asymmetric in the direction of the wind, indicating that there is greater rates of reaction on the down-wind edge of the reaction zone. The magnitude of the forward spread is in the order of 3 times that of the backing (i.e. counter-flow) spread. The degree of lateral spread (i.e. perpendicular to the wind flow) is similar to the backing spread. The spread of the high temperature zone appears to stop with subsequent iterations and the maximum temperature in the domain decreases, suggesting the reactions are slowing. Again, this is a result of the divergence in the solution and corresponding onset of unreal conditions.

Reaction products

Figures 6.6–6.8 (pgs. 134–136) show the plan view of the spatial distribution on the floor of the wind tunnel of the mole fractions of four gas phase product species: H_2O, H_2O(l), CO_2 and $C_6H_{10}O_5$ (levoglucosan); and one gas phase reactant species: O_2, from the thermal degradation and oxidation reactions (p. 201), and the Arrhenius reaction rates for reaction #3 (p. 201), the flaming combustion reaction. As with the total temperature in the system, there is a distinct asymmetry in the distribution of the species in the direction of the air flow.

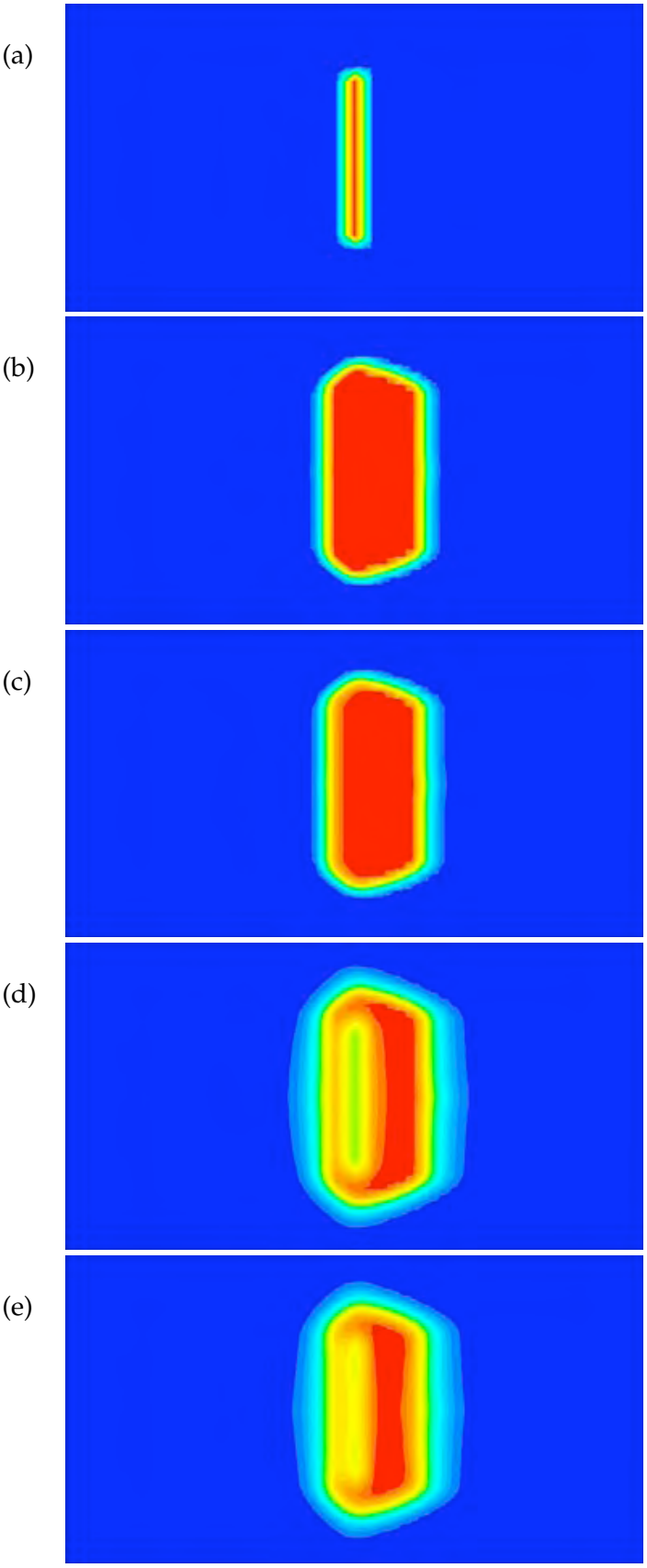

Figure 6.5: Sequence of total temperature contour maps of experiment #1 in which the fire is lit from a line mid-way down the wind tunnel at (a) ignition at t = 0 s, (b) t = 1 s, (c) t = 2 s, (d) t = 3 s and (e) t = 4 s. Red indicates regions of maximum temperature in the domain (in the order of 5000 K), blue indicates regions of ambient temperature (310 K) with other colours interpolated between.

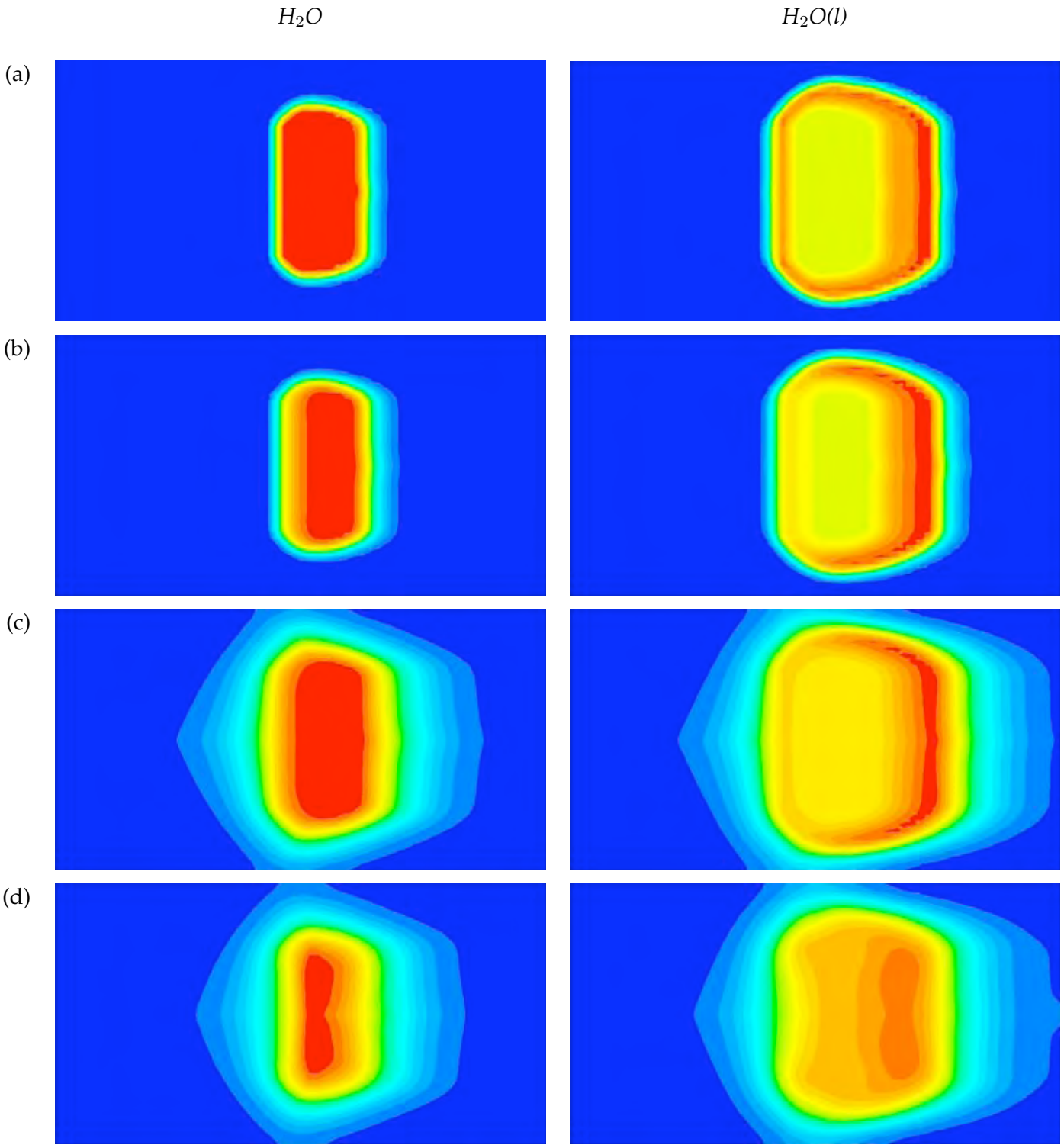

Figure 6.6: Sequence of mole fraction contours for H_2O (left) and H_2O(l) (right) of experiment #1 at (a) t = 1 s, (b) t = 2 s, (c) t = 3 s and (d) t = 4 s. Red indicates regions of highest mole fraction for each species, blue indicates lowest mole fraction (generally zero) with other colours interpolated between.

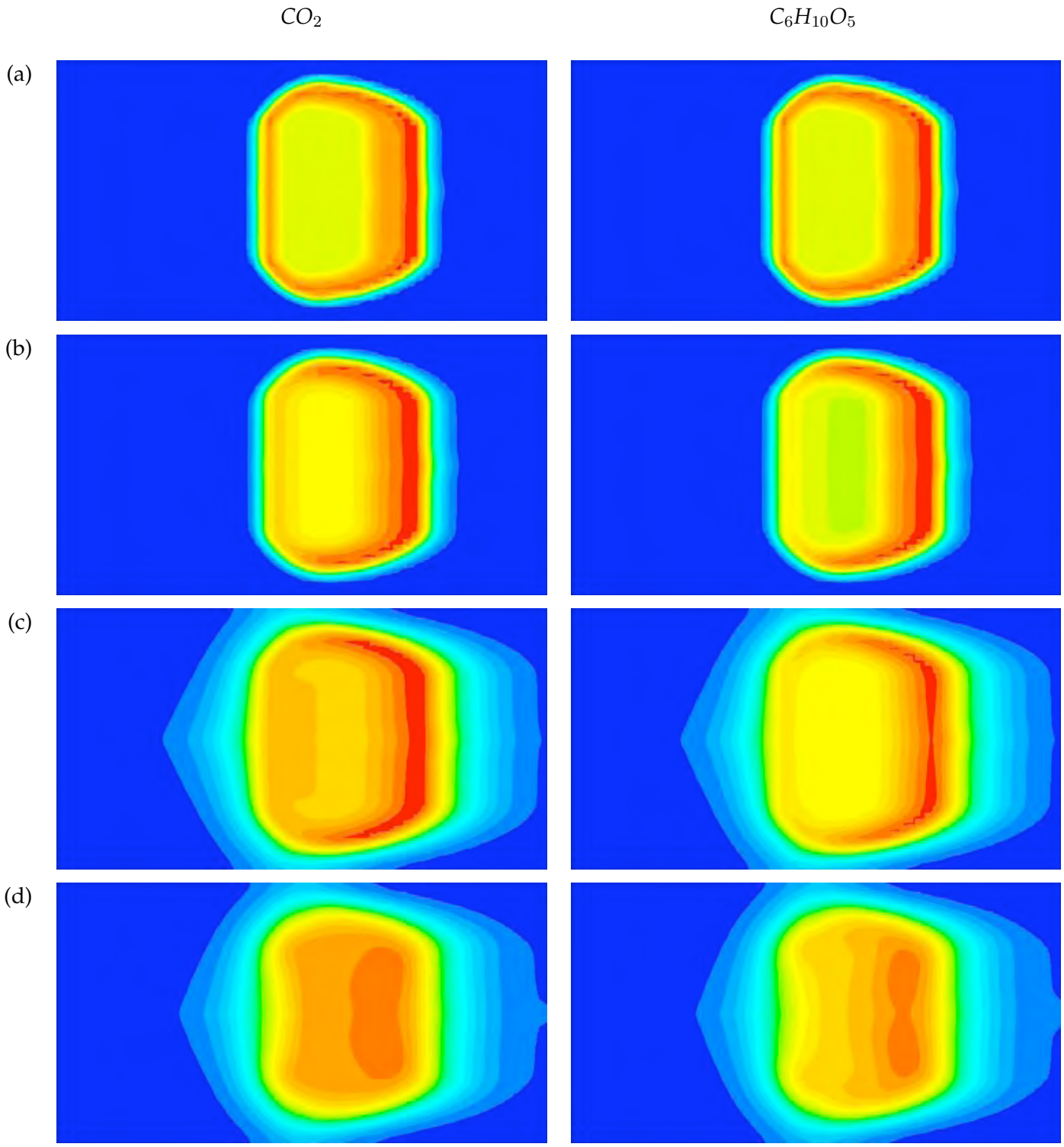

Figure 6.7: Sequence of mole fractions for CO_2 (left) and levoglucosan (right) of experiment #1 at (a) t = 1 s, (b) t = 2 s, (c) t = 3 s and (d) t = 4 s. Red indicates regions of highest mole fraction for each species, blue indicates lowest mole fraction (generally zero) with other colours interpolated between.

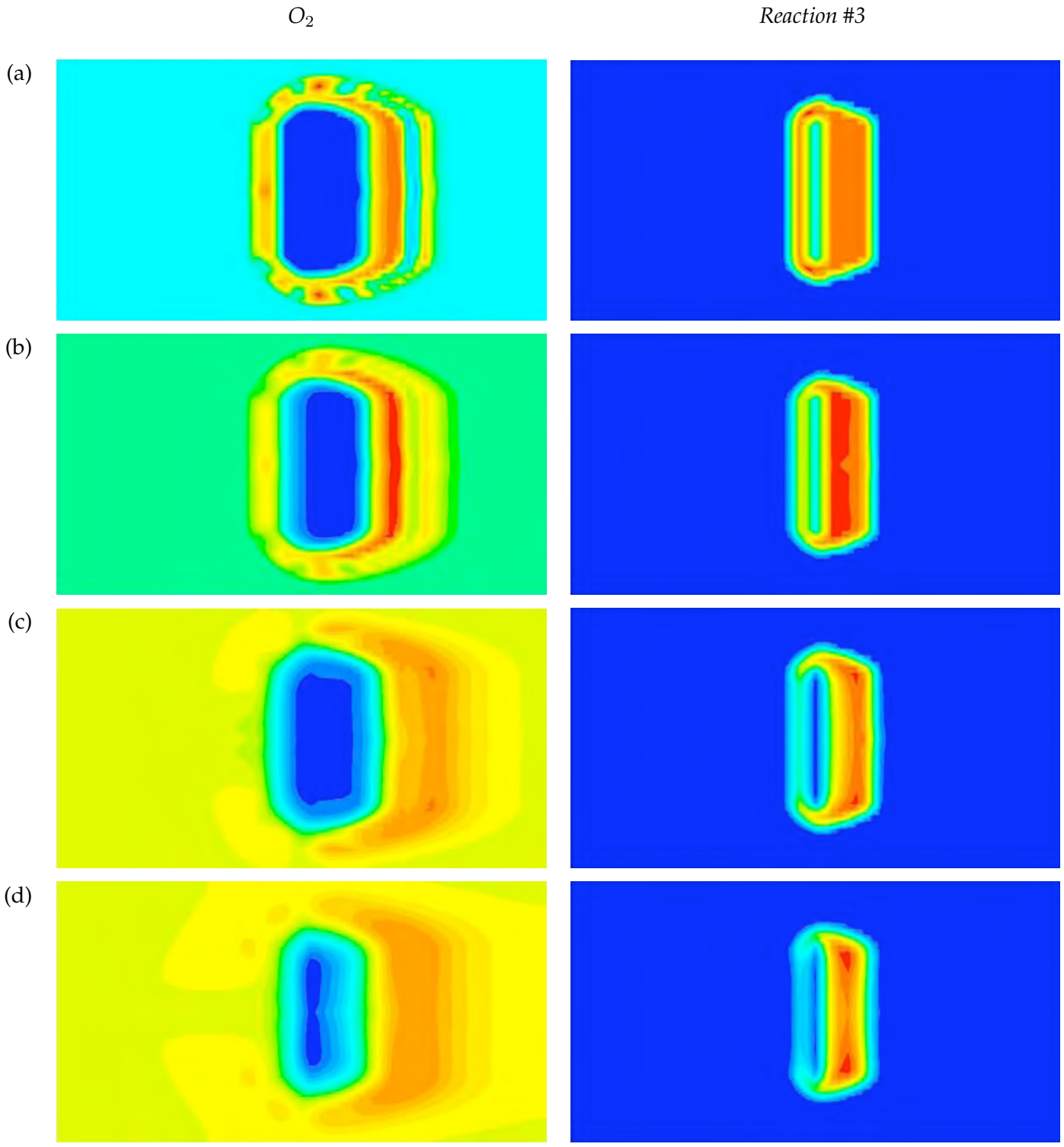

Figure 6.8: Sequence of mole fraction of O_2 (left) and Arrhenius reaction rate for flaming combustion (reaction #3) (right) of experiment #1 at (a) t = 1 s, (b) t = 2 s, (c) t = 3 s and (d) t = 4 s. Red indicates regions of highest mole fraction for O_2 and highest reaction rate (kgmol m^{-3} s^{-1}) for reaction #3, blue indicates lowest mole fraction O_2 (generally zero) and zero reaction rate for reaction #3 with other colours interpolated between.

The degree of asymmetry for most of the reaction products (i.e. $H_2O(l)$, CO_2 and $C_6H_{10}O_5$) is greater than that of the total temperature distributions for the same iterations, although in relative terms it is similar (i.e. about 3 times). The primary reason is that these products are involved in reactions that are endothermic or only slightly exothermic. Only H_2O correlates with the temperature distributions because it is the only product associated solely with oxidation reactions, and hence with the bulk of the heat production. While CO_2 is also associated with the oxidation reactions, it is also a product of the formation of the charcoal and thus is closely related in distribution to $H_2O(l)$.

The shape of the mole fraction distribution for each product (except H_2O) shows that the reaction front producing the reaction products is tending towards a parabolic shape as a result of the effect of the flow and the reaction kinetics (although by the time the simulation ceases it has not yet reached this shape). The similar counter-flow and lateral spread results in near circular expansion on the upwind edge and flanks.

The asymmetrical shapes of the product mole fractions also indicate the relative production rates of the individual species. In all cases, the location of maximum product is found on the downwind side of the reaction zone, with decreasing amounts around the flanks and rear, confirming that the reaction rates are highest on the downwind side. The region of maximum oxidation, indicated by the region of lowest mole fraction of O_2 (Fig. 6.8 left, p. 136), coincides with the region of maximum H_2O (Fig. 6.6 left, p. 134), a product of oxidation. It is interesting to note the increase of O_2 mole fraction immediately downwind of this zone, suggesting there has been some type sweeping of oxygen from adjacent areas, possibly due to convective action.

Pressure and wind velocity

The dynamic pressure (Fig. 6.9, left) reveals the first distinct symptoms that the results presented so far are affected by numerical instability and divergence in the solution. The first two iterations produce results that appear reasonable, however, the third iteration (Fig. 6.9, c left) shows that the dynamic pressure has suddenly increased by 11 orders of magnitude from the previous time step, indicating that the solution is no longer valid.

The wind velocity for the final two iterations (Figs. 6.10c and d (p. 139) and 6.11c and d (p. 139)) has suddenly increased by 5 orders of magnitude in each time step, resulting in velocities faster than the speed of light, which are obviously incorrect.

For the purposes of exploring the role of wind in the spatial context of the thermal degradation reactions it is assumed that the results prior to the iterations producing these erroneous values are valid. Thus, all subsequent analysis and discussion are restricted to the first two iterations.

3D perspective

Figure 6.12 (p. 140) shows a 3D perspective of the temperature for the first two iterations. The 3D perspective is constructed from the intersection of two planes: the floor of the wind tunnel and a vertical plane through the centre of the wind tunnel. Red indicates contours of maximum temperature and blue indicates contours of ambient (310 K) temperature. This reveals that although there is significant heat down wind from the ignition line in the 2D perspective (Fig. 6.5, p. 133), there is in fact a greater spread

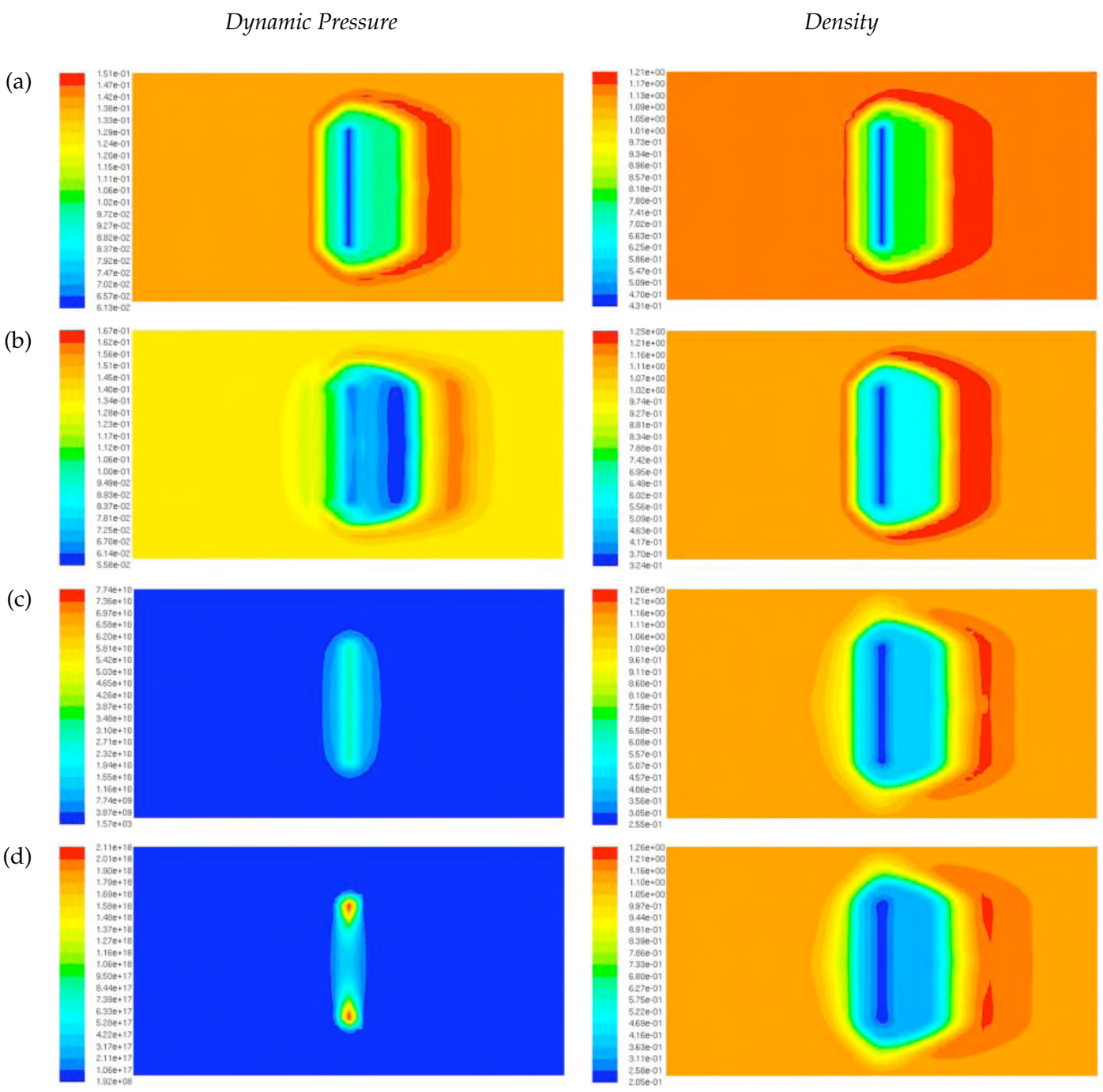

Figure 6.9: Sequence of dynamic pressure (left) and density (right) of experiment #1 at (a) t = 1 s, (b) t = 2 s, (c) t = 3 s and (d) t = 4 s. Red indicates regions of highest dynamic pressure and density, blue indicates regions of lowest dynamic pressure and density with other colours interpolated between, as represented by the legends.

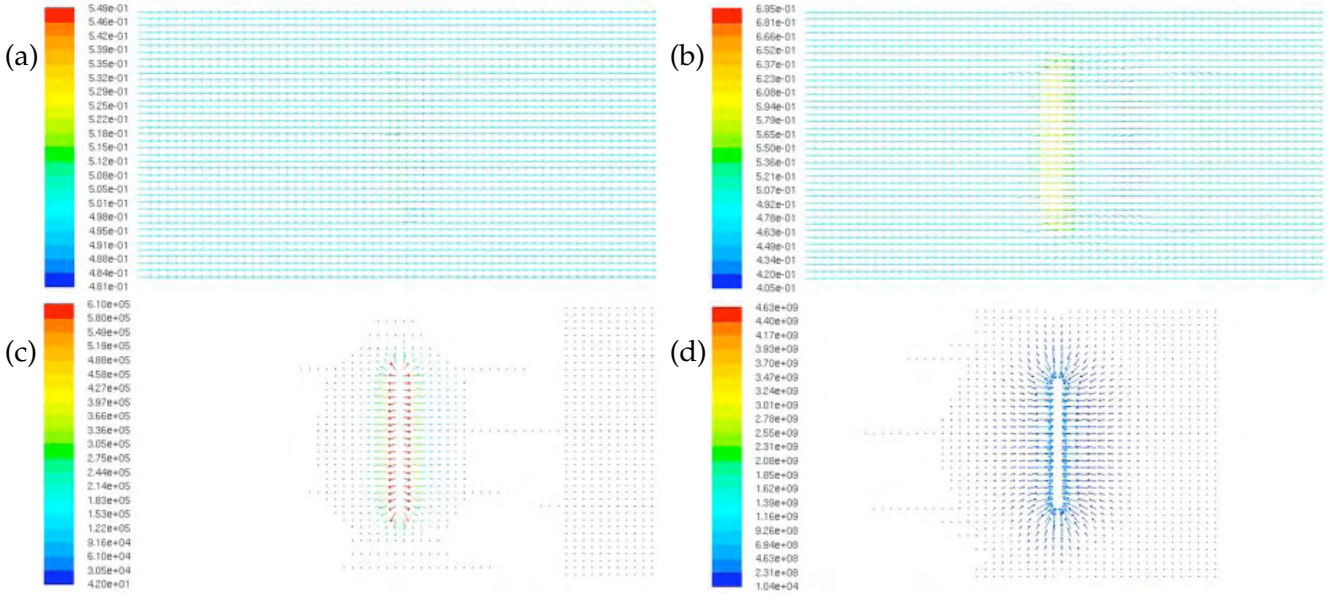

Figure 6.10: Sequence of vectors of wind velocity on a horizontal plane 0.05 m above the floor of the wind tunnel of experiment #1 at (a) t = 1 s, (b) t = 2 s, (c) t = 3 s and (d) t = 4 s. Velocity magnitudes are indicated by the colour in the legends.

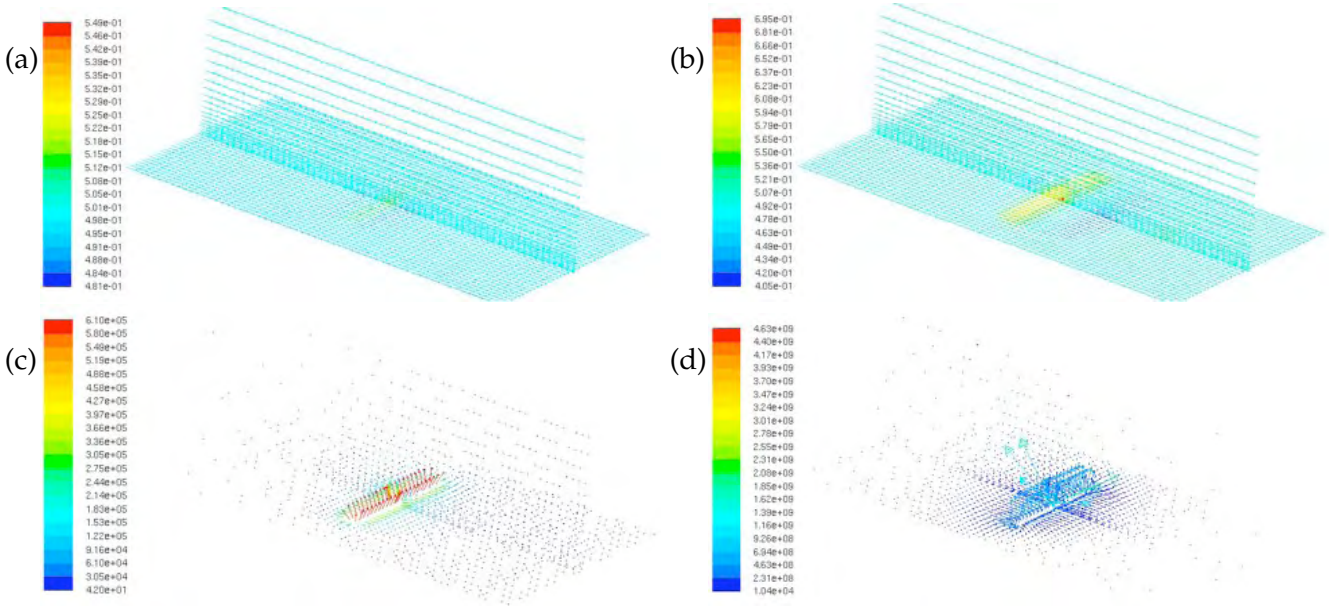

Figure 6.11: Sequence of vectors of wind velocity from of experiment #1 on a horizontal plane 0.05 m above the floor of the wind tunnel and the vertical plane through the centre of the wind tunnel at (a) t = 1 s, (b) t = 2 s, (c) t = 3 s and (d) t = 4 s. Velocity magnitudes are indicated by the colour in the legends.

of heat vertically at the line of ignition and the vertical structure decreases downwind. This supports the observation that the bulk of the heat comes from the combustion of the charcoal in the centre of the reaction zone.

However, the corresponding 3D distributions of H_2O, CO_2 and levoglucosan for the first two iterations (Fig. 6.13), shows that that is a much more even vertical distribution of these product species than of the temperature. Indeed, the vertical profile shows that

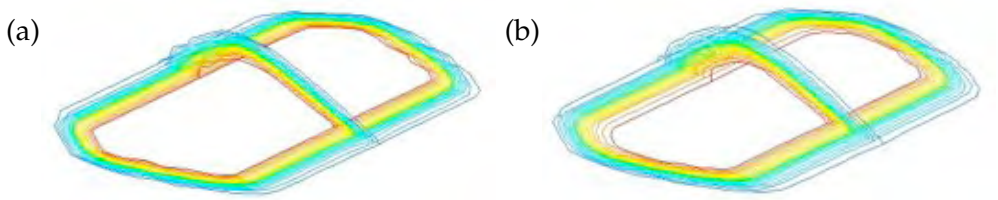

Figure 6.12: 3D perspective of experiment #1, created by the floor of the wind tunnel and a vertical plane through the centre of the wind tunnel, of the temperature at (a) t = 1 s and (b) t = 2 s. Red indicates contours of maximum temperature and blue indicates contours of ambient (310 K) temperature with other colours interpolated between.

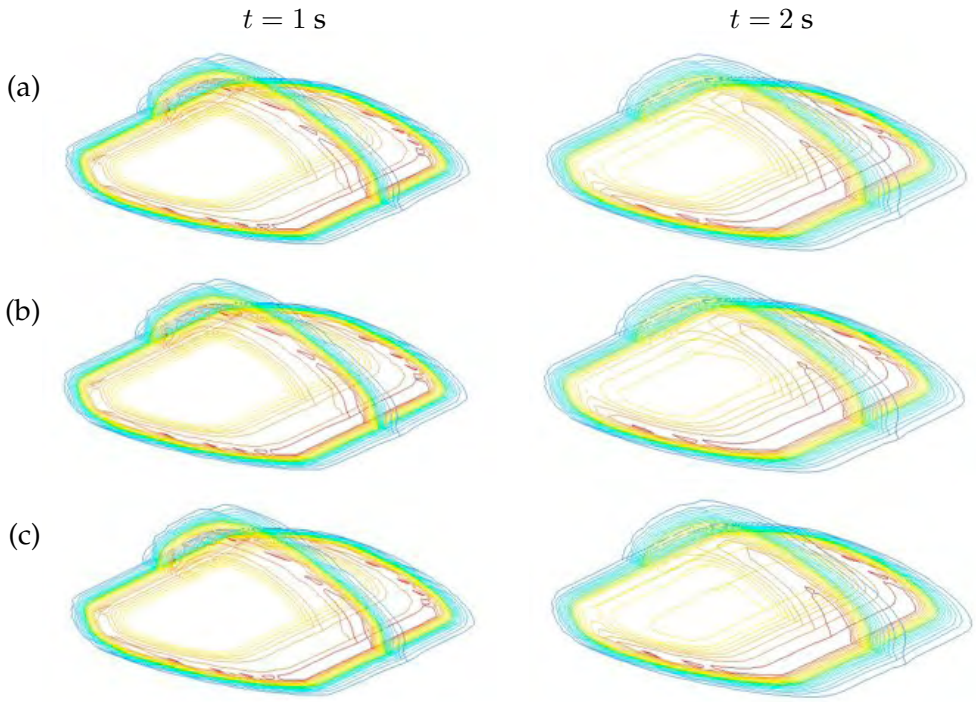

Figure 6.13: 3D perspective of experiment #1, created by the floor of the wind tunnel and a vertical plane through the centre of the wind tunnel, of the distribution of (a) H_2O(l), (b) CO_2 and (c) levoglucosan at t = 1 s (left) and t = 2 s (right). Red indicates contours of maximum mole fraction and blue indicates contours of low (generally zero) mole fraction.

the zone of highest mole fraction for each species extends from the downwind edge on the floor of the wind tunnel a short distance upstream, and some distance off the floor, possibly due to a slow vertical dispersion as the reaction front has progressed downwind.

6.3.3 Numerical experiment #2: 0 m s^{-1}

A primary test of any fire spread simulation model is not just its performance under a given wind, but also its performance under no wind. Many fire simulation models treat a zero wind situation as a special condition and rely upon a different spread mechanism than that used for non-zero wind situations. A fire ignited from a point under these

Table 6.4: Solver parameters used for 3D Experiment #2.

Solver Parameter	Value	Comment
Total time (s)	3	
Time step (s)	1	
Reaction	on	
Ignition type	rectangle	600 K
	(0.2 × 0.16 m)	ignition patch
Horiz. wind vel. (m s^{-1})	0	

conditions will show no bias in its spread and thus form an expanding circle. In this experiment, the initial domain wind speed is set to 0 m s^{-1}, i.e. still wind conditions, and a 'point' ignition rather than a line is used and an ambient temperature of 310 K (Table 6.4).

The ignition point consists of a patch of 4 × 4 = 16 cells, with a final size of 0.2 m × 0.16 m (due to the non-equal grid structure in the x and y directions, i.e. $\Delta x = 5$ cm and $\Delta y = 4$ cm, respectively). This is placed in the centre of the wind tunnel floor, mid-way down the tunnel's length.

Two iterations at 1 s time-step were achieved before the solver suffered divergence and numerical instability issues. As with experiment #1, this is not ideal but does at least provide sufficient results to analyse.

Temperature

Figure 6.14 shows a sequence of contours of total temperature on the floor of the domain under plan view (i.e. looking down) for the first 3 seconds prior to the onset of divergence in the solution and termination of the simulation. The initial, near-circular expansion of the high temperature zone as ignition occurs is clearly evident in the first time step (Fig. 6.14b). However, as with previous experiments, the high temperature zone does not continue to spread and the magnitude of values decrease with subsequent iterations. Again, this is a result of the divergence in the solution and corresponding onset of unreal conditions.

The high temperature zone has taken on a slightly rounded elliptical shape, elongated along the long axis of the wind tunnel (length:breadth ratio 1.25). While this differs from the expected symmetry due to the lack of wind, it is most likely a result of the non-circular ignition patch used and, indeed has the same aspect ratio as the ignition patch. This is supported by the uniformity in the width of the intermediate temperature zones. This is not the case in the wind-driven results of experiment #1 (Fig. 6.5, p. 133).

Reaction products

Figures 6.15-6.17 (ps. 143–145) show the plan view of the spatial distribution on the floor of the wind tunnel of the mole fractions of four gas phase product species: H_2O, H_2O(l), CO_2 and $C_6H_{10}O_5$ (levoglucosan); and one gas phase reactant species: O_2, and the Arrhenius reaction rates for reaction #3, the flaming combustion reaction.

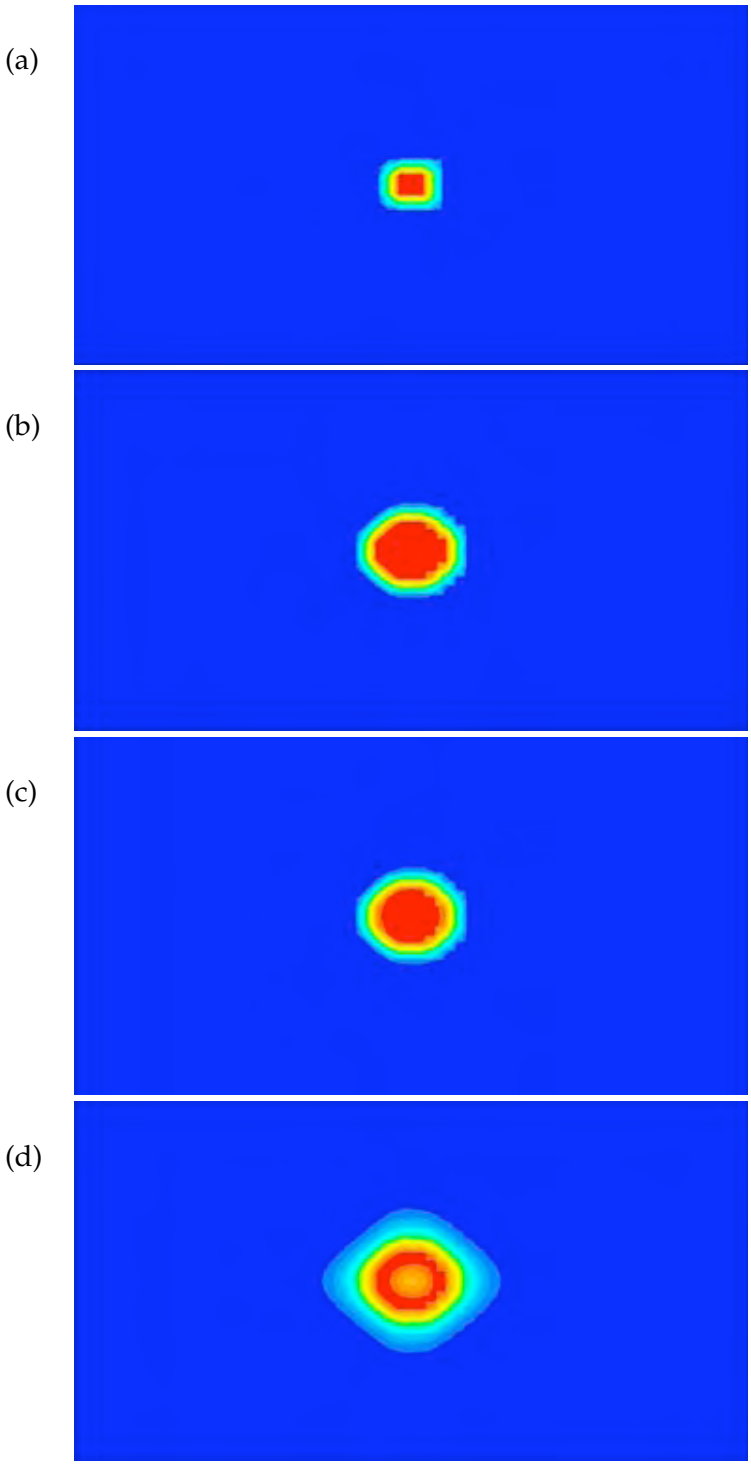

Figure 6.14: Sequence of total temperature contour maps of experiment #2 in which the fire is lit from a squarish patch in the centre of the wind tunnel at (a) ignition at t = 0 s, (b) t = 1 s, (c) t = 2 s and (d) t = 3 s. Red indicates regions of maximum temperature in the domain (in the order of 5000 K), blue indicates regions of ambient temperature (310 K) with other colours interpolated between.

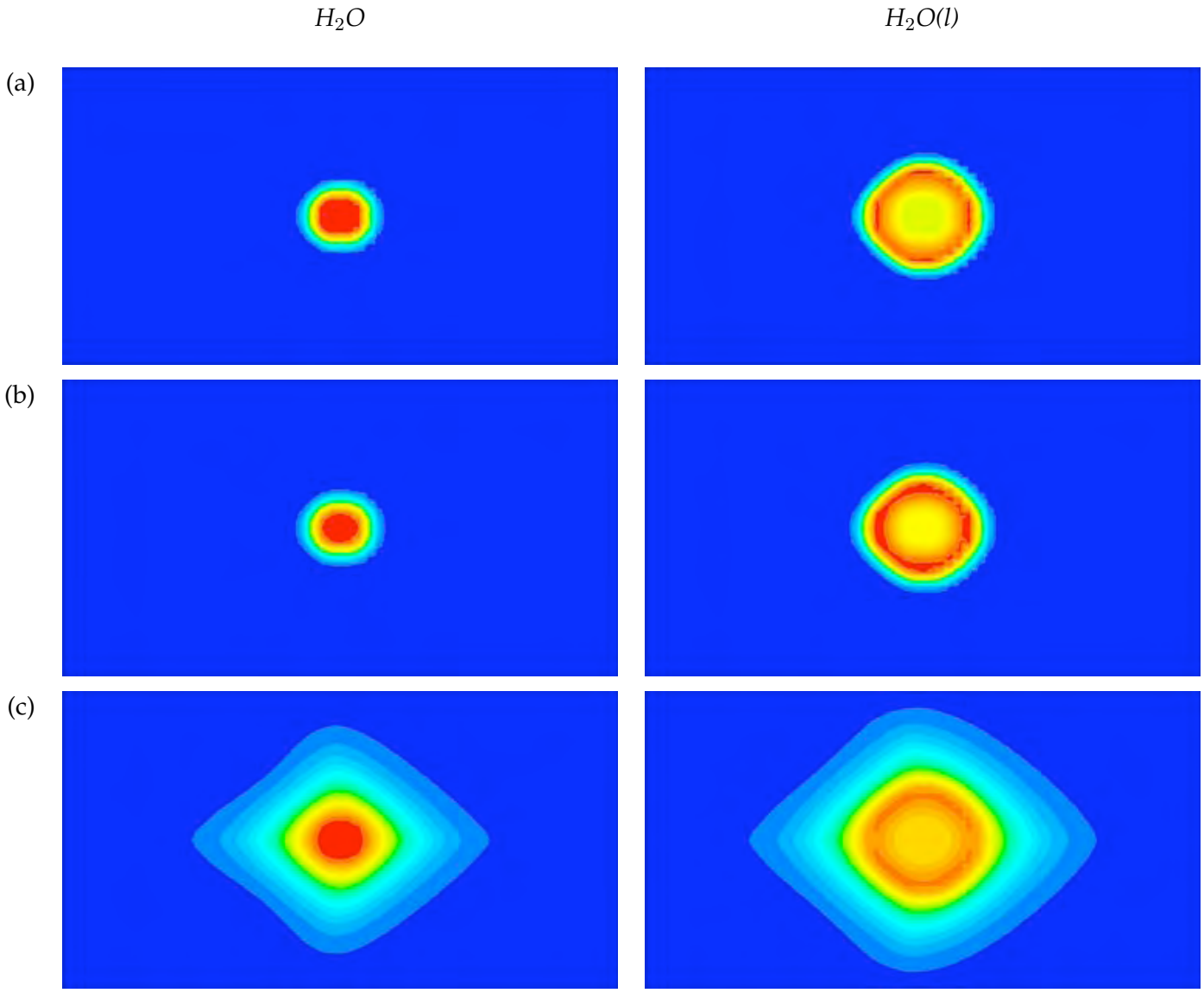

Figure 6.15: Sequence of mole fraction contours for H_2O (left) and H_2O(l) (right) of experiment #2 at (a) ignition at (a) t = 1 s, (b) t = 2 s and (c) t = 3 s. Red indicates regions of highest mole fraction for each species, blue indicates regions of lowest mole fraction (generally zero) with other colours interpolated between.

As with the total temperature in the system, there is a slight asymmetry in the distribution of the species in the direction of the long axis of the wind tunnel. In the final iteration, the shape takes on a distinct rhomboid shape as the solution becomes divergent and unreal.

Unlike the results of experiment #1, where the extent of asymmetry for most of the reaction products (i.e. H_2O(l), CO_2 and $C_6H_{10}O_5$) was greater than that of the total temperature for the same iterations, there is actually a decrease in the asymmetry seen in the reaction products here. At the first iteration, the length:breadth ratio of all three prod-

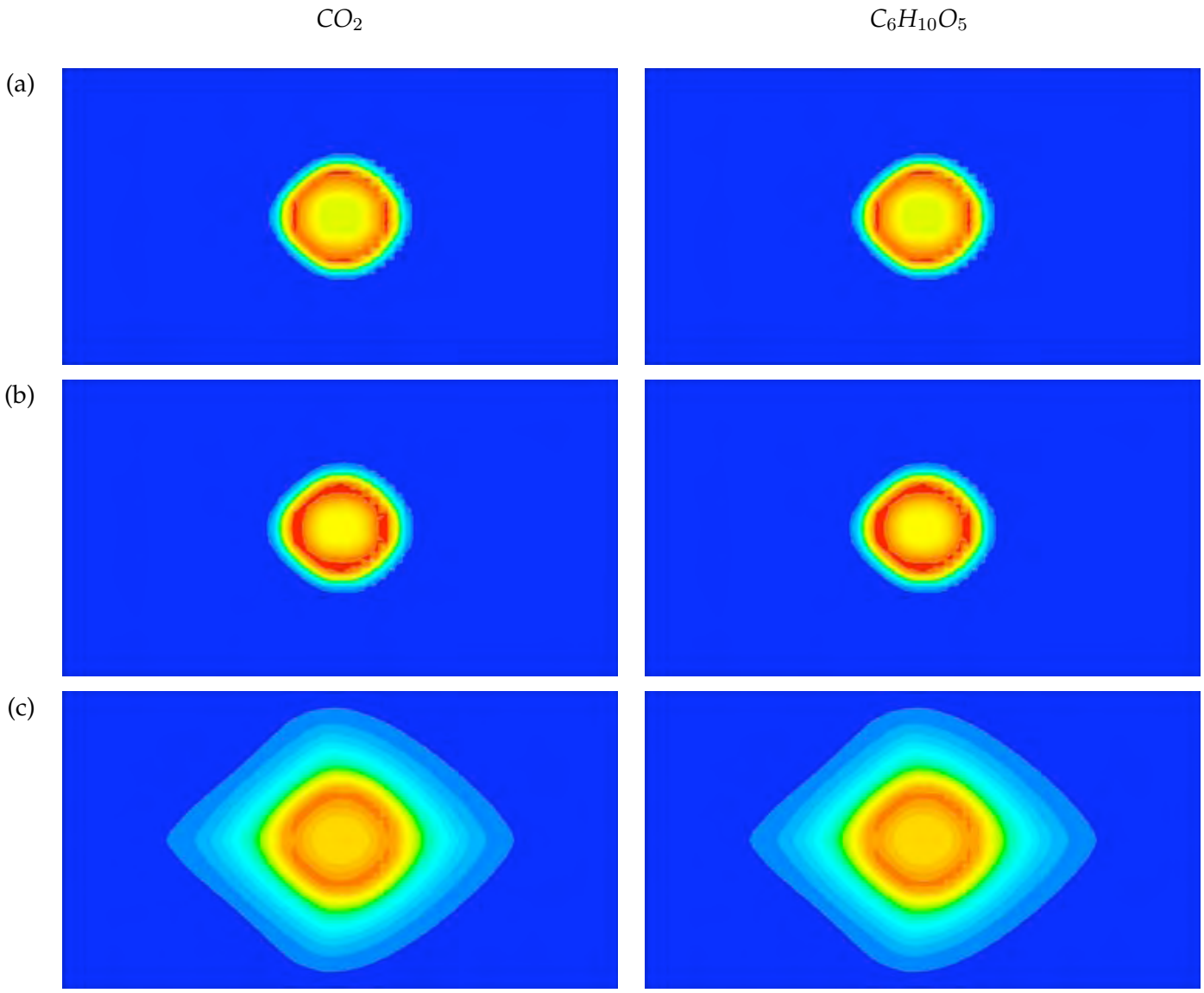

Figure 6.16: Sequence of mole fractions for CO_2 (left) and levoglucosan (right) of experiment #2 at (a) t = 1 s, (b) t = 2 s and (c) t = 3 s. Red indicates regions of highest mole fraction for each species, blue indicates regions of lowest mole fraction (generally zero) with other colours interpolated between.

ucts is approximately 1.16 (*c.f* 1.25), with a correspondingly closer approximation to a circular shape.

Only H_2O correlates with the temperature distributions directly because it is the only product associated solely with the oxidation reactions, and hence with the bulk of the heat production. While CO_2 is also associated with the oxidation reactions, it is also a product of the formation of the charcoal and thus is more closely related in distribution to H_2O(l).

The near-circular shape of the mole fraction distribution for the product (with the

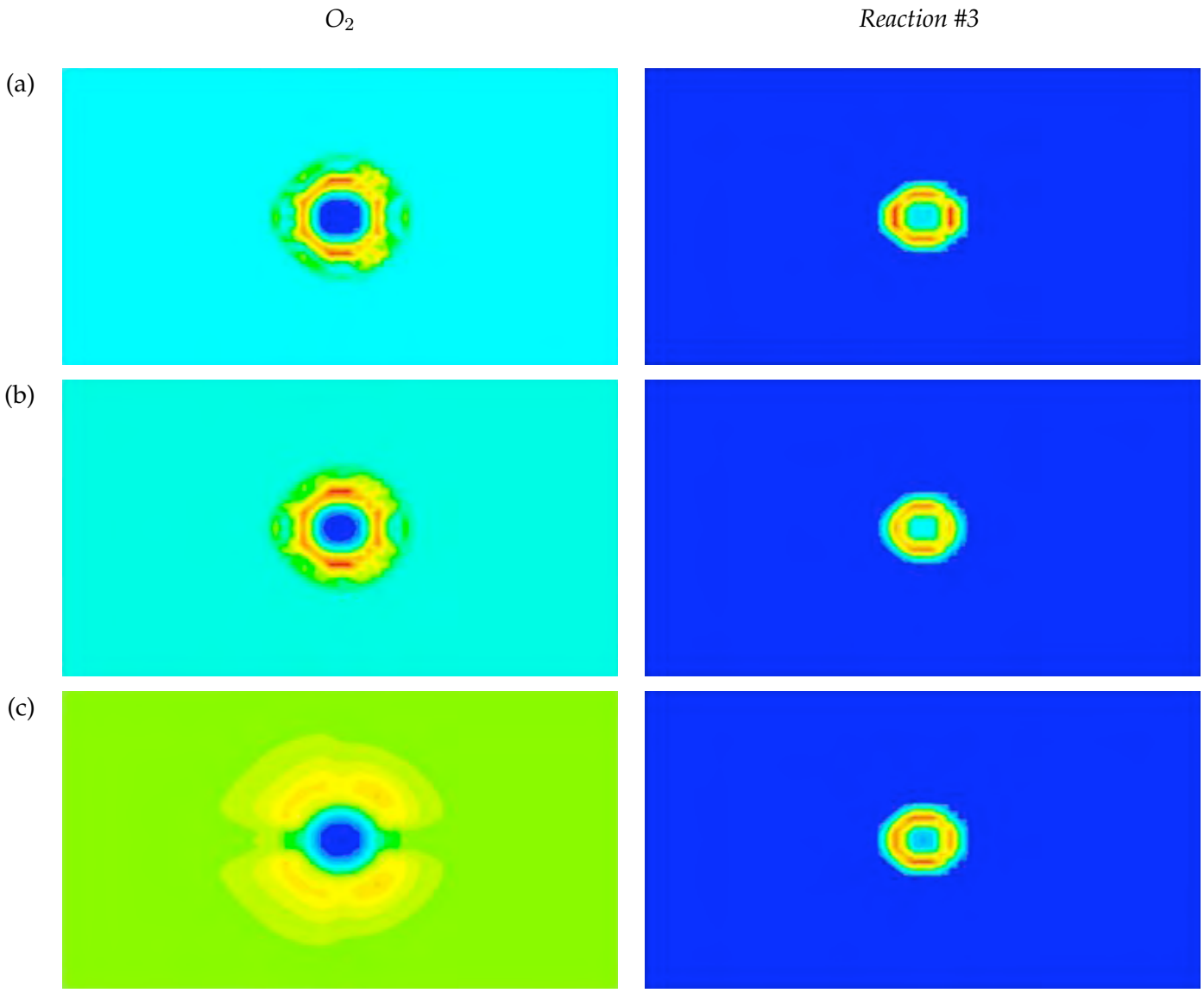

Figure 6.17: Sequence of mole fraction of O_2 (left) and Arrhenius reaction rate for flaming combustion (reaction #3) (right) of experiment #2 at (a) t = 1 s, (b) t = 2 s and (c) t = 3 s. Red indicates regions of highest mole fraction for O_2 and highest reaction rate (kgmol m^{-3} s^{-1}) for reaction #3, blue indicates regions of lowest mole fraction O_2 (generally zero) and zero reaction rate for reaction #3 with other colours interpolated between.

exception of H_2O) confirms the understanding of zero-wind fire behaviour. That is, the reaction front producing the reaction products is unbiased and occurs equally around the fire perimeter (despite some apparent minor discontinuities in the distributions), resulting in even spread outwards and a circular perimeter. The location of the maximum mole fractions for each reaction product (*sans* H_2O) coincide, supporting the argument.

The region of maximum oxidation, indicated by the region of lowest mole fraction of O_2 (Fig. 6.17 left), coincides with the region of maximum H_2O (Fig. 6.15 left, p. 143),

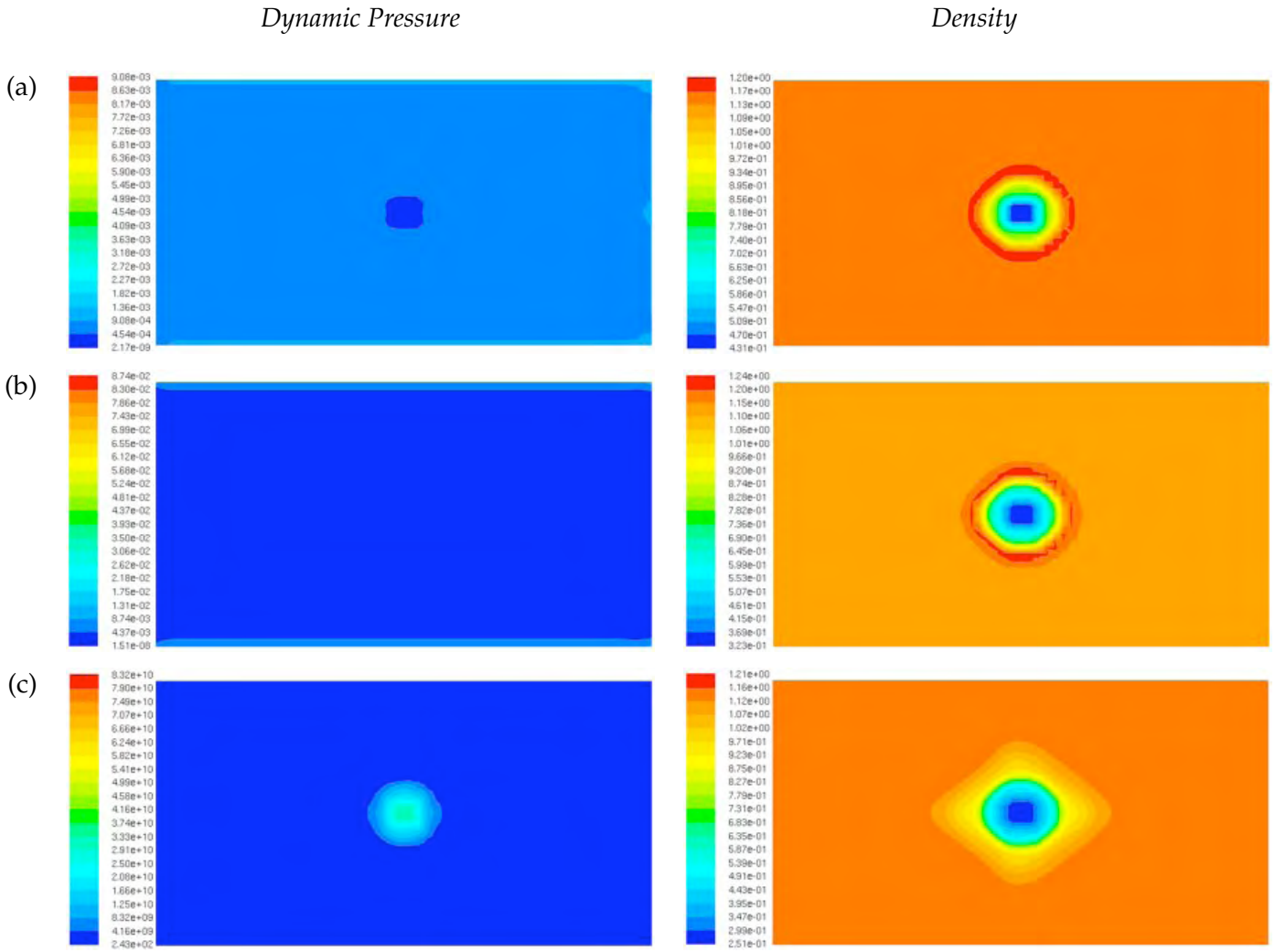

Figure 6.18: Sequence of dynamic pressure (left) and density (right) of experiment #2 at (a) t = 1 s, (b) t = 2 s and (c) t = 3 s. Red indicates regions of highest dynamic pressure and density, blue indicates regions of lowest dynamic pressure and density with other colours interpolated between, as represented by the legend.

a product of oxidation. Again, it is interesting to note an increase of O_2 mole fraction immediately adjacent to this zone, which is clearly asymmetrical, possibly due to convective action and the interaction of the wall.

Pressure and wind velocity

The dynamic pressure (Fig. 6.18, left) again reveals the first symptoms arising from numerical instability and divergence in the solution. The first two iterations again produce results that appear reasonable. The third iteration (Fig. 6.18, left c), however, shows that the dynamic pressure has suddenly increased by 12 orders of magnitude from the previous time step, indicating that the solution is no longer valid. The wind velocity for the final iteration (Figs. 6.19c and 6.20c, p. 148) has again suddenly increased by 6 orders of magnitude.

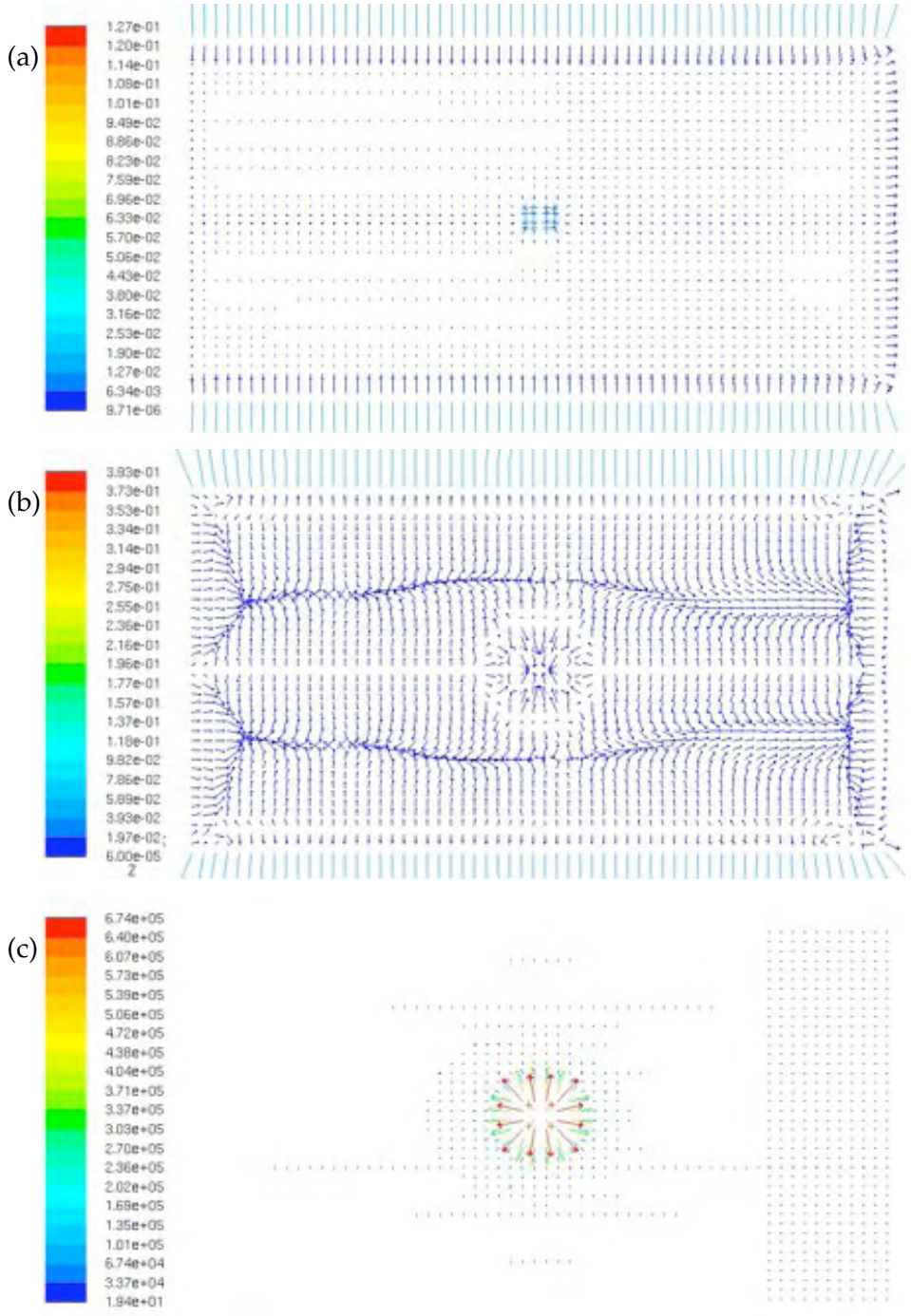

Figure 6.19: Sequence of vectors of wind velocity on a horizontal plane 0.05 m above the floor of the wind tunnel of experiment #2 at (a) t = 1 s, (b) t = 2 s and (c) t = 3 s.

As with experiment #1 all subsequent analysis and discussion of experiment #2 is constrained to the first two iterations where the results are assumed to be valid.

Figure 6.19b shows the formation of interesting structures in the wind near the floor of the wind tunnel. In-flow from the ends of the wind tunnels, albeit of very small magnitude, is clearly apparent, presumably matched by an outflow of air out the ends at the roof of the wind tunnel due to buoyancy. Two lines of convergence are visible, running down the long axis of the wind tunnel, about a third of the way across the tunnel from the outer walls. The lines bow around the presence of the fire in the middle of the tunnel.

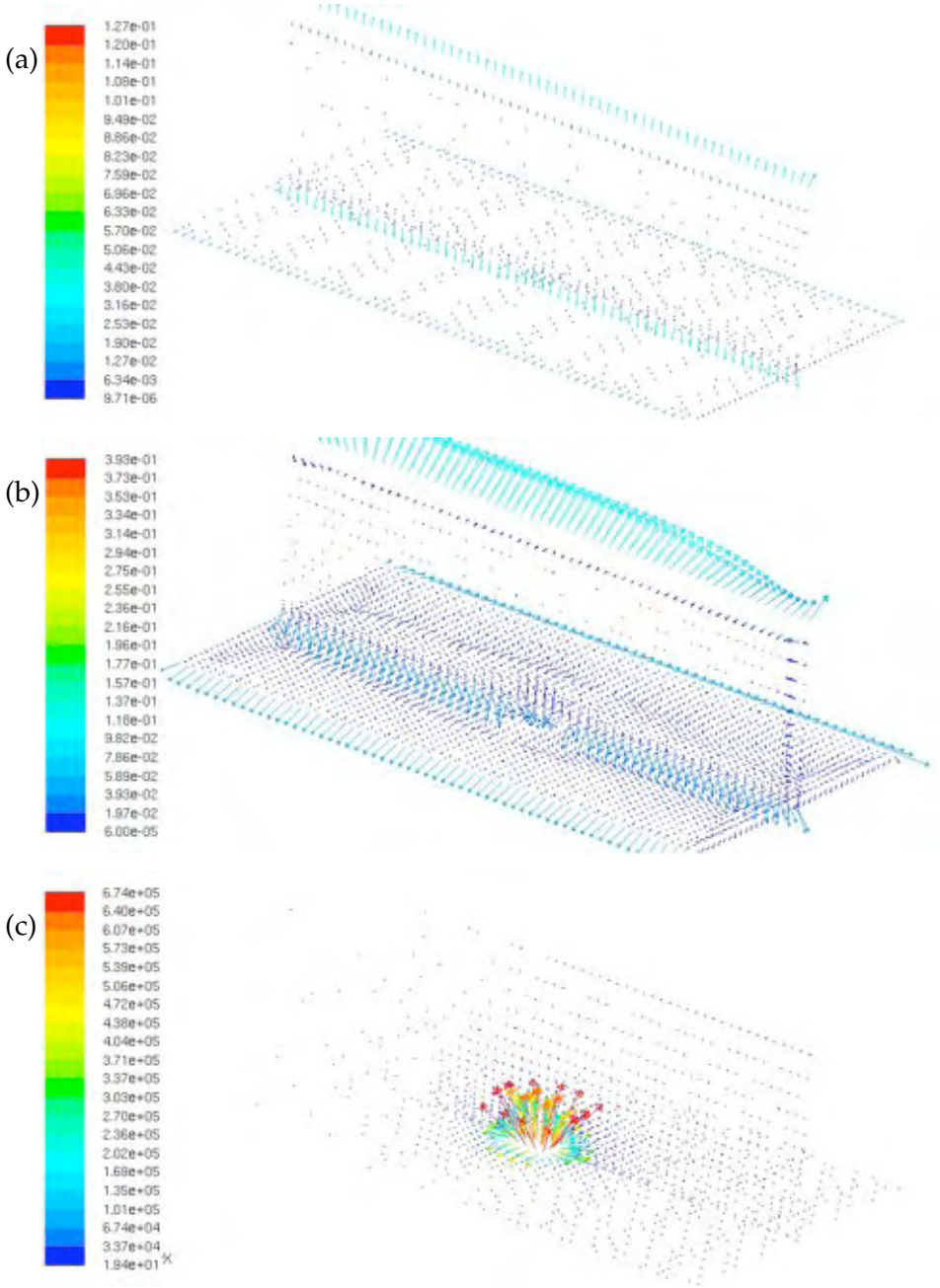

Figure 6.20: Sequence of vectors of wind velocity from of experiment #2 on a horizontal plane 0.05 m above the floor of the wind tunnel and the vertical plane through the centre of the wind tunnel at (a) t = 1 s, (b) t = 2 s and (c) t = 3 s.

The lines are asymmetric in that there is a different form of the convergent structures on the right when compared to the left.

3D perspective

Figure 6.21 shows a 3D perspective of the temperature for the first two iterations. This perspective, constructed from the intersection of two planes: the floor of the wind tunnel and a vertical plane through the centre of the wind tunnel, reveals that the heat distribution vertically is generally uniform. A slight non-linear vertical distribution is visible in the first iteration (Fig. 6.21 left), but this is less apparent in the second iteration (Fig. 6.21 right).

The corresponding 3D distributions of H_2O, CO_2 and levoglucosan for the first two iterations (Fig. 6.22), shows an essentially even vertical distribution of these product species.

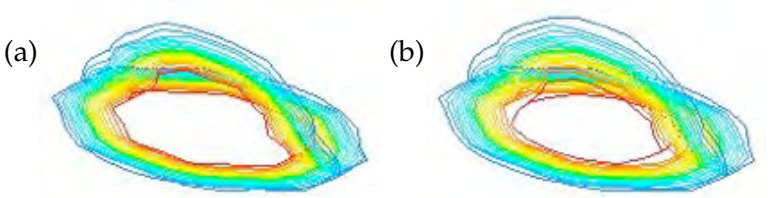

Figure 6.21: 3D perspective of the temperature contours of the first two iterations at (a) 1s and (b) 2 s of experiment #2. These are created by the floor of the wind tunnel and a vertical plane through the centre of the wind tunnel, of the temperature for the first two iterations. Red indicates contours of maximum temperature and blue indicates contours of ambient (310 K) temperature with other colours interpolated between.

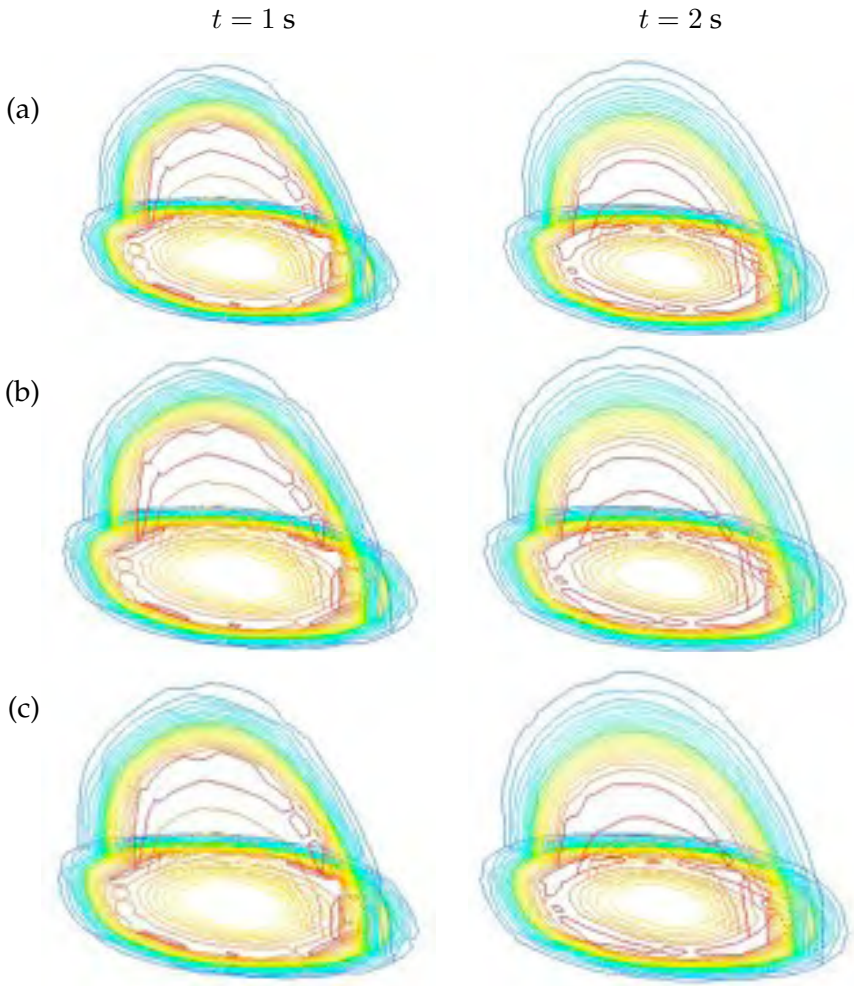

Figure 6.22: 3D perspective of experiment #2, created by the floor of the wind tunnel and a vertical plane through the centre of the wind tunnel, of the distribution of (a) H_2O(l), (b) CO_2 and (c) levoglucosan at t = 1 s (left) and t = 2s (right). Red indicates contours of maximum mole fraction and blue indicates contours of minimum (generally zero) mole fraction with other colours interpolated between.

6.4 Discussion

The primary aim of this CFD modelling was to determine the spatial impact of the competitive formation of charcoal and levoglucosan during thermal degradation in conditions open to an ambient air flow. It is difficult to obtain a direct comparison of the formation rates of charcoal with respect to levoglucosan, due to the fact that the charcoal species ($C_{11}H_4$) is a solid phase species and thus its mole fraction is not tracked by FLUENT (designed primarily for fluid flows). However, we know that H_2O(l) is only formed in the reaction that forms $C_{11}H_4$ and that 8 moles of H_2O(l) are formed for every mole of $C_{11}H_4$ formed (Eq. A3.1, p. A3.1). Thus, dividing the distribution of the mole fraction of H_2O(l) by 8 gives the mole fraction of $C_{11}H_4$ but not necessarily the spatial distribution of the charcoal, as H_2O(l) is modelled as a gas phase species and can be advected away from the site of its formation. However it will be assumed that distribution of the mole fraction of water will provide a simulacrum of the distribution of the mole fraction of char on the floor.

Figures 6.23 and 6.24 show the contours of mole fraction at t = 2 s of experiments #1 and #2 respectively for: a) charcoal (estimated from the mole fraction of H_2O(l)), and (b) levoglucosan (same as figures 6.7 (p. 135) and 6.16 b, right (p. 144)). The distributions appear at first glance to be identical but closer inspection reveals two significant differences.

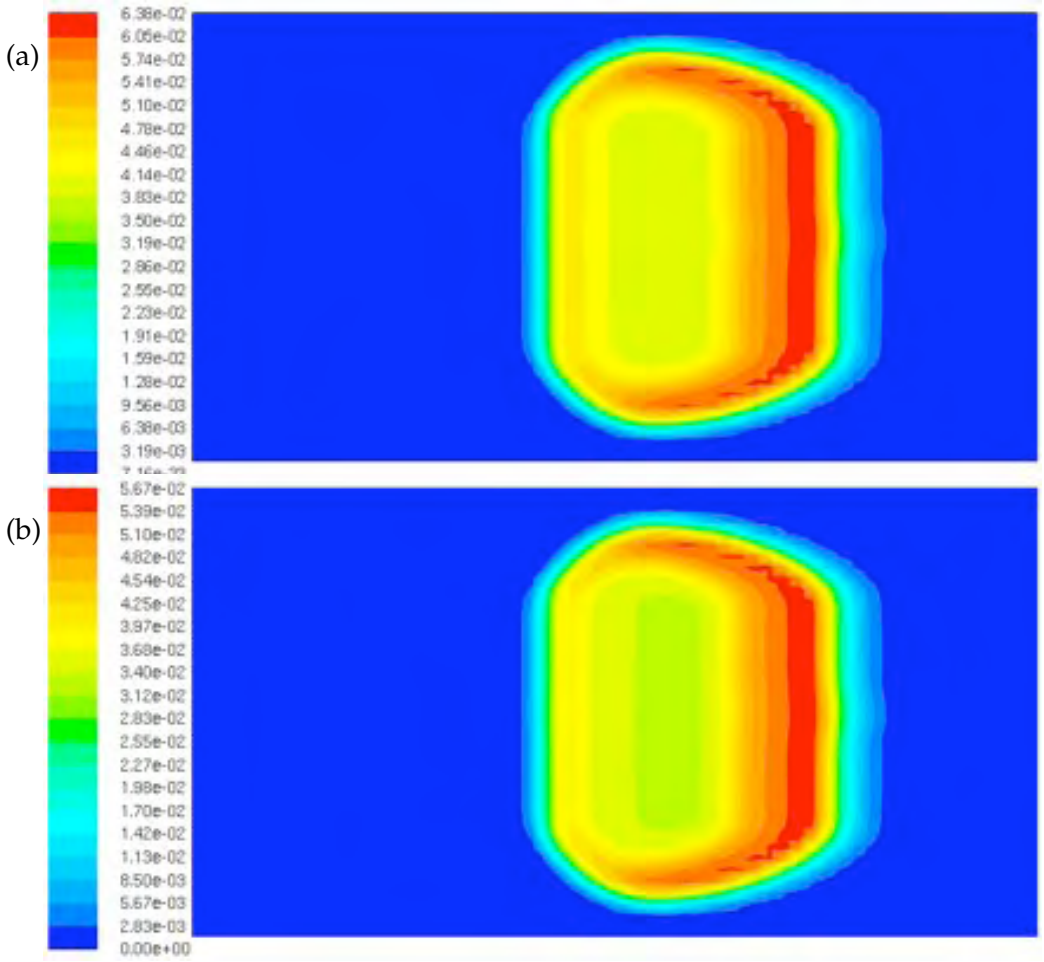

Figure 6.23: 2D contours of mole fraction of (a) charcoal (estimated from mole fraction of H_2O(l)) and (b) levoglucosan on the floor of the wind tunnel from experiment #1.

The first is in the absolute amount of product (as revealed by the scale on the left of the figures). In experiment #1 (Fig. 6.23), the amount of charcoal is uniformly greater than the amount of levoglucosan by 12.2–13.3%, with an average of 12.4% (s.d. 0.27). In experiment #2 ((Fig. 6.24), the amount of charcoal is also uniformly greater than that of levoglucosan by 12.2–13.3% but with a slightly greater average, 12.5% (s.d. 0.29). This suggests that in both cases, the competition between the formation of the charcoal and levoglucosan lies only slightly in favour of the charcoal (and ever slightly more so in the case of the zero wind experiment). The fact that the levoglucosan has not ignited to any great degree (as shown by the contours of the flaming combustion reaction (Fig. 6.8 right, p. 136), CO_2 (Fig. 6.7 left, p. 135), and temperature (Fig. 6.5, p. 133)), suggests that the combustion conditions are marginal and thus would not be expected to be dominated by levoglucosan formation and flaming combustion.

The second is in the spatial distribution of the two thermal degradation products. Figure 6.25 shows the areas of difference between the two contours of mole fraction for the second iteration for experiment #1 (Fig. 6.25a) and experiment #2 (Fig. 6.25b) superimposed on the contours of mole fraction of levoglucosan. In the former figure, the differences are shown as cross-hatched regions, in the latter as regions of white. In the wind-driven case (experiment #1), the majority of the difference occurs in the centre and rear of the fire area. In the zero-wind case (experiment #2) there are only very slight differences scattered around the fire perimeter.

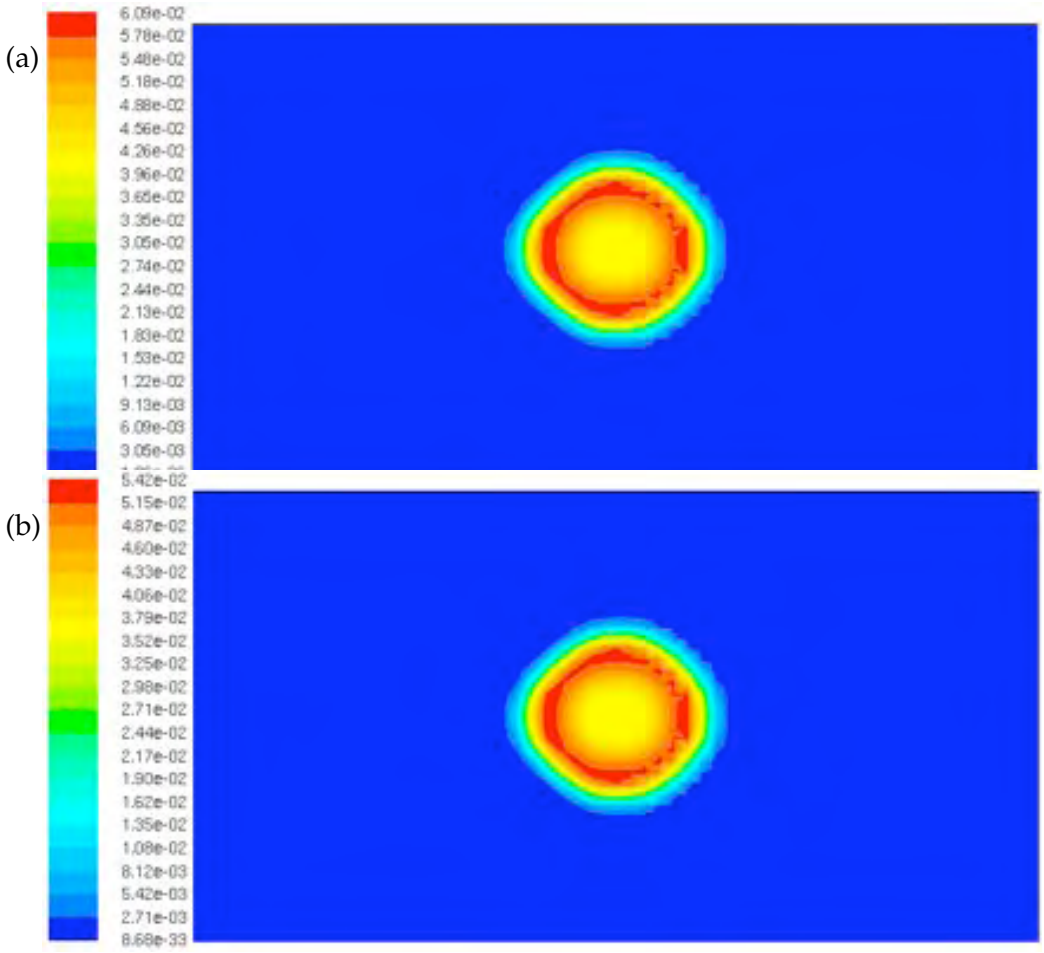

Figure 6.24: 2D contours of mole fraction of (a) charcoal (estimated from mole fraction of $H_2O(l)$) and (b) levoglucosan on the floor of the wind tunnel from experiment #2.

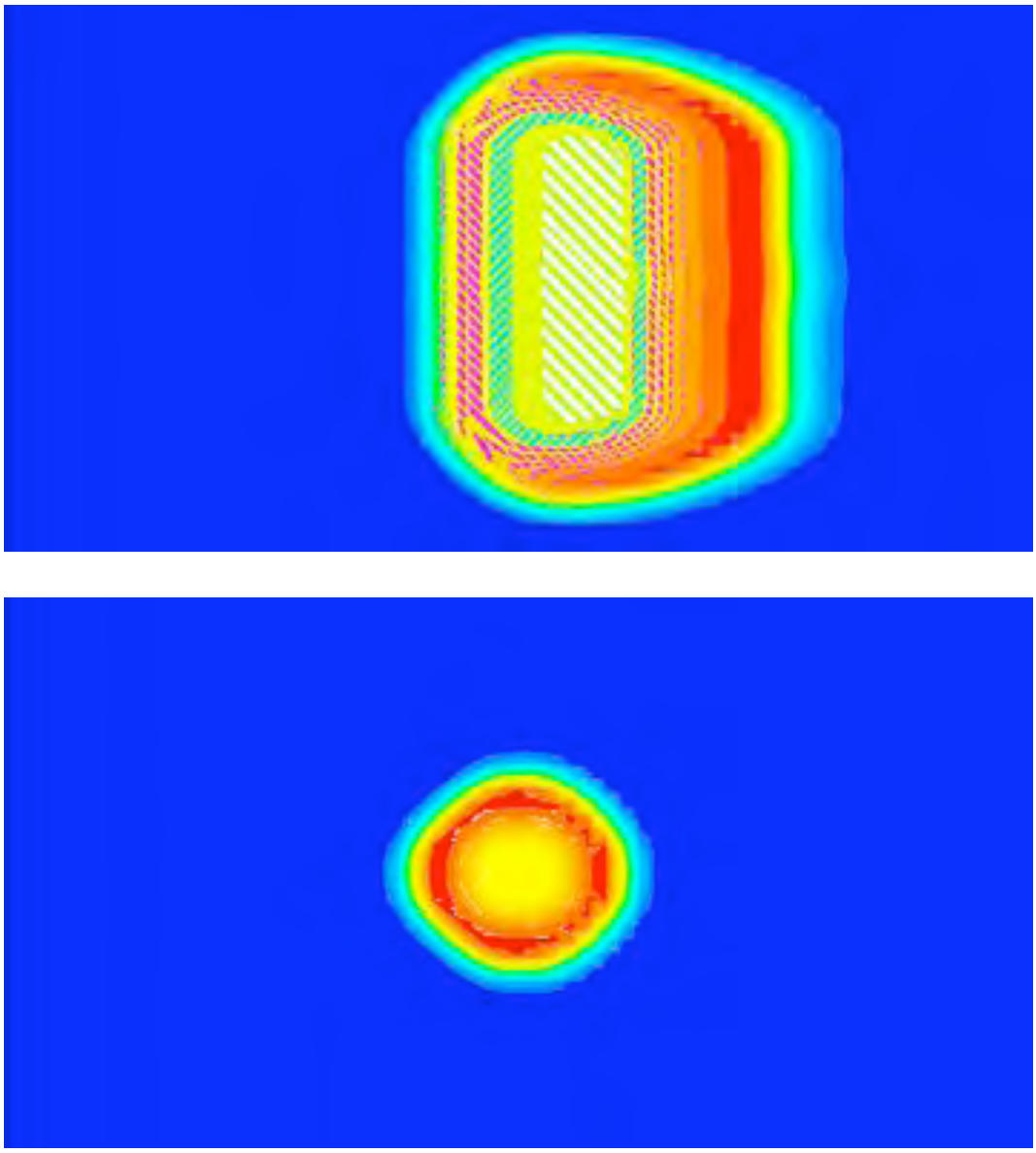

Figure 6.25: Areas of differences in the spatial distribution between the charcoal mole fraction contours and the levoglucosan (represented as cross-hatching) for (a) experiment #1 and (b) experiment #2. White cross-hatching indicates an absolute increase in charcoal mole fraction of 0.73 or 121.5%; green cross-hatching indicates an absolute increase in charcoal of 0.76 or 121.5%; and orange cross-hatching indicates regions of absolute increase of 0.79 or 120.6% of the levoglucosan mole fraction.

The white cross-hatching in the centre of the fire indicates an absolute increase in charcoal mole fraction of 0.73 or 121.5% of the levoglucosan mole fraction. The green cross-hatching indicates an absolute increase in charcoal of 0.76 or 121.5% of the levoglucosan mole fraction. The orange cross-hatching indicates regions of absolute increase of 0.79 or 120.6% of the levoglucosan mole fraction.

The lack of bias under no wind in the formation of reaction products in general, and charcoal and levoglucosan in particular, illustrates the temperature dependence of these reactions such that rates for all reactions increase similarly throughout the domain. The

development of a bias under wind shows that there is a differential in the reaction zone temperatures, presumably as a result of the action of the wind since all else is equal. The relative increase in the formation of charcoal in comparison with levoglucosan predominantly on the upwind side of the reaction zone suggests that its lower activation energy allows it to form in competition with levoglucosan much more readily under the conditions where it is open to the flow of the ambient wind.

6.5 Conclusions

This chapter has detailed the definition and construction of a computational fluid dynamics model of the competitive combustion of cellulose, known as CC-CFD, using the commercial CFD code FLUENT. The initial form of this model used a two-step, three path reaction model in which cellulose undergoes a primary reaction (thermal degradation) to charcoal, either directly or in the presence of water, or levoglucosan (incorporating implicitly the thermal degradation of cellulose to intermediate forms (levoglucosan-end and hydrolysed cellulose) and conversion to volatile (levoglucosan) and charcoal in one step). The rates of these reactions are limited by the rates of formation of the end products. The enthalpy of formation of the charcoal is negative (i.e. exothermic) while that of the levoglucosan is positive (endothermic). Secondary reactions of the oxidation of charcoal and levoglucosan in the processes of glowing combustion and flaming combustion respectively form water and carbon dioxide. The enthalpy of formation of these products are based on those contained in the FLUENT materials database.

The competitive combustion chemistry was put in the context of a wind tunnel experiment in order to provide a contained domain for numerical purposes, i.e. so that the flows being simulated were relatively simple and constrained. The wind tunnel measured 3 m long, 1.6 m wide and 1 m high. A thin layer of cellulose fuel was laid upon the floor of the tunnel such that the combustion reaction takes the form of a surface reaction on the floor. Air enters the wind tunnel in a uniform flow at speeds that can be varied in a number of ways, and exits the other end.

This experimental design paradigm was implemented in two computational grids or meshes. The first was a 2-dimensional mesh which was used to develop and refine the numerical simulation. This mesh was a central longitudinal cross-section along the length of the wind tunnel. The second was a fully 3-dimensional mesh that allowed the spatial aspects of the competitive combustion chemistry to be investigated. The objective of the numerical experiments was to investigate the interaction of the air flow in the wind tunnel with the competitive thermal degradation and combustion reactions. The aim was to determine if there is a spatial difference in the thermal degradation reactions as a result of the ambient air flow and the activation energies of the competitive reactions.

Difficulties in the form of numerical instability and divergence in the solution were encountered in the solutions of both the 2D and 3D formulations. A recognised issue with FLUENT is the difficulty of obtaining a convergent stable solution for problems that involve rapid and high heat release rates. A simplified set of thermal degradation reactions was implemented to try to improve the numerical stability of the simulation. The direct formation of charcoal was omitted, resulting in a competing two-path two-step reaction set. The liquid phase of water ($H_2O(l)$) was used to differentiate the formation of

water (liquid) in the charcoal formation reaction from the formation of water (gaseous) in the oxidation reactions. Numerical instability and divergence were still experienced in the solutions after a short number of time-steps and which limited the usability of the model. However it was assumed that the results produced prior to the onset of instability were valid enough to make observations and analyses and draw conditional conclusions. The extreme magnitude of the maximum temperature in these solutions suggest that even these results may be questionable but at least provide a starting point.

Two limited experiments were conducted to investigate the influence of wind on the thermal degradation and oxidation reactions: a constant 0.5 m s^{-1} wind of ambient (i.e. 310 K) temperature from the left hand end of the wind tunnel; and a zero wind also of ambient temperature. Experiment #1 provided evidence of a bias in the shape of the contours of total temperature in the domain due to the wind. Although the simulations ceased due to numerical stability before the final perimeter shape was achieved, this bias tended toward the shape of a crescent or parabola curved into the wind. This shape is similar to that found for head fires burning freely in a wind.

The spatial distribution of the formation of thermal degradation products, H_2O(l), CO_2 and levoglucosan, also tended towards the parabolic head fire shape, although more pronounced than that observed in the contours of temperature. The spatial distribution of products also showed that the regions of maximum mole fraction (i.e. the percentage of moles of chemical present) occured in a crescent form on the downwind edge of the combustion zone, indicating that the region of maximum reaction rate, and thus reaction temperature, also occurs in this shape. The mole fraction of charcoal (inferred from the mole fraction of H_2O(l)) was found to be uniformly greater than that of levoglucosan by about 12%. This suggests that the competition between the formation of the thermal degradation products is only slightly in the favour of charcoal and that the oxidation (and thus the greater rate of heat release) of levoglucosan is marginal (i.e. not much flaming combustion), as shown by the relatively low rates of the flaming combustion reaction.

While the regions of maximum product formation appear similar for all products on the downwind edge, a greater degree of difference is apparent on the upwind edge of the fire zone. Here it was found that the mole fraction of charcoal was in the order of 20% greater than the mole fraction of levoglucosan. This suggests that formation of charcoal in the competition between the two thermal degradation pathways is more favoured at the rear of the fire zone than the formation of levoglucosan.

These results are far from conclusive but provide an insight into the nature of the interaction of environmental conditions with the reactions of thermal degradation. To the extent that they may be considered valid they support the thermokinetic modelling of Chapter 5 in which the maximum reaction rate occurs where a) the temperature is highest and b) reactants are present. The maximum temperature in the domain is behind the crescent of reaction forming the charcoal and levoglucosan, in the zone where the charcoal is oxidising (forming H_2O), but there would be little reactant (i.e. cellulose) remaining at this point. Thus, the region of maximum reaction rate is elsewhere. The passage of air over the region of maximum temperature acts to increase the temperature of the air, mainly through convective mixing. In conjunction with the transfer of heat through radiation from the region of maximum temperature, the region immediately downwind is heated sufficiently to achieve the maximum reaction rates in the domain.

Experiment #2 using no wind showed no bias in the either formation of the thermal degradation products (H_2O(l), CO_2 and levoglucosan) or in the contours of maximum temperature (other than that formed as a result of the rectangular ignition patch). Although the spatial distribution of products was not exactly uniform around perimeter of the fire, they were very nearly identical, with only a very minor amount of difference between charcoal (through H_2O(l)) and levoglucosan. This shows that the lack of a bias in the wind over the reaction zone results in no spatial bias in the thermal degradation reaction around the fire perimeter. All things being equal, this will result in an even distribution of charcoal formation and levoglucosan formation around the perimeter.

The fact that there is a significant difference between the spatial distribution of thermal degradation products with and without a wind provides support for the argument that it is the direction of the wind (through its temperature) in relation to the fire perimeter that dictates the outcome of the competitive reactions involved in the thermal degradation of cellulose. The lower activation energy of the charcoal formation is statistically favoured under the conditions where the influence of the more ambient temperature wind lowers the temperature of the reacting zone, as found on the upwind edge of the fire perimeter. Where the wind has increased in temperature to something significantly more than ambient temperature, resulting in a statistically greater occurrence of the activation energy of the levoglucosan formation reaction, the ratio of levoglucosan to charcoal increases.

The situation where the levoglucosan formation was statistically favoured over the charcoal formation was not encountered in the limited set of experiments conducted here. With a more robust CFD model that is not beset with numerical instability, a more complete set of experiments (which includes flaming combustion) might achieve more conclusive and convincing results. Steps to improve the numerical stability of FLUENT (Graham[5] pers. comm., July 2007) include employing a much finer (> 10 times finer than the current) domain mesh, using an initial time step in the order of 1×10^{-6} seconds and more controlled use of number of iterations per time step to ensure solution convergence at each time step before incrementing to the next time. Once this is achieved it may be possible to revert to the original 'ideal' CC-CFD model with the original reaction rate constants. This will provide a more robust representation of the competitive combustion reactions and more reliable results. Ideally, implementing a more fundamental 3-path, 3-step model that includes the formation of the intermediate cellulose species (i.e. hydrolysed cellulose and levoglucosan-end cellulose) will produce a more realistic representation of the thermal degradation of cellulosic fuels. It is possible that the non-convergence issues encountered with FLUENT may be due to the inability of FLUENT to properly handle the rapid chemical kinetics and high thermal gradients and other CFD packages may need to be investigated to study the competitive thermokinetics of cellulosic fuels.

Once a robust model has been constructed, investigation of ambient versus elevated air temperatures, non-uniform, non-steady wind speed and direction and oxygen-free environments may be possible. Validation of these numerical experiments could be achieved under controlled conditions in a suitably designed laboratory. More complicated CFD models that include more realistic representations of bushfire fuel itself, larger computational domains, and more realistic environmental conditions may be possible.

[5]David Graham, consultant, LEAP Australia, ANSYS LTD Australian representative.

The computational requirements for the full CFD solution of a detailed and large scale simulation of a bushfire is prohibitive in terms of the cost, time and data required. The next chapter takes the qualitative results of CFD modelling carried out in this chapter and attempts to build the framework of a model that simplifies the physical and chemical processes involved in the spread of a bushfire such that the computational requirements are more suited to an operational model of fire behaviour.

Chapter 7

A framework for a new model of bushfire spread

In which the outline for a spatial model of bushfire spread based on the understanding of the competitive thermal degradation and resulting combustion of cellulosic fuels shown in the preceding chapters is proposed and discussed. A detailed network model of the interactions of the spatial aspects of the key competing chemistry and the heat transfer processes is constructed to describe the evolution of a fire perimeter. This network model could provide the basis of a dynamical systems model or a cellular automata model of bushfire spread.

Four university professors—an engineer, a physicist, a chemist, and a statistician—are called in to see the vice chancellor. Just as they arrive, the vice chancellor is called out of his office, leaving the four professors fuming in annoyance. As they sit waiting they become alarmed when they see a fire in the VC's waste paper basket.

The engineer leaps to his feet. "Brute force is the answer," he says. "If we stomp on it hard enough we can put it out".

The physicist leaps up and stops the engineer. "Wait! I know what to do! We have to cool down the materials until their temperature is lower than their ignition temperature and then the fire will go out."

"No, no, no!" the chemist says excitedly. "We must cut off the supply of oxygen so that the combustion reactions will cease due to lack of one of the reactants."

While the three argue about what they should do, they become aware of the statistician running around the room lighting other fires. "What are you doing?" they scream.

The statistician stops and looks at his colleagues. "Isn't it obvious? I'm trying to get an adequate sample size."

7.1 Introduction

The initial aim of this project had been to investigate the interaction between the atmosphere and a fire in an effort to explain some of the fundamental behaviour observed in bushfires, particularly under extreme fire weather conditions, and to incorporate the

results in a model of bushfire spread. The growing field of complex systems science (CSS) appeared to offer a different approach to the investigation of bushfires than that traditionally employed which might reveal new and different insights.

7.1.1 Complex Systems Science

Before the discovery of chaos, physical processes were generally categorised into two groups: periodic behaviour and random behaviour; both are simple, in that the former repeats in time, and the latter provides a reduced statistical description (Crutchfield and Young 1989). The study of chaos has shown that there is a broad spectrum of behaviour between the two (e.g. Lorenz (1963)). CSS has evolved to investigate the behaviours of systems in this space.

A complex system is considered to be one in which the whole is greater than the sum of its parts (Kelly 1992; Cohen and Stewart 1994). This may seem trite, but captures the essence of CSS in juxtaposition to the traditional reductionist science which arrived with the Enlightenment of the 18th Century. The reductionist approach to science strives to break down a problem or process into its component parts. These can then be investigated in isolation from the rest of the system, allowing problem simplification and an iterative progress toward a solution to the problem. This approach has generally been successful in a very wide range of endeavours, from building a bridge to putting a man on the moon, however it struggles when a subcomponent of a problem or process cannot be treated in isolation. This flaw was recognised very early on and led to one of the first tools of CSS, namely statistical mechanics used in the study of thermodynamics by Boltzmann, Gibbs and company, but was generally ignored for the sake simplicity. However, increasingly more complicated problems, such as many-body interactions (such as seen in the motion of the planets), turbulence, ecology, economics, and quantum mechanics, showed that a reductionist approach failed to capture the necessary detail of a problem and provide useful solutions (Cohen and Stewart 1994). Thus, CSS has become recognised in recent times as an important field in the development of understanding of systems which are, at best, highly complicated and, at worst, highly complex.

The primary attribute of a complex system is what is called an 'emergent property' or 'emergence' (Seeley 2000; Green 2000), in which a behaviour or property is said to 'emerge' from the interactions of the elements of the system, rather than being a fundamental part of the system itself. This can take the form of self-organisation, in which the system of elements forms itself into a particular pattern or behaviour without any external influence. Quantification of self-organisation is problematic, mainly because it has yet to be rigorously defined (Shalizi *et al*. 2004). Many attempts have been made to do this, ranging initially from changes in thermodynamic and then information theoretic entropy (Shannon 1948), through to measures of complexity based on causal state representations based on ϵ-machines (Crutchfield and Young 1989) or appropriately defined notions of 'order' and 'disorder' (Shiner *et al*. 1999).

It is the emergence of a complex behaviour from an otherwise seemingly simple system that forms the major paradigm of CSS. That is, much of the complexity observed in real systems (be they biological, physical, societal, economic) is a result of interactions of (possibly very simple) elements that comprise the system being observed. Thus, a complex system can be defined as comprising many independent but interacting elements or components (Green 2000). Other qualities that are used to define a complex system

include the spanning of a large range of spatial and temporal scales, and irregular or non-linear interactions between elements.

It is the interactions between the components, rather than any inherent complexity of the components themselves, that provides the complexity of the behaviour of the system. However, the interactions may not necessarily be complex or complicated in order for the system to exhibit complex behaviour. One of the basic tenets of the CSS approach is that much of the complex behaviours exhibited in a system are the result of simple rules of interaction (Wolfram 2002). Understanding and quantifying the governing rules of interactions is the aim of CSS.

This aim is achieved via a diverse range of tools and techniques. The most fundamental is based on the idea that the basic behaviour of a complex system can be synthesised by capturing some suitable simplified approximation of the key characteristics of the system. In the field of turbulence this is called 'coarse-graining' (i.e. reducing the detail or resolution of the system to some simpler form that still captures the basic system behaviours) (McComb 2006) and is based upon the techniques developed in quantum field theory known as renormalisation (RN) theory and renormalisation group (RNG) theory (McComb 2004). These techniques endeavour to quantify a particular physical quantity at a certain scale and 'renormalise' it to a mean-field quantity at a larger scale, effectively reducing the resolution needed to describe the attributes of that quantity. This is only truly successful if the information contained in the reduced-resolution, larger-scale version is equal to the information contained in the original version, but there will always be trade-offs.

Shalizi *et al*. (2004) formalised the measure of statistical complexity, C, developed by Grassberger (1986) and Crutchfield and Young (1989), in which complexity was defined as the least amount of information about a system's state needed for a maximally accurate prediction of the system's future state. In a thermodynamic setting, this is the amount of information a full set of macroscopic variables contains about a system's microscopic state (Shalizi and Moore 2003). The canonical example of this is found in the field of thermodynamics in which the macroscopic variables such as temperature and pressure contain information about the microscopic state of the gas molecules that are interacting to produce the macroscopic variables.

Other CSS tools and techniques developed or coopted to study complex systems include (but are not restricted to) cellular automata, graph theory (encompassing network theory), dynamical systems theory, agent-based modelling, hidden Markov models, genetic algorithms and computational mechanics. Topic areas that have been investigated include economics/share markets, gene expression/regulation, ecology, condensed matter, flocking/schooling of birds and fish, turbulence, and much more.

7.1.2 CSS and bushfire behaviour

A scoping study (Sullivan *et al*. 2003b) found that, based on the formalisms used in CSS to define a complex system, an individual bushfire can be considered a complex system: it is comprised of many independent but interconnected components (the fire, the fuel (including individual fuel elements), the topography, the atmosphere (including large and small scale structures within the atmosphere), the components span a large range of scales (see Table 2.1, p. 18), the connections between these components are irregular and in many cases non-linear, and behaviour emerges from the self-organisation of the

elements that is not inherent in any of the components of the system (the rate of spread of the fire could be considered an emergent quantity as it depends on interactions of the system components).

Bushfire (in the form of idealised forest fires at landscape scales) has been used as a real-world example (along with earthquakes and avalanches) of self-organised criticality in which the distribution of fire size and fire occurrence follow a power-law which is scale invariant (Bak *et al*. 1990; Bak 1996). That is, the frequency of occurrence decreases with increasing fire size. However, the behaviour of an individual bushfire had never before been considered from the point of view of CSS and thus presented an opportunity to apply the tools of CSS and perhaps develop a new type of bushfire spread model.

The disadvantages, in terms of computational and data requirements, formulations and validation, of the full physical modelling of bushfire behaviour (i.e. the chemistry and physics of combustion and heat transfer, as for example in FIRETEC (Linn 1997; Linn *et al*. 2002; Linn and Cunningham 2005), WFDS (Mell *et al*. 2006, 2007) and IUSTI (Larini *et al*. 1998; Porterie *et al*. 2000, 2007)) mean that it will be a considerable time before these models provide the useful and timely results required for operational bushfire spread prediction (Sullivan 2007b). The empirical approach to fire behaviour modelling, used to develop operational systems currently in use, limits the applicability, flexibility and range of such systems and relies heavily on the choice of statistical models by the modeller (Sullivan 2007c). There is a need for a 'best-of-both-worlds' type solution, in which the fundamental processes and interactions on which the physical models are based are solved in a manner that gives the timeliness, robustness and confidence normally associated with empirical models such that the results can be used operationally. CSS was seen as an approach that could potentially provide such a result.

An initial attempt concentrated on attempting to reduce the interactions between the convection column of a fire with the bulk motion of the atmosphere over the fire in order to replicate the characteristic parabolic head fire shape. This took the form of a hybrid 2-dimensional, 3-state cellular automata fire spread model linked to a simplified quasi-physical model of the fire's convection column (Sullivan and Knight 2004). It used local cell-based spread rules that incorporated semi-stochastic rules (allowing discontinuous, non-near neighbour spread) with a spread direction based on the vector summation of the mean wind field vector and a vector from the cell to the centre of convection.

The initial aim of this PhD study had been to extend and develop further this approach to modelling the interaction of the fire with the atmosphere, as this was seen as the source of much of the non-linear behaviour in bushfires (e.g. Clark *et al*. (1996a,b, 2004)). However, upon commencement of this project and the realisation of the importance of the role of competitive thermal degradation of cellulosic fuels in the non-linearity of bushfire behaviour, the direction of work changed dramatically (as detailed in the preceding chapters). It has not, however, changed the basic need for a more robust, computationally-feasible and fundamental approach to the building of an operational fire spread model.

Thus this penultimate chapter in this thesis will present and discuss the framework for a fire spread model that uses as its basis the competitive thermal degradation and combustion of cellulosic fuels in combination with the CSS paradigm of identifying and coarse-graining the processes involved in the behaviour and spread of bushfires.

7.2 Network models of bushfire behaviour

Green (2000) stated that all complex systems can be represented as digraphs (directed graphs) or networks, in which the connections (called edges) between elements of the complex system (called nodes) define the interactions. Indeed, Green goes on to say that matrix models, dynamical systems and cellular automata are all isomorphic to digraphs. If this is the case, and if an individual bushfire is considered a complex system, then a bushfire must be representable as a network of interconnected nodes. Green[1] (pers. comm., 2006) suggested that the structure of such a network for a bushfire would be based on the spatial aspect of the fuel through which a fire would burn. That is, that the elements of a cellular representation of the landscape would form the nodes of the network and the connections would presumably be the physical contact between the cells representing the landscape. For example, a square lattice would result in each cell having four near-neighbours (the von Neumann neighbourhood) and four next-near-neighbours (the Moore neighbourhood).

This, in fact, is how many cellular automata (CA) models of fire spread (e.g. Green *et al*. (1990); Li and Magill (2000); Hargrove *et al*. (2000); Dunn and Milne (2004); Johnston *et al*. (2006); Dunn (2007); Encinas *et al*. (2007)) represent the landscape and the spread of fire across it. However, this representation fails to capture the key aspects involved in the behaviour of a bushfire, in many instances reducing the nature of combustion to a simple 'contagion'-like mechanism in which a cell ignites only through contact (moderated through various threshold requirements) with an already burning cell, ignoring the influence of non-local mechanisms such as radiative and convective heat transfer, solid mass transfer, and the nature of biomass combustion (although these can be addressed via non-near-neighbour interactions).

A network is the easiest method of representing the key elements in a complex systems and the directions of interactions linking them. This not only provides a visual representation of the system but can also allow other types of models, such as a dynamical model, to be developed from it. The remainder of this section will work towards the development of a network representation of the elements and interactions involved in the behaviour of a bushfire.

7.2.1 The combustion triangle

The simplest network model of fire is based on that of the traditional fire combustion triangle (Fig. 7.1a). The fire combustion triangle consists of the three components necessary for combustion to occur—fuel, oxygen and heat. To represent this triangle as a network (Fig. 7.1b), the vertices of the triangle define the nodes or elements of the network and the sides define the edges or interactions. One could argue, however, that there is very little interaction between the three ingredients so we must introduce a fourth node—combustion itself—and redefine the interactions in this context (Fig. 7.1c). This figure shows that oxygen, fuel and heat all contribute to combustion but also that combustion contributes to heat, thus providing a mechanism for continued combustion.

[1]Professor David G. Green, School of Information Technology, Monash University.

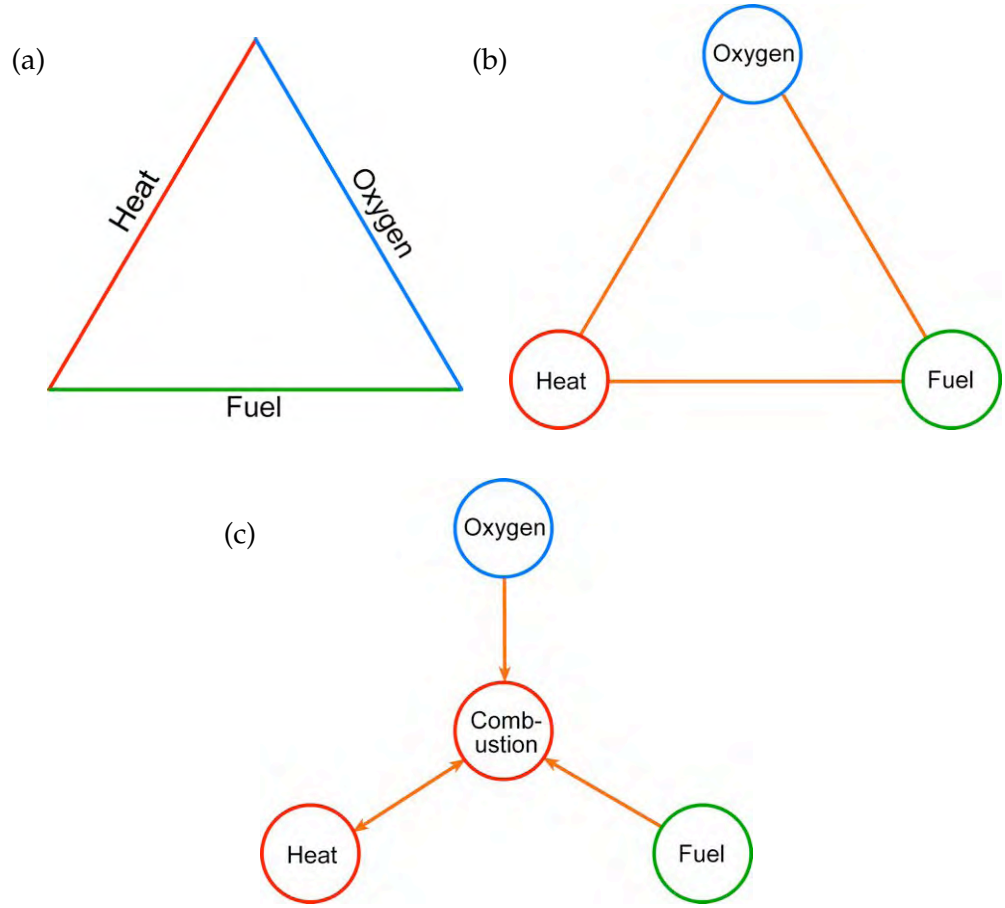

Figure 7.1: (a) The traditional fire combustion triangle in which the three key ingredients necessary for combustion are identified. (b) This triangle can be represented as a simple network in which the vertices become nodes. (c) Identifying the connections between the nodes defines one possible configuration of interactions in the network. In this case a simple feedback between heat and the combustion leading to ongoing combustion is identified.

7.2.2 The fire behaviour triangle

Countryman (1966) extended the idea of the fire combustion triangle to illustrate the primary components that govern the behaviour of a bushfire, that is fuel, weather and topography, forming the fire behaviour (or fire environment) triangle surrounding the fire itself (Fig. 7.2a). Converting this triangle to a network (Fig. 7.2b), the vertices become the network nodes and the sides become the edges. Determining the direction of the interactions is the next task. Topography can affect the weather and the fuel but the converse is not true. All three elements influence the behaviour of the fire but it may be said that the fire can only influence the weather, and then only under the most extreme of circumstances. One must also be aware of the temporal scale of the interactions; weather and topography do influence fuel but only over extremely long periods, much greater than the timescale of the fire (in this case, *weather* is probably more correctly termed *climate*). Figure 7.2c shows one possible resulting configuration of the interactions. This representation is very similar to the more general fire system model proposed by Byram (1959b) (see the next section).

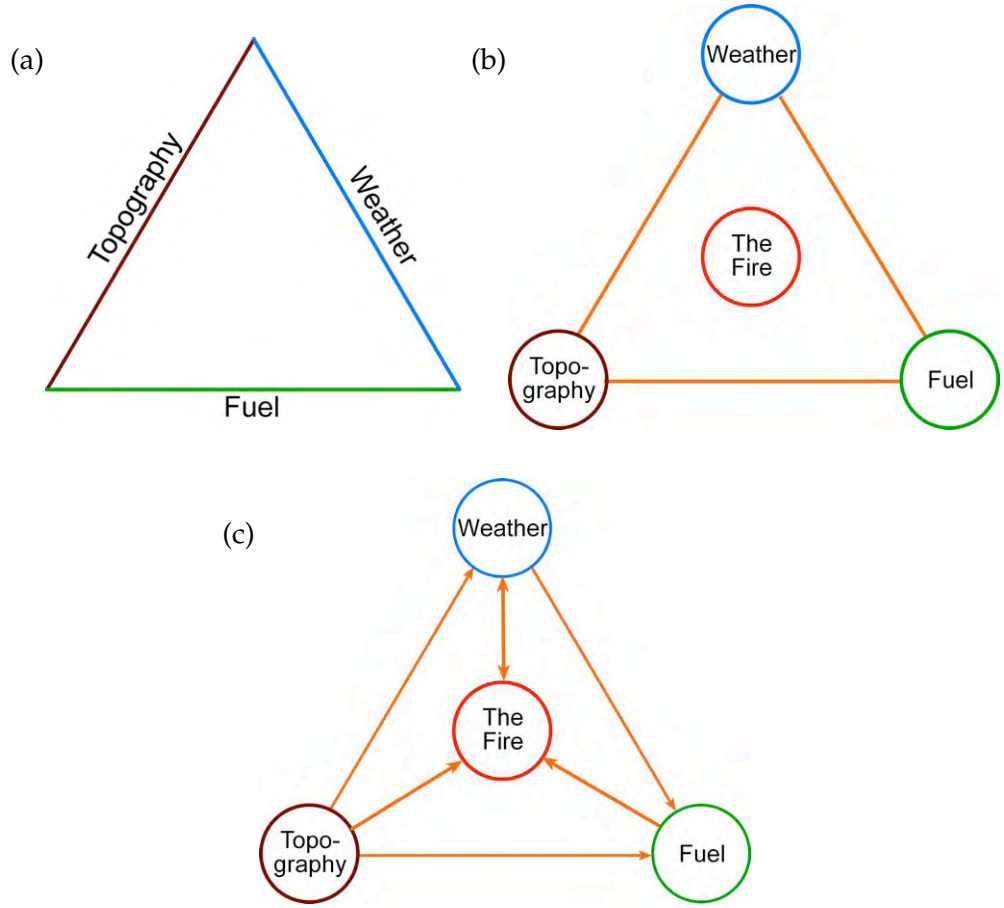

Figure 7.2: (a) The fire behaviour triangle identifies the key components that control the behaviour of a fire in the landscape. (b) This triangle can be represented as a network in which the vertices become nodes. (c) Identifying possible connections between the nodes defines the network. Care must be taken with differing timescales between interactions (e.g. weather and topography would have only a very slow influence on fuel).

7.2.3 Byram's fire system model

In an attempt to develop a unifying concept of bushfire behaviour and a physical system in which to describe the diverse and sometimes contradictory behaviour observed in bushfires, Byram (1959b, p. 99) proposed the fire system model (Fig. 7.3). This system, intended to represent the behaviour of bushfires of all sizes and intensities, identifies four essential elements:

1. the Earth's gravitational field;
2. a compressible fluid (the Earth's atmosphere);
3. a boundary surface beneath the fluid (the Earth's surface);
4. a heat source at or near the boundary surface.

The deliberate replacement of familiar fire concepts with abstract elements not normally associated with bushfire (e.g. the gravitational field), was an attempt by Byram to avoid the trap of minutiae that too easily becomes fire-specific and to capture only those key physical interactions that influence the behaviour of bushfires at all scales. This

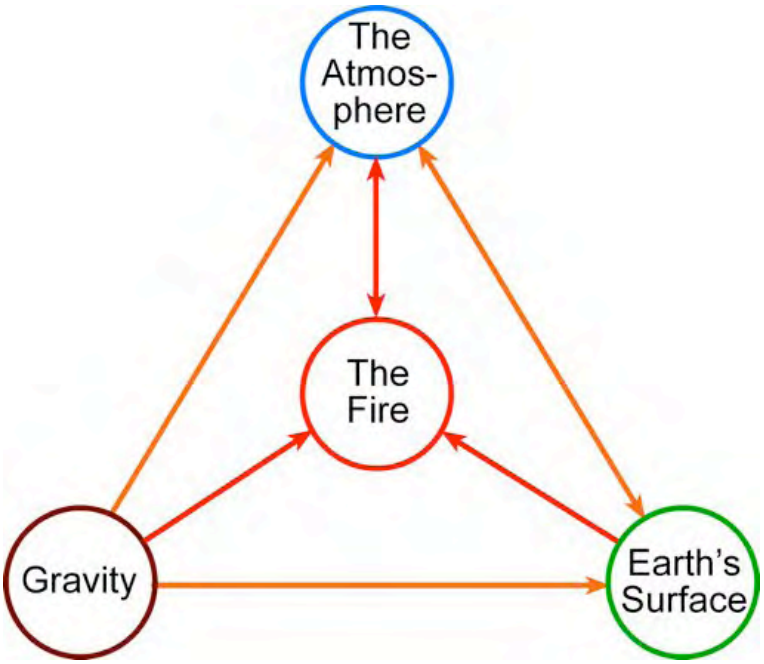

Figure 7.3: Byram's conceptual model of the primary elements of bushfire behaviour—the fire system model—composed of abstract forms of the key elements involved in determining the behaviour of bushfires.

model highlights the interaction between the fire and the atmosphere and led to the formulation of Byram's energy criterion (Byram 1959b; Nelson 1993, 2003) that quantified the power of the fire and the power of the wind driving the fire. While Byram's work has led to development of other non-dimensional quantities used to investigate the ratio of the dynamic and buoyant forces involved in bushfire behaviour (such as, for example, Clark *et al.*'s (1996b) convective Froude number), no complete system model of fire behaviour, as envisaged by Byram, has been developed.

In the light of the work presented previously in this thesis, it can be seen that the representation of the fire in all three networks presented above (even the abstract version proposed by Byram) can be seen to be an oversimplification of the complex nature of the combustion of cellulosic fuels. Thus, a slightly more detailed model of the important elements involved in fire behaviour must be introduced. The danger exists, however, that in doing so one may fall into Byram's trap of minutiæ.

7.3 A network model of competitive combustion

The first step in developing a network representation of any phenomenon is to define what it is we wish to capture in our network. This can be done by stating a series of observations or facts about our system:

1. Wind:
   (a) Wind temperature controls thermal degradation reactions;
   (b) Wind direction and perimeter position control effective wind temperature.

2. Thermal degradation:
   (a) High wind temperature produces more volatile gas;
   (b) Low wind temperature produces more charcoal.
3. oxidation:
   (a) Volatile oxidation provides the fastest heat release;
   (b) Volatile oxidation provides broadest transfer of heat to unburnt fuel;
   (c) Charcoal oxidation provides slowest but greatest heat release.
4. Heat transfer:
   (a) Heat transfer is collectively radiation, convection and conduction (inc. flame contact);
   (b) Wind turbulence/mixing increases heat transfer from volatile oxidation to unburnt fuel;
   (c) Charcoal oxidation is only local and not affected by wind.

The second step is to select the scale at which we will attempt capture the essence of the system. In fire there are three main scales:

1. the fine "fuel element' scale;
2. the medium "fuel bed" scale;
3. the large "landscape" scale.

While it is possible to nest networks within networks, we will restrict ourselves to a single layer network representing the phenomenon at one scale. Initially, we will look only at the competitive combustion process at the "fuel element" scale, and then we will look at fire behaviour at the "fuel bed" scale.

The third step in building a network model is to identify the nodes that represent the key aspects of the system at our scale of interest. These are the *system variables* and might comprise local variables, parameters, forces or processes. As Byram stated, the more abstract the state variable, the more generally applicable the resultant model (alternately, the more mechanistic the model, the more one gains precision and realism but at the cost of generality (Levins 1966)). However, the choice of a set of suitable abstract system variables is quite difficult and dependent to a certain degree on personal choice and in many instances may be quite arbitrary. Initially, we will restrict ourselves to a literal interpretation of the physical aspects of the thermal degradation and combustion of cellulosic fuel.

Figure 7.4[2] shows one possible representation of a particular set of the above facts concerned with the competitive combustion of a cellulosic fuel at the fine "fuel element" scale. In this representation, the competitive thermal degradation reactions have been reduced to the formation of volatiles and charcoal in competition. Arrow-ended edges indicate positive contributions to the node and the ball-end edges indicate negative contributions.

This is obviously much more complicated that the traditional combustion network (Fig. 7.1, p. 162) but essentially contains the same four elements—oxygen (air), fuel, heat—but fire has been split into two competing paths, each with two steps. The edges,

[2]All figures of network structures were constructed using PowerPlay, a freeware Java-based digraph editor written at the University of Oregon (http://www.ent.orst.edu/loop/download.aspx).

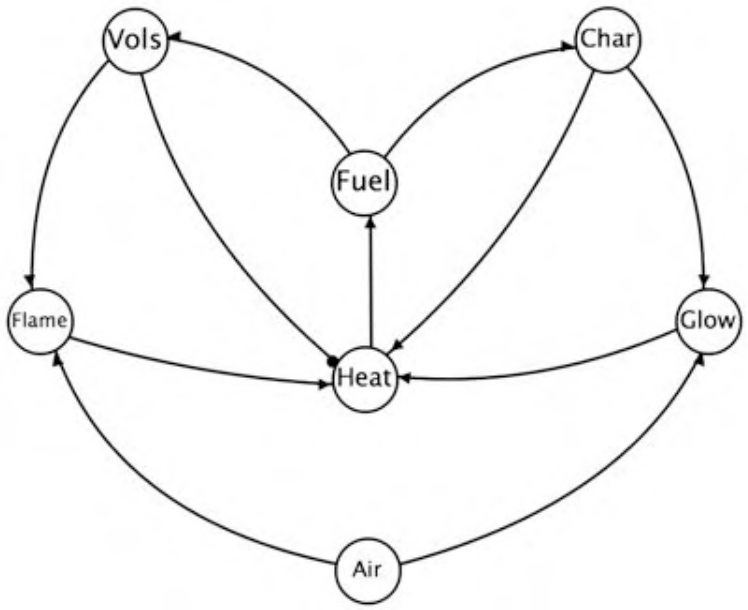

Figure 7.4: One possible network representation of the competitive combustion of cellulosic fuel at the fuel element scale, simplifying the competitive thermal degradation reactions to the formation of volatiles and charcoal in competition and the resultant flaming combustion (Flame) and glowing combustion (Glow). Arrow-ended edges indicate positive contributions to the node and the ball-end edges indicate negative contributions.

E(Fuel,Vols) and E(Fuel, Char), are not mutually exclusive and indeed occur simultaneously at this scale under the competitive processes discussed previously. The network appears to be symmetrical about the heat-fuel axis, but closer inspection shows the exothermic addition of heat to the Heat node from the Char node and the endothermic substraction of heat from the Vols node, resulting in asymmetry.

Two predominant loops are formed (Fig. 7.5), one each for the formation and oxidation of charcoal (red) and volatiles (blue), representing the feedback of heat from these reactions to the heat reservoir. An additional loop is formed through the exothermic formation of charcoal (green). All three loops provide possible pathways by which combustion can be self-sustaining. This representation is graphically equivalent to the simplified chemical reaction scheme used in Chapter 6 in the computational fluid dynamics simulations.

This model does not, however, provide us with a mechanism for predicting the spread of fire. To do that we must at least look at the medium "fuel bed" scale.

7.4 A network model of fire spread

The key message of this thesis is that the competitive thermal degradation and combustion of cellulosic fuels is controlled by the temperature of the air around the reaction zone—the hotter the air, the more volatilisation occurs; the cooler the air, the more charcoal formation occurs. Unless it has been affected by its passage over previously burned/burning ground, wind temperature will be ambient. Thus, a model of the spread

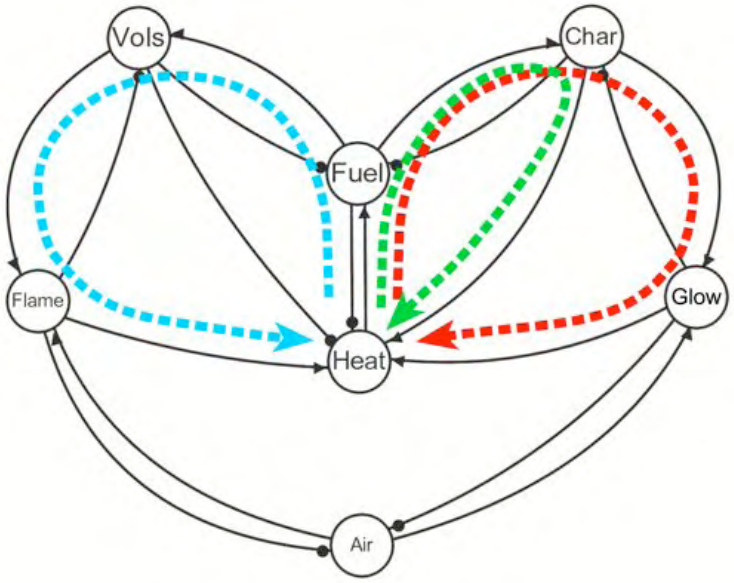

Figure 7.5: Three possible feedback paths are formed in the combustion network, providing possible pathways by which combustion can be self-sustaining: charcoal formation and combustion (dashed red line), volatiles formation and combustion (dashed blue line) and charcoal formation only (dashed green line).

of a bushfire must be able to determine the temperature of the wind as a function of the wind direction and the burnt area of the fire.

Strictly speaking, this is a fluid dynamics problem, but we can avoid the interaction of the motion of the air and the heat release of the fire (and the need for a solution to the Navier-Stokes equations) by approximating the interaction of the wind and the fire using prescribed behaviours. This will reduce computational demand as well as the requirement for detailed input data.

By considering the direction of the mean wind and direction of the normal of the fire perimeter, we can determine the section of the perimeter we are dealing with and the likely wind temperature solely through geometry. When the wind direction and the normal to fire perimeter are parallel, we are dealing with the head fire and thus the air in the reaction region will be at its maximum (i.e. in the order of 600-700 K, just outside the reaction zone). As the angle between the mean wind direction and the normal of the fire perimeter increases, the effective temperature of the wind decreases. When they are orthogonal or greater (approaching anti-parallel) the wind temperature approaches its minimum (i.e. ambient).

Figure 7.6 shows a network for one possible interpretation of our fire behaviour 'facts' for a segment of the fire perimeter composed of an element of the fuel bed. The competitive thermal degradation has been reduced to flaming or glowing combustion, occurring in competition, determined as a function of the temperature of the fuel substrate as modified by the wind temperature (through a fuel/wind coupling coefficient). The Fuel node represents both the mass of the fuel as well as its heat reservoir (i.e. the fuel substrate temperature); Flame and Glow act to reduce the mass of the fuel segment and to also provide heat into the fuel segment.

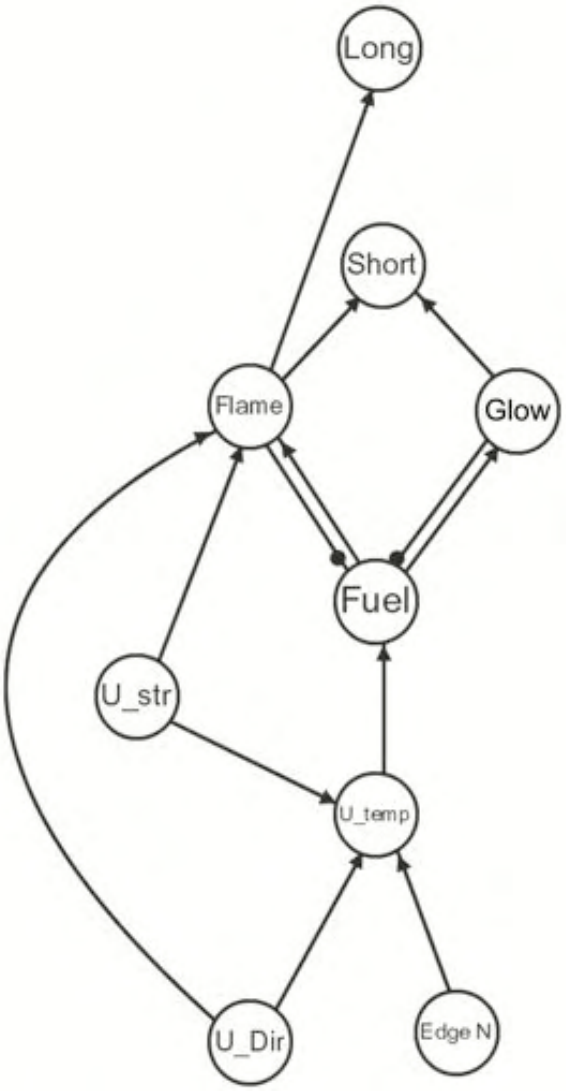

Figure 7.6: One possible network interpretation of the fire behaviour 'facts' for a segment of the fire perimeter composed of an element of the fuel bed. The competitive thermal degradation has been reduced to flaming or smouldering combustion, determined as a function of the temperature affecting the fuel element.
Legend: U_dir = wind direction, U_temp = wind temperature, U_str = wind speed, Edge N = the direction normal to the fire edge, Fuel = the fuel bed element, Flame = flaming combustion, Glow = glowing combustion, Short = short distance (i.e. adjacent) heat transfer, Long = extended (non-local) heat transfer.

A fuel segment can both glow and flame according to the understanding of competitive combustion. The relative amounts of each combustion mode is determined by the temperature of the fuel substrate. The amount of heat released once combustion commences is also predetermined, following the convolution of two different evolutions, one for the slower, greater heat released from charcoal combustion in glowing (Fig. 7.7, solid red line) and a faster, lesser heat released from volatile combustion in flaming (Fig. 7.7, dashed blue line). These are based on idealised rates for the oxidation reactions. The peak of heat release in flaming combustion corresponds to about 5–10 seconds of

tall flame observed in fire fronts, whereas the glowing combustion occurs over a period more closely related to the burnout time of the fuel (60-120 seconds, depending on fuel type).

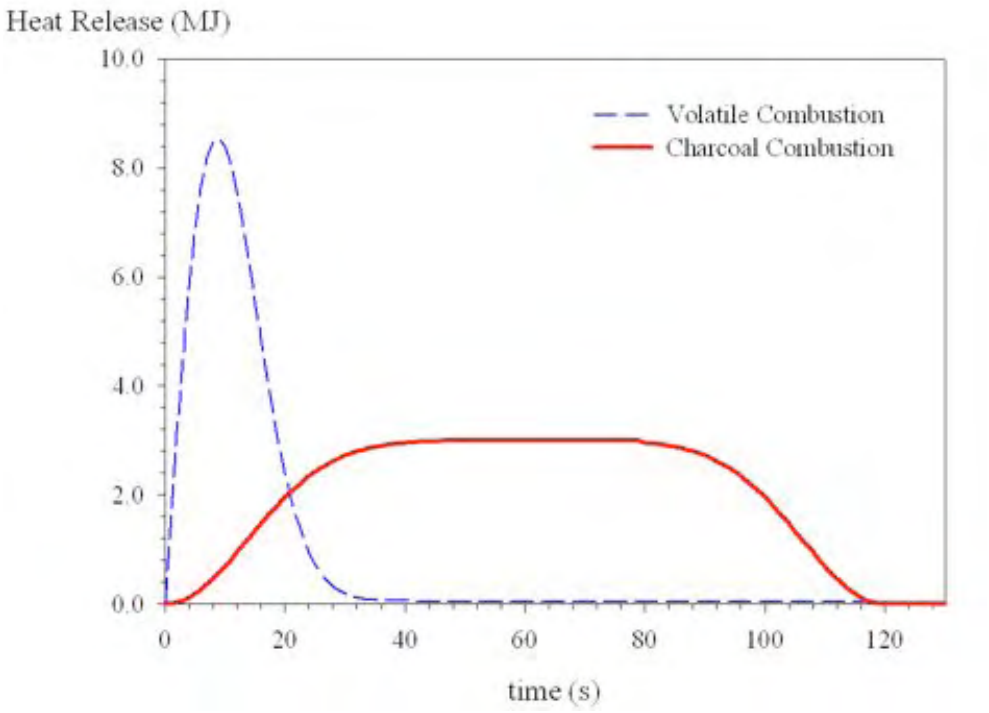

Figure 7.7: Idealised heat release evolution curves for charcoal oxidation via smouldering combustion (solid red line), and volatile oxidation via flaming combustion (dashed blue line). Flaming combustion releases its heat rapidly, whereas smouldering combustion releases more heat over a longer time.

The heat released by the combustion processes occurs at two scales: glowing combustion only occurs over the short-distance scale (i.e. the immediate or adjacent fuel elements); the flaming combustion occurs over both the short-distance and the long-distance (i.e. non-local transfer). It is assumed that all heat transfer occurs predominantly in the direction of the wind. The only exception would be for the short distance heat transfer which might be isotropic. At this scale, heat transfer does not necessarily need to be specific (i.e. radiation, convection or conduction) but kept general.

The short- and long-distance heat transfer mechanisms link the combustion of the fuel element at this perimeter segment to the adjacent fuel elements. The rate of spread of the fire is thus then determined by the rate at which perimeter segments achieve flaming combustion. The transition of the fuel segment from non-burning (but receiving heat) to combustion (glowing and/or flaming) is determined by two fixed ignition heat thresholds, one for glowing and one for flaming at a slightly higher value based on the activation energies for the reactions.

7.5 Discussion and conclusion

A network model of a phenomenon allows the model developer to identify both the perceived key elements of a system and the perceived interactions between the elements. This graphical representation of a model of understanding can then be used to develop other forms of the model that are more suitable for implementing the prediction of the future behaviour of the system, such as differential equations or a cellular automata. We shall not, however, progress to that end but rather leave the network models as a proposed framework for such development.

The network model of competitive combustion extends the simple fire combustion triangle model to represent the competitive pathways present in the thermal degradation of cellulosic fuels and the thermal feedback explored in some detail in Chapter 4 and 5. The low activation energy, exothermic reaction of the formation of charcoal feeds heat back into the fuel element, steadily building up the reservoir of energy until the higher activation energy—but endothermic—pathway to volatilisation can occur. When the activation energy of the oxidation reactions is reached, ignition occurs and the rapid consumption of the fuel element ensues.

The proposed network model of bushfire spread necessarily simplifies the thermal degradation processes that compose the competitive combustion network to provide a mechanism that is driven by the fuel element temperature, modified by the wind temperature. The main direct feedback in this model is the thermal feedback from the short-distance heating from the charcoal formation back into the current fuel element. A secondary feedback exists in the flaming combustion, representing the negative thermal feedback of the endothermic formation of volatiles. It is this mechanism that inhibits the positive feedback and stops the system from simply exploding. No other direct feedback mechanism is present because the fire spread process itself is not stationary and thus not self-contained. However, indirect feedbacks through the rapid transfer of non-local heat may be possible.

This framework provides a possible explanation for the observed behaviour of bushfires in which the maximum rate of spread of a fire for the prevailing conditions is governed by the width and shape of the fire. The basic scale of the model at the fire perimeter segment (in the order of, say, 1 m) provides a method of determining the degree to which flaming or smouldering combustion dominates around the perimeter. A wide, broad fire front will result in a greater number of fire perimeter segments that have the mean wind direction parallel (or very near to) to the normal of the fire perimeter; a narrow, pointed fire front will result in a lesser number of segments that have the mean wind direction parallel to the normal of the fire perimeter. The upshot of this is that a broad, wide fire front will have more length of perimeter that is producing flaming combustion and thus greater non-local heating of unburnt fuel, resulting in a greater rate of spread.

While this framework does not include any consideration of the interaction of the fire with the atmosphere via the convection column, and thus does not provide any feedback mechanism between the two components, it is possible that such a mechanism can be built in at a later date. This would entail expanding the scale of consideration to that of the landscape, as the atmospheric processes involved primarily exist at this scale. However, the simple geometric basis of determining the spatial distribution of volatilisation and charring will have difficulty with complicated fire perimeters in which fingers of flame front have formed at the head of the fire. The model will under-estimate the extent

of volatilisation on the flanks of these fingers because, even though the flanks are parallel with the direction of the wind, the bulk of the head fire remains behind the fingers and thus will result in elevated temperatures rather than the assumed ambient temperatures. It may be possible to include information about the burning area as a whole rather than just the local perimeter segment to determine the likely burning regime at the segment.

The effect of topography is also not included in this framework. The mechanisms involved in the interaction between slope are not clearly understood, but have been approximated to be similar to that of the interaction between wind and the fire. If this is the case, then the framework could be modified to cater for the effect of slope by altering the scope of the long, non-local heat transfer.

Converting the network model to a set of differential equations would create a dynamical system model of the interactions defined therein. Such a model would provide the opportunity to investigate the presence of fixed point behaviours and transitions but would not necessarily provide a useful tool for predicting the rate of spread of a bushfire. To do this the network model needs to be applied to a model of the landscape. Here 2D cellular automata is particularly well-suited to modelling phenomena over a landscape and both the network form and the dynamical system model can be implemented on a cellular automata.

Chapter 8

Summary, conclusions and implications

In which the work detailed in the previous chapters of this thesis is summarised and conclusions about the role of wind in the combustion of biomass fuel and the subsequent impact on the behaviour of bushfires drawn. The importance of the temperature of the wind in the highly temperature-sensitive reactions involved in the thermal degradation of cellulosic fuels has implications for the behaviour and spread of bushfires, particularly the rate of spread and shape of the fire perimeter. Implications on diverse aspects of bushfires are briefly discussed and outlines of possible future work given.

A doctor, a lawyer and a physicist were discussing the relative merits of having a wife or a girlfriend.

The lawyer said, "A girlfriend is better, for sure. If you have a wife and want a divorce, it causes all sorts of legal and financial problems."

"Oh no," the doctor commented. "It's far better to have a wife, because the sense of security and stability in your life lowers your stress and is good for your health."

"You're both wrong," the physicist snickered. "It's best to have one of each. That way when your wife thinks you're with your girlfriend and your girlfriend thinks you're with your wife, you can spend more time working in the lab.

8.1 Introduction

One goal of this thesis has been to present the current understanding of the chemistry and physics of the thermal degradation and combustion of cellulose in the context of the behaviour of bushfires. Cellulose is the predominant component of all biomass and is the most common organic material on the surface of the planet (Harris 1999). Much of the understanding of the combustion of cellulose, and thus biomass, has been confined to industrial-type energy conversion systems in which conditions are strictly controlled and the aim is to maximise a particular aspect of the system (e.g. energy output, product yield, etc.). Perversely, the field of bushfire behaviour research, which has at its core the need for understanding of the very same processes involved in industrial biomass

burners, has not taken advantage of the considerable amount of work that has been undertaken on the fundamentals of biomass combustion.

A critical development in the understanding of the thermal degradation and subsequent combustion of cellulosic fuels was the discovery in the mid-1960s (with refinements in the 1970s and 1980s) of the competitive reactions leading to the formation of volatiles (primarily levoglucosan) and charcoal. The source of competition in these reactions lies in two possible nucleophiles that can attack the cellulose chain following thermolytic scission at the glycosidic link. Inter-molecular nucleophilic addition via a water molecule forms hydrolysed cellulose which can undergo dehydration, decarbonylation and cross-linking reactions under further heating, forming what is known as charcoal. Intra-molecular nucleophilic substitution via a hydroxyl group leads to cyclisation and the formation of a levoglucosan-end which is impervious to the dehydration and cross-linking reactions. Under further heating this levoglucosan-end cellulose can undergo depolymerisation, forming levoglucosan, which is volatile and can readily decompose to other species which are the primary source of gas-phase fuel in flaming combustion.

The charcoal formation reactions are characterised by a relatively low activation energy and a net exothermicity. By comparison, the levoglucosan forming reactions have a higher activation energy and a net endothermicity. Thermal and chemical feedbacks between the cellulose substrate, the formation of charcoal, and the formation of volatiles, provide the ability for these reactions to become self-sustaining. Secondary reactions involving the oxidation of products of the thermal degradation reactions release even more heat, producing the characteristics commonly associated with 'fire'—smoke and flame—and ensure that, once conditions are suitable, the thermal degradation and combustion reactions become self-sustaining. Oxidation of volatile occurs as a turbulent non-premixed reaction that releases light and heat in the form of flames. Rapid, chaotic mixing can result in incomplete combustion and dark-coloured smoke. Oxidation of charcoal occurs as a solid-air interface reaction that releases considerable heat slowly in glowing (or smouldering) combustion and leaves a fine white ash residue which may impede further oxidation.

Much of the past industrial combustion research has focussed on well-defined and controlled conditions in order to improve the production yield of one or another product. The effect of uncontrolled conditions, as found in the case of a bushfire, has not been investigated. In particular, the role of wind, which is the most significant variable in the behaviour of bushfires, in the thermal degradation reactions was not known. At the same time, much of bushfire research has concentrated upon the development of empirical models of behaviour that eschew fundamental understanding for simpler, more pragmatic and implementable operational systems of bushfire spread prediction.

Evidence of the competitive combustion reactions in bushfires is quite apparent in observations of the non-linear behaviour of bushfires. Under essentially constant conditions differences in the amount and colour of flame, the amount and colour of ash residue and the speed of progression and behaviour of the fire perimeter, can be observed around the perimeter of a bushfire. Previous attempts to explain these differences have focussed on the interaction of the fire and its convection column with the atmosphere, leading to more and more complicated physical models that require more and more computational resources to model atmospheric phenomena. Geometric models have been used to simulate the different rates of spread observed around the perimeter by applying tem-

plate shapes based on a standard perimeter form and the speed of the wind to simulate propagation of the perimeter. Yet no adequate physical explanation for the observed behaviour has been produced. A robust understanding of the role of the thermal degradation of cellulose plays in the behaviour of bushfires will lead to safer and more effective suppression.

This thesis has proposed that much of the non-linear behaviour of bushfires, incorporating the spread and propagation of the fire perimeter, can be attributed to the competitive nature of the thermal degradation and the subsequent combustion of cellulosic fuels. It is further propounded that it is the influence of the wind flow over and around the reaction zone of the thermal degradation processes that provides a controlling mechanism in the competitive formation of volatiles and charcoal. The subsequent combustion of these products results in the behaviour observed in bushfires.

8.2 Findings of this thesis

8.2.1 Thermokinetic model of competitive cellulosic combustion

The starting point for the exploration of the hypothesis was a zero-dimensional thermokinetic model of the thermal degradation of cellulose obtained from the literature (Ball *et al*. 1999a). This model was extended to include the secondary oxidation reactions of the thermal degradation products and modified to provide two coupled temperatures for reactions in the substrate as well as the gas phase above it. The model does not simulate the rise in fuel temperature from ambient, instead it assumes that an external heat source is applied that raises the temperature to that around which the thermal degradation reactions commence. This allows investigation of the onset of ignition due to the thermal degradation of the fuel to be undertaken. The effect of wind (strength and temperature) was modelled through a variable coupled to the temperature equations of the model and through the advection of volatile away from the reaction zone.

The model was shown to simulate the exothermic and endothermic nature of the formation of charcoal and volatile, respectively, and, under certain initial conditions, to show a net exothermicity that leads to the commencement of secondary reactions and an extremely rapid increase in system temperatures (i.e. both substrate and gas phase), representative of ignition. A large series of numerical experiments (in excess of 630) was conducted to investigate the role of initial bound moisture and constant wind, both in isolation and in combination, on the evolution of system enthalpies and temperatures, substrate mass and reaction products. The model was shown to evaporate initial bound moisture at temperatures below that of initiation of the thermal degradation, thus consuming energy from the system and correctly replicating loss of water prior to the onset of combustion reactions.

The effect of constant wind was found to be more complex. The dual impact of wind temperature and advection of volatiles resulted in a complicated response of system temperatures around critical wind values whereby the system would undergo exothermic and endothermic periods that would either progress to ignition or lead to reaction cessation, depending on which side of the critical value the wind strength was initially set.

The temperature of the wind was found to dictate the dominant regime of thermal degradation and subsequently the rate of substrate consumption and time to ignition. Wind temperatures of around ambient values (i.e. $\simeq 300$ K) predominantly produced

hydrolysed cellulose and charcoal, which through its exothermicity led, depending on the initial substrate temperature, to ignition. Wind temperatures at elevated values (in the order of the initial substrate temperature, i.e. $\geq$ 580 K) predominantly produced levoglucosan-end cellulose and, subsequently, volatiles that rapidly led to the onset of ignition and the rapid consumption of substrate.

The effect of the wind, through its temperature, is to modify the reaction zone temperature which controls the competitive temperature-sensitive reactions of charcoal and volatile formation. In the open, the wind by definition is ambient and thus, any reaction open to ambient wind should result in the preferential formation of charcoal. However, at the fire front, the ambient-temperature wind is prevented from reaching the reaction zone by two mechanisms: the first is the heating of the air in its passage over the burned and burning ground such that it is no longer of ambient temperature; the second is the interception of the wind behind the fire front and the deflection into the convection column. The result is that the air temperature inside the reaction zone is far from ambient temperature, causing the preferential formation of volatiles.

The model may be extended further by including a component to simulate the interception of heat from an external source (such as a nearby burning fuel element) to allow investigation of the commencement of the combustion reactions from ambient temperatures.

The spatial aspect of the above interpretation cannot be investigated using the zero-dimensional thermokinetic model. The question of how the formation of volatiles and charcoal and the subsequent combustion differs around the fire perimeter can only be answered by a full 3-dimensional simulation of the air flow over and around the reaction zones formed in the competitive combustion of cellulosic fuel. This was done using a commercial computational fluid dynamics package.

8.2.2 Computational fluid dynamics of competitive cellulosic combustion

The commercial computational fluid dynamics (CFD) package FLUENT was selected for the spatial investigation of the competitive combustion of cellulose because of its turbulent reactive flow modelling capabilities. The modelling paradigm was that of a fire burning across a thin cellulosic fuel layer placed on the floor of a large rectangular-section wind tunnel 3 m long by 1 m high and 1.6 m wide. A 3-dimensional computation domain formed the basis of the competitive combustion model in which radiation, turbulence and species transport models and a solution solver were selected to form the competitive combustion CFD (CC-CFD) model. Issues with numerical instability and divergence in the solutions forced a simplification of the intended idealised thermal degradation reactions, to a two-step, two-path reaction driven by the fastest reaction rates.

Despite further numerical instability problems with this simplified model, solutions for a very small number of iterations prior to the onset of divergence were obtained and assumed to be valid. Although these results are not conclusive they did provide at least sufficient results for preliminary analysis. Two numerical experiments were conducted: the first using an ambient-temperature wind of 0.5 m s^{-1}; and the second using no wind (i.e. zero wind speed). Comparison of the results of these two experiments highlighted the different aspects of the competitive combustion reactions.

In the 0.5 m s^{-1} wind experiment a distinct asymmetry in the fire perimeter was clearly evident in the contours of temperature as well as reaction products. That is, the

downwind edge of the fire reaction zone travelled further from the line of ignition than the upwind edge. The rate of spread of the flanks of the fire was in the same order as the rear, resulting in the downwind edge tending towards the characteristic parabolic head fire shape noted in field experiments. The amount of charcoal by mole fraction produced at the downwind edge was consistently more (by approximately 12%) than that of volatile, although the contours were exactly the same, suggesting that the reaction regime was not conducive to the preferential formation of volatile, only just favouring charcoal, and that flaming combustion had not commenced prior to the onset of numerical instability. However, significant differences in the both the contours of mole fraction as well as the relative amounts of both products were apparent along the upwind edge of the fire. This suggests that along this edge, which is more open to the ambient temperature wind than the downwind edge, the formation of charcoal is much more favoured (by 20–22%) than the formation of volatile. A possible future experiment to explore this would be to conduct a similar experiment with the temperature of the wind in the range of 600-700 K, which should produce more volatile than charcoal.

In the still wind condition no asymmetry in the fire perimeter as defined by the contours of temperature or reaction products was observed. Again, the amount of charcoal by mole fraction was greater than that of volatile indicating that the conditions favoured the formation of charcoal, but the lack of asymmetrical formation showed that there was no bias in the reactions due to the lack of bias in the temperature of the flow of air over the reaction zone.

In comparison with the 0.5 m s^{-1} wind experiment this leads to the conclusion that the action of the wind does play a role in the thermal degradation reactions and that ambient temperature wind ($\simeq$ 300 K) leads to the preferential formation of charcoal on the upwind edge of the fire zone (i.e. the back of the fire). The fact that the formation of charcoal was of the same order as the formation of volatiles at the head of the fire suggests that the conditions were not conducive to the favouring of volatilisation and flaming combustion.

Thus to the extent that these findings may be relied upon, they do confirm those of the zero-dimension thermokinetic modelling that the ambient wind plays a role in determining the preferential formation of charcoal and volatiles during the thermal degradation of cellulosic fuels. Subsequent combustion through oxidation of these products results in the phenomenological aspects that characterise the behaviour of bushfires.

Improvements to the CC-CFD model to solve the issues with numerical instability, which might include finer resolution of the computation domain and tighter time-step and residual controls, should provide a more reliable model capable of investigating a number of aspects of fire behaviour. It is possible that the issues encountered with FLUENT may not be overcome due to deficiencies in the software. Alternative CFD packages capable of investigating the detailed chemical kinetics of solid and gas phase combustion in a turbulent reactive flow may need to be examined in order to provide a more robust simulation of these aspects.

Future numerical experiments might include the effect of slope, the effect of wind temperature, combustion under an inert atmosphere to investigate the role of oxidation, or single-path combustion (removing one of the competitive pathways). More CFD advanced experiments might include more realistic representations of fuels (i.e. rather than a thin continuous layer) such that gross fuel characteristics such as bulk density, struc-

ture and load be included; non-constant wind flow (both temporally and spatially) and larger volume domains. These simulations could also form the basis of laboratory experiments that would serve to both validate the modelling but also to investigate other aspects of biomass combustion.

8.2.3 A network model of fire spread

The complete modelling of the behaviour and spread of a bushfire from first principles, incorporating the chemistry of combustion and the physics of heat transfer in a self-consistent manner, is possible but is computationally intensive. Also the requirements for data describing the initial and varying conditions at the resolution and precision required for accurate computation would be beyond most experimental situations and certainly beyond any operational setting.

The importance of the role of the competitive combustion of cellulosic fuels in determining the behaviour of a bushfire, from its spread to its response to changes in conditions, requires that some aspect of this role be included in a prediction model suitable for operational use. A framework for a compromise between the full physical model solution of fire and the operationally-suitable empirical model of fire behaviour was proposed using a network representation of the critical components and their interactions controlling the behaviour of a bushfire.

This framework simplifies the competitive nature of the thermal degradation of cellulosic fuel to a one-step, two-path mechanism in which a particular fuel element can produce both flaming combustion and glowing combustion to differing extents, dependent upon the interaction of the temperature of the wind with the temperature of the fuel element. This interaction is represented by the cross-product of the direction of the wind with the direction normal to the tangent of the fire edge. The transfer of heat is dictated by the type of combustion—flaming combustion transfers heat over longer distances (modified by the strength of the wind) than that of glowing combustion. Idealised heat release rates provide the temporal basis of the combustion—smouldering combustion releases more heat over a longer period than flaming combustion which releases a higher initial rate of heat.

The framework is in a form that can be converted to a set of ordinary differential equations that are suitable for parameterisation and analysis (using tools such as stability or bifurcation theory), or can be implemented in a 2D cellular automata for spatial modelling. These are two possible directions of further work.

8.2.4 Summary of conclusions

It was shown in this thesis that the competitive formation of volatiles and charcoal in the thermal degradation of cellulosic fuels is strongly affected by the temperature of the fuel that is undergoing heating, due primarily to the difference in activation energy of the competing pathways. Chemical and thermal feedbacks in the thermal degradation process (through differences in heat and catalytic requirements) provide a source of non-linearity in the behaviour of combustion.

In the context of a bushfire burning in the open, the formation of both volatiles and charcoal occur simultaneously at each point around the fire perimeter. However, the extent to which one formation process dominates the other is determined by total heat flux

received by the fuel which may be moderated by the modification of the fuel temperature by interaction with the ambient-temperature wind. At the rear of the fire, where the reaction zone is open to the ambient-temperature wind, charcoal is formed preferentially over volatiles. At the head of the fire, where the reaction zone is essentially blocked from the effect of ambient-temperature wind, volatile formation dominates (while in-flow of ambient air to the reaction zone ahead of the fire due to the effect of buoyancy may occur in fires that are restricted in their spread—such as slash burns—the head fires of free-burning bushfires are less affected by this convective cooling due to the high heating rates ahead of the fire). The flanks of the fire alternate between heading and backing behaviours, depending on the fine scale shifts in wind direction.

Both charcoal and volatiles combust in air through oxidation but produce different morphologies—volatile combustion produces flames with rapid heat release, while charcoal combustion produces glowing combustion with a slow but greater heat release. As a result of both the change in preferential formation of thermal degradation species around the fire perimeter and the difference in their combustion morphology, there is a distinct difference in the observed spread and behaviour around a fire perimeter. Minor changes in wind direction cause a change in the ratio of product formation and result in changes in the behaviour and spread of the fire on the applicable sections of fire perimeter, resulting in the expansion of the fire perimeter. Major changes in wind direction cause a substantial shift in the ratios of product. Along the flanks and at the rear of the fire, where the exothermic charcoal formation predominates, the considerable reservoir of heat stored in the fuels allow the rapid transition to volatile formation and associated increased spread, which have caught firefighters unaware (Cheney *et al*. 2001).

The low activation energy exothermic charcoal formation and the higher activation energy endothermic formation of volatiles and the strong dependence of these reactions upon temperature also provides an explanation for the observed stop-start behaviour of bushfires (i.e. the seemingly capricious nature of bushfires as illustrated in Figure 1.1, p. 9). Efforts to correlate the short-term spread of the fire with the gust structure of the wind (e.g. Albini (1982); Taylor *et al*. (2004)) have found no relation between the two, suggesting that the stop-start spread of a bushfire is not primarily the result of the gust structure in the wind, although the wind certainly plays a critical role in the behaviour of the flames. The understanding of the competitive thermal degradation of biomass fuel suggests that the interaction between the exothermic and endothermic reactions at the head of a bushfire will result in a see-sawing of the energy release as the exothermicity drives the reactions toward volatilisation and as the rapid release of volatiles drives the system toward charcoal formation and so on, resulting in alternating bursts of rapid forward spread and little or no forward spread, giving the appearance of stop-start behaviour.

8.3 Implications of competitive combustion in bushfires

The fundamental competitive reactions at the heart of the thermal degradation and combustion of cellulosic fuels provide a source of hitherto unconsidered non-linearity in the behaviour of a bushfire as a whole and raises a number of implications for the study of bushfires. Until this work was undertaken the current understanding of the dynamics of the competitive thermal degradation of cellulosic fuels has not had a significant impact

upon the knowledge base used to develop models of bushfire behaviour. Indeed, much of the knowledge used in the teaching of bushfire behaviour is based upon the work of a small handful of workers from the 1950s and has not incorporated any of the advances in knowledge of the nature of biomass combustion since that time.

In this section I attempt to identify some of the tropes of bushfire research and highlight where an understanding of competitive combustion makes an impact.

8.3.1 Heat yield and Byram's fireline intensity

The seminal work of Byram (1959a,b) provided the basic understanding of bushfire behaviour from which many of the modern texts on bushfire behaviour have descended (Luke and McArthur 1978; Vines 1981; Pyne *et al*. 1996) and from which all operation fire behaviour prediction systems have evolved. A key development was Byram's fireline intensity (Byram 1959a):

$$I = Hwr \tag{8.1}$$

where I is the fireline intensity (kW m^{-1}), r is the rate of forward spread of the fire m s^{-1}, w is the mass of fuel consumed per unit area (kg m^{-2}) and H is the heat yield of the fire (kJ kg^{-1}). I has become a psuedo-fundamental quantity (even though it cannot be directly measured) and has been used to develop models of flame length (Byram 1959a), fire power (Byram 1959b; Nelson 2003), rate of spread (e.g. Rothermel (1972)), suppression difficulty (Cheney 1981) and fire severity.

r and w are quite straight forward conceptually, if somewhat difficult to measure accurately in the field. H, however, has caused some difficulties in the past. Heat of combustion is the total amount of energy released when a quantity of fuel is oxidised completely (Pyne *et al*. 1996) under adiabatic conditions (no losses of sensible or latent heat) (Van Wagner 1972) and is normally determined in a bomb calorimeter. Heat yield is defined as the low heat of combustion and is the heat of combustion less heat losses due to latent heat of vaporisation, radiation and incomplete combustion (Byram 1959a). Heat yield is used as the more 'field-like' quantity and is considered to be pretty much a constant property of a particular fuel species which does not vary greatly in biomass fuels (Byram 1959a; Pyne *et al*. 1996), and is dependent only upon the moisture content of the fuel (Luke and McArthur 1978). Generally, a figure of 16,000–18,000 kJ kg^{-1} is used (Luke and McArthur 1978; Pyne *et al*. 1996).

However, the use of heat of combustion and heat yield as determined in a bomb calorimeter does not take into account the way in which the fuel is consumed. That is, it treats all mechanisms of combustion equally and takes no account of the differences in the enthalpy of the chemical reactions in thermal degradation. We know from work in previous chapters in this thesis that there is a significant difference in the amount and way heat is released, depending upon the formation of charcoal or volatiles due to the thermal degradation processes. It is interesting to note that the range of values selected for average heat yields lies between the values given in the literature for charcoal combustion (32,000 kJ kg^{-1}, Eghlimi *et al*. (1999)) and volatile combustion (14,000 kJ kg^{-1}, Parker and LeVan (1989)). Thus, assuming a constant heat yield will grossly underpredict the amount of heat released purely via charcoal combustion and over-predict heat released purely by volatile combustion.

It may be that the heat yield value is a quasi-average figure considering that volatile combustion and charcoal combustion occur simultaneously at each location around the

fire perimeter, but it is a gross approximation to treat 'combustion' as singular process. That is, all fires are not the same and should not be treated as such. Methods such as that of Catchpole *et al*. (1982) where the Byram fireline intensity around a fire perimeter is calculated using the geometric change in rate of outward spread around the perimeter and the head fire heat yield oversimplify the nature of combustion and misrepresent the likely heat release rate around the perimeter.

8.3.2 Carbon sequestration and greenhouse gas modelling

The understanding that not all fires are equal is of prime importance when considering the process of carbon sequestration and the modelling of greenhouse gas emissions (such as CO_2 and H_2O) from biomass fires. As we have seen, the competitive thermal degradation reactions differ greatly in their stoichiometry in regard to CO_2 formation. Per mole of double-unit cellulose thermally degraded, charcoal formation (based on our example charcoal species of $C_{11}H_4$, releases one mole of CO_2; the formation of levoglucosan releases no CO_2. From a carbon sequestration standpoint, the formation of charcoal is much preferred to the formation of levoglucosan, which is volatile and can degrade into other, less useful, species. Charcoal is the primary component of what is called black carbon (Forbes *et al*. 2006) which can reside in the environment for considerable lengths of time. A growing use of fire to mitigate greenhouse gas emission and sequester carbon focuses on the timing of burning to reduce fuel that might get burnt later in the fire season (Williams[1] general comment, 2007).

Thus, in order to sequester carbon and keep it out of the atmosphere, the formation of charcoal should be favoured over the formation of volatiles. This is possible through an understanding of the conditions in which charcoal formation is favoured, i.e. low heating rates in the presence of suitable levels of moisture. Rapid heating rates under very dry conditions will encourage the formation of volatiles. Lighting fires in such a way as to reduce the relative size of the head fire and increase the size of the flanks and rear of the fire—through, for example, the use of backing fires—would also achieve this aim.

However, if our charcoal is allowed to combust, it will release 11 moles of CO_2 for every mole of our charcoal species oxidised, due to its carbon-rich structure. On the other hand, levoglucosan will release only 5 moles of CO_2 for every mole of levoglucosan oxidised. Therefore, while the formation of charcoal is a desired outcome, its oxidation should be discouraged or in total it will release 2.4 times as much CO_2 as flaming combustion. Thus, fires lit to encourage the formation of charcoal must be extinguished prior to the initiation of the oxidation reactions. This will not be easily achieved.

Estimates of the amount of charcoal (and thus the sequestration of carbon) produced by uncontrolled bushfires (or conversely estimates of the amount of area burnt based on the amount of charcoal present (Scott and Glasspool 2006)) should not assume that the distribution of charcoal is constant across the burnt area. An estimate must be made of the area that was burnt under backing conditions and that which was burnt under heading conditions.

While there will be carbon present in the head fire ash due to incomplete combustion, it will not be in a form such as charcoal that will remain present for any great length of

[1] R.J. Williams, Senior Principal Research Scientist, CSIRO Sustainable Ecosystems, Darwin, NT.

time. This type of black carbon is called black ash (Forbes *et al*. 2006). The structural rigidity of the charcoal formed via the crosslinking and dehydration of hydrolysed cellulose results in a form of charcoal that is much more robust and less likely to be transported and thus provide a stable sink for carbon. Marris (2006) and Lehmann (2007) suggests that a similar sort of process was used by the indigenous peoples of the Amazon thousands of years ago to create high-carbon content ($\simeq 9\%$) black fertile soils.

8.3.3 Can't see the fire for the flames

A major change in wind direction, shifting a previously quiescent flanking or backing fire to a head fire, is a serious safety issue for firefighters, particularly those undertaken indirect suppression (Cheney *et al*. 2001). It was previously assumed that the behaviour of such a fire would necessarily go through a growth phase before achieving the rates of spread associated with a well-developed head fire. However, Cheney *et al*. showed in a number of case studies of fatalities that, following a major wind change, flank fires achieved head fire spread rates near-instantaneously, catching firefighters unaware, often before the flames achieved their full height. This behaviour supports the hypothesis of competitive combustion presented here in that, although the flank fire flames appear much smaller than that of the head fire, the reservoir of heat maintained by the formation and combustion of charcoal provides the necessary energy to immediately generate the behaviour associated with the head fire.

The primary mechanism for the propagation of a bushfire has traditionally been assumed to be that of radiation from the flames (e.g. Rothermel and Anderson (1966); Anderson (1968, 1969); Albini (1985); de Mestre *et al*. (1989). However, the role of flame radiation in fire spread is not so straightforward. Observations of laboratory-based fire spread experiments in which the fuel ahead of the fire was shielded from the flame radiation (Catchpole and de Mestre 1986), field experiments in which the rate of spread of the fire was observed to be consistent regardless of flame height (Gould *et al*. 2007) and physical modelling (Cunningham and Linn 2007), show that the energy required for the thermal degradation of cellulosic fuels is not greatly dependent upon the radiation intercepted from the flames.

Given that at the level of fuel immediately in front of the reaction zone, only the first few centimetres of flame actually has any impact on the radiation intercepted by that fuel through the apparent optical thickness of the flame. That is, the bulk of the radiation from high flames is from optically thin flames and is also radiated away from the fuel.

Many attempts have been made to relate the rate of spread of a bushfire to the geometry of the flame (height, length, flame angle) (e.g. Burrows (1999); Anderson *et al*. (2006)) and the resultant radiative load but the turbulent non-premixed gas phase oxidation of the volatiles is so dependent upon the mixing of fuel gas and oxygen, resulting in very random combustion that can lead to detached envelopes of volatiles oxidising well above the level of the fuel. As a result it is difficult to see a consistent causal relation between the rate of spread of a fire and its flames. That is, the flames are not the cause of the spread of the fire but a result of the thermal degradation reactions that define the fire. Recent work (Finney *et al*. 2006) suggests that it is ignition by direct flame contact that controls the spread of fire in discontinuous fuels but this, too, is a result of the turbulent nature of flames and therefore inconsistent.

One aspect of bushfire flames that has not been investigated is the formation of shockwaves. All turbulent diffusion flames form shockwaves (E. Oran[2], pers. comm, 2006) as a result of the rapid expansion of the reaction zone and the occurrence of Richtmyer-Meshkov instabilities in the flame edge, acting to trigger Kelvin-Helmholtz instabilities which in turn interact and increase the surface area of the flame and the energy released (Oran and Gamezo 2007). While these shockwaves have been studied numerically in some detail in the context of premixed combustion in closed channels and found to be important in the transition to detonation, the effect of shockwaves from large scale, non-premixed turbulent diffusion combustion in the open has not been addressed and may play a role in the behaviour of extreme high intensity bushfires.

8.3.4 Other implications

An understanding of the competitive nature of the combustion of cellulosic fuel and the fact that not all combustion processes are equal in biomass fire, leads to implications about many other aspects of bushfire behaviour.

Suppression and mop-up

The primary tool for suppression bushfires and mopping-up afterwards is water. In fine fuels, water is effective at removing heat and breaking up the fuel, reducing its thermal capacity. However, suppression of smouldering fuels has always caused problems, particular after the passage of the main front when all fine fuels have been consumed and only larger material remains to burn. Anecdotal evidence has shown than trying to extinguish large material (i.e. logs and tree trunks) with water during the mop-up phase (that period after the main fire has been extinguished and the fire perimeter is being patrolled for residual burning) can be time-consuming and problematic.

The glowing or smouldering combustion phase, as we have seen, is a result of the hydrolysation of cellulose and the formation of charcoal, which is both exothermic and encouraged by the presence of water. While addition of water should not really affect the formation charcoal, the heat that is released during the formation of the charcoal and the oxidation of the charcoal is quite considerable and since generally these fuels are large and bulky, the effect of water in breaking up the fuel and reducing its thermal capacity is restricted. The addition of water may act to limit the volatilisation process by removing some energy but, as a result, drives the system to more charcoal formation and thus more heat generation.

Given time, the water may evaporate and recommence volatilisation, essentially 're-igniting' well after the fire was thought extinguished. Time and effort is generally required to ensure that large woody smouldering material does not reignite to cause further problems, especially on days of very high to extreme fire danger.

Peat and root fires

The exothermic formation of charcoal is also important in fires other than bushfires. The mistaken belief that 'fire' is isomorphic to 'flames' and requires oxygen to occur leads

[2]Dr. Elaine S. Oran, Senior Scientist for Reactive Flow Physics, Laboratory for Computational Physics & Fluids Dynamics, US Naval Research Laboratory.

to difficulties dealing with the spread of fire where oxygen is limited. Generally, these types of fires occur underground and include peat fires and tree root fires and manage to propagate without oxygen due to the exothermicity of the charcoal formation. The process is long and slow but self-sustaining as long as the fuel is continuous and the fire can then pop out unexpectedly at the surface and, if the conditions are suitable, cause significant trouble.

Effect of insignificant recent rain

Anecdotal evidence (e.g. McArthur (1967)) suggests that the effect of small amounts of rain can have a positive rather than negative effect on the behaviour and spread of bushfires. One possible explanation of this is the catalytic effect of water on the exothermic formation of charcoal, resulting in a moderating effect on the conditions required for the onset of combustion. As a result, perfectly dry fuel which will require higher input energy to undergo volatilisation (with the resulting endothermicity) may form charcoal with the addition of a minor amount of water, generating enough heat to progress quickly to volatilistion and flaming combustion.

8.4 Conclusion

It has been about ninety years since research into the behaviour of bushfires began in earnest. In that time many advances in the understanding of one of the world's most fascinating and deadly natural phenomena have been made. However, despite the considerable effort that has been expended on this endeavour, we are still no closer to building a complete theory of the behaviour of a bushfire. That is, there is still no set of governing equations that describe—and are able to predict—the behaviour of a bushfire in all naturally occurring conditions. It is hoped that the work presented in this thesis has taken a small step in that direction by highlighting and exploring the importance of the role of the nature of cellulosic thermal degradation and combustion in determining the behaviour of a bushfire.

Moreover, the unique chemical attributes of cellulosic fuels and the way it thermally degrades are important, not only for fires in the bush, but also for fires where cellulosic fuels are the dominant layer carrying the fire. Large scale urban fires such as the Great Fire of London in 1666 (Tinniswood 2004), the Great Chicago Fire in 1871, and the mass conflagration fires of the Second World War (Carrier *et al*. 1985), burning through predominantly wooden structures behaved more like bushfires than structural fires once the scale of the fire became large enough to integrate the individual dwellings into a heterogeneous fuel layer, revealing behaviour that is fundamental to the combustion of biomass fuels.

With a greater understanding of the fundamental mechanisms involved in the thermal degradation and combustion of cellulosic fuels it is hoped that the groundwork for a unifying theory of bushfire behaviour will be possible.

Afterword

A theory is something nobody believes, except the person who made it. An experiment is something everybody believes, except the person who did it.

Albert Einstein

All models are wrong, but some are useful.

George E. P. Box

The jokes[3] used to open each chapter in this thesis serve two primary purposes. The first is as an attempt at levity in a form of literature that traditionally has spurned such literary frivalence—why shouldn't a PhD thesis also be an enjoyable read and perhaps raise a smile? The jokes are intended to remind the reader that the real world is much more complex than the simplified version that gets portrayed in scientific publications.

The second, and more important, purpose is to highlight the huge disparities that exist between the various science disciplines. Bushfire research is not unique in its varied multi-disciplinary research needs—there are many other areas of endeavour that involve just as widely spread scientific disciplines. But bushfire research is one area that has suffered from the great divides between the various disciplines involved.

As discussed in the introductory chapter, the bulk of the research into the behaviour of bushfires over the past century has been undertaken by the land management agencies and professions for whom bushfires had the greatest impact. The pragmatic solutions that were developed provided methods for providing useful information about the behaviour of bushfires but did not progress the understanding of the processes involved. Other disciplines have contributed over the decades but generally only in a sporadic manner with generally sporadic results, with perhaps the exception of the seminal work of George M. Byram during the 1940s, '50s and '60s, who brought a unique blend of mathematics, physics and understanding to fire behaviour research.

Byram's legacy in bushfire research has stretched into the 21st Century. However, that legacy has been a two-edged sword. While the advances that Byram brought to the field have provided the basis for many of the operational systems in use around the world, they may have also had the unintended consequence of providing too sound a foundation for further work within the traditional bushfire research community, effectively stifling the continuation of his investigation of the physical processes involved in the behaviour of bushfires.

[3]The jokes have been modified from those found in a number of sources, including http://www.physlink.com/Fun/Jokes.cfm, http://www.thatwasfunny.com.

The distinctly multi-disciplinary nature of bushfire behaviour requires a distinctly multi-disciplinary approach that is applied in a concentrated, rather than sporadic, way. There is much that the broad disciplines of chemistry, physics and mathematics can bring to the field of bushfire research, not the least of which is a different perspective. The advances in the field of combustion are testament to the advantages brought by the coherent application of multiple scientific disciplines—advances that have had no impact on bushfire research, surely one of the major application areas of combustion in the world.

This thesis has shown that the advances that have been made in the understanding of the chemistry involved in combustion have more than an esoteric role in the understanding of bushfire behaviour in general. Closer ties between the disciplines is necessary for further progress to be made in the understanding of bushfire behaviour and the development of robust operational fire prediction systems.

Appendix 1: Nomenclature of thermokinetic symbols

Table A1.1: Nomenclature of symbols used in the thermokinetic modelling in this thesis. Where applicable, the equation number of the quantity is given.

Symbol	Name	Unit	Primary Equation No.	Page No.
S	Substrate mass	–	4.25	67
LG	Levoglucosan-end mass	–	4.13	64
OH	Hydrolysed cellulose mass	–	4.26	68
V	Volatile mass	–	4.27	68
C	Charcoal mass	–	4.28	68
W_b	Bound water mass	–	4.29	68
W_g	Water vapour mass	–	4.30	68
G	Gas mass	–	4.31	67
T_s	Solid phase temperature	K	4.32	68
T_v	Gas phase temperature	K	4.33	68
T_a	Ambient wind temperature	K		68
R	Universal gas constant	J K^{-1} mol^{-1}	=8.314472	
f	Wind speed	–		68
dt (or Δt)	Time step	s		67
k_{xn}	Reaction rate constant	–	Table 4.1 or 4.2	65 or 69
ΔH_x	Species enthalpy	J g^{-1}	Table 4.1 or 4.2	65 or 69
qn	Heat of reaction	J	4.36–4.40	69
E_a	Activation energy	J mol^{-1}		69
$\bar{C}_x$	Weighted specific heat	J g^{-1} K^{-1}		68
m–t	Stoichiometry constants	–		67–68
ϵ_g	Gas coupling coefficient	–		67–68
ϵ_s	Substrate coupling coefficient	–		67–68
ζ	Wind coupling coefficient	–		67–68
γ	Heat transfer coefficient	–		67–68

Other symbols not included here are used infrequently and defined in the text where used. Quantities reported without units are considered non-dimensional.

Appendix 2: Thermokinetic model ODE files

A2.1 Dual_Core_T.ODE–Constant simulations

```
# Dual_CoreT.ode
# 19 February 2007
# A simplified model of the global kinetics of cellulose degradation
# in which water hydrolyses the cellulose and the hydrolysed product
# forms char separately.  Two phases of water are modelled : gas (wg)
# and bound (wb) water, in order to control the type used in char form-
# ation. Ball (1999) yield coefficients are used, in addition to 'd'
# species formed from cleavage. A heat transfer coefficient, gamma is
# restrict amount of heat from volatile combustion that is transferred
# to the fuel substrate.  Debugging stuff added as aux at end.

# This version is based on water_gamma.ode.  This version now has two
# regimes for the tracking of temperature.  The first is the substrate,
# u_s, which is essentially the temperature of the core of the solid
# fuel.  The second is the vapour phase temperature, u_v, which is
# essentially the temperature of the gas above the substrate and the
# surface of the substrate itself.

# nUmerics:
# Bounds = 1000, dt = 0.01, Total = 200, Method=stiff
# Start temp u = 550 in order to start thermal degradation process

# Just discovered that the above options can be set directly into the
# ODE file, so here goes:
@ BOUND=1500,DT=1,TOTAL=2000, METH=stiff, MAXSTOR=500000

#=====================================================================
# Variable and parameter initiation
#=====================================================================
init s=1,lg=0,oh=0,wg=0,wb=0.0001,c=0,v=0,g=0,u_v=300,u_s=550

p za1=6.7e5,za2=2.8e19,za3=6.9e22,zd=1.3e10
p zb1=3.2e14,zb2=1.3e10,zb3=1.3e10,zb4=3.2e14,zv=1.3e10
p Ea1=110000,Ea2=240000,Ea3=220000,Ed=145000
p Eb1=198000,Eb2=153000,Eb3=145000,Eb4=198000,Ev=153000

p f=0,B=0,R=8.3144,wf=0,l=1,u_a=300
p qc=1000,qv=-300
p m=0.44,n=0.42,p=0.14
p nd=0.89

# Specific heats for substrate, char and gas,two phases of water (J/g/K)
p ca=1.38,cc=0.67,cg=1.1,cwv=2.02,cws=4.183, rho0=250
```

```
44
45 # Advection mixing control parameter
46 p epsilon_g=0.01, epsilon_s=0.01,zeta=1
47
48 # Heat transfer coefficient
49 p gamma=1
50
51 # Heat of combustion, char, volatiles
52 p qs=32000, qf=14000
53
54 # Heat of vaporisation of water
55 p qw=-2272
56
57 # Volatile combustion coefficients and yields
58 p zcf=2.55e13, Ef=188000
59 p y1=0.75, y3=0.25
60
61 # Char combustion coefficients and yields
62 p zcs=1.4e11, Es=183000
63 p y2=0.93, y4=0.07
64
65 # Water vaporisation coefficient values taken from Sexton, Macaskill
66 # and Gray (2001)
67 p zev=3.41e4, Evp=42000
68
69 #=================================================
70 # Reaction rates calculated from rate constants, activation energy and
71 # temperature
72 #=================================================
73 ka1=za1*exp(-Ea1/(R*u_s))
74 #kd=zd*exp(-Ed/(R*u_s))
75 ka2=za2*exp(-Ea2/(R*u_s))
76 ka3=za3*exp(-Ea3/(R*u_s))
77 kb1=zb1*exp(-Eb1/(R*u_s))
78 kb2=zb2*exp(-Eb2/(R*u_s))
79 kb3=zb3*exp(-Eb3/(R*u_s))
80 kb4=zb4*exp(-Eb4/(R*u_s))
81 kv=zv*exp(-Ev/(R*u_s))
82
83 #equation for evaporation of water
84 kev=zev*exp(-Evp/(R*u_s))
85
86 # Volatile combustion reaction rate
87 kf=zcf*exp(-Ef/(R*u_v))
88
89 # Char combustion reaction rate
90 ks=zcs*exp(-Es/(R*u_s))
91
92 # old code Heat capacity is averaged across all components
93 # old code cp=((a+d+blg+boh)*ca+c*cc+(wg+wb+v+g)*cg)/rho0
94
95 # heat capacity of solid (non-gaseous) fuels (including bound water and
96 # char)
97
98 cp_s = ((s+lg+oh)*ca + wb*cws + c*cc)
99
```

```
100 # heat capacity of gases (inc water vapour) (assumes air as dominate
101 # species)
102 cp_g = (1-(v+g+wg))*1.01+(v+g)*cg + wg*cwv
103
104 #=========================================================
105 # ODEs for evolution of substrate and products
106 #=========================================================
107
108 # Cellulose substrate degrades and is not renewed
109 ds/dt = -ka1*s - ka2*s - ka3*s*wb
110
111 # Cellulose with Levoglucosan end formation
112 dlg/dt = ka2*s-kb1*lg-kb2*lg
113
114 # Hydrolysed cellulose formation
115 doh/dt = ka3*s*wb - kb3*oh - kb4*oh
116
117 # Water formation (+ water from combustion)
118 # Gaseous water from combustion + evaporation
119 dwg/dt=f*(wf-wg)+y3*kf*v*(1-f) + y4*ks*c + kev*wb
120
121 # Bound water from thermal degradation - char formation - evaporation
122 dwb/dt = (1-nd)*ka1*s + m*kb3*oh + m*kb2*lg + m*kv*v - ka3*s*wb - kev*wb
123
124 #Char formation (includes char combustion loss)
125 dc/dt = n*kb3*oh + n*kb2*lg + n*kv*v - ks*c
126
127 # Volatiles formation (includes advection and combustion)
128 dv/dt = kb1*lg + kb4*oh - kv*v - f*v - kf*v*(1-f)
129
130 # Gas formation (includes CO2, CO, etc) (+ combustion sources)
131 dg/dt = p*kb2*lg + p*kb3*oh + p*kv*v - f*g + y1*kf*v*(1-f)+y2*ks*c
132
133 #=================================================
134 # Heats of formation and combustion of the various products
135 #=================================================
136
137 # Heat of formation (volatiles)
138 q1=qv*(kb1*lg + kb4*oh)
139
140 # Heat of formation (Char)
141 q2=qc*(kb2*lg + kb3*oh + kv*v)
142
143 # Heat of combustion (volatiles)
144 q3=gamma*qf*kf*v
145
146 # Heat of combustion (char)
147 q4=qs*ks*c
148
149 # Heat of vaporisation of bound water
150 q5=qw*kev*wb
151
152 #=================================================
153 # Temperature evolution equations
154 #=================================================
155
```

```
156 # Coupled temperature equations for solid (u_s) and vapour (u_v) via
157 # zeta coupling parameter
158 # C*du = dH
159
160 du_s/dt=(q1+q2+q4+q5+epsilon_s*f*(u_a-u_s)+zeta*(u_v-u_s))/cp_s
161 du_v/dt=(q3+epsilon_g*f*(u_a-u_v)-zeta*(u_v-u_s))/cp_g
162
163 #===================================
164 # Auxilary quantities for debugging
165 #===================================
166
167 aux HV=q1
168 aux HC=q2
169 aux HCV=q3
170 aux HCC=q4
171 aux HWV=q5
172 #Char heat
173 aux Char=q2+q4
174 # Volatile heat
175 aux Vols=q1+q3
176 # total heat
177 aux TotalHeat=q1+q2+q3+q4+q5
178
179 done
```

A2.2 Unsteady_F.ODE–Unsteady flow simulations

```
# Unsteady_F.ode
# 4 April 2007

# A simplified model of the global kinetics of cellulose degradation in
# which water hydrolyses the cellulose and the hydrolysed product forms
# char separately.  Two phases of water are modelled : gas (wg) and
# bound (wb) water, in order to control the type used in char formation.
# Ball (1999) yield coefficients are used, in addition to 'd' species
# formed from cleavage. A heat transfer coefficient, gamma is restrict
# amount of heat from volatile combustion that is transferred to the fuel
# substrate.  Debugging stuff added as aux at end.

# This version is based on dual_core_t.ode.  The stream flow variable, f
# is now allowed to vary rather than be fixed constant.  This is done by
# making f a sinusoidal function of time such that f fluctuates over a
# set period around a mean value with a set amplitude.

# nUmerics:
# Bounds = 1000, dt = 0.01, Total = 3000, Method=stiff
# Start temp u = 550 in order to start thermal degradation process

# Just discovered that the above options can be set directly into the ODE
# file, so here goes:
@ BOUND=1500000,DT=0.01,TOTAL=3000, METH=stiff, MAXSTOR=5000000


#=====================================================================
# Variable and parameter initiation
#=====================================================================
init s=1,lg=0,oh=0,wg=0,wb=0,c=0,v=0,g=0,u_v=550,u_s=580

p za1=6.7e5,za2=2.8e19,za3=6.9e22,zd=1.3e10
p zb1=3.2e14,zb2=1.3e10,zb3=1.3e10,zb4=3.2e14,zv=1.3e10
p Ea1=110000,Ea2=240000,Ea3=220000,Ed=145000
p Eb1=198000,Eb2=153000,Eb3=145000,Eb4=198000,Ev=153000

p B=0,R=8.3144,wf=0,l=1,u_a=300
p qc=1000,qv=-300
p m=0.44,n=0.42,p=0.14
p nd=0.89

# Function for time varying wind speed f
p f_amp=0.02,f_mean=0.01,f_period=60,gust_on=1
f = gust_on*((f_amp/2)*sin(2*pi/f_period*t)+f_mean)+((1-gust_on)*f_mean)

# Specific heats for substrate, char and gas,two phases of water (J/g/K)
p ca=1.38,cc=0.67,cg=1.1,cwv=2.02,cws=4.183, rho0=250

# Advection mixing control parameter
p epsilon_g=0.01, epsilon_s=0.01,zeta=1

# Heat transfer coefficient
p gamma=1

```

```
55 # Heat of combustion, char, volatiles
56 p qs=32000, qf=14000
57
58 # Heat of vaporisation of water
59 p qw=-2272
60
61 # Volatile combustion coefficients and yields
62 p zcf=2.55e13, Ef=188000
63 p y1=0.75, y3=0.25
64
65 # Char combustion coefficients and yields
66 p zcs=1.4e11, Es=183000
67 p y2=0.93, y4=0.07
68
69 # Water vaporisation coefficient values taken from Sexton, Macaskill
70 # and Gray (2001)
71 p zev=3.41e4, Evp=42000
72
73 #=====================================================
74 # Reaction rates calculated from rate constants, activation energy and
75 # temperature
76 #=====================================================
77 ka1=za1*exp(-Ea1/(R*u_s))
78 ka2=za2*exp(-Ea2/(R*u_s))
79 ka3=za3*exp(-Ea3/(R*u_s))
80 kb1=zb1*exp(-Eb1/(R*u_s))
81 kb2=zb2*exp(-Eb2/(R*u_s))
82 kb3=zb3*exp(-Eb3/(R*u_s))
83 kb4=zb4*exp(-Eb4/(R*u_s))
84 kv=zv*exp(-Ev/(R*u_s))
85
86 #equation for evaporation of water
87 kev=zev*exp(-Evp/(R*u_s))
88
89 # Volatile combustion reaction rate
90 kf=zcf*exp(-Ef/(R*u_v))
91
92 # Char combustion reaction rate
93 ks=zcs*exp(-Es/(R*u_s))
94
95 # old code Heat capacity is averaged across all components
96 # old code cp=((a+d+blg+boh)*ca+c*cc+(wg+wb+v+g)*cg)/rho0
97
98 # heat capacity of solid (non-gaseous) fuels (including bound water
99 # and char)
100 cp_s = ((s+lg+oh)*ca + wb*cws + c*cc)
101
102 # heat capacity of gases (inc water vapour) (assumes air as dominate
103 # species)
104 cp_g = (1-(v+g+wg))*1.01+(v+g)*cg + wg*cwv
105
106 #=========================================================
107 #ODEs for evolution of substrate and products
108 #=========================================================
109
110 # Cellulose substrate degrades and is not renewed
```

```
111 ds/dt = -ka1*s - ka2*s - ka3*s*wb
112
113 # Cellulose with Levoglucosan end formation
114 dlg/dt = ka2*s-kb1*lg-kb2*lg
115
116 # Hydrolysed cellulose formation
117 doh/dt = ka3*s*wb - kb3*oh - kb4*oh
118
119 # Water formation (+ water from combustion)
120 # Gaseous water from combustion + evaporation
121 dwg/dt=f*(wf-wg)+y3*kf*v*(1-f) + y4*ks*c + kev*wb
122
123 # Solid water from thermal degradation - char formation - evaporation
124 dwb/dt = (1-nd)*ka1*s+m*kb3*oh+m*kb2*lg+m*kv*v-ka3*s*wb-kev*wb
125
126 #Char formation (includes char combustion loss)
127 dc/dt = n*kb3*oh + n*kb2*lg + n*kv*v - ks*c
128
129 # Volatiles formation (includes advection and combustion)
130 dv/dt = kb1*lg + kb4*oh - kv*v - f*v - kf*v*(1-f)
131
132 # Gas formation (includes CO2, CO, etc) (+ combustion sources)
133 dg/dt = p*kb2*lg + p*kb3*oh + p*kv*v - f*g + y1*kf*v*(1-f)+y2*ks*c
134
135 #=================================================
136 # Heats of formation and combustion of the various products
137 #=================================================
138
139 # Heat of formation (volatiles)
140 q1=qv*(kb1*lg + kb4*oh)
141
142 # Heat of formation (Char)
143 q2=qc*(kb2*lg + kb3*oh + kv*v)
144
145 # Heat of combustion (volatiles)
146 q3=gamma*qf*kf*v
147
148 # Heat of combustion (char)
149 q4=qs*ks*c
150
151 # Heat of vaporisation of bound water
152 q5=qw*kev*wb
153
154 #=================================================
155 # Temperature evolution equations
156 #=================================================
157
158
159 # Coupled temperature equations for solid (u_s) and vapour (u_v) via
160 # zeta coupling parameter
161
162 du_s/dt=(q1+q2+q4+q5+epsilon_s*f*(u_a-u_s)+zeta*(u_v-u_s))/cp_s
163 du_v/dt=(q3+epsilon_g*f*(u_a-u_v)-zeta*(u_v-u_s))/cp_g
164
165 #===================================
166 # Auxilary quantities for debugging
```

```
#==================================

aux HV=q1
aux HC=q2
aux HCV=q3
aux HCC=q4
aux HWV=q5

#Char heat
aux Char=q2+q4
# Volatile heat
aux Vols=q1+q3
# total heat
aux TotalHeat=q1+q2+q3+q4+q5

aux wind=f
aux phase_diff_v = f-q1-q3
aux phase_diff_c = f-q2-q4

done
```

Appendix 3: CC-CFD model numerical instability

This appendix details some of the numerical experiments conducted in 2D that highlighted some of the limitations of the FLUENT and the CC-CFD model as defined in section 6.2 (p. 117), the 'ideal' CC-CFD model. Issues with numerical stability and divergence in the solutions in both 2D and 3D formulations required the simplification of the 'ideal' model to a highly approximated one that still reflected the behaviour of the competitive thermal degradation in a spatial context.

A3.1 Numerical experiment, 2D domain, 600K—Failed ignition

Using the 'ideal' formulation for the CC-CFD model in a 2D domain and an ignition patch temperature of 600 K (Experiment #1, Table A3.1) resulted in a failed ignition, in which the high temperature zone of the ignition patch slowly migrated downwind under the influence of the 0.5 m s^{-1} wind.

Table A3.1: Solver parameters used for 2D Experiment 600 K

Solver Parameter	Value	Comment
Total time (s)	15	
Time step (s)	0.01	
No. iterations/time step	1	(max.)
Reaction	on	600 K ignition patch
Horiz. wind vel. (m s^{-1})	0.5	constant

The maximum temperature in the domain decreases exponentially (Fig. A3.1) under the influence of the ambient temperature (310 K) air in the wind tunnel, suggesting that the rates of the thermal degradation reactions and, more importantly, the oxidisation reactions are decreasing. This implies that ignition of the system has not taken place.

A3.2 Numerical experiment 2D domain, 650 K—Numerical instability

The results of experiment #1 suggested that the initial patch temperature of 600 K was not sufficient to initiate the exothermic reactions that provide the self-sustaining energy requirements of the combustion processes. A higher initial patch temperature was implemented.

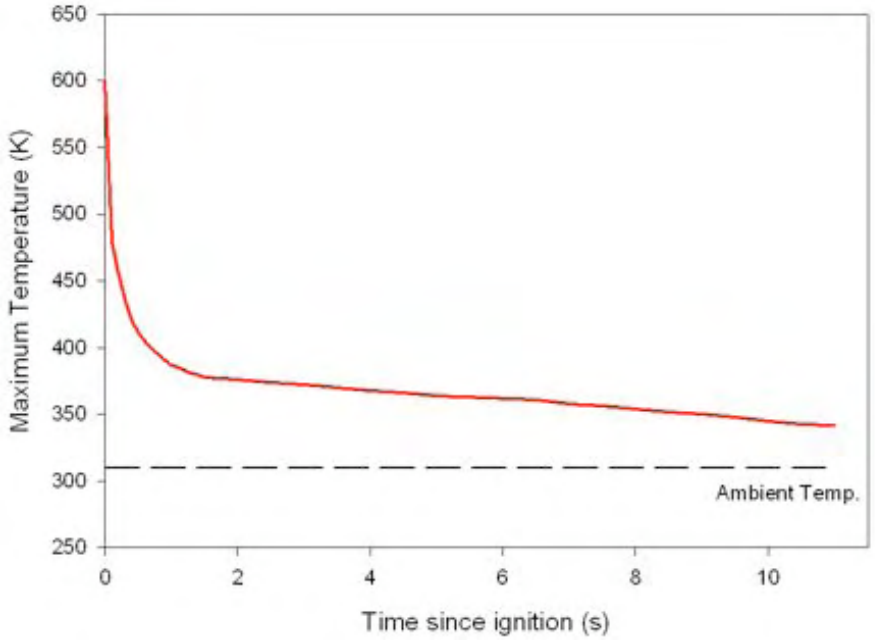

Figure A3.1: Evolution of maximum temperature of experiment #1. Maximum temperature in the domain decreases exponentially with time suggesting the exothermic reactions (mainly oxidisation) are not occurring and that ignition has not taken place.

Using similar simulation settings as Experiment #1 (Table A3.2), the initial patch temperature was increased to 650 K in order to try to initiate the exothermic reactions to the point that the thermal degradation reactions become self-sustaining. However, doing so revealed a major issue with the use of FLUENT to simulate fast, highly exothermic, reactive flows. Numerical instability occurred, resulting in divergence in the solution and a forced halt of the simulation with errors.

Table A3.2: Solver parameters used for 2D Experiment #2

Solver Parameter	Value	Comment
Total time (s)	< 1	Instability encountered
Time step (s)	0.01	Adaptive: Δ t/2
No. iterations/time step	1	(max.)
Reaction	on	650 K ignition patch
Horiz. wind vel. (m s^{-1})	0.5	constant

Numerical stability is the ability of a method of solving a differential equation to approximate the exact solution to the equation. An unstable numerical solution will result in growth of errors in the solution, particularly stiff differential equations which contain terms that can lead to rapid variation in the solution. Numerical instability can lead to divergence in the solution in which the solution does not asymptote toward a particular limit value, resulting in oscillation, unrestricted growth or chaotic behaviour. Reducing

the time step (to extremely small values in the case of stiff equations) can improve numerical stability and assist in the convergence of the solution (particularly in explicit method solver). Obtaining a converged solution in a reacting flow is acknowledged as being difficult in FLUENT (Fluent Inc 2001c, p. 13-37): "...the impact of the chemical reaction on the basic flow pattern may be strong, leading to a model in which there is a strong coupling between the mass/momentum balances and the species transport equations. This is especially true in combustion, where the reactions lead to a large heat release and subsequent density changes and large accelerations in the flow."

A second convergence issue involves reactions with very rapid rates (i.e. much more rapid than the rates of convection and diffusion); the solution of the species transport equations become numerically difficult (i.e. stiff). Symptoms of the onset of numerical instability experienced in Experiment #2 included negative absolute temperatures and very large velocity magnitudes which resulted in divide by zero leading to the fatal error 'NAN:Not a number'.

Prior to the fatal errors, the simulation of Experiment #2 performs remarkably well, showing the initiation of the exothermic reactions prior to ignition of the volatiles and the increase in the system temperature. Figure A3.2 shows the maximum system temperature (solid red line) of one particular run in Experiment #2. This run uses an adaptive time step mechanism in which the time step is halved at each time step in an attempt to improve the numerical stability of the solution. The initial time step of 0.01 s is retained for the first 6 iterations and then begins to halve for each subsequent iteration (dashed blue line). After a total of 10 iterations, the time step is 6.2500×10^{-4} s and the total time elapsed is 0.069375 s.

This figure shows the initial patch temperature of 650 K rapidly being reduced by the action of the ambient (310 K) surroundings. After a very short time, however, the temperature plateaus as the exothermic reactions begin to occur at significant rates. The resulting release of heat then begins to increase the maximum temperature in the system at an increasingly rapid rate. From the 11th iteration (0.069687 s) to the 20th iteration (0.069999 s), the temperature increases a total of 24 K, an average rate of increase in temperature of 76923 K s^{-1}. This is extremely rapid, and in the next iteration the simulation halts with a fatal NAN error. Divergences were detected in the solution from the 18th iteration and the Courant number automatically decreased from 5 initially to 0.05 in order to obtain a convergent solution. These measures failed in the 21st iteration. In the last iteration, the time step was 6.1035×10^{-7} s.

This rapid increase in temperature is attributable to the onset of the ignition of the highly exothermic oxidisation reactions and is similar in nature to the rapid increase in system temperature observed in the zero-dimensional thermokinetic modelling undertaken in Chapter 4. However, where the onset of ignition of the volatiles was considered an endpoint in those numerical experiments (and thus cessation of the simulations due to the failure of the solver not perceived to be a problem), the flaming combustion is a vital component of the interactions of the heat, wind and reaction kinetics in these numerical experiments and needed to be solved.

The user manual (Fluent Inc 2001c, p. 13-37) offers several suggestions to attempt to improve the numerical stability and convergence of solutions, including 'cold starting' the simulation (running the simulation for a number of time steps with the reactive chemistry turned off in order to allow the flow to settle down then re-engaging the

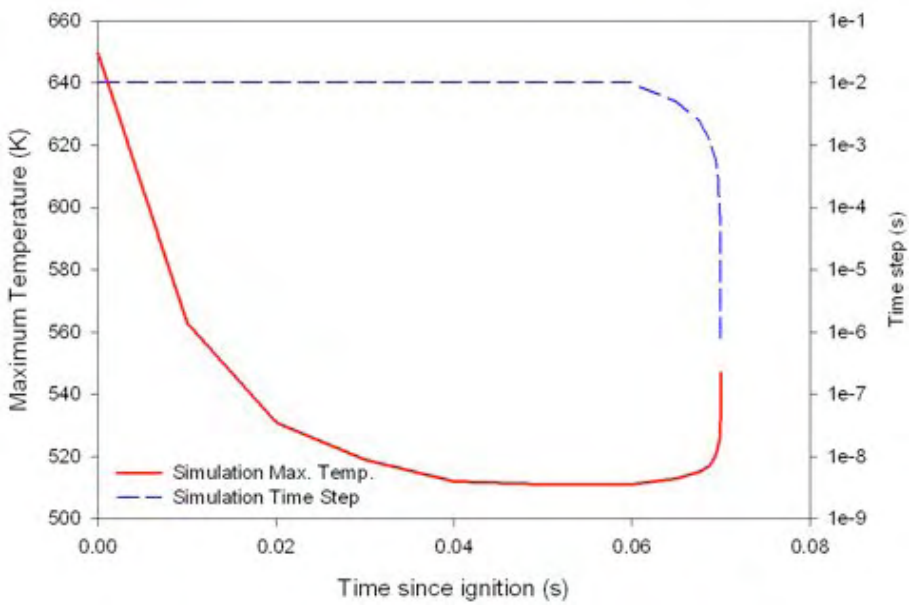

Figure A3.2: Evolution of maximum temperature of experiment #1. Maximum temperature in the domain (red line) decreases exponentially with time for the first few tenths of seconds and then plateaus at around 510 K. The exothermic reactions in the system then begin to react causing the maximum temperature in the system to increase extremely rapidly, causing numerical instability and divergence in the solutions. The time step (blue dashed line) is halved from an initial 0.01 s at each time step from 0.06 s onwards in an unsuccessful attempt to improve numerical stability.

chemical and energy solvers), under-relaxing the solution to the equations (reducing the change of each variable during each time step), using the double-precision version of the solver to reduce the risk of computational (i.e. numerical) rounding and truncation errors, reducing the time step of the solver, using adaptive time-stepping, changing the specific heat of the mixture and the reaction products to better model the effect of rapid heat release.

No improvement with these modifications was found, either individually or in combination. Additional, more extreme, modifications were made to the problem definition and solvers selected. These included using combinations of other turbulence, radiation and species transport models, reducing the spatial resolution of the mesh by a factor of 5, applying other solver methods (segregated and coupled-explicit), and reordering the combustion reactions. Again, no improvement in the situation was forthcoming.

In light of the deadlines associated with this project, the decision was made to implement a simplified formulation of the CC-CFD model based on a simplified two-step, two-path reaction chemistry in order to at least provide interim results.

A3.3 CC-CFD model simplification

A simplified model of the thermokinetics of thermal degradation and combustion of cellulosic fuels, was constructed (Fig. A3.3).

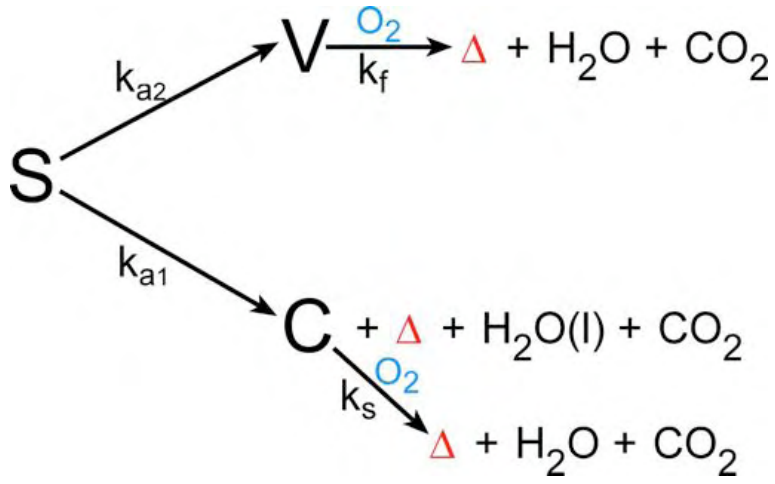

Figure A3.3: Schematic of the simplified chemistry used in revised version of the CC-CFD model in an attempt to improve numerical stability and achieve a convergent flow.

This model ignores the role of water in the production of char, simplifying the two-path charcoal formation process into a single path. The formation of volatiles and the oxidisation of the volatiles and charcoal remain the same:

Charcoal

The formation of our charcoal species ($C_{11}H_4$) is given by:

$$2(C_6H_{10}O_5)_s \rightarrow C_{11}H_4 + CO_2 + 8H_2O(l) \tag{A3.1}$$

Levoglucosan

The formation of levoglucosan is given by :

$$(C_6H_{10}O_5)_s \rightarrow C_6H_{10}O_{5_g}. \tag{A3.2}$$

Flaming combustion

Oxidation of levoglucosan is assumed to proceed to H_2O and CO_2 with no intermediates formed:

$$C_6O_5H_{10_g} + 6O_{2_g} \rightarrow 6CO_{2_g} + 5H_2O_g. \tag{A3.3}$$

Glowing combustion

Oxidation of the charcoal is assumed to proceed to H_2O and CO_2 with no intermediates formed:

$$C_{11_s}H_4 + 12O_{2_g} \rightarrow 11CO_{2_g} + 2H_2O_g. \tag{A3.4}$$

These changes had very little effect on the enthalpy of the formation reactions (1 order of magnitude) and no discernible effect on the reaction kinetics but allowed the formation reaction of charcoal to be identified separately from the oxidisation reactions. Pre-exponential factor and activation energy values for each reaction, as well as reaction type, are given in Table A3.3. The primary difference between this version and that of the original 'ideal' version is that the activation energies and pre-exponential factors used for the charcoal and levoglucosan formation reactions are that of the *fastest* reactions in the pathway, not the slowest. It is unknown if this makes a difference to the stability of the computations.

Table A3.3: Activation energy, pre-exponential factor and reaction type for reactions used in CFD model.

Reaction	**Pre-exponential Factor (s^{-1})**	**Activation Energy (kJ mol^{-1})**	**Reaction Type**
Charcoal	6.9×10^{22}	220	Wall surface
Levoglucosan	2.8×10^{19}	240	Wall surface
Glowing	1.4×10^{11}	183	Wall surface
Flaming	2.55×10^{13}	188	Volumetric

The component models of the simplified CC-CFD model remained, for the most part, the same as the 'ideal' CC-CFD model. That is, the models for the RSM turbulence model, the DO radiation model, the EDC reaction model were selected. Instead of the implicit coupled solver, the unsteady segregated solver was selected as it provided at least two time steps (at 1 s intervals) before numerical instability occurred. Smaller time steps (0.1–0.0001) appeared to make little difference, particularly in regard to the occurrence of solution divergence.

Appendix 4: Summary FLUENT file for CC-CFD model

A4.1 FLUENT CC-CFD summary

```
FLUENT
Version: 3d, segregated, spe, RSM, unsteady (3d, segregated,  species, Reynolds stress model, unsteady)
Release: 6.2.16
Title:

Models
------

   Model                              Settings
   ---------------------------------------------------------------------
   Space                              3D
   Time                               Unsteady, 1st-Order Implicit
   Viscous                            Reynolds stress model
   Wall Treatment                     Standard Wall Functions
   RSM Wall Reflection Effects Option Disabled
   RSM Wall B.C. Option (solve k)     Enabled
   Quadratic Pressure-Strain Option   Disabled
   Heat Transfer                      Enabled
   Solidification and Melting         Disabled
   Radiation                          Discrete Ordinate Model
   Species Transport                  Reacting (6 species)
   Coupled Dispersed Phase            Disabled
   Pollutants                         Disabled
   Soot                               Disabled

Boundary Conditions
-------------------

   Zones

      name               id   type
      ---------------------------------------
      tunnel_interior    17   fluid
      inlet              9    velocity-inlet
      sym_wall           11   symmetry
      outlet             12   pressure-outlet
      outer_wall         13   wall
      roof               14   wall
      floor              15   wall
      default-interior   16   interior

   Boundary Conditions

      tunnel_interior

         Condition                                  Value
         ---------------------------------------------------------------------------------------------------------------------------------
         Material Name                              thermal_degradation
         Specify source terms?                      no
         Source Terms                               ((mass (inactive . #f) (constant . 0) (profile  )) (x-momentum (inactive . #f
         Specify fixed values?                      no
         Local Coordinate System for Fixed Velocities no
         Fixed Values                               ((x-velocity (inactive . #f) (constant . 0) (profile  )) (y-velocity (inactiv
         Motion Type                                0
         X-Velocity Of Zone                         0
         Y-Velocity Of Zone                         0
         Z-Velocity Of Zone                         0
         Rotation speed                             0
         X-Origin of Rotation-Axis                  0
         Y-Origin of Rotation-Axis                  0
         Z-Origin of Rotation-Axis                  0
         X-Component of Rotation-Axis               0
         Y-Component of Rotation-Axis               0
         Z-Component of Rotation-Axis               1
         Participates in radiation                  yes
         Deactivated Thread                         no
         Laminar zone?                              no
         Porous zone?                               no
         Conical porous zone?                       no
         X-Component of Direction-1 Vector          1
         Y-Component of Direction-1 Vector          0
         Z-Component of Direction-1 Vector          0
         X-Component of Direction-2 Vector          0
         Y-Component of Direction-2 Vector          1
```

Z-Component of Direction-2 Vector	0
X-Coordinate of Point on Cone Axis	1
Y-Coordinate of Point on Cone Axis	0
Z-Coordinate of Point on Cone Axis	0
Half Angle of Cone Relative to its Axis	0
Direction-1 Viscous Resistance	0
Direction-2 Viscous Resistance	0
Direction-3 Viscous Resistance	0
Direction-1 Inertial Resistance	0
Direction-2 Inertial Resistance	0
Direction-3 Inertial Resistance	0
C0 Coefficient for Power-Law	0
C1 Coefficient for Power-Law	0
Porosity	1
Solid Material Name	cellulose_substrate
Reaction Mechanism	0
Activate reaction mechanisms?	yes
Surface-Volume-Ratio	0

inlet

Condition	Value
Velocity Specification Method	2
Reference Frame	0
Velocity Magnitude	0.5
Coordinate System	0
X-Velocity	0
Y-Velocity	0
Z-Velocity	0
X-Component of Flow Direction	1
Y-Component of Flow Direction	0
Z-Component of Flow Direction	0
X-Component of Axis Direction	1
Y-Component of Axis Direction	0
Z-Component of Axis Direction	0
X-Coordinate of Axis Origin	0
Y-Coordinate of Axis Origin	0
Z-Coordinate of Axis Origin	0
Angular velocity	0
Temperature	310
Turbulence Specification Method	3
Turb. Kinetic Energy	1
Turb. Dissipation Rate	1
Turbulence Intensity	0.1
Turbulence Length Scale	1
Hydraulic Diameter	1
Turbulent Viscosity Ratio	10
Reynolds-Stress Specification Method	0
UU Reynolds Stresses	1
VV Reynolds Stresses	1
WW Reynolds Stresses	1
UV Reynolds Stresses	0
VW Reynolds Stresses	0
UW Reynolds Stresses	0
	(((constant . 0) (profile)) ((constant . 0) (profile)) ((constant . 0) (profile)) ((constant . 0
External Black Body Temperature Method	0
Black Body Temperature	300
Internal Emissivity	1
is zone used in mixing-plane model?	no

sym_wall

Condition	Value

outlet

Condition	Value
Gauge Pressure	0
Radial Equilibrium Pressure Distribution	no
Backflow Total Temperature	310
Backflow Direction Specification Method	1
Coordinate System	0
X-Component of Flow Direction	1
Y-Component of Flow Direction	0
Z-Component of Flow Direction	0
X-Component of Axis Direction	1
Y-Component of Axis Direction	0
Z-Component of Axis Direction	0
X-Coordinate of Axis Origin	0
Y-Coordinate of Axis Origin	0
Z-Coordinate of Axis Origin	0
Turbulence Specification Method	3
Backflow Turb. Kinetic Energy	1
Backflow Turb. Dissipation Rate	1
Backflow Turbulence Intensity	0.1
Backflow Turbulence Length Scale	1
Backflow Hydraulic Diameter	1
Backflow Turbulent Viscosity Ratio	10
Reynolds-Stress Specification Method	0
Backflow UU Reynolds Stresses	1
Backflow VV Reynolds Stresses	1
Backflow WW Reynolds Stresses	1
Backflow UV Reynolds Stresses	0

Backflow VW Reynolds Stresses	0
Backflow UW Reynolds Stresses	0
External Black Body Temperature Method	0
Black Body Temperature	300
Internal Emissivity	1
Backflow	(((constant . 0) (profile)) ((constant . 0) (profile)) ((constant . 0) (profi
is zone used in mixing-plane model?	no
Specify targeted mass-flow rate	no
Targeted mass-flow	1

outer_wall

Condition	Value
Wall Thickness	0
Heat Generation Rate	0
Material Name	cellulose_substrate
Thermal BC Type	0
Temperature	310
Heat Flux	0
Convective Heat Transfer Coefficient	0
Free Stream Temperature	300
Enable shell conduction?	no
Wall Motion	0
Shear Boundary Condition	0
Define wall motion relative to adjacent cell zone?	yes
Apply a rotational velocity to this wall?	no
Velocity Magnitude	0
X-Component of Wall Translation	1
Y-Component of Wall Translation	0
Z-Component of Wall Translation	0
Define wall velocity components?	no
X-Component of Wall Translation	0
Y-Component of Wall Translation	0
Z-Component of Wall Translation	0
Internal Emissivity	1
External Emissivity	1
External Radiation Temperature	300
Wall Roughness Height	0
Wall Roughness Constant	0.5
Radiation BC Type	3
X-Component of Radiation Direction	1
Y-Component of Radiation Direction	0
Z-Component of Radiation Direction	0
Theta Width of Beam	1.744e-08
Phi Width of Beam	1.744e-08
	(((constant . 0) (profile)))
	(1)
Apply Irradiation Parallel to the Beam?	yes
Use Beam Direction from Solar Parameters?	no
Use Total Irradiation from Solar Parameters?	no
Activate Reaction Mechanisms	no
	(0 0 0 0 0)
	(((constant . 0) (profile)) ((constant . 0) (profile)) ((constant .
Rotation Speed	0
X-Position of Rotation-Axis Origin	0
Y-Position of Rotation-Axis Origin	0
Z-Position of Rotation-Axis Origin	0
X-Component of Rotation-Axis Direction	0
Y-Component of Rotation-Axis Direction	0
Z-Component of Rotation-Axis Direction	1
X-component of shear stress	0
Y-component of shear stress	0
Z-component of shear stress	0
Surface tension gradient	0
Reaction Mechanisms	0
Specularity Coefficient	0

roof

Condition	Value
Wall Thickness	0.2
Heat Generation Rate	0
Material Name	cellulose_substrate
Thermal BC Type	0
Temperature	310
Heat Flux	0
Convective Heat Transfer Coefficient	0
Free Stream Temperature	300
Enable shell conduction?	no
Wall Motion	0
Shear Boundary Condition	0
Define wall motion relative to adjacent cell zone?	yes
Apply a rotational velocity to this wall?	no
Velocity Magnitude	0
X-Component of Wall Translation	1
Y-Component of Wall Translation	0
Z-Component of Wall Translation	0
Define wall velocity components?	no
X-Component of Wall Translation	0
Y-Component of Wall Translation	0
Z-Component of Wall Translation	0
Internal Emissivity	1
External Emissivity	1
External Radiation Temperature	300

```
      Wall Roughness Height                             0
      Wall Roughness Constant                           0.5
      Radiation BC Type                                 3
      X-Component of Radiation Direction                1
      Y-Component of Radiation Direction                0
      Z-Component of Radiation Direction                0
      Theta Width of Beam                               1.744e-08
      Phi Width of Beam                                 1.744e-08
                                                        (((constant . 0) (profile  )))
                                                        (1)
      Apply Irradiation Parallel to the Beam?           yes
      Use Beam Direction from Solar Parameters?         no
      Use Total Irradiation from Solar Parameters?      no
      Activate Reaction Mechanisms                      no
                                                        (0 0 0 0 0)
                                                        (((constant . 0) (profile  )) ((constant . 0) (profile  )) ((constant . 0) (profile  )) (
      Rotation Speed                                    0
      X-Position of Rotation-Axis Origin                0
      Y-Position of Rotation-Axis Origin                0
      Z-Position of Rotation-Axis Origin                0
      X-Component of Rotation-Axis Direction            0
      Y-Component of Rotation-Axis Direction            0
      Z-Component of Rotation-Axis Direction            1
      X-component of shear stress                       0
      Y-component of shear stress                       0
      Z-component of shear stress                       0
      Surface tension gradient                          0
      Reaction Mechanisms                               0
      Specularity Coefficient                           0

   floor

      Condition                                         Value
      ------------------------------------------------------------------------------------------------------------------------------------------------------
      Wall Thickness                                    0
      Heat Generation Rate                              0
      Material Name                                     cellulose_substrate
      Thermal BC Type                                   0
      Temperature                                       310
      Heat Flux                                         0
      Convective Heat Transfer Coefficient              0
      Free Stream Temperature                           300
      Enable shell conduction?                          no
      Wall Motion                                       0
      Shear Boundary Condition                          0
      Define wall motion relative to adjacent cell zone? yes
      Apply a rotational velocity to this wall?         no
      Velocity Magnitude                                0
      X-Component of Wall Translation                   1
      Y-Component of Wall Translation                   0
      Z-Component of Wall Translation                   0
      Define wall velocity components?                  no
      X-Component of Wall Translation                   0
      Y-Component of Wall Translation                   0
      Z-Component of Wall Translation                   0
      Internal Emissivity                               1
      External Emissivity                               1
      External Radiation Temperature                    300
      Wall Roughness Height                             0
      Wall Roughness Constant                           0.5
      Radiation BC Type                                 3
      X-Component of Radiation Direction                1
      Y-Component of Radiation Direction                0
      Z-Component of Radiation Direction                0
      Theta Width of Beam                               1.744e-08
      Phi Width of Beam                                 1.744e-08
                                                        (((constant . 0) (profile  )))
                                                        (1)
      Apply Irradiation Parallel to the Beam?           yes
      Use Beam Direction from Solar Parameters?         no
      Use Total Irradiation from Solar Parameters?      no
      Activate Reaction Mechanisms                      yes
                                                        (0 0 0 0 0)
                                                        (((constant . 0) (profile  )) ((constant . 0) (profile  )) ((constant . 0) (profile  )) (
      Rotation Speed                                    0
      X-Position of Rotation-Axis Origin                0
      Y-Position of Rotation-Axis Origin                0
      Z-Position of Rotation-Axis Origin                0
      X-Component of Rotation-Axis Direction            0
      Y-Component of Rotation-Axis Direction            0
      Z-Component of Rotation-Axis Direction            1
      X-component of shear stress                       0
      Y-component of shear stress                       0
      Z-component of shear stress                       0
      Surface tension gradient                          0
      Reaction Mechanisms                               0
      Specularity Coefficient                           0

   default-interior

      Condition   Value
      -----------------

Solver Controls
---------------
```

Equations

Equation	Solved
Flow	yes
Turbulence	yes
Reynolds Stresses	yes
h2o<l>	yes
h2o	yes
co2	yes
o2	yes
c6h10o5	yes
Energy	yes
Discrete Ordinates	yes

Numerics

Numeric	Enabled
Absolute Velocity Formulation	yes

Unsteady Calculation Parameters

Time Step (s)	1
Max. Iterations Per Time Step	1

Relaxation

Variable	Relaxation Factor
Pressure	0.3
Density	0.3
Body Forces	1
Momentum	0.7
Turbulence Kinetic Energy	0.3
Turbulence Dissipation Rate	0.3
Turbulent Viscosity	0.5
Reynolds Stresses	0.5
h2o<l>	0.8
h2o	0.8
co2	0.8
o2	0.8
c6h10o5	0.8
Energy	0.5
Discrete Ordinates	1

Linear Solver

Variable	Solver Type	Termination Criterion	Residual Reduction Tolerance
Pressure	V-Cycle	0.1	
X-Momentum	Flexible	0.1	0.7
Y-Momentum	Flexible	0.1	0.7
Z-Momentum	Flexible	0.1	0.7
Turbulence Kinetic Energy	Flexible	0.1	0.7
Turbulence Dissipation Rate	Flexible	0.1	0.7
Reynolds Stresses	Flexible	0.1	0.7
h2o<l>	Flexible	0.1	0.7
h2o	Flexible	0.1	0.7
co2	Flexible	0.1	0.7
o2	Flexible	0.1	0.7
c6h10o5	Flexible	0.1	0.7
Energy	Flexible	0.1	0.7
Discrete Ordinates	Flexible	0.1	0.7

Discretization Scheme

Variable	Scheme
Pressure	Standard
Momentum	First Order Upwind
Turbulence Kinetic Energy	First Order Upwind
Turbulence Dissipation Rate	First Order Upwind
Reynolds Stresses	First Order Upwind
h2o<l>	First Order Upwind
h2o	First Order Upwind
co2	First Order Upwind
o2	First Order Upwind
c6h10o5	First Order Upwind
Energy	First Order Upwind
Discrete Ordinates	First Order Upwind

Solution Limits

Quantity	Limit
Minimum Absolute Pressure	1
Maximum Absolute Pressure	5e+10
Minimum Temperature	1
Maximum Temperature	5000
Minimum Turb. Kinetic Energy	1e-14
Minimum Turb. Dissipation Rate	1e-20
Maximum Turb. Viscosity Ratio	100000

```
Material Properties
-------------------

   Material: (levoglucosan . thermal_degradation) (fluid)

      Property                     Units       Method     Value(s)
      ------------------------------------------------------------
      Cp (Specific Heat)           j/kg-k      constant   1500
      Molecular Weight             kg/kgmol    constant   162
      Standard State Enthalpy      j/kgmol     constant   48600000
      Standard State Entropy       j/kgmol-k   constant   0
      Reference Temperature        k           constant   298.14999
      L-J Characteristic Length    angstrom    constant   0
      L-J Energy Parameter         k           constant   0
      Degrees of Freedom                       constant   0
      Speed of Sound               m/s         none       #f

   Material: (cellulose<s> . thermal_degradation) (fluid)

      Property                     Units       Method     Value(s)
      ------------------------------------------------------------
      Cp (Specific Heat)           j/kg-k      constant   1220
      Molecular Weight             kg/kgmol    constant   162
      Standard State Enthalpy      j/kgmol     constant   0
      Standard State Entropy       j/kgmol-k   constant   5731.7471
      Reference Temperature        k           constant   298
      L-J Characteristic Length    angstrom    constant   3.711
      L-J Energy Parameter         k           constant   78.6
      Degrees of Freedom                       constant   0
      Speed of Sound               m/s         none       #f

   Material: (char . thermal_degradation) (fluid)

      Property                     Units       Method     Value(s)
      ------------------------------------------------------------
      Cp (Specific Heat)           j/kg-k      constant   1220
      Molecular Weight             kg/kgmol    constant   136
      Standard State Enthalpy      j/kgmol     constant   2.57e+08
      Standard State Entropy       j/kgmol-k   constant   5731.7471
      Reference Temperature        k           constant   298
      L-J Characteristic Length    angstrom    constant   0
      L-J Energy Parameter         k           constant   0
      Degrees of Freedom                       constant   0
      Speed of Sound               m/s         none       #f

   Material: (carbon-dioxide . thermal_degradation) (fluid)

      Property                     Units       Method       Value(s)
      ------------------------------------------------------------------------------------------------------------------------------------------------------------------------
      Cp (Specific Heat)           j/kg-k      polynomial   (300-1000: 429.92889 1.8744735 -0.0019664851 1.2972514e-06 -3.9999562e-10) (1000-5000: 841.37
      Molecular Weight             kg/kgmol    constant     44.009949
      Standard State Enthalpy      j/kgmol     constant     -3.9353235e+08
      Standard State Entropy       j/kgmol-k   constant     213720.2
      Reference Temperature        k           constant     298.14999
      L-J Characteristic Length    angstrom    constant     3.941
      L-J Energy Parameter         k           constant     195.2
      Degrees of Freedom                       constant     0
      Speed of Sound               m/s         none         #f

   Material: (water-liquid . thermal_degradation) (fluid)

      Property                     Units       Method     Value(s)
      ------------------------------------------------------------
      Cp (Specific Heat)           j/kg-k      constant   4182
      Molecular Weight             kg/kgmol    constant   18.0152
      Standard State Enthalpy      j/kgmol     constant   0
      Standard State Entropy       j/kgmol-k   constant   69902.211
      Reference Temperature        k           constant   298.15
      L-J Characteristic Length    angstrom    constant   0
      L-J Energy Parameter         k           constant   0
      Degrees of Freedom                       constant   0
      Speed of Sound               m/s         none       #f

   Material: cellulose<s> (fluid)

      Property                          Units       Method      Value(s)
      ------------------------------------------------------------------
      Density                           kg/m3       constant    2000
      Cp (Specific Heat)                j/kg-k      constant    1220
      Thermal Conductivity              w/m-k       constant    0.045400001
      Viscosity                         kg/m-s      constant    1.72e-05
      Molecular Weight                  kg/kgmol    constant    162
      Standard State Enthalpy           j/kgmol     constant    0
      Standard State Entropy            j/kgmol-k   constant    5731.7471
      Reference Temperature             k           constant    298
      L-J Characteristic Length         angstrom    constant    3.711
      L-J Energy Parameter              k           constant    78.6
      Absorption Coefficient            1/m         constant    0
      Scattering Coefficient            1/m         constant    0
      Scattering Phase Function                     isotropic   #f
      Thermal Expansion Coefficient     1/k         constant    0
      Refractive Index                              constant    1
      Degrees of Freedom                            constant    0
      Speed of Sound                    m/s         none        #f
```

Material: water-liquid (fluid)

Property	Units	Method	Value(s)
Density	kg/m3	constant	998.2
Cp (Specific Heat)	j/kg-k	constant	4182
Thermal Conductivity	w/m-k	constant	0.6
Viscosity	kg/m-s	constant	0.001003
Molecular Weight	kg/kgmol	constant	18.0152
Standard State Enthalpy	j/kgmol	constant	0
Standard State Entropy	j/kgmol-k	constant	69902.211
Reference Temperature	k	constant	298.15
L-J Characteristic Length	angstrom	constant	0
L-J Energy Parameter	k	constant	0
Absorption Coefficient	1/m	constant	0
Scattering Coefficient	1/m	constant	0
Scattering Phase Function		isotropic	#f
Thermal Expansion Coefficient	1/k	constant	0
Refractive Index		constant	1
Degrees of Freedom		constant	0
Speed of Sound	m/s	none	#f

Material: char (fluid)

Property	Units	Method	Value(s)
Density	kg/m3	constant	2000
Cp (Specific Heat)	j/kg-k	constant	1220
Thermal Conductivity	w/m-k	constant	0.045400001
Viscosity	kg/m-s	constant	1.72e-05
Molecular Weight	kg/kgmol	constant	136
Standard State Enthalpy	j/kgmol	constant	-7353
Standard State Entropy	j/kgmol-k	constant	5731.7471
Reference Temperature	k	constant	298
L-J Characteristic Length	angstrom	constant	0
L-J Energy Parameter	k	constant	0
Absorption Coefficient	1/m	constant	0
Scattering Coefficient	1/m	constant	0
Scattering Phase Function		isotropic	#f
Thermal Expansion Coefficient	1/k	constant	0
Refractive Index		constant	1
Degrees of Freedom		constant	0
Speed of Sound	m/s	none	#f

Material: carbon-dioxide (fluid)

Property	Units	Method	Value(s)
Density	kg/m3	constant	1.7878
Cp (Specific Heat)	j/kg-k	constant	840.37
Thermal Conductivity	w/m-k	constant	0.0145
Viscosity	kg/m-s	constant	1.37e-05
Molecular Weight	kg/kgmol	constant	44.00995
Standard State Enthalpy	j/kgmol	constant	-3.9353235e+08
Standard State Entropy	j/kgmol-k	constant	213720.2
Reference Temperature	k	constant	298.15
L-J Characteristic Length	angstrom	constant	3.941
L-J Energy Parameter	k	constant	195.2
Absorption Coefficient	1/m	constant	0.43
Scattering Coefficient	1/m	constant	0
Scattering Phase Function		isotropic	#f
Thermal Expansion Coefficient	1/k	constant	0
Refractive Index		constant	1
Degrees of Freedom		constant	0
Speed of Sound	m/s	none	#f

Material: levoglucosan (fluid)

Property	Units	Method	Value(s)
Density	kg/m3	constant	1
Cp (Specific Heat)	j/kg-k	constant	1500
Thermal Conductivity	w/m-k	constant	0.045400001
Viscosity	kg/m-s	constant	1.72e-05
Molecular Weight	kg/kgmol	constant	162
Standard State Enthalpy	j/kgmol	constant	1850
Standard State Entropy	j/kgmol-k	constant	0
Reference Temperature	k	constant	298.14999
L-J Characteristic Length	angstrom	constant	0
L-J Energy Parameter	k	constant	0
Absorption Coefficient	1/m	constant	0
Scattering Coefficient	1/m	constant	0
Scattering Phase Function		isotropic	#f
Thermal Expansion Coefficient	1/k	constant	0
Refractive Index		constant	1
Degrees of Freedom		constant	0
Speed of Sound	m/s	none	#f

Material: cellulose_substrate (solid)

Property	Units	Method	Value(s)
Density	kg/m3	constant	700
Cp (Specific Heat)	j/kg-k	constant	2310
Thermal Conductivity	w/m-k	constant	0.17299999
Absorption Coefficient	1/m	constant	0

Scattering Coefficient	1/m	constant	0.5
Scattering Phase Function		isotropic	#f
Refractive Index		constant	1

Material: thermal_degradation (mixture)

Property	Units	Method	Value(s)
Mixture Species		names	((h2o<l> h2o co2 o2 c6h10o5 n2) (c11h4 <c6h10o5>n) ())
Reaction		finite-rate	((reaction-1 ((<c6h10o5>n 1 0 1)) ((c6h10o5 1 0 1)) ((h2o<l> 0 1) (h2o 0 1) (c
Mechanism		reaction-mechs	((mechanism-1 (reaction-type . all) (reaction-list reaction-1 reaction-2 react
Density	kg/m3	incompressible-ideal-gas	#f
Cp (Specific Heat)	j/kg-k	mixing-law	#f
Thermal Conductivity	w/m-k	constant	0.045400001
Viscosity	kg/m-s	constant	1.72e-05
Mass Diffusivity	m2/s	constant-dilute-appx	(2.8799999e-05)
Absorption Coefficient	1/m	constant	0
Scattering Coefficient	1/m	constant	0
Scattering Phase Function		isotropic	#f
Thermal Expansion Coefficient	1/k	constant	0
Refractive Index		constant	1

Material: (nitrogen . thermal_degradation) (fluid)

Property	Units	Method	Value(s)
Cp (Specific Heat)	j/kg-k	constant	1040.67
Molecular Weight	kg/kgmol	constant	28.0134
Standard State Enthalpy	j/kgmol	constant	0
Standard State Entropy	j/kgmol-k	constant	191494.78
Reference Temperature	k	constant	298.15
L-J Characteristic Length	angstrom	constant	3.621
L-J Energy Parameter	k	constant	97.53
Degrees of Freedom		constant	0
Speed of Sound	m/s	none	#f

Material: nitrogen (fluid)

Property	Units	Method	Value(s)
Density	kg/m3	constant	1.138
Cp (Specific Heat)	j/kg-k	constant	1040.67
Thermal Conductivity	w/m-k	constant	0.0242
Viscosity	kg/m-s	constant	1.663e-05
Molecular Weight	kg/kgmol	constant	28.0134
Standard State Enthalpy	j/kgmol	constant	0
Standard State Entropy	j/kgmol-k	constant	191494.78
Reference Temperature	k	constant	298.15
L-J Characteristic Length	angstrom	constant	3.621
L-J Energy Parameter	k	constant	97.53
Absorption Coefficient	1/m	constant	0
Scattering Coefficient	1/m	constant	0
Scattering Phase Function		isotropic	#f
Thermal Expansion Coefficient	1/k	constant	0
Refractive Index		constant	1
Degrees of Freedom		constant	0
Speed of Sound	m/s	none	#f

Material: (oxygen . thermal_degradation) (fluid)

Property	Units	Method	Value(s)
Cp (Specific Heat)	j/kg-k	constant	919.31
Molecular Weight	kg/kgmol	constant	31.9988
Standard State Enthalpy	j/kgmol	constant	0
Standard State Entropy	j/kgmol-k	constant	205026.86
Reference Temperature	k	constant	298.15
L-J Characteristic Length	angstrom	constant	3.458
L-J Energy Parameter	k	constant	107.4
Degrees of Freedom		constant	0
Speed of Sound	m/s	none	#f

Material: oxygen (fluid)

Property	Units	Method	Value(s)
Density	kg/m3	constant	1.2999
Cp (Specific Heat)	j/kg-k	constant	919.31
Thermal Conductivity	w/m-k	constant	0.0246
Viscosity	kg/m-s	constant	1.919e-05
Molecular Weight	kg/kgmol	constant	31.9988
Standard State Enthalpy	j/kgmol	constant	0
Standard State Entropy	j/kgmol-k	constant	205026.86
Reference Temperature	k	constant	298.15
L-J Characteristic Length	angstrom	constant	3.458
L-J Energy Parameter	k	constant	107.4
Absorption Coefficient	1/m	constant	0
Scattering Coefficient	1/m	constant	0
Scattering Phase Function		isotropic	#f
Thermal Expansion Coefficient	1/k	constant	0
Refractive Index		constant	1
Degrees of Freedom		constant	0
Speed of Sound	m/s	none	#f

Material: (water-vapor . thermal_degradation) (fluid)

```
   Property                    Units       Method       Value(s)
   ------------------------------------------------------------------------------------------------------------------------------------------
   Cp (Specific Heat)          j/kg-k      polynomial   (300-1000: 1563.0767 1.6037546 -0.0029327841 3.2161008e-06 -1.1568267e-09)
   Molecular Weight            kg/kgmol    constant     18.015341
   Standard State Enthalpy     j/kgmol     constant     -2.418379e+08
   Standard State Entropy      j/kgmol-k   constant     188696.44
   Reference Temperature       k           constant     298.14999
   L-J Characteristic Length   angstrom    constant     2.605
   L-J Energy Parameter        k           constant     572.4
   Degrees of Freedom                      constant     0
   Speed of Sound              m/s         none         #f

Material: water-vapor (fluid)

   Property                          Units       Method      Value(s)
   ------------------------------------------------------------------------
   Density                           kg/m3       constant    0.5542
   Cp (Specific Heat)                j/kg-k      constant    2014
   Thermal Conductivity              w/m-k       constant    0.0261
   Viscosity                         kg/m-s      constant    1.34e-05
   Molecular Weight                  kg/kgmol    constant    18.01534
   Standard State Enthalpy           j/kgmol     constant    -2.418379e+08
   Standard State Entropy            j/kgmol-k   constant    188696.44
   Reference Temperature             k           constant    298.15
   L-J Characteristic Length         angstrom    constant    2.605
   L-J Energy Parameter              k           constant    572.4
   Absorption Coefficient            1/m         constant    0.54
   Scattering Coefficient            1/m         constant    0
   Scattering Phase Function                     isotropic   #f
   Thermal Expansion Coefficient     1/k         constant    0
   Refractive Index                              constant    1
   Degrees of Freedom                            constant    0
   Speed of Sound                    m/s         none        #f

Material: air (fluid)

   Property                          Units       Method      Value(s)
   ------------------------------------------------------------------------
   Density                           kg/m3       constant    1.225
   Cp (Specific Heat)                j/kg-k      constant    1006.43
   Thermal Conductivity              w/m-k       constant    0.0242
   Viscosity                         kg/m-s      constant    1.7894e-05
   Molecular Weight                  kg/kgmol    constant    28.966
   Standard State Enthalpy           j/kgmol     constant    0
   Standard State Entropy            j/kgmol-k   constant    0
   Reference Temperature             k           constant    298.15
   L-J Characteristic Length         angstrom    constant    3.711
   L-J Energy Parameter              k           constant    78.6
   Absorption Coefficient            1/m         constant    0
   Scattering Coefficient            1/m         constant    0
   Scattering Phase Function                     isotropic   #f
   Thermal Expansion Coefficient     1/k         constant    0
   Refractive Index                              constant    1
   Degrees of Freedom                            constant    0
   Speed of Sound                    m/s         none        #f

Material: aluminum (solid)

   Property                    Units    Method      Value(s)
   ------------------------------------------------------------
   Density                     kg/m3    constant    2719
   Cp (Specific Heat)          j/kg-k   constant    871
   Thermal Conductivity        w/m-k    constant    202.4
   Absorption Coefficient      1/m      constant    0
   Scattering Coefficient      1/m      constant    0
   Scattering Phase Function            isotropic   #f
   Refractive Index                     constant    1
```

Bibliography

Albini, F. A. (1975). Computer-based models of wildland fire behavior: a user's manual. Unnumbered publication, USDA Forest Service, Intermountain Forest and Range Experimental Station, Odgen UT.

Albini, F. A. (1979). Spot fire distance from burning trees–a predictive model. General Technical Report INT-56, USDA Forest Service, Intermountain Forest and Range Experimental Station, Odgen UT.

Albini, F. A. (1982). Response of free-burning fires to non-steady wind. *Combustion Science and Technology*, 29:225–241.

Albini, F. A. (1985). A model for fire spread in wildland fuels by radiation. *Combustion Science and Technology*, 42:229–258.

Albini, F. A. and Baughman, R. G. (1979). Estimating windspeeds for predicting wildland fire behaviour. Research Paper INT-221, USDA Forest Service, Intermountain Forest and Range Experimental Station, Odgen UT.

Alexander, M. E. (1985). Estimating the length to breadth ratio of elliptical forest fire patterns. In *Proceedings of the Eighth Conference on Forest and Fire Meteorology*, pages 287–304. Society of American Foresters.

Anderson, D. H., Catchpole, E. A., de Mestre, N. J., and Parkes, T. (1982). Modelling the spread of grass fires. *Journal of Australian Mathematics Society, Series B*, 23:451–466.

Anderson, H. E. (1964). Mechanisms of fire spread. Research Paper INT-8, USDA Forest Service, Intermountain Forest & Range Experiment Station, Ogden, UT.

Anderson, H. E. (1968). Fire spread and flame shape. *Fire Technology*, 4:51–58.

Anderson, H. E. (1969). Heat transfer and fire spread. Research Paper INT-69, USDA Forest Service, Intermountain Forest & Range Experiment Station, Ogden, UT.

Anderson, H. E. (1983). Predicting wind-driven wild land fire size and shape. Research Paper INT-305, USDA Forest Service Intermountain Forest and Range Experiment Station, Intermountain Forest & Range Experiment Station, Ogden, UT.

Anderson, T. B. and Jackson, R. (1967). Fluid mechanical description of fluidized beds: Equations of motion. *Industrial & Engineering Chemistry. Fundamentals*, 6(4):527–539.

Anderson, W., Pastor, E., Butler, B., Catchpole, E., Dupuy, J.-L., Fernandes, P., Guijarro, M., Mendes-Lopes, J.-M., and Ventura, J. (2006). Evaluating models to estimate flame characteristics for free-burning fires using laboratory and field data. *Forest Ecology and Management*, 234(Supplement 1):S77–.

Andrews, P. (1986). BEHAVE: fire behaviour prediction and fuel modelling system - BURN subsystem, part 1. General Technical Report INT-194, USDA Forest Service, Intermountain Forest and Range Experiment Station, Ogden, UT, Intermountain Forest & Range Experiment Station, Ogden, UT.

Antal, M. J. and Várhegyi, G. (1995). Cellulose pyrolysis kinetics: The current state of knowledge. *Industrial & Engineering Chemistry Research*, 34(3):703–717.

Antal, M. J., Várhegyi, G., and Jakab, E. (1998). Cellulose pyrolysis kinetics: Revisited.

Industrial & Engineering Chemistry Research, 37(4):1267–1275.

Babrauskas, V. (2003). *Ignition Handbook*. Fire Science Publishers, Issaquah, WA.

Bachelard, G. (1938). *The Psychoanalysis of Fire*. Quartet Books, London. (orig. *La Psychanalyse du Feu*, trans. Alan C.M. Ross, 1964).

Backreedy, R., Fletcher, L., Jones, J., Ma, L., Pourkashanian, M., and Williams, A. (2005). Co-firing pulverised coal and biomass: a modeling approach. *Proceedings of the Combustion Institute*, 30(2):2955–2964.

Bak, P. (1996). *How Nature Works: The Science of Self-organised Criticality*. Springer-Verlag Telos, New York, USA.

Bak, P., Chen, K., and Tang, C. (1990). A forest-fire model and some thoughts on turbulence. *Physics Letters A*, 147(5-6):297–300.

Baker, A., Helbert, W., Sugiyama, J., and Miles, M. (2000). New insight into cellulose structure by atomic force microscopy shows the i_α crystal phase at near-atomic resolution. *Biophysical Journal*, 79:1139–1145.

Ball, R., McIntosh, A., and Brindley, J. (1999a). The role of char-forming processes in the thermal decomposition of cellulose. *Physical Chemistry Chemical Physics*, 1:5035–5043.

Ball, R., McIntosh, A., and Brindley, J. (1999b). Thermokinetic models for simultaneous reactions: a comparitive study. *Combustion Theory and Modelling*, 3:447–468.

Ball, R., McIntosh, A. C., and Brindley, J. (2004). Feedback processes in cellulose thermal decomposition: implications for fire-retarding strategies and treatments. *Combustion Theory and Modelling*, 8(2):281–291.

Bari, S. and Naser, J. (2005). Simulation of smoke from a burning vehicle and pollution levels caused by traffic jam in a road tunnel. *Tunneling and Underground Space Technology*, 20(3):281–290.

Barrow, G. M. (1973). *Physical Chemistry*. McGraw-Hill Kogakusha, Tokyo, Japan, 3rd edition.

Batchelor, G. (1967). *An Introduction to Fluid Mechanics*. Cambridge University Press, London, 1970 edition.

Batt, K. L. and Leslie, L. M. (1998). Verification of output from a very high resolution numerical weather prediction model: the 1996 Sydney to Hobart yacht race. *Meteorological Applications*, 5(4):321–327.

Baum, H. and Mell, W. (1998). A radiative transport model for large-eddy fire simulations. *Combustion Theory and Modelling*, 2:405–422.

Beall, F. C. and Eickner, H. W. (1970). Thermal degradation of wood components: A review of the literature. Research Paper FPL 130, USDA Forest Service, Madison, Wisconsin.

Beer, T. (1990). The Australian National Bushfire Model Project. *Mathematical and Computer Modelling*, 13(12):49–56.

Beer, T. (1991). The interaction of wind and fire. *Boundary-Layer Meteorology*, 54(2):287–308.

Belcher, S. E. and Hunt, J. C. R. (1998). Turbulent flow over hills and waves. *Annual Review of Fluid Mechanics*, 30:507–538.

Bond, H., Mackinnon, K., and Noar, P. (1967). Report on the meteorological aspects of the catastrophic bushfires in south-eastern Tasmania on 7 February 1967.

Boutin, O., Ferrer, M., and Lédé, J. (1998). Radiant flash pyrolysis of cellulose-Evidence

for the formation of short life time intermediate liquid species. *Journal of Analytical and Applied Pyrolysis*, 47:13–31.

Bradbury, A. G. W., Sakai, Y., and Shafizadeh, F. (1979). A kinetic model for pyrolysis of cellulose. *Journal of Applied Polymer Science*, 23:3271–3280.

Branca, C. and di Blasi, C. (2004). Parallel- and series-reaction mechanisms of wood and char combustion. *Thermal Science*, 8(2):51–63.

Broido, A. (1976). Kinetics of solid-phase cellulose pyrolysis. In Shafizadeh, F., Sarkanen, K. V., and Tillman, D. A., editors, *Thermal Uses and Properties of Carbohydrates and Lignins*, chapter 2, pages 19–36. Academic Publishing, New York.

Broido, A., Javier-son, A., Ouano, A., and Barrall II, E. (1973). Molecular weight decrease in the early pyrolysis of crystalline and amorphous cellulose. *Journal of Applied Polymer Science*, 17:3627–3635.

Broido, A. and Nelson, M. A. (1975). Char yield on pyrolysis of cellulose. *Combustion and Flame*, 24:263–268.

Búcsi, A. and Rychlý, J. (1992). A theoretical approach to understanding the connection between ignitability and flammability parameters of organic polymers. *Polymer Degradation and Stability*, 38(1):33–40.

Burgan, R. E. (1988). 1988 revisions to the 1978 National Fire-Danger Rating System. Research Paper SE-273, USDA Forest Service, , Southeastern Forest Experiment Station, Asheville NC.

Burrows, N. D. (1999). Fire behaviour in jarrah forest fuels: 1. Laboratory experiments. *CALMScience*, 3(1):31–56.

Butler, B. W., Finney, M., Bradshaw, L., Forthofer, J., McHugh, C., Stratton, R., and Jimenez, D. (2006). Wind Wizard: A new tool for fire management decision support. In Andrews, P. L. and Butler, B. W., editors, *Fuels Management—How to Measure Success: Conference Proceedings. RMRS-P-41*, pages 787–796. USDA Forest Service, Rocky Mountain Research Station, Fort Collins, CO. 28-30 March 2006, Portland OR.

Byram, G. M. (1954). Atmospheric conditions related to blowup fires. Station Paper No. 35, USDA Forest Service, Southeastern Forest Experiment Station, Asheville NC.

Byram, G. M. (1959a). Combustion of forest fuels. In Davis, K., editor, *Forest Fire Control and Use*, chapter 3, pages 61–89 pp. McGraw-Hill, New York.

Byram, G. M. (1959b). Forest fire behaviour. In Davis, K., editor, *Forest Fire Control and Use*, chapter 4, pages 90–123. McGraw-Hill, New York.

Canadian Forest Service (1970). *Canadian Forest Fire Weather Index*. Canadian Forest Service.

Carrier, G. F., Fendell, F. E., and Feldman, P. S. (1985). Firestorms. *Journal of Heat Transfer*, 107:19–27.

Catchpole, E. A., de Mestre, N. J., and Gill, A. M. (1982). Intensity of fire at its perimeter. *Australian Forest Research*, 12:47–54.

Catchpole, T. and de Mestre, N. (1986). Physical models for a spreading line fire. *Australian Forestry*, 49(2):102–111.

Catchpole, W. R., Catchpole, E. A., Butler, B. W., Rothermel, R. C., Morris, G. A., and Latham, D. J. (1998). Rate of spread of free-burning fires in woody fuels in a wind tunnel. *Combustion Science and Technology*, 131:1–37.

Chandler, C., Cheney, P., Thomas, P., Trabaud, L., and Williams, D. (1983a). *Fire in Forestry*

1: Forest Fire Behaviour and Effects. John Wiley & Sons, New York.

Chandler, C., Cheney, P., Thomas, P., Trabaud, L., and Williams, D. (1983b). *Fire in Forestry 2: Forest Fire Management and Organization*. John Wiley & Sons, New York.

Cheney, N. P. (1968). Predicting fire behaviour with fire danger tables. *Australian Forestry*, 32(2):71–79.

Cheney, N. P. (1976). Bushfire disasters in Australia. *Australian Forestry*, 39:73–79.

Cheney, N. P. (1981). Fire behaviour. In Gill, A., Groves, R., and Noble, I., editors, *Fire and the Australian Biota*, chapter 5, pages 151–175. Australian Academy of Science, Canberra.

Cheney, N. P. and Gould, J. S. (1995). Fire growth in grassland fuels. *International Journal of Wildland Fire*, 5:237–247.

Cheney, N. P. and Gould, J. S. (1997). Fire growth and acceleration. *International Journal of Wildland Fire*, 7(1):1–5.

Cheney, N. P., Gould, J. S., and Catchpole, W. R. (1993). The influence of fuel, weather and fire shape variables on fire-spread in grasslands. *International Journal of Wildland Fire*, 3(1):31–44.

Cheney, N. P., Gould, J. S., and Catchpole, W. R. (1998). Prediction of fire spread in grasslands. *International Journal of Wildland Fire*, 8(1):1–13.

Cheney, P., Gould, J., and McCaw, L. (2001). The dead-man zone–a neglected area of firefighter safety. *Australian Forestry*, 64(1):45–50.

Cheney, P. and Sullivan, A. (1997). *Grassfires: Fuel, Weather and Fire Behaviour*. CSIRO Publishing, Collingwood, Australia.

Cheng, P. (1964). Two-dimensional radiating gas flow by a moment method. *American Institute of Aeronautics and Astronautics Journal*, 2(9):1662–1664.

Clark, T. L., Coen, J., and Latham, D. (2004). Description of a coupled atmosphere-fire model. *International Journal of Wildland Fire*, 13(1):49–63.

Clark, T. L., Jenkins, M. A., Coen, J., and Packham, D. (1996a). A coupled atmosphere-fire model: Convective feedback on fire-line dynamics. *Journal of Applied Meteorology*, 35(6):875–901.

Clark, T. L., Jenkins, M. A., Coen, J. L., and Packham, D. R. (1996b). A coupled atmosphere-fire model: Role of the convective Froude number and dynamic fingering at the fireline. *International Journal of Wildland Fire*, 6(4):177–190.

Coblentz, W. W. (1905). Infra-red absorption spectra, II: Liquids and solids. *The Physical Review*, 20(6):337–363.

Cohen, J. and Stewart, I. (1994). *The Collapse of Chaos*. Viking, New York, NY.

Cohen, J. D. and Burgan, R. E. (1979). Hand-held calculator for fire danger/fire behaviour. *Fire Management Notes*, 40(1):8–9.

Coleman, J. R. and Sullivan, A. L. (1996). A real-time computer application for the prediction of fire spread across the Australian landscape. *Simulation*, 67(4):230–240.

Colman, J. J. and Linn, R. R. (2003). Non-local chemistry implementation in HIGRAD/FIRETEC. In *Fifth Symposium on Fire and Forest Meteorology, 16-20 November 2003, Orlando, Florida.* American Meteorological Society.

Colman, J. J. and Linn, R. R. (2005). Separating combustion from pyrolysis in HIGRAD/FIRETEC. In *Sixth Symposium on Fire and Forest Meteorology, 25-27 October 2005, Canmore, Alabama.* American Meteorological Society.

Colman, J. J. and Linn, R. R. (2007). Separating combustion from pyrolysis in HI-

GRAD/FIRETEC. *International Journal of Wildland Fire*, 16(4):493–502.

Consalvi, J. L., Porterie, B., and Loraud, J. C. (2002). A formal averaging procedure for radiation heat transfer in particulate media. *International Journal of Heat and Mass Transfer*, 45(13):2755–2768.

Countryman, C. M. (1966). The concept of the fire environment. *Fire Control Notes*, 27:8–10.

Cox, G. (1998). Turbulent closure and the modelling of fire by using computational fluid dynamics. *Philosophical Transactions of the Royal Society A: Mathematical, Physical and Engineering Sciences*, 356(1748):2835–2854.

Crane, W. J. B. (1982). Computing grassland and forest fire behaviour, relative humidity and drought index by pocket calculator. *Australian Forestry*, 45:89–97.

Crutchfield, J. P. and Young, K. (1989). Inferring statistical complexity. *Physical Review Letters*, 63(2):105–108.

CSIRO (1997). CSIRO Grassland Fire Spread Meter. Cardboard meter, Styrox Pty Ltd.

Cunningham, P. and Linn, R. R. (2007). Numerical simulations of grass fires using a coupled atmosphere-fire model: Dynamics of fire spread. *Journal Of Geophysical Research-Atmospheres*, 112(D5):5108–5108.

Curry, J. R. and Fons, W. L. (1938). Rate of spread of surface fires in the Ponderosa pine type of California. *Journal of Agricultural Research*, 57(4):239–267.

Curry, J. R. and Fons, W. L. (1940). Forest-fire behaviour studies. *Mechanical Engineering*, 62:219–225.

CWFGM Steering Committee (2004). *Prometheus User Manual v.3.0.1*. Canadian Forest Service.

de Mestre, N. J., Catchpole, E. A., Anderson, D. H., and Rothermel, R. C. (1989). Uniform propagation of a planar fire front without wind. *Combustion Science and Technology*, 65:231–244.

Deeming, J. E., Burgan, R. E., and Cohen, J. D. (1977). The National Fire-Danger Rating System - 1978. General Technical Report INT-39, USDA Forest Service, Intermountain Forest and Range Experiment Station, Ogden, UT.

Deguchi, S., Tsujii, K., and Horikoshi, K. (2006). Cooking cellulose in hot and compressed water. *Chemical Communications*, 11(31):3293–3295.

Di Blasi, C. (1993). Modeling and simulation of combustion processes of charring and non-charring solid fuels. *Progress in Energy and Combustion Science*, 19(1):71–104.

Di Blasi, C. (1998). Comparison of semi-global mechanisms for primary pyrolysis of lignocellulosic fuels. *Journal of Analytical and Applied Pyrolysis*, 47(1):43–64.

Diebold, J. P. (1994). A unified, global model for the pyrolysis of cellulose. *Biomass and Bioenergy*, 7(1-6):75–85.

Douglas, D. R. (1957). Forest Fire Weather Studies in South Australia. Bulletin No. 9, South Australia Woods and Forests Department.

Drake, M. C. and Haworth, D. C. (2007). Advanced gasoline engine development using optical diagnostics and numerical modeling. *Proceedings of the Combustion Institute*, 31(1):99–124.

Drysdale, D. (1985). *An Introduction to Fire Dynamics*. John Wiley and Sons, Chichester, UK.

Dunn, A. (2007). *A Model of Wildfire Propagation Using the Interacting Spatial Automata Formalism*. PhD thesis, University of Western Australia School of Computer Science

and Software Engineering.

Dunn, A. and Milne, G. (2004). Modelling wildfire dynamics via interacting automata. In Sloot, P. M. A., Chopard, B., and Hoekstra, A. G., editors, *ACRI*, volume 3305 of *Lecture Notes in Computer Science*, pages 395–404. Springer.

Dupuy, J. (1995). Slope and fuel load effects on fire behaviour: Laboratory experiments in pine needle fuel beds. *International Journal of Wildland Fire*, 5(3):153–164.

Eghlimi, A., Lu, L., Sahajwalla, V., and Harris, D. (1999). Computational modelling of char combustion particles based on the structure of char particles. In *Second International Conference of CFD in the Minerals and Process Industries, 6-8 December, 1999*, Melbourne, Australia. CSIRO.

Elliot, J. A. (1993). Plasma kinetic theory. In Dendy, R. O., editor, *Plasma Physics: an Introductory Course*, chapter 2, pages 29–53. Cambridge University Press, Cambridge, UK.

Ellis, P. F. M. (2000). *The aerodynamic and combustion characteristics of eucalypt bark: A firebrand study*. PhD thesis, The Australian National University School of Forestry, Canberra, ACT, Australia.

Emmons, H. W. (1966). Fundamental problems of the free burning fire. *Fire Research Abstracts and Reviews*, 8(1):1–17.

Encinas, L. H., White, S. H., del Rey, A. M., and Sanchez, G. R. (2007). Modelling forest fire spread using hexagonal cellular automata. *Applied Mathematical Modelling*, 31(6):1213–1227.

Ermentrout, B. (2002). *Simulating, Analyzing, and Animating Dynamical Systems: A Guide to XPPAut for Researchers and Students*. Society for Industrial & Applied Mathematics, Philadelphia, PA.

Ferziger, J. H. and Perić, M. (1996). *Computational Methods for Fluid Dynamics*. Springer-Verlag, Berlin, Germany.

Finney, M. A. (1998). FARSITE: Fire area simulator–model development and evaluation. Research Paper RMRS-RP-4, USDA Forest Service, Rocky Mountain Research Station,.

Finney, M. A., Cohen, J. D., Grenfell, I. C., and Yedinak, K. M. (2006). Experiments on fire spread in discontinuous fuel beds. *Forest Ecology and Management*, 234:S99–S99.

Finnigan, J. (2000). Turbulence in plant canopies. *Annual Review Of Fluid Mechanics*, 32:519–571.

Finnigan, J. J. and Brunet, Y. (1995). Turbulent airflow in forests on flat and hilly terrain. In Coutts, M. P. and Grace, J., editors, *Wind and Trees*, chapter 1, pages 3–40. Cambridge University Press, UK.

Fluent Inc (2001a). *FLUENT 6.0 User's Guide Volume 1*. Fluent Inc, Lebanon, NH.

Fluent Inc (2001b). *FLUENT 6.0 User's Guide Volume 2*. Fluent Inc, Lebanon, NH.

Fluent Inc (2001c). *FLUENT 6.0 User's Guide Volume 3*. Fluent Inc, Lebanon, NH.

Fluent Inc (2001d). *GAMBIT 2 Modeling Guide Volume 1*. Fluent Inc, Lebanon, NH.

Flynn, J. H. (1980). The effect of heating rate upon the coupling complex reactions. I. Independent and competitive reactions. *Thermochimica Acta*, 37:225–238.

Fons, W. L. (1946). Analysis of fire spread in light forest fuels. *Journal of Agricultural Research*, 72(3):93–121.

Forbes, M. S., Raison, R. J., and Skjemstad, J. O. (2006). Formation, transformation and transport of black carbon (charcoal) in terrestrial and aquatic ecosystems. *Science*

of The Total Environment, 370(1):190–206.

Forestry Canada Fire Danger Group (1992). Development and structure of the Canadian Forest Fire Behavior Prediction System. Information Report ST-X-3, Forestry Canada Science and Sustainable Development Directorate, Ottawa, ON.

Frandsen, W. H. (1971). Fire spread through porous fuels from the conservation of energy. *Combustion and Flame*, 16:9–16.

Gavalas, G. R. (1968). *Nonlinear Differential Equations of Chemically Reacting Systems*. Springer, Berlin.

Gaydon, A. and Wolfhard, H. (1960). *Flames: Their Structure, Radiation and Temperature*. Chapman and Hall Ltd, London, 2nd edition.

Gibson, M. M. and Launder, B. E. (1978). Ground effects on pressure fluctuations in the atmospheric boundary layer. *Journal of Fluid Mechanics*, 86(3):491–511.

Gill, A. M. (1981). Adaptive responses of Australian vascular plant species to fire. In Gill, A., Groves, R., and Noble, I., editors, *Fire and the Australian Biota*, chapter 11, pages 244–272. Australian Academy of Science, Canberra.

Gisborne, H. T. (1927). The objectives of forest fire-weather research. *Journal of Forestry*, 25(4):452–456.

Gisborne, H. T. (1929). The complicated controls of fire behaviour. *Journal of Forestry*, 27(3):311–312.

Gisborne, H. T. (1933). The wood cylinder method of measuring forest inflammability. *Journal of Forestry*, 31:673–679.

Gisborne, H. T. (1947). Fundamentals of fire behavior. *Fire Control Notes*, 9(1):13–24.

Goldstein, R. J., Ibele, W. E., Patankar, S. V., Simon, T. W., Kuehn, T. H., Strykowski, P. J., Tamma, K. K., Heberlein, J. V. R., Davidson, J. H., Bischof, J., Kulacki, F. A., Kortshagen, U., Garrick, S., and Srinivasan, V. (2006). Heat transfer: A review of 2003 literature. *International Journal of Heat and Mass Transfer*, 49(3-4):451–534.

Gould, J. and Sullivan, A. (2004). Fuel hazard development. Client Report No. 1468, CSIRO Forestry and Forest Products, Canberra, ACT.

Gould, J. S. (2006). Development of bushfire spread of the Wangary Fire 10th and 11th January 2005, Lower Eyre Pennisula, South Australia. Technical report, CSIRO/Ensis, Canberra, ACT.

Gould, J. S., Cheney, N. P., Hutchings, P. T., and Cheney, S. (1996). Prediction of bushfire spread. Final Report for IDNDR Project: 4/95, CSIRO Forestry and Forest Products, Canberra.

Gould, J. S., McCaw, W. L., Cheney, N. P., Ellis, P. F., Knight, I. K., and Sullivan, A. L. (2007). *Project Vesta–Fire in Dry Eucalypt Forest: fuel structure, dynamics and fire behaviour*. Ensis-CSIRO, Canberra ACT, and Department of Environment and Conservation, Perth WA.

Grassberger, P. (1986). Toward a quantitative theory of self-generated complexity. *International Journal of Theoretical Physics*, 25(9):907–938.

Gray, B. F., Griffiths, J. F., and Hasko, S. M. (1984). Spontaneous ignition hazards in stockpiles of cellulosic materials: Criteria for safe storage. *Journal of Chemical Technology and Biotechnology. Chemical Technology*, 34(8):453–463.

Gray, B. F., Sexton, M. J., Halliburton, B., and Macaskill, C. (2002). Wetting-induced ignition in cellulosic materials. *Fire Safety Journal*, 37(5):465–479.

Green, D. (2000). Self-organisation in complex systems. In Bossomaier, T. and Green,

D., editors, *Complex Systems*, chapter 2, pages 11–50. Cambridge University Press, Cambridge, UK.

Green, D. G., Gill, A. M., and Noble, I. R. (1983). Fire shapes and the adequacy of fire-spread models. *Ecological Modelling*, 20(1):33–45.

Green, D. G., Tridgell, A., and Gill, A. M. (1990). Interactive simulation of bushfires in heterogeneous fuels. *Mathematical and Computer Modelling*, 13(12):57–66.

Greenberg, J. P., Friedli, H., Guenther, A. B., Hanson, D., Harley, P., and Karl, T. (2006). Volatile organinc emissions from the distillation and pyrolysis of vegetation. *Atmospheric Chemistry and Physics*, 6:81–91.

Grishin, A. M. (1997). *Mathematical modeling of forest fires and new methods of fighting them*. Publishing House of Tomsk State University, Tomsk, Russia, English translation edition. Translated from Russian by Marek Czuma, L. Chikina and L. Smokotina, edited by Frank Albini.

Grishin, A. M., Gruzin, A. D., and Gruzina, E. E. (1984). Aerodynamics and heat exchange between the front of a forest fire and the surface layer of the atmosphere. *Journal of Applied Mechanics and Technical Physics*, 25(6):889–894.

Grishin, A. M., Gruzin, A. D., and Zverev, V. G. (1983). Mathematical modeling of the spreading of high-level forest fires. *Soviet Physics Doklady*, 28(4):328–330.

Güllü, D. and Demirbaş, A. (2001). Biomass to methanol via pyrolysis process. *Energy Conversion and Management*, 42(11):1349–1356.

Hallam, S. (1975). *Fire and hearth : a study of Aboriginal usage and European usurpation in south-western Australia*. Australian Institute of Aboriginal Studies.

Hargrove, W. W., Gardner, R. H., Turner, M. G., Romme, W. H., and Despain, D. G. (2000). Simulating fire patterns in heterogeneous landscapes. *Ecological Modelling*, 135(2-3):243–263.

Harris, P. (1999). On charcoal. *Interdisciplinary Science Reviews*, 24(4):301–306.

Hawley, L. F. (1926). Theoretical considerations regarding factors which influence forest fires. *Journal of Forestry*, 24(7):7.

Hurst, D. F., Griffith, D. W. T., and Cook, G. D. (1994). Trace gas emissions from biomass burning in tropical australian savannas. *Journal of Geophysical Research*, 99(D8):16441–16456.

Jane, F. W. (1956). *The Structure of Wood*. The Macmillan Company, New York, NY.

Jenkins, M. A., Clark, T., and Coen, J. (2001). Coupling atmospheric and fire models. In Johnson, E. and Miyanishi, K., editors, *Forest Fires: Behaviour and Ecological Effects*, chapter 5, pages 257–302. Academic Press, San Diego, CA, 1st edition.

Jiménez, J. (2006). The numerical computation of turbulence. In Shats, M. and Punzmann, H., editors, *Lecture Notes On Turbulence And Coherent Structures In Fluids, Plasmas And Nonlinear Media*, volume 4 of *Lecture Notes in Compex Systems*, chapter 6, pages 281–307. World Scientific, Singapore.

Johnston, P., Milne, G., and Kelso, J. (2006). A heat transfer simulation model for wildfire spread. *Forest Ecology and Management*, 234:S78–S78.

Karplus, W. J. (1977). The spectrum of mathematical modeling and systems simulation. *Mathematics and Computers in Simulation*, 19(1):3–10.

Keeves, A. and Douglas, D. R. (1983). Forest fires in South Australia on 16 February 1983 and consequent future forest management aims. *Australian Forestry*, 46(3):148–162.

Kelly, K. (1992). A distributed Santa Fe system. *Bulletin of the Santa Fe Institute*, 7(1):4–6.

Kemp, E. M. (1981). Pre-quaternary fire in Australia. In Gill, A., Groves, R., and Noble, I., editors, *Fire and the Australian Biota*, chapter 1, pages 3–21. Australian Academy of Science, Canberra.

King, A. and Linton, M. (1963). Report on moisture variation in forest fuels : equilibrium moisture content. Technical report, CSIRO Division of Physical Chemistry, Melbourne.

King, N. K. (1971). Simulation of the rate of spread of an aerial prescribed burn. *Australian Forest Research*, 6(2):1–10.

King, N. K. (1972). The influence of water vapour on the emission spectra of flames. *Combustion Science and Technology*, 6:247–256.

Knight, I. and Coleman, J. (1993). A fire perimeter expansion algorithm based on huygens' wavelet propagation. *International Journal of Wildland Fire*, 3(2):73–84.

Knight, I. K. and Sullivan, A. L. (2004). A semi-transparent model of bushfire flames to predict radiant heat flux. *International Journal of Wildland Fire*, 13(2):201–207.

Kolmogorov, A. N. (1941). The local structure of turbulence in incompressible viscous fluid for very large reynolds numbers. *Soviet Physics Doklady*, 30:301–305. Reprinted in *Proceedings of the Royal Society of London: Mathematical and Physical Sciences* 434(1890), 9-13 (1991).

Koufopanos, C. A., Maschio, G., and Lucchesi, A. (1989). Kinetic modelling of the pyrolysis of biomass and biomass components. *The Canadian Journal of Chemical Engineering*, 67:75–84.

Koufopanos, C. A., Papayannakos, N., Maschio, G., and Lucchesi, A. (1991). Modelling of the pyrolysis of biomass particles. Studies on kinetics, thermal and heat transfer effects. *The Canadian Journal of Chemical Engineering*, 69(8):907–915.

Kourtz, P. H., Nozaki, S., and O'Regan, W. G. (1977). Forest fires in a computer : A model to predict the perimeter location of a forest fire. Information Report FF-X-65, Fisheries and Environment Canada.

Kourtz, P. H. and O'Regan, W. G. (1971). A model for a small forest fire...to simulate burned and burning areas for use in a detection model. *Forest Science*, 17(1):163–169.

Larini, M., Giroud, F., Porterie, B., and Loraud, J. C. (1998). A multiphase formulation for fire propagation in heterogeneous combustible media. *International Journal of Heat and Mass Transfer*, 41(6-7):881–897.

Launder, B. E., Reece, G. J., and Rodi, W. (1975). Progress in the development of a Reynolds-stress turbulence closure. *Journal of Fluid Mechanics*, 68(3):537–566.

Le Goff, P. (1999). Issues of vocabulary : thermostatics, thermokinetics thermodynamics. *International Journal of Thermal Science*, 38(6):463–464.

Lehmann, J. (2007). A handful of carbon. *Nature*, 447:143–144.

Leslie, L. M. and Skinner, T. C. L. (1994). Real-time forecasting of the Western Australia summertime trough: Evaluation of a new regional model. *Weather and Forecasting*, 9:371–383.

Levins, R. (1966). The strategy of model building in population biology. In Sober, E., editor, *Conceptual Issues in Evolutionary Biology*, page 1827. MIT Press, Cambridge MA, 2nd edition. 1984.

Li, X. and Magill, W. (2000). Modelling fire spread under environmental influence using a cellular automaton approach. *Complexity International*, 8.

Lignini, F., Uzan-Elbez, J., Girard, J. P., Porfiri, M. T., Rodríguez-Rodrigo, L., and EISS Team (2005). Fire risk analysis in ITER tritium building. *Fusion Engineering and Design*, 75-79:1097–1102.

Linn, R., Reisner, J., Colman, J. J., and Winterkamp, J. (2002). Studying wildfire behavior using FIRETEC. *International Journal of Wildland Fire*, 11(3-4):233–246.

Linn, R. R. (1997). A transport model for prediction of wildfire behaviour. PhD Thesis LA-13334-T, Los Alamos National Laboratory. Reissue of PhD Thesis accepted by Department of Mechanical Engineering, New Mexico State University.

Linn, R. R. and Cunningham, P. (2005). Numerical simulations of grass fires using a coupled atmosphere-fire model: Basic fire behavior and dependence on wind speed. *Journal of Geophysical Research*, 110:D13107.

Linn, R. R. and Harlow, F. H. (1998). FIRETEC: A transport description of wildfire behaviour. In *Second Symposium on Fire and Forest Meteorology, 11-16 January 1998, Pheonix, Arizona*, pages 14–19. American Meteorological Society.

Loane, I. T. and Gould, J. S. (1986). *Aerial suppression of bushfires - Cost/benefit study for Victoria*. National Bushfire Research Unit, CSIRO Division of Forest Research, Canberra ACT.

Lockwood, F. C. and Shah, N. G. (1981). A new radiation solution method for incorporation in general combustion prediction procedures. In *Proceedings of the 18th Symposium (International) on Combustion*, pages 1405–1416, The Combustion Institute, Pittsburgh, PA.

Lorenz, E. N. (1963). Deterministic nonperiodic flow. *Journal of the Atmospheric Sciences*, 20(2):130–141.

Luke, R. (1953). Fire control manual. NSW Bushfire Committee.

Luke, R. H. (1961). *Bush Fire Control in Australia*. Hodder and Stoughton, Melbourne.

Luke, R. H. and McArthur, A. G. (1978). *Bushfires in Australia*. Australian Government Publishing Service, Canberra.

Mamleev, V., Bourbigot, S., and Yvon, J. (2007a). Kinetic analysis of the thermal decomposition of cellulose: The change of the rate limitation. *Journal of Analytical and Applied Pyrolysis*, 80(1):151–165.

Mamleev, V., Bourbigot, S., and Yvon, J. (2007b). Kinetic analysis of the thermal decomposition of cellulose: The main step of mass loss. *Journal of Analytical and Applied Pyrolysis*, 80(1):151–165.

Marris, E. (2006). Black is the new green. *Nature*, 442:624–626.

Mason, P. J. (1994). Large-eddy simulation: A critical review of the technique. *Quarterly Journal of the Royal Meteorological Society*, 120(515):1–26.

Matthews, S. (2006). A process-based model of fine fuel moisture. *International Journal of Wildland Fire*, 15(2):155–168.

McAlpine, R. and Wakimoto, R. (1991). The acceleration of fire from point source to equilibrium spread. *Forest Science*, 37(5):1314–1337.

McArthur, A. G. (1958). The preparation and use of fire danger tables. In *Proceedings of Fire Weather Conference, Australian Bureau of Meteorology, Melbourne, July 1958*. 24 pp.

McArthur, A. G. (1960). Fire danger rating tables for annual grasslands. Forestry and timber bureau, Commonwealth Department of National Development, Canberra.

McArthur, A. G. (1962). Control burning in eucalypt forests. Forestry and Timber Bureau

Leaflet 80, Commonwealth Department of National Development, Canberra.

McArthur, A. G. (1966). Weather and grassland fire behaviour. Forestry and Timber Bureau Leaflet 100, Commonwealth Department of National Development, Canberra.

McArthur, A. G. (1967). Fire behaviour in eucalypt forests. Forestry and Timber Bureau Leaflet 107, Commonwealth Department of National Development, Canberra.

McArthur, A. G. (1969). The Tasmanian bushfires of 7th February, 1967, and associated fire behaviour characteristics. In *Mass Fire Symposium, 10-12 February 1969, Collected Papers*, volume 1, Maribyrnong, Victoria. Defence Standards Laboratory. Paper A7, 24 pp.

McArthur, A. G. (1973). McArthur Mk V Forest Fire Danger Meter. Cardboard meter.

McArthur, A. G. and Luke, R. H. (1963). Fire behaviour studies in Australia. *Fire Control Notes*, 24(4):87–92.

McComb, D. (2006). Renormalization and statistical methods. In Shats, M. and Punzmann, H., editors, *Lecture Notes On Turbulence And Coherent Structures In Fluids, Plasmas And Nonlinear Media*, volume 4 of *Lecture Notes in Compex Systems*, chapter 2, pages 21–80. World Scientific, Singapore.

McComb, W. D. (2004). *Renormalization Methods: A Guide for Beginners*. Oxford University Press, Oxford, UK.

Mell, W., Jenkins, M. A., Gould, J., and Cheney, P. (2007). A physics based approach to modeling grassland fires. *International Journal of Wildland Fire*, 16(1):1–22.

Mell, W. E., Manzello, S. L., and Maranghides, A. (2006). Numerical modeling of fire spread through trees and shrubs. *Forest Ecology and Management*, 234:S82–S82.

Mills, G. (2005a). Lower atmospheric drying, stability, and increased wildfire activity. In *Sixth Symposium on Fire and Forest Meteorology*. Paper 1.2, 5 pp.

Mills, G. (2005b). On the subsynoptic-scale meteorology of two extreme fire weather days during the Eastern Australian fires of January 2003. *Australian Meteorological Magazine*, 54(4).

Milosavljevic, I., Oja, V., and Suuberg, E. M. (1996). Thermal effects in cellulose pyrolysis: Relationship to char formation process. *Industrial & Engineering Chemistry Research*, 35:653–662.

Mitchell, J. A. (1937). Rule of thumb for determining rate of spread. *Fire Control Notes*, 2:395–396.

Mok, W. S. L., Antal, M. J., Szabo, P., Várhegyi, G., and Zelei, B. (1992). Formation of charcoal from biomass in a sealed reactor. *Industrial & Engineering Chemistry Research*, 31(4):1162–1166.

Moore, W. J. (1963). *Physical Chemistry*. Longmans Green and Co Ltd, London, 4th edition.

Morrison, R. T. and Boyd, R. N. (1983). *Organic Chemistry*. Allyn and Bacon, Inc., Boston, Mass., 4th edition.

Morvan, D. and Dupuy, J. L. (2004). Modeling the propagation of a wildfire through a mediterranean shrub using a multiphase formulation. *Combustion and Flame*, 138(3):199–210.

Morvan, D., Dupuy, J. L., Pimont, F., and Linn, R. R. (2006). Numerical study of grassland fires behaviour using a physical multiphase formulation. *Forest Ecology and Management*, 234:S90–S90.

Nelson, M. I. (1997). A dynamical systems model of autoignition in the cone calorimeter.

In Hasemi, Y. and Tsukuba, E., editors, *Fire Safety Science: Proceedings of the Fifth International Symposium*, volume 5, pages 547–558. International Association for Fire Safety Science.

Nelson, M. I. (1998). Ignition mechanisms of thermally thin thermoplastics in the cone calorimeter. *Proceedings of the Royal Society A: Mathematical, Physical and Engineering Sciences*, 454(1971):789–814.

Nelson, Jr., R. M. (1993). Byram's derivation of the energy criterion for forest and wildland fires. *International Journal of Wildland Fire*, 3(3):131–138.

Nelson, Jr., R. M. (2003). Power of the fire–a thermodynamic analysis. *International Journal of Wildland Fire*, 12(1):51–65.

Noble, I. R., Bary, G. A. V., and Gill, A. M. (1980). McArthur's fire-danger meters expressed as equations. *Australian Journal of Ecology*, 5:201–203.

Oran, E. S. and Gamezo, V. N. (2007). Origins of the deflagration-to-detonation transition in gas-phase combustion. *Combustion and Flame*, 148:4–47.

Orfao, J. J. M., Antunes, F. J. A., and Figueiredo, J. L. (1999). Pyrolysis kinetics of lignocellulosic materials: three independent reactions model. *Fuel*, 78(3):349–358.

O'Sullivan, A. C. (1997). Cellulose: the structure slowly unravels. *Cellulose*, 4(3):173–207.

Pagni, P. J. and Peterson, T. G. (1973). Flame spread through porous fuels. In *Proceedings of the 14th (International Symposium) on Combustion*, pages 1099–1107, Pittsburgh, PA. The Combustion Institute.

Parker, W. J. and LeVan, S. L. (1989). Kinetic properties of the components of douglas-fir and the heat of combustion of their volatile pyrolysis products. *Wood and Fiber Science*, 21(3):289–305.

Pastor, E., Zarate, L., Planas, E., and Arnaldos, J. (2003). Mathematical models and calculation systems for the study of wildland fire behaviour. *Progress in Energy and Combustion Science*, 29(2):139–153.

Peet, G. B. (1965). A fire danger rating and controlled burning guide for the northern jarrah (Euc. Marginata Sm.) forest of Western Australia. Bulletin No 74, Forests Department, Perth, Western Australia.

Pielke, R. A., Cotton, W. E., Walko, R. L., Tremback, C. J., Lyons, W. A., Grasso, L. D., Nicholls, M. E., Moran, M. D., Wesley, D. A., Lee, T. J., and Copeland, J. H. (1992). A comprehensive meteorological modeling system – RAMS. *Meteorology and Atmospheric Physics*, 49:69–91.

Plucinski, M. P. (2003). *The investigation of factors governing ignition and development of fires in heathland vegetation*. PhD thesis, School of Mathematics and Statistics University of New South Wales, Australian Defence Force Academy, Canberra, ACT, Australia.

Pompe, A. and Vines, R. G. (1966). The influence of moisture on the combustion of leaves. *Australian Forestry*, 30(3):231–241.

Porterie, B., Consalvi, J. L., Loraud, J. C., Giroud, F., and Picard, C. (2007). Dynamics of wildland fires and their impact on structures. *Combustion and Flame*, 149(3):314–328.

Porterie, B., Morvan, D., Larini, M., and Loraud, J. C. (1998). Wildfire propagation: A two-dimensional multiphase approach. *Combustion Explosion and Shock Waves*, 34(2):139–150.

Porterie, B., Morvan, D., Loraud, J. C., and Larini, M. (2000). Fire spread through fuel

beds: Modeling of wind-aided fires and induced hydrodynamics. *Physics of Fluids*, 12(7):1762–1782.

Potter, B. E. (1996). Atmospheric properties associated with large wildfires. *International Journal of Wildland Fire*, 6(2):71–76.

Potter, B. E. (2002). A dynamics based view of atmosphere-fire interactions. *International Journal of Wildland Fire*, 11(3-4):247–255.

Potter, B. E. (2005). The role of released moisture in the atmospheric dynamics associated with wildland fires. *International Journal of Wildland Fire*, 14(1):7784.

Pyne, S. J. (1991). *Burning Bush: A Fire History of Australia*. University of Washington Press, Seattle, WA, 1998 paperback edition.

Pyne, S. J. (2001). *Year of the Fires : The Story of the Great Fires of 1910*. Viking, New York.

Pyne, S. J., Andrews, P. L., and Laven, R. D. (1996). *Introduction to Wildland Fire*. John Wiley and Sons, New York, 2nd edition.

Raithby, G. D. and Chui, E. H. (1990). A finite-volume method for predicting radiant heat transfer in enclosures with participating media. *Journal of Heat Transfer*, 112:415–423.

Rawson, R. P., Billing, P. R., and Duncan, S. F. (1983). The 1982-83 forest fires in Victoria. *Australian Forestry*, 46(3):163–172.

Rehm, R. G. and Baum, H. R. (1978). The equations of motion for thermally driven, buoyant flows. *Journal of Research of the National Bureau of Standards*, 83(3):297–308.

Reisen, F., Brown, S., and Cheng, M. (2006). Air toxics in bushfire smoke–firefighters exposure during prescribed burns. *Forest Ecology and Management*, 234(Supplement 1):S144–S144.

Richards, G. D. (1995). A general mathematical framework for modeling two-dimensional wildland fire spread. *International Journal of Wildland Fire*, 5:63–72.

Richards, G. D. and Bryce, R. W. (1996). A computer algorithm for simulating the spread of wildland fire perimeters for heterogeneous fuel and meteorological conditions. *International Journal of Wildland Fire*, 5(2):73–79.

Richardson, L. F. (1922). *Weather Prediction by Numerical Process*. Cambridge Univeristy Press.

Rodger, G. J. (1961). Report of the Royal Commission on the bush fires of December 1960 and January, February and March 1961 in Western Australia. Western Australia State Parliament.

Rothermel, R. C. (1972). A mathematical model for predicting fire spread in wildland fuels. Research Paper INT-115, USDA Forest Service, Intermountain Forest and Range Experimental Station, Odgen UT.

Rothermel, R. C. (1983). How to predict the spread and intensity of forest and range fires. General Technical Report INT-143, USDA Forest Service, Intermountain Forest and Range Experimental Station, Odgen UT.

Rothermel, R. C. and Anderson, H. E. (1966). Fire spread characteristics determined in the laboratory. Research Paper INT-30, USDA Forest Service, Intermountain Forest and Range Experimental Station, Odgen UT.

Sacadura, J. F. (2005). Radiative heat transfer in fire safety science. *Journal of Quantitative Spectroscopy & Radiative Transfer*, 93:5–24.

Scott, A. (2005). *Encyclopedia of Nonlinear Science*. Routledge, New York, NY.

Scott, A. C. and Glasspool, I. J. (2006). The diversification of paleozoic fire systems and

fluctuations in atmospheric oxygen concentration. *PNAS*, 103(29):10861–10865. Proceedings of the National Academy of Sciences of the United States of America.

Seeley, D. A. (2000). Network evolution and the emergence of structure. In Bossomaier, T. and Green, D., editors, *Complex Systems*, chapter 3, pages 51–89. Cambridge University Press, Cambridge, UK.

Semenoff, N. N. (1928). Zur theorie des verbrennungsprozesses. *Zeitschrift für Physik*, 48(7-8):571–582.

Sexton, M. J., Macaskill, C., and Gray, B. F. (2001). Self-heating and drying in two-dimensional bagasse piles. *Combustion Theory and Modelling*, 5:517–536.

Shafizadeh, F. (1982). Introduction to pyrolysis of biomass. *Journal of Analytical and Applied Pyrolysis*, 3(4):283–305.

Shafizadeh, F. and Chin, P. P. S. (1977). Thermal deterioration of wood. In Goldstein, I. S., editor, *Wood Technology: Chemical Aspects*, number 43 in ACS Symposium Series, pages 57–81, Washington, DC. American Chemical Society.

Shalizi, C. R. and Moore, C. (2003). What is a macrostate? subjective observations and objective dynamics. *arXiv:*, cond-mat/0303625v1:15 pp.

Shalizi, C. R., Shalizi, K. L., and Haslinger, R. (2004). Quantifying self-organization with optimal predictors. *Physical Review Letters*, 93(11):118701.

Shampine, L. F. (1980). What everyone solving differential equations should know. In Gladwell, I. and Sayers, D. K., editors, *Computational Techniques for Ordinary Differential Equations*, chapter 1, pages 1–17. Academic Press, London, UK.

Shannon, C. E. (1948). A mathematical theory of communication. *The Bell System Technical Journal*, 27:379–423, 623–656.

Shiner, J. S., Davison, M., and Landsberg, P. T. (1999). Simple measure for complexity. *Physical Review E*, 59(2):1459–1464.

Smith, J. M. B. (1979). Biogeographic history of Australian flora and fauna. In Recher, H. F., Lunney, D., and Dunn, I., editors, *A Natural Legacy: Ecology in Australia*, chapter 2, pages 13–26. Pergamon Press, Sydney.

Springett, B. P. (1979). Biogeographic history of Australian flora and faunaneed proper title here. In Recher, H. F., Lunney, D., and Dunn, I., editors, *A Natural Legacy: Ecology in Australia*, chapter 7, pages 90–103. Pergamon Press, Sydney.

Stocks, B. J., Alexander, M. E., and Lanoville, R. A. (2004). Overview of the International Crown Fire Modelling Experiment (ICFME). *Canadian Journal of Forest Research*, 34(8):1543–1547.

Stocks, B. J., Lawson, B. D., Alexander, M. E., Van Wagner, C. E., McAlpine, R. S., Lynham, T. J., and Dubé, D. E. (1991). The Canadian system of forest fire danger rating. In Cheney, N. and Gill, A., editors, *Conference on Bushfire Modelling and Fire Danger Rating Systems*, pages 9–18, Canberra. CSIRO.

Stott, J. B. (1960). Influence of moisture on the spontaneous heating of coal. *Nature*, 188(4744):54.

Sullivan, A. (2004). Nature of severe fire events. Client Report No. 1470, CSIRO Forestry and Forest Products, Yarralumla, ACT.

Sullivan, A. L. (2007a). Convective Froude number and Byram's energy criterion of Australian experimental grassland fires. *Proceedings of the Combustion Institute*, 31(2):2557–2564.

Sullivan, A. L. (2007b). A review of wildland fire spread modelling, 1990-present, 1: Physical and quasi-physical models. *arXiv:0706.3074v1 [physics.geo-ph]*. 46 pp.

Sullivan, A. L. (2007c). A review of wildland fire spread modelling, 1990-present, 2: Empirical and quasi-empirical models. *arXiv:0706.4128v1[physics.geo-ph]*. 32 pp.

Sullivan, A. L. (2007d). A review of wildland fire spread modelling, 1990-present, 3: Simulation and mathematical analogues. *arXiv:0706.4130v1[physics.geo-ph]*. 29 pp.

Sullivan, A. L., Ellis, P. F., and Knight, I. K. (2003a). A review of the use of radiant heat flux models in bushfire applications. *International Journal of Wildland Fire*, 12(1):101–110.

Sullivan, A. L. and Knight, I. K. (2001). Estimating error in wind speed measurements for experimental fires. *Canadian Journal of Forest Research*, 31(3):401–409.

Sullivan, A. L. and Knight, I. K. (2004). A hybrid cellular automata/semi-physical model of fire growth. In *Proceedings of the 7th Asia-Pacific Conference on Complex Systems, 6-10 December 2004, Cairns*, pages 64–73.

Sullivan, A. L., Knight, I. K., Weber, R. O., and Finnigan, J. F. (2003b). Application of complex systems science to the analysis of the behaviour of bushfires: A scoping study. Client Report No. 1293, CSIRO Forestry and Forest Products, Canberra.

Swanson, M. A. (1948). Studies on the structure of polysaccharides. IV. Relation of the iodine color to the structure. *Journal of Biological Chemistry*, 172(2):825–837.

Taylor, S. W., Wotton, B. M., Alexander, M. E., and Dalrymple, G. N. (2004). Variation in wind and crown fire behaviour in a northern jack pine - black spruce forest. *Canadian Journal of Forest Research*, 34:1561–1576.

Tinniswood, A. (2004). *By Permission of Heaven: The True Story of the Great Fire of London*. Riverhead, New York, NY.

Tolhurst, K. G. and Chatto, K. (1998). Behaviour and threat of a plume driven bushfire in west-central Victoria, Australia. In *Proceedings of 13th Fire and Forest Meteorology Conference, Lorne, Australia, 1996*, volume 2, pages 321–331. IAWF.

Turner, J. S. (1973). *Buoyancy effects in fluids*. Cambridge University Press, Cambridge. Paperback edition 1979.

van Boekel, M. A. J. S. (2001). Kinetic aspects of the Maillard reaction: a critical review. *Nahrun/Food*, 45(3):150–159.

Van Wagner, C. E. (1969). A simple fire-growth model. *The Forestry Chronicle*, 45(1):103–104.

Van Wagner, C. E. (1972). Heat of combustion, heat yield and fire behaviour. Information Report PS-X-35, Environment Canada, Petawawa Forest Experiment Station, Chalk River, Ontario.

Van Wagner, C. E. (1977). Effect of slope on fire spread rate. *Canadian Forestry Service Bi-Monthly Research Notes*, 33:7–8.

Van Wagner, C. E. (1985). Fire spread from a point source. Memo PI-4-20 dated January 14, 1985 to P. Kourtz (unpublished), Canadian Forest Service, Petawawa National Forest Institute, Chalk River, OT.

Van Wagner, C. E. (1987). Development and Structure of the Canadian Forest Fire Weather Index System. Forestry Technical Report 35, Canadian Forestry Service, Petawawa National Forest Institute, Chalk River, OT.

Van Wagner, C. E. and Pickett, T. L. (1985). Equations and FORTRAN program for the Canadian Forest Fire Weather Index System. Forestry Technical Report 33, Cana-

dian Forestry Service, Petawawa National Forestry Institute, Chalk River, OT.

Várhegyi, G., Antal, M. J., Jakab, E., and Szabó, P. (1997). Kinetic modeling of biomass pyrolysis. *Journal of Analytical and Applied Pyrolysis*, 42(1):73–87.

Várhegyi, G., Szabó, P., Mok, W. S.-L., and Antal, Jr., M. J. (1993). Kinetics of the thermal decomposition of cellulose in sealed vessels at elevated pressures. Effects of the presence of water on the reaction mechanism. *Journal of Analytical and Applied Pyrolysis*, 26:159–174.

Viegas, D. X. (2005). A mathematical model for forest fires blowup. *Combustion Science and Technology*, 177(1):27–51.

Viegas, D. X. (2006). Parametric study of an eruptive fire behaviour model. *International Journal of Wildland Fire*, 15(2):169–177.

Vines, R. G. (1981). Physics and chemistry of rural fires. In Gill, A., Groves, R., and Noble, I., editors, *Fire and the Australian Biota*, pages 129–150. Australian Academy of Science, Canberra.

Viney, N. R. (1991). A review of fine fuel moisture modelling. *International Journal of Wildland Fire*, 1(4):215–234.

Watt, S. D., Staggs, J. E. J., McIntosh, A. C., and Brindley, J. (2001). A theoretical explanation of the infuence of char formation on the ignition of polymers. *Fire Safety Journal*, 36(5):421–436.

Weber, R. O. (1989). Analytical models of fire spread due to radiation. *Combustion and Flame*, 78:398–408.

Weber, R. O. (1991a). Modelling fire spread through fuel beds. *Progress in Energy Combustion Science*, 17(1):67–82.

Weber, R. O. (1991b). Toward a comprehensive wildfire spread model. *International Journal of Wildland Fire*, 1(4):245–248.

Weise, D. R. and Biging, G. S. (1997). A qualitative comparison of fire spread models incorporating wind and slope effects. *Forest Science*, 43(2):170–180.

Williams, F. A. (1982). Urban and wildland fire phenomenology. *Progress in Energy Combustion Science*, 8:317–354.

Williams, F. A. (1985). *Combustion Theory: The Fundamental Theory of Chemically Reacting Flow Systems*. Addison-Wesley Publishing Company, Massachusetts, 2nd edition. 1994.

Williams, J. (2004). Managing fire-dependent ecosystems: we need a public lands policy debate. *Fire Management Today*, 64(2):6–11.

Wodley, F. A. (1971). Pyrolysis products of untreated and flame retardant-treated α-cellulose and levoglucosan. *Journal of Applied Polymer Science*, 15(4):835–851.

Wolfram, S. (2002). *A New Kind of Science*. Wolfram Media, Inc., Illinois, USA.

World Meteorological Organisation (1988). *World Meterological Organisation Technical Regulations Vol 1: General meterological standards and recommended practices*. Number 49. Secretariat of the World Meterological Organisation, Geneva, Switzerland.

Wright, J. G. (1932). Forest-fire hazard research: As developed and conducted at the petawawa forest experiment station. Department of the Interior Canada Forest Service, Ottawa, Canada.

Wu, Y., Xing, H. J., and Atkinson, G. (2000). Interaction of fire plume with inclined surface. *Fire Safety Journal*, 35(4):391–403.

Xue, H., Ho, J. C., and Cheng, Y. M. (2001). Comparison of different combustion models

in enclosure fire simulation. *Fire Safety Journal*, 36(1):37–54.

Yakot, V. and Orszag, S. A. (1986). Renormalization group analysis of turbulence. I. Basic theory. *Journal of Scientific Computing*, 1(1):3–51.

Zhbankov, R. G., Firsov, S. P., Buslov, D. K., Nikonenko, N. A., Marchewka, M. K., and Ratajczak, H. (2002). Structural physico-chemistry of cellulose macromolecules. Vibrational spectra and structure of celllulose. *Journal of Molecular Structure*, 614:117–125.

Zou, X., Gurnagul, N., Uesaka, T., and Bouchard, J. (1994). Accelerated aging of papers of pure cellulose: mechanism of cellulose degradation and paper embrittlement. *Polymer Degradation and Stability*, 43(3):393–402.